Enhancement of Carotenoid Biosynthesis and Antioxidant Responses in Diatoms by Light Modulation

Thesis

Enhancement of carotenoid biosynthesis and antioxidant responses in microalgae by light modulation

Arianna Smerilli

Master of Science in Biological Monitoring

University of Genova, Italy

Doctor of Philosophy
in Life and Biomolecular Science

The Open University – Milton Keynes, UK
Stazione Zoologica Anton Dohrn - Napoli, Italy

September 2017

Enhancement of carotenoid biosynthesis and antioxidant responses in microalgae by light modulation

Arianna Smerilli

Doctor of Philosophy in Life and Biomolecular Science

Director of Studies

Dr Christophe Brunet

Stazione Zoologica Anton Dohrn

Naples, Italy

External Supervisor

Prof Alexander Ruban

Queen Mary University

London, UK

September 2017

The Open University

ABSTRACT

The ecological success of diatoms is mostly attributed to their ability to adjust biological performances to the variable environmental conditions they experience in the water column. While the efficient photoacclimative and photoprotective mechanisms in diatoms are already reported, the involvement of the antioxidant network in lowering or repairing light stress or damage is poorly understood.

My thesis consists of the concomitant investigation of the photoprotective and antioxidant network functioning in the coastal diatom *Skeletonema marinoi*, and during an experiment at sea in the Gulf of Naples. The aims of my work are to explore the antioxidant network in diatoms to better understand its activation in coping with light variation, and the functional link between antioxidant molecules synthesis/activity and photoprotection.

Results showed the spectral light dependent activity of antioxidant enzymes such as ascorbate peroxidase, catalase, and superoxide dismutase. They act in complementarity of the antioxidant molecules synthesis. A high concentration of ascorbic acid, phenolics compounds and among them flavonoids were found in diatoms. These molecules respond to light variations in terms of spectral composition, photon flux density, daily light dose, light shape distribution and photoperiod duration. Also, in a natural microalgal community, these molecules were found at high concentration following a dynamics that relied on light, nutrient stress and photosynthetic regulation.

The photoprotective xanthophyll cycle, involving the pigments diatoxanthin and diadinoxanthin, is activated by light and modulated in concordance with antioxidant molecules synthesis. Indeed, under different light climates, a link between these two defense processes was found. I also show that the xanthophyll cycle pigments have a high antioxidant activity. This feature explains why they increase together with antioxidant molecules during cell senescence. More generally, the physiological state of the cells modulates the antioxidant and photoprotective network in diatoms.

ACKNOWLEDGMENTS

My acknowledgments go to the people that turned this PhD project into reality.

First of all, I would like to thank Stazione Zoologica Anton Dohrn which provided for the financial and technical support to fulfill this project.

I am grateful to my director of studies Dr Christophe Brunet for introducing me to this fascinating world of microalgae and photophysiology, and for trusting and supporting me during these years.

My gratitude also goes to my external supervisor Prof. Alexander Ruban, who kept track of my progress and provided precious comments and suggestions which improved the research work.

I would like to thank also Federico Corato, the Master of Lights.

Indeed, one of the persons which greatly contributed to this work was Dr Ida Orefice, without whom all of this would have been impossible. She gave me the basis for working with these tiny and sometimes bossy organisms, we had fruitful discussions to improve the work, from the smallest practical issues till the bigger theoretical ones, and above all supported and comforted me during the harshest moments.

Then, surely I have to thank all the amazing people I had the chance to meet here in Stazione, sometimes for their providential help in the work, but mostly for the fun, the non-sense, the GOT evenings, the food, the affection, the hysterical crying and the big laughs. So, thank you Laura, Laura, Greta, Eleonora, Maira, Vincenzo, Cecilia, Romain, Chetan, and all the other friends. Yeah, even you Maria Paola and Katerina.

I must say thank you to Riccardo, for supporting and put up with me all these years, for the invaluable advices and comfort, for the love, the travels, the Sundays on the couch.

Finally, I would like to express my infinite gratitude to my family. Firstly to my mother, my rock, for her unconditional love, always ready to help me in all the ways possible and even impossible.

Of course to my father, for occasionally faking some interest into my work.

And lastly to my brothers, without whom part of myself would be lacking.

TABLE OF CONTENTS

LIST OF FIGURES

LIST OF TABLES

LIST OF ABBREVIATIONS

^{1}Chl* chlorophyll singlet excited state

$^1O_2$ singlet oxygen

^{3}Chl* chlorophyll triplet excited state

a* cell-specific absorption coefficient

ABTS 2,2'-azino-bis (3-ethylbenzothiazoline-6-sulphonic acid)

AEq ascorbic acid equivalent

ANOVA analysis of variance

AP-1 activator protein-1

APX ascorbate peroxidase

ARA arachidonic acid

ARE antioxidant responsive elements

AsA ascorbic acid

ATP adenosine triphosphate

Ax antheraxanthin

B blue

BR blue+red

BSA bovine serum albumin

Byr billion years

bZIP basic region leucine zipper

CAT catalase

CCM carbon concentrating mechanism

CET PSI cyclic electron transport around PSI

CET PSII cyclic electron transport around PSII

Chl *a* chlorophyll a

Chl *c* chlorophyll c

CP chlorophyll-protein complex

CRY cryptochrome

cyt b_6/*f* cytochrome b_6/*f*

DASH CRY *Drosophila, Arabidopsis, Synechococcus, Homo* cryptochrome

DCMU 3-(3,4-dichlorophenyl)-1,1-dimethylurea

Dd diadinoxanthin

DES de-epoxidation state

DHA docosahexaenoic acid

DHAR dehydroascorbate reductase

DMAPP dimethylallyl diphosphate

DOC dissolved organic carbon

DPPH 2,2-diphenyl-1-picrylhydrazyl

Dt diatoxanthin

DU degree of unsaturation

DW dry weight

E irradiance

Ek light saturation index for photosynthesis

EPA eicosapentaenoic acid

ETR electron transport rate

F_0 minimal fluorescence

FA fatty acid

FAD flavin adenine dinucleotide

FCP fucoxanthin chlorophyll *a*/*c* binding protein complex

Fe^{2+} ferrous ion

Fe^{3+} ferric ion

FeS Rieske iron-sulfur protein

Fm maximal fluorescence

FNR ferredoxin-NADP oxidoreductase

FSW filtered sea water

Fuco fucoxanthin

Fv variable fluorescence

Fv/Fm photochemical efficiency of the PSII

G3P 3-phosphoglicerate

GAEq gallic acid equivalent

GGPP geranylgeranyl pyrophosphate

GMO genetically modified organism

GPX glutathione peroxidase

GR glutathione reductase

GSH reduced glutathione

GSSH oxidized glutathione

H_2O_2 hydrogen peroxide

H_{II} phase inverted hexagonal phase

His histidine

HPLC high performance liquid chromatography

IC_{50} half maximal inhibitory concentration

Ile isoleucine

IPP isopentenyl pyrophosphate

IR infrared

$L^{\bullet}$ fatty acid radical

LC/MS liquid chromatography-mass spectrometry

LCBY lycopene β-cyclase

LED light-emitting diode

Leu leucine

LH lipid

LHC light harvesting complex

$LOO^{\bullet}$ peroxyl-fatty acid radical

LOOH lipid hydroperoxides

LOV light, oxygen, voltage

LUT1 carotene epsilon-monooxygenase; lutein like protein

MAPK mitogen-activated protein kinase

MDHAR monodehydroascorbate reductase

MEP methylerythritol phosphate

MEV mevalonate

MGDG monogalactosyldiacylglycerol

MTHF methenyltetrahydrofolate

Myr million years

NADH nicotinamide adenine dinucleotide

NADPH nicotinamide adenine dinucleotide phosphate

NDH NAD(P)H dehydrogenase complex

NF-kB nuclear factor-k

NOX NADPH oxidase

NPQ Non-photochemical quenching of chlorophyll *a* fluorescence

Nrf2 nuclear factor 2

Nx neoxanthin

$O_2^{\bullet-}$ superoxide ion

OH^- hydroxyl ion

$OH^{\bullet}$ hydroxyl radical

PAM pulse amplitude modulation

PAR photosynthetic active radiation

PC plastocyanin

PCA principal component analysis

PDS Phytoene desaturase

PFD photon flux density

Phe phenylalanine

Pheo pheophytin

POC particulate organic carbon

PQ plastoquinone

Prep-HPLC preparative high performance liquid chromatography

PSI photosystem I

PSII photosystem II

PSY phytoene synthase

PTOX plastid terminal oxidase

PUFA polyunsaturated fatty acid

PUR photosynthetic usable radiation

qE energy-dependent quenching

QEq quercetin equivalent

qI photoinhibitory quenching

qT state transition quenching

R red

RC reaction center

$_{rel}ETR_{max}$ maximal relative rate of linear electron transport

RFU relative fluorescence unit

RGB red green blue

ROS reactive oxygen species

RT room temperature

Rubisco ribulose-1,5-bisphosphate carboxylase oxygenase

RuBP ribulose 1,5-bisphosphate

SA specific activity

SD standard deviation

SOD superoxide dismutase

SQDG sulfoquinovosyldiacylglycerol

SS sum of squares

Sy.x standard deviation of the residuals

TCA trichloroacetic acid

TEAC trolox equivalent antioxidant capacity

TFC total flavonoid content

Thr threonine

TPC total phenolic content

Tyr tyrosine

UV ultraviolet

VDE violaxanthin de-epoxidase

Vx violaxanthin

WWC water-water cycle

XC xanthophyll cycle

XOD xanthine oxidase

ZDS ζ-carotene desaturase

Zeax zeaxanthin

ZEP zeaxanthin epoxidase

α maximum light use efficiency

β-car β-carotene

μ growth rate

ϕ_p quantum yield of photochemistry

1. General introduction

1.1 The microalgal realm and the group of Bacillariophyceae

1.1.1 Microalgal diversity

The term *microalgae* is used to indicate a polyphyletic assemblage of microorganisms. They do not share a common origin, following multiple and independent evolutionary lines, but they do show physiological coherence: oxygenic photosynthesis (Andersen, 1992).

These both prokaryotic and eukaryotic microorganisms populate all the aquatic environments, from the marine to the brackish and freshwaters.

Microalgae show an impressive biodiversity and they are widespread among all different habitats. According to this feature, they can be divided into three groups: the free floating ones, also known as phytoplankton; the ones that live attached to submerged structures and vegetation, also known as periphyton; and the ones that grow on the bottom sediments, the benthic microalgae.

Phytoplankton, corresponding to the group of microalgae that inhabits the water column, floating or drifting in the water mass, is the most important group. There are about 25.000 morphologically defined forms of phytoplankton, distributed among seven major phyla (Fig. 1.1)(Falkowski *et al.*, 2004).

The prokaryotic part of phytoplankton is composed by the cyanobacteria, while the eukaryote members comprise diatoms, dinoflagellates, coccolithophores, green algae, etc.

Although representing less than 1% of the global primary producer biomass, microalgal contribution to Earth's primary productivity is similar to the photosynthetic terrestrial productivity (46.2% and 53.8% respectively)(Field *et al.*, 1998). These astonishing rates are due to the high metabolic activity and the fast turnover (Kolber, 2007).

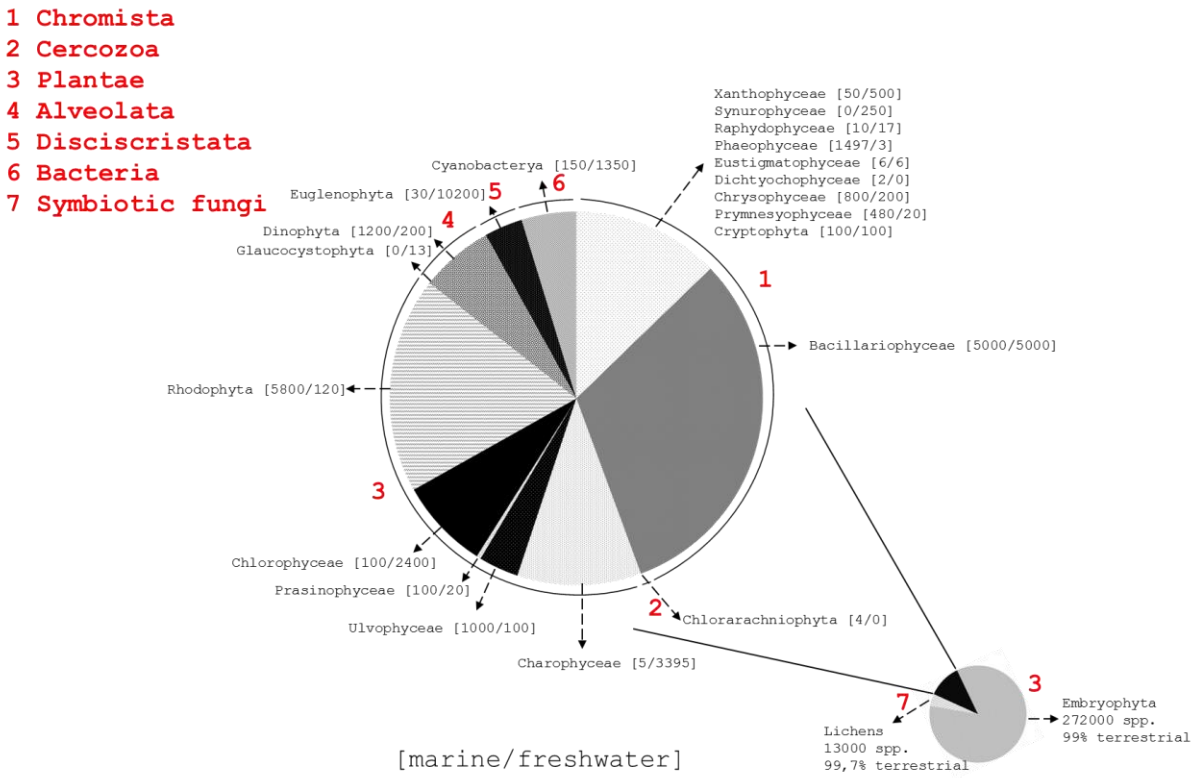

Figure 1.1: Phylogenetic distribution of terrestrial and aquatic photoautotrophs based on morphological characteristics (modified from Falkowski *et al.*, 2004).

Microalgae represent the base of the aquatic food webs, providing organic carbon that reaches higher trophic levels. Indeed, they play a central role in the biogeochemical cycling of elements and nutrients, producing oxygen required for aerobic life and strongly contributing to the biological carbon pump. The latter is the process through which fixed carbon is sequestered over geologically relevant time-scale in the deep sea, assuring the survival of all the organisms that live beneath the photic zone, i.e. the upper layer characterized by the presence of enough light energy which allows the occurrence of photosynthetic process (Smetacek, 1999, Bowler *et al.*, 2009).

They evolved reaching the ability not only to survive but even thrive in the harshest conditions, thanks also to their capacity to produce a multitude of compounds with protective and nourishing properties. The result is a high level of structural and chemical diversity, coming from different metabolic pathways (Cardozo *et al.*, 2007).

The high functional diversity covers a broad range of adaptive traits regarding the morphology (e.g. cell size, shape, presence of flagellum, single or colonial cells), the

utilization of resources (e.g. light, nutrients) or physiology (e.g. optimal temperature, osmoregulation).

1.1.2 The Diatoms

1.1.2.1 The rise of diatoms

The most diversified group of phytoplankton in contemporary oceans is constituted by diatoms. They belong to the class *Bacillariophyceae* within the phylum *Heterokonta* or *Stramenopiles.*

While Guiry (2012) estimated that diatoms species should be around 20.000 (8.000 undiscovered diatoms species, and the 12.000 already described ones), Mann and Droop (1996) estimated that there should be more than 200.000 different species. Kooistra *et al.* (2007) raise the issue of the cryptic species, not distinguishable following classical morphological study, but now analysable with molecular tools. According to them, there should be more than 100.000 cryptic diatom species.

The ecological success of diatoms is reflected not only by the number of species, but also by their biomass and primary productivity. Diatoms' ecological weight could be better understood by saying that the oxygen in every fifth breath we take come from them (Nelson *et al.*, 1995, Field *et al.*, 1998).

The frail nature of diatom's external structure prevented their conservation in the sediments, making it difficult to precisely determine their first appearance on Earth (Falkowski *et al.*, 2004). The earliest diatom fossil dates back to the Early Jurassic, so 190 million years (Myr) ago (Kooistra *et al.*, 2007), but according to molecular-clock-based estimates, it seems that they arose in the Triassic period, some 250 Myr ago (Armbrust, 2009). Their rising, together with coccolitophorids and dinoflagellates, led to a major change of the organic carbon cycling, progressively reducing the atmospheric CO_2, which at that time was almost eight times higher than today, and increasing the O_2 levels. Furthermore, the sinking of these phytoplanktonic species at the sea bottom created part of the current petroleum reserves (Armbrust, 2009).

The first diatom lineage was the radial centric, while the bi- and multi-polar centric appeared in the early Cretaceous (115 Myr ago ca)(Kooistra *et al.*, 2007, Bowler *et al.*, 2010b). The most recent lineage is represented by the pennates: araphid ones popped up 90 Myr ago, and the raphid ones later, almost 60 Mya, after the Cretaceous–Tertiary (K–T) mass extinction (Kooistra *et al.*, 2007, Bowler *et al.*, 2010b) (Fig. 1.2).

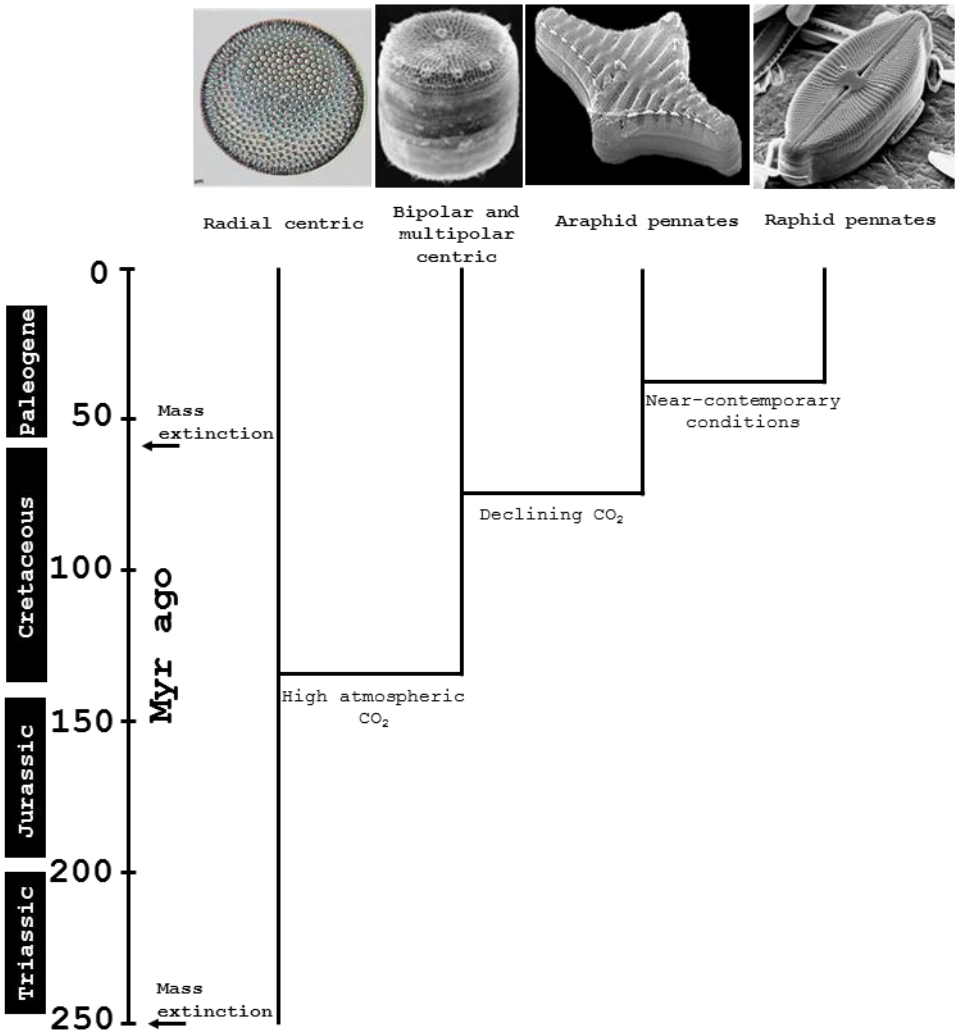

Figure 1.2: Estimated timing of divergence of the four major diatom lineages (modified from Armbrust, 2009).

Following the endosymbiotic theory, 1.5 billion years (Byr) ago, or even before following the newest findings on fossil records (Bengtson *et al.*, 2017), an eukaryotic heterotroph engulfed a cyanobacterium, the first life form able to perform photosynthesis. This first event led to the rise of Plantae, the major group that includes green and red algae and land

plants. After that, various secondary endosymbiosis events involving both green and red algae occurred several times independently (Keeling, 2013). *Circa* 1 Byr ago, a heterotroph engulfed a red alga, which progressively became the plastid of the super-group of the *Chromalveolates*, which includes *Stramenopiles* (diatoms belong to this *phylum*), *Haptophyta*, *Cryptophyta* and *Alveolata* (Keeling, 2010).
These plastids are surrounded by four membranes: the two original plastid membranes, the plasma membrane of the endosymbiotic alga, and the phagosomal membrane of the eukaryotic host (Keeling, 2013). Other findings suggest that another endosymbiotic event involving a green alga may have occurred (Moustafa *et al.*, 2009)(Fig. 1.3).

As consequence of endosymbiosis, many algal genes both from the plastid and from the nucleus were lost, but many others were transferred to the host nucleus (Armbrust, 2009, Keeling, 2013). Interestingly, at least 5% of diatoms genes show bacterial origin, indicating multiple lateral gene transfer events (Bowler *et al.*, 2008, Finazzi *et al.*, 2010). The final result is a mixed genome, chimera of genes from different sources (heterotrophic host, green and red algae, bacteria) that provides diatoms a range of attributes that are a combination of animal and plant features. This may be the reason of their ecological success, which, for example, allows them to survive in prolonged period of darkness, or to bloom from their resting stage in optimal environmental conditions (Kooistra *et al.*, 2007, Armbrust, 2009, Clemens & Christian, 2013).

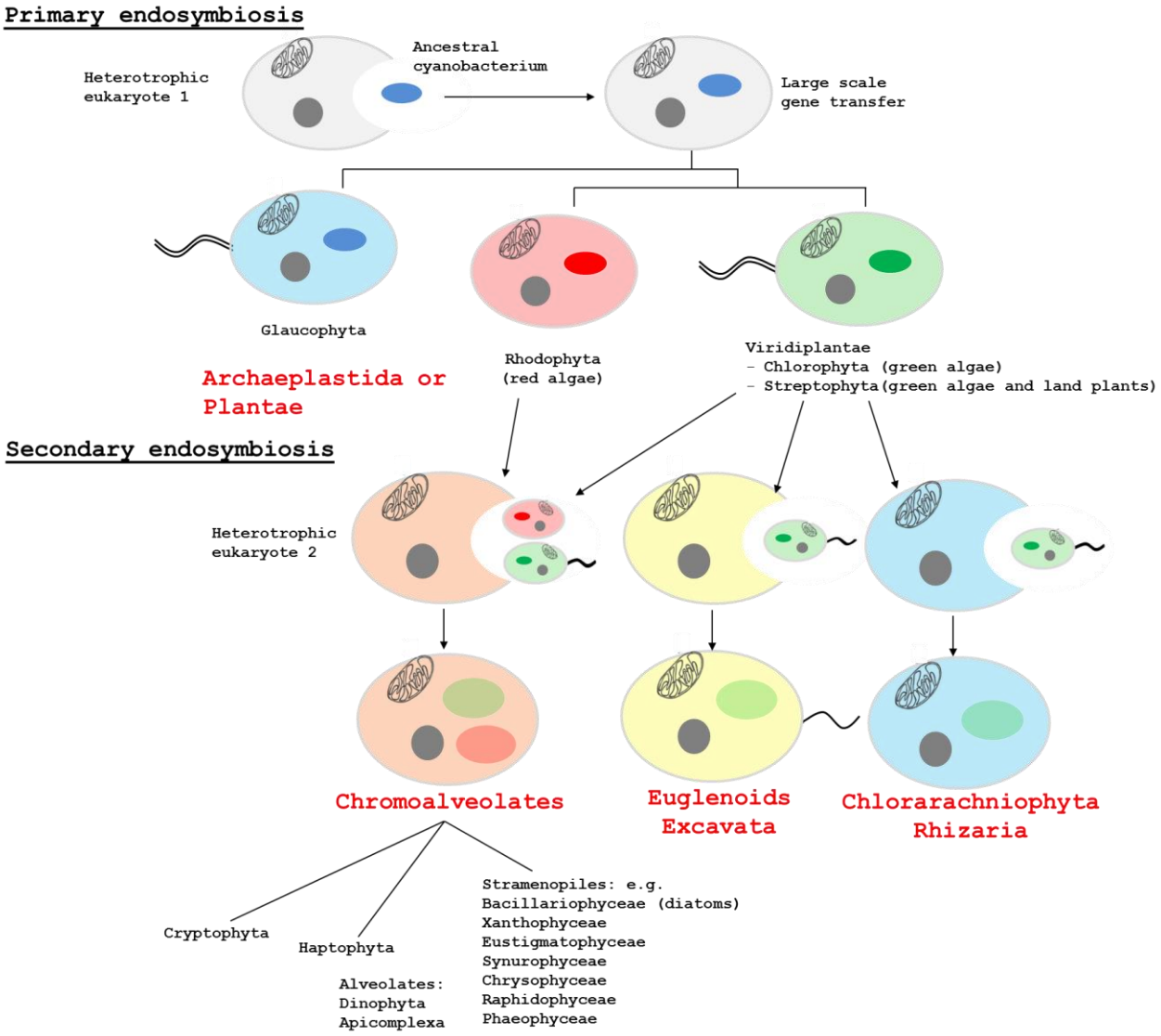

Figure 1.3: Endosymbiotic events and evolution of eukaryotic algal groups (modified from Clemens & Christian, 2013).

1.1.2.2 Ecological success of diatoms

The modern oceans, which cover more than the 70% of the Earth surface, are dominated by the eukaryotic red-plastid derived secondary endosymbionts (diatoms), while in the terrestrial environment prevails the green-plastid lineage (Falkowski *et al.*, 2004).

The extraordinary ecological success of this class of algae relies upon their biological peculiarities (Kooistra *et al.*, 2007) and refined mechanisms evolved in order to cope with environmental changes (Vardi *et al.*, 2006, Bowler *et al.*, 2008, Brunet *et al.*, 2014).

Diatoms are more successful than other phytoplankton groups in turbulent and nutrient-rich waters thanks to the high plasticity of their photosynthetic apparatus (Falkowski *et al.*, 2004).

They have an efficient nutrient uptake that depends on their size. The small ones tend to bloom after a nutrient pulse due to the high surface to volume ratio that facilitates the acquisition of limiting nutrients. The larger species instead are able to store nutrients in their vacuole, an organelle present only in diatoms and not in the other planktonic heterokontophycean, haptophycean and dinoflagellates (Kooistra *et al.*, 2007, Litchman *et al.*, 2009). The nutrient storage capability is very useful in the aquatic ecosystems, where the nutrient availability is circumscribed to short temporal pulses. The vacuole also confers other advantages such as the regulation of the buoyancy: diatoms can sink along the water column to stock nutrients and move up to the nutrient-deficient surface layer to photosynthesize (Kooistra *et al.*, 2007). The daily migratory behavior represents an adaptation against the grazers, which show an opposite movement towards the surface in the evening and down in the morning (Kooistra *et al.*, 2007). Diatom's combination of animal- and plant-like features allows them to survive in the harshest conditions, such as under prolonged period of darkness, and resume growth when they return to light (e.g., in the poles) (Armbrust, 2009). They can form resting stages, a characteristic that probably come from the heterotrophic host (Kooistra *et al.*, 2007); they are able to generate chemical energy from the breakdown of fat, like animals, and to generate metabolic intermediates from the breakdown, like plants (Armbrust, 2009).

Their high efficiency in CO_2 fixation, despite its low concentration in marine environment with a pH of ca. 8.2-8.1, is probably due to their capability of a direct uptake of HCO_3^-, the

mainly available form of inorganic carbon at sea, coupled with biophysical carbon concentrating mechanisms (CCMs), such as bicarbonate transporters and carbonic anhydrases, saturating the carboxylase reaction of Rubisco (Bowler *et al.*, 2010b, Raven *et al.*, 2012, Raven *et al.*, 2014, Young *et al.*, 2016). It has also been hypothesized, that diatoms have a C4 concentrating mechanism (Johnston *et al.*, 2001). Another hypothesis explaining their efficient photosynthesis come from the fact that diatoms could recover inorganic carbon and nitrogen losses from photorespiration in the mitochondria through the urea cycle, a metabolic pathway that would come from their animal origin (Allen *et al.*, 2006).

Last, but not least, their ability to photoprotect in order to cope with large fluctuations in light intensity and periodic exposures to high light (see section 1.3.3 Photoprotection)(Lavaud *et al.*, 2004, Brunet *et al.*, 2014) might be another key aspect that contributes to the large ecological success.

1.1.2.3 Morphology, chloroplast structure and pigment content of diatoms

The word "diatom" comes from the ancient Greek, being formed by the two words διά (diá, "through") and τέμνειν (témnein, "to cut"), meaning "to cut through" or more clearly, "cut in two". The etymology perfectly describes the distinguishing character of this class of microalgae: they are surrounded by a silicic theca, the frustule, which consists of two slightly unequal parts, the epi-theca and the hypo-theca, that fit together like a lid on a box.
Their size span from few micrometres (e.g. *Cyclotella* spp. has a minimum diameter of ca. 3 µm) to few millimetres (e.g., *Ethimodiscus* has a maximum diameter of ca. 2 mm) (Snoeijs *et al.*, 2002). Cell size differs between the marine and freshwater diatoms: the first ones are bigger, some species can reach a cell volume higher than 10^9 μm^3, while the freshwater ones are almost 3 times smaller, reaching a maximum cell size equal to 10^6 μm^3 (Litchman *et al.*, 2009).
There are two major types of diatoms: the centric and the pennate ones (Fig. 1.4).

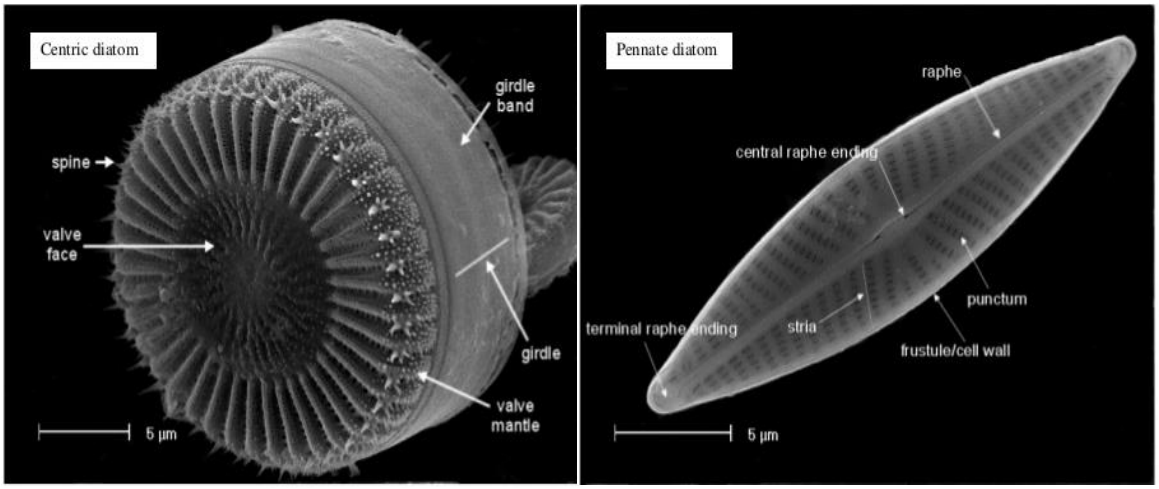

Figure 1.4: Centric and pennate diatoms, from https://westerndiatoms.colorado.edu. In the centric diatoms is visible the theca (valve face) which is linked to the other one by a series of linking, siliceous bands. Each band is called girdle band, or copula. Plural form is cingula, or girdle. The mantel is the downturned side of the valve surrounding the valve face. The spines are silica extension of the valve, and can show different morphologies. In the pennate diatom are visible the raphe, one or two slits through the valve face of monoraphid and biraphid diatoms. The punctum is a round or oval perforation in the silica cell wall; usually many of them are grouped to forma a stria.

Centric diatoms have a radial symmetry in valve view that can be unipolar or multipolar. They contain several small plastids and are oogamous, meaning that their gametes are an egg and motile spermatozoids with one flagellum. Pennate diatoms, instead, are elongated cells with bilateral symmetry. Along their long axis they may show a slit called raphe, through which they secrete mucilage used to stick to a substrate or glide over it. They contain one or few large plastids and are isogamous, meaning that their gametes are of equal shape and without flagella.

Diatoms can grow as single cells, but the planktonic ones are able to form chains. The reason why they acquired this ability remains unclear. Hypothetically, it confers major resistance to grazers, allows the adjustment of buoyancy, facilitates sexual reproduction and helps in optimizing the nutrient uptake (Kooistra *et al.*, 2007).

The organization and protein/pigment composition of diatom chloroplast differ from those of other photosynthetic organisms. It is included in four membranes and characterized by the presence of three thylakoids, the so-called girdle lamella, surrounding groups of parallel

bands of three loosely appressed thylakoids (Pyszniak & Gibbs, 1992, Lavaud, 2007), unlike green algal thylakoids which are composed by stacked (grana) and unstacked membrane regions (lamellae) (Ruban & Johnson, 2015) (Fig. 1.5).

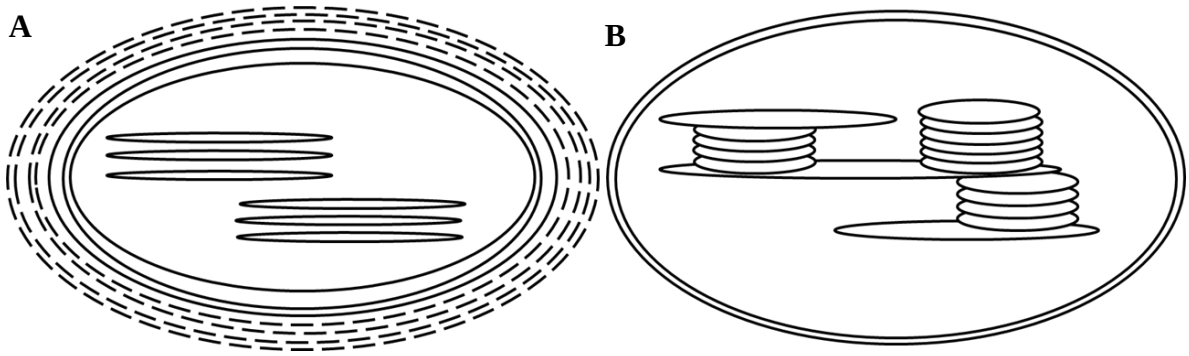

Figure 1.5: Schematic drawing of chloroplasts (A) diatom chloroplast: the groups of three loosely appressed thylakoids are included in the girdle lamellae (full ellipses) and the four membranes (dashed ellipses); (B) green alga chloroplast: two membranes include the thylakoids, which are composed by stacked (grana) and unstacked (lamellae) regions.

The diatom's thylakoids don't show the same separation between PSII (photosystem II) and PSI (photosystem I) as in higher plants, although a certain degree of PSI segregation has been observed (Pyszniak & Gibbs, 1992, Lepetit *et al.*, 2012, Bína *et al.*, 2016).

Both PSII and PSI are surrounded by the major peripheral FCP antenna, but in addition to that, diatoms seem to have a specific FPC antenna connected to PSI (Veith *et al.*, 2009, Lepetit *et al.*, 2010).

Peripheral light harvesting antenna of diatoms consists of fucoxanthin chlorophyll *a*/*c* binding protein (FCP) complexes. It is constituted by three different protein families: the Lhcf that are the main ones, the Lhcr that comprise the specific antenna of the PSI, related to the red algal LHCI proteins, and the Lhcx involved in the photoprotective mechanisms (Lepetit *et al.*, 2010, Büchel, 2015).

In diatoms, the oligomeric state of these complexes seems to be species-specific: in *Phaeodactylum tricornutum* the basic unit is a trimer, but probably in the native thylakoid membrane the main oligomeric state is a hexamer; in *Cyclotella meneghiniana* instead, were found both trimeric and hexameric oligomers, named FCPa and FCPb, respectively (Wilhelm *et al.*, 2014).

The antennae pigment composition, as well as a higher chlorophyll/carotenoid ratio with respect to higher plants, increase diatoms' ability to absorb the blue wavelengths mostly found in the aquatic environment (Beer *et al.*, 2006, Bertrand, 2010).

The Chl *a* plays a central role in light energy conversion, and absorbs in the red and blue regions of the light spectrum. The accessory pigment Chl *c* shows a lower absorbance in the red, but a stronger absorption in the blue region (Kuczynska *et al.*, 2015)(Fig. 1.6).

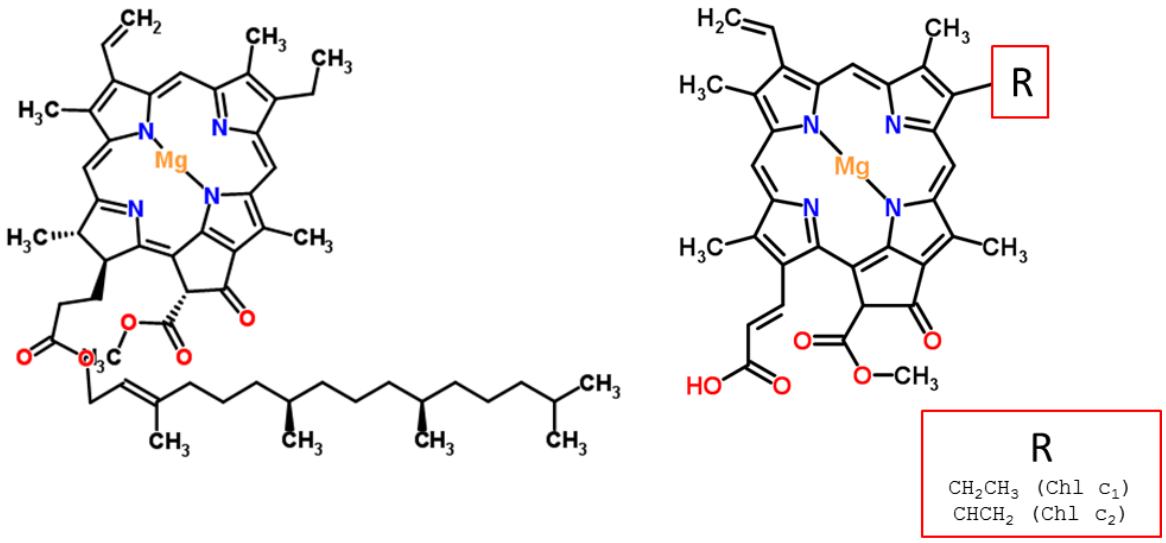

Figure 1.6: Chlorophyll *a* and chlorophyll *c* pigment structure.

The carotenoid content in diatom is limited to eight inter-related species. The four main ones are β-carotene (β-car) precursor of the xanthophylls fucoxanthin (Fuco), diadinoxanthin (Dd), diatoxanthin (Dt). Other xanthophylls such as neoxanthin (Nx), zeaxanthin (Zeax), violaxanthin (Vx) and antheraxanthin (Ax) can also be present.

Apart from Fuco that also participates in the light harvesting, the other carotenoids are mainly involved in photoprotective mechanism.

In diatoms, the xanthophyll with a photoprotective role is Dt, being synthesized from its precursor Dd. The other xanthophylls Zeax, Ax, Vx and Nx are involved as precursors of Fuco and Dd. The biosynthetic pathway through which diatoms pigments are formed is still not clear (Kuczynska *et al.*, 2015).

Depending on the growth rate and the taxon, the early carotenoid biosynthesis follows two different pathways, the mevalonate (MEV) and the methylerythritol phosphate (MEP), both

producing dimethylallyl diphosphate (DMAPP) and its isomer, isopentenyl pyrophosphate (IPP). DMAPP is converted to geranylgeranyl pyrophosphate (GGPP) by the GGPP synthase (GGPS) and then to phytoene by the phytoene synthase (PSY). Phytoene desaturase (PDS) converts phytoene into ζ-carotene, which in turns is converted into lycopene by ζ-carotene desaturase (ZDS). Lycopene is cyclized by lycopene β-cyclase (LCBY) to β-car. Then the hydroxylation reaction which converts β-car into the xanthophyll Zeax is ascribed to the enzyme LUT1, a monoxygenase. Then the conversion of Zeax into Ax and then Vx is catalyzed by Zeax epoxidase (ZEP); the reverse reaction instead is catalyzed by Vx de-epoxidase (VDE). Currently there are two models which explain the formation of the other xanthophylls. Surely the conversion from Dd into Dt and *vice-versa* is catalyzed by VDE and ZEP respectively, but the previous steps and the Fuco biosynthesis are still under debate. Lohr and Wilhelm (2001) proposed that Vx is the precursor of Dd, from which Dt and Fuco are formed. Dambek *et al*. (2012) instead proposed that Nx is the precursor of both Fuco and Dd, but the enzyme responsible for the conversion of Vx into Nx was still not found and sometimes neither Nx has been detected (Kuczynska *et al.*, 2015)(Fig. 1.7)

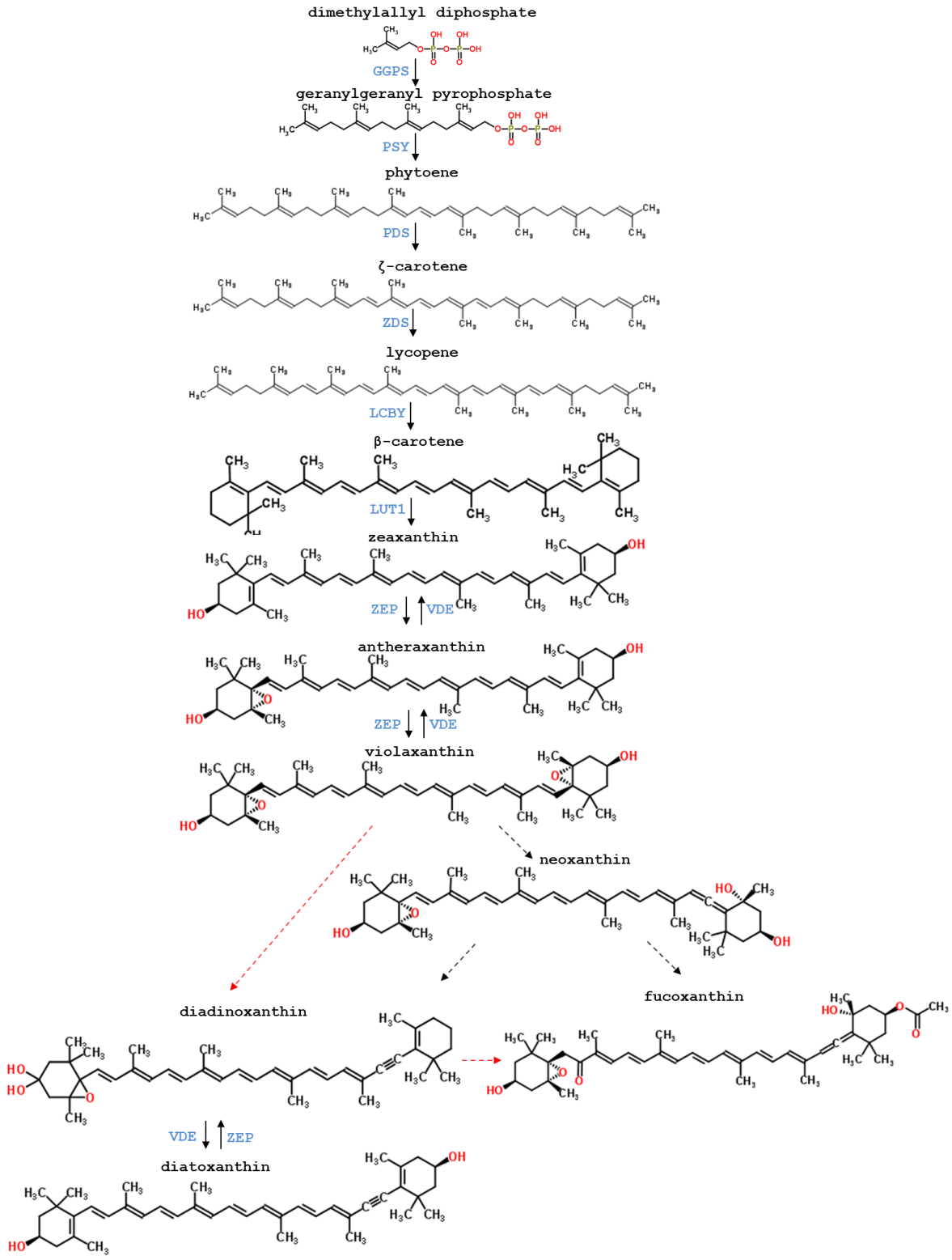

Figure 1.7: Biosynthetic pathway of carotenoids in diatoms following Lohr & Wilhelm (2001), red dashed arrows, and Dambek *et al.*, (2012), black dashed arrows.

1.2. Microalgae in biotechnology

1.2.1 The state of art and potential of using microalgae in biotechnology

The exploitation of microalgae by humans begun in ancient times: 2000 years ago Chinese populations started to eat the cyanobacterium *Nostoc* during famine; also the cyanobacteria *Spirulina* and *Aphanizomenon* have been used as food for thousands of years (Jensen *et al.*, 2001, Spolaore *et al.*, 2006).
The large-scale cultivation of microalgae started just few decades ago in the 60's with a Japanese plant producing *Chlorella*, a green alga; later on in the 70's another plant was built in Mexico for the production of *Spirulina* (Spolaore *et al.*, 2006). The research at that time had the purpose to finding an alternative protein supply with respect to the traditional agricultural crops in order to feed the increasing world population.

The use of microalgae as microorganisms able to convert efficiently light energy and carbon dioxide into energy-rich and valuable products in a sustainable way became in recent years a research area of renewed and growing interest.
Compared to the other agricultural crop, they have a high growth rate and need just water, light and some space - smaller than for higher plants - to grow. These are great advantages in an economical perspective (Olaizola, 2003, Barra *et al.*, 2014).

There are two main categories of market products derived from microalgae: the dried algae directly sold as a dietary supplement (mostly *Spirulina* and *Chlorella*) and products extracted and isolated from them (Enzing *et al.*, 2014).
Microalgae indeed may be considered as a powerful mean for the production of biofuels and bioactive molecules such as pigments, carotenoids, vitamins, proteins, phenolic compounds that could be widely used for the production of nutraceuticals, pharmaceuticals, animal feed additives, and cosmetics (Borowitzka, 1995, Pulz & Gross, 2004, Spolaore *et al.*, 2006, Mata *et al.*, 2010, Borowitzka, 2013, Barra *et al.*, 2014, Enzing *et al.*, 2014, Pérez-López *et al.*, 2014, Vigani *et al.*, 2015).
These microalgal high value products have a larger market value than dried algae, although their smaller production volumes (Vigani *et al.*, 2015).

Among the most important compounds produced by microalgae, carotenoids occupy the place of honour. β-carotene was the first commercialized pigment from the microalga *Dunaliella salina*; lately, *Haematococcus pluvialis* was used to commercialize astaxanthin. Surely, microalgae are a potential source of other carotenoids of interest, such as zeaxanthin, fucoxanthin, lutein, phytoene, but for now the poor yield compared to the former two discourage their industrial-scale production (Borowitzka, 2013). The commercial importance of carotenoids is ascribed, besides as colour agents, for their provitamin A activity, as well as for their intrinsic antioxidant activity, and so they can be employed in the cosmetic, nutraceutic and pharmaceutic industry (Begum *et al.*, 2016).

Aside from carotenoids, microalgae are able to produce other molecules with proven antioxidant activity. They are a source of ascorbic acid, tocopherol, phenolic compounds, glutathione, phycobiliproteins, not counting the antioxidant enzymes (Snoeijs *et al.*, 2012, Goiris *et al.*, 2012, Barra *et al.*, 2014). They can be applied in the formulation of cosmetics, such as the sun-protective ones, or in the food and nutraceutic industry, or even in pharmaceutic for the treatment of diseases that imply oxidation processes, such as inflammation (Pulz & Gross, 2004).

Another important class of compounds produced by these organisms is represented by the fatty acids. Thanks to their high content of lipids, microalgae can be employed for the formulation of biofuels (Mata *et al.*, 2010). But also, like higher plants, they are able to produce the long-chain polyunsaturated fatty acids (PUFAs), largely employable in food, feed and cosmetic industry, substituting those extracted from fishes (Pulz & Gross, 2004, Li *et al.*, 2014). These compounds are also important from a medical point of view. Eicosapentaenoic acid (EPA) and docosahexaenoic acid (DHA), two ω-3fatty acids, showed positive effects on human metabolism, reducing for example the levels of cholesterol and triglycerides, preventing stroke, Alzheimer's disease, rheumatoid arthritis and even certain types of cancer (Gouveia *et al.*, 2010).

The dietary bioactive compounds promote human health also *via* the activation of transcription factors which activate the transcription of genes encoding for metabolic and defence enzymes (Foyer & Noctor, 2009).

Yet, microalgal polysaccharides have different applications, both for their rheological properties as gelling and thickening agents and for their potential in the pharmacologic

industry, thanks to their antiviral, antibacterial, anti-inflammatory, cytotoxic activities (Kraan, 2012, de Jesus Raposo *et al.*, 2015).

The employability of microalgae in the food industry is also supported by their vitamin and mineral content. They produce almost all the essential vitamins (i.e., A, B_1, B_2, B_6, B_{12}, C, E, nicotinate, biotin, folic acid and pantothenic acid) and have a balanced mineral content (i.e., Na, K, Ca, Mg, Fe, Zn and trace minerals) (Gouveia *et al.*, 2010).

Apart from the known compounds that microalgae produce in medium-large amount, secondary metabolites, produced in low quantity, have important pharmaceutical applications (Borowitzka, 1995, Barra *et al.*, 2014). Indeed, microalgae evolved the ability to produce potent bioactive molecules in order to survive in the harshest aquatic environment, populated by planktivorous grazers or environmental rivals (Berry *et al.*, 2008). Some species of dinoflagellates are famous for their toxicity. For example, *Alexandrium* and *Pyrodinium* produce the saxitoxins that affect nerve and muscle cells through the inhibition of the voltage-gated sodium channels. This feature makes this toxin a possible drug candidate for anesthesia, although it has not been used yet in the clinic (Llewellyn, 2006). *Dinophysis* and *Prorocentrum* produce okadaic acid, a protein phosphatase inhibitor (Cohen, 2010). *Gambierdiscus toxicus* has the prize to produce the most potent non-peptidic natural toxin known today, the maitotoxin, which induces cell death damaging calcium channels, thus altering cell homeostasis. These few examples of toxins illustrate the potential potent biochemical tools available for pharmacological study.

1.2.2 Microalgal resources and challenges

The advantage offered by the exploitation of microalgal ability to produce high-added value products directly from CO_2, water and light is double. It allows the use of renewable source of energy while reducing the on-going climate change *via* the consumption of the main heat-trapping gas (CO_2), thus representing an environmental and economic priority.

However, the biotechnological research related to the utilization of microalgae is still at the beginning. The main issue to be solved to fully exploit the huge microalgal potential is the reduction of the effective costs of production (Vigani *et al.*, 2015), lowering them to entice the market interest. Under this objective, it has to be enhanced the biomass productivity, acting on the way of production as well as in selecting organisms containing high

concentration of the desired product, otherwise the downstream processes of separation and purification would have high costs.

Currently, most microalgal production occurs in outdoor open ponds, but the relatively low costs and easy construction and operation are counterbalanced by the non-optimal conditions for the manufacture of most high value products. These systems do not allow the control of essential parameters such as light, temperature and CO_2, and they are prone to contamination. These problems led to the development of closed photobioreactors – for indoor or outdoor production. However, most of them are still too inefficient, requiring further development and optimization. The design of next-generation of photobioreactors, addressed towards the manufacture of high added value products, should optimize the product yield through to the manipulation of the culture conditions, chosen specifically for each microalgal species according to its unique physiological and growth characteristics. To reach this goal and enhance microalgal production, a better understanding of the (photo)physiology, the metabolic pathways and the environmental cues they respond to is needed. In this way it will be possible to improve the culturing condition with a productivity-driven purpose.

In fact, algal growth, physiology and molecular composition are strongly controlled by environmental parameters, light as first one, being the latter the most relevant ecological axis driving photosynthetic and division rate, and success of microalgae in the water column (Lemoine & Schoefs, 2010, Brunet *et al.*, 2013, Chandrasekaran *et al.*, 2014, Fields *et al.*, 2014).

The new lighting technology constituted by the light-emitting diodes (LEDs) allows the modulation of the light environment, not only in terms of photoperiod or intensity, but also in terms of light spectrum, being able to produce a wide colour gamut by the independent adjustment of the single diodes. Therefore, it might represent an ideal means of controlling microalgal growth and productivity (Brunet *et al.*, 2014). In addition to the possible modification of the light environment, this technology shows high energy efficiency with respect to the older ones constituted by incandescent bulbs or fluorescent lamps, so this artificial system might meet with the market need of decrease the industrial scale production costs.

Another approach for improving microalgal production could be the use of genetically modified organisms (GMOs), optimized by genetic engineering for the production of

secondary metabolites. The genetic manipulation of microalgae, apart from few successful transformations, is still in its infancy (León-Bañares *et al.*, 2004), and is associated with many uncertainties, e.g., on the productive *vs*. growth performance. Also, the acceptability of products from GMOs by the market is perceived as problematic (Amin *et al.*, 2013).

Despite their huge biodiversity, only few thousands of microalgal strains are kept in collection, only few hundreds have been studied for their chemical content and, up to now, only around 20 microalgal species have a biotechnological use (Olaizola, 2003, Barra *et al.*, 2014). In order to boost this field, new target species have to be investigated, with a focus on their production efficiency, as well as their ecological and physiological traits. In this way, it will be possible to discover new photosynthetic microorganisms for the production of specific compounds and/or discover new bioactive molecules.

To pursue this goal, diatoms, the most dominant group of photosynthetic microorganisms in aquatic environment, have a great potential which is almost completely unused (Lebeau & Robert, 2003, Bozarth *et al.*, 2009, Dubinsky & Stambler, 2009, Barra *et al.*, 2014). This class of microalgae show a high diversity and physiological plasticity that can feed the different biotechnological interests.

Currently, some of them like *Chaetoceros*, *Phaeodactylum*, *Skeletonema*, and *Thalassosira* are used in molluscs and shrimp aquaculture, thanks to their high degree of digestibility (Barra *et al.*, 2014).

Diatoms are a wide source of PUFAs such as EPA and DHA, both ω-3fatty acids, and arachidonic acid (ARA) an ω-6 fatty acid (Lebeau & Robert, 2003).

Thanks to their capacity to biomineralize silica, they could be also employed in the nanotechnology field for the construction of nanostructures with myriads of applications, from the chemical and biological sensing and diagnosis, to drug delivery, or in microelectronic devices, or for the nanofiltration (Bozarth *et al.*, 2009).

They produce peculiar pigments such as fucoxanthin, a pigment with proven antioxidant, anti-inflammatory, anticancer, anti-obese, and antidiabetic activities (Peng *et al.*, 2011), the xanthophylls diadinoxanthin and diatoxanthin with a putative antioxidant activity (Goss & Lepetit, 2015), in addition to the common β-carotene, a pigment with provitamine-A,

antioxidant, hepatoprotective activities (Stahl & Sies, 2003, Sangeetha *et al.*, 2009, Martin & Sabina, 2017).

Apart from the known molecules, their extracts possess antioxidant, antibacterial, antifungicidal, antitumoral, anti-inflammatory activities, although the active molecules are not yet identified (Lebeau & Robert, 2003, Ingebrigtsen *et al.*, 2016, Lauritano *et al.*, 2016, Sansone *et al.*, 2017).

They can be also a putative future replacement of fossil fuel, behind the discovering by the scientific community of the molecular and physiological factors controlling the lipid production and accumulation (Levitan *et al.*, 2014). In fact, the lipid extraction for biofuel manufacturing is nowadays limited by the poor yield, determining higher costs with respect of fossil fuel. It is known that lipid content enhancement could be achieved under nutrient starvation (Guerra *et al.*, 2013, Bellou *et al.*, 2014), but such condition alters photosynthetic energy conversion efficiency and thus growth. Another way to improve oil production is the exploration of genetic transformations, even though, until now, this way still did not give the expected results (Dunahay *et al.*, 1995).

Another issue associated with diatoms massive cultivation is their need of silica addition in growth medium and its subsequent recovery from the biomass, determining higher cost of production, although no information on silica's projected costs is available (Hildebrand *et al.*, 2012). In order to reach economic competitiveness, microalgal lipid extraction should be coupled with high-value compounds production, such as pigments, phenolic compounds, or other secondary bioactive metabolites, increasing the financial viability of the process (Bellou *et al.*, 2014, Wang & Seibert, 2017).

1.3 Light-driven processes in the marine microalgae

1.3.1 Light in marine environment

Light is one of the most important parameters that modulates the growth and productivity of photosynthetic microorganisms (Kirk, 1983, Lavaud *et al.*, 2007, Perrine *et al.*, 2012, Brunet *et al.*, 2014, Chandrasekaran *et al.*, 2014, Giovagnetti *et al.*, 2014, Wilhelm *et al.*, 2014).

The spectral range between 400 and 700 nm is used by autotrophs in the process of photosynthesis and is known as photosynthetic active radiation (PAR). It corresponds to the visible part of the light, i.e. the portion of the light spectrum that a functional human eye can perceive. Photons with shorter wavelength, such as the ultraviolet (UV) radiation, between 200 and 400 nm, carry too much energy and could therefore damage cells and tissues through oxidative stress or even direct DNA damage. UV light is mostly absorbed by the stratospheric ozone layer, but part of it still penetrates in aquatic systems affecting planktonic organisms and fishes (Häder *et al.*, 2007). The photons at longer wavelengths (> 700 nm) are too weak to support oxygenic photosynthesis (Fig. 1.8).

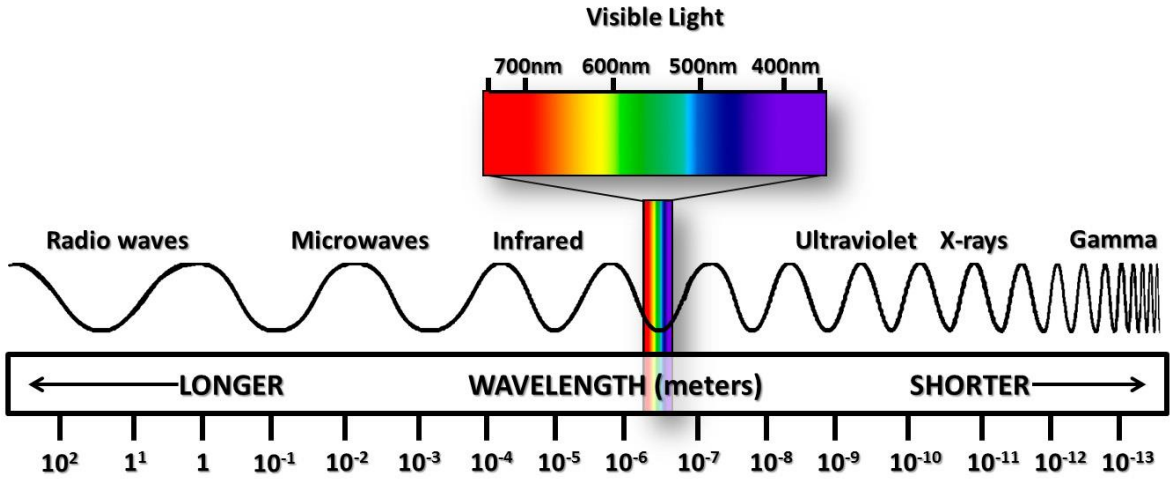

Figura 1.8: Electromagnetic spectrum (from http://www.ces.fau.edu/nasa/module-2/radiation-sun.php).

In aquatic ecosystems, light displays a huge variability in terms of photon flux density (PFD), spectral composition and photoperiod as a result of the vertical gradient, turbulent mixing, time of the day, seasonality, and the absorptive and scattering processes of the water itself due to the suspended particulate matter (Kirk, 1994, Depauw *et al.*, 2012, Brunet *et al.*, 2014), making the underwater light climate extremely distinct with respect of the terrestrial one (Depauw *et al.*, 2012). These features contribute differently in the various regions of the hydrosphere, for instance in the eutrophic *vs*. oligotrophic regions, or marine *vs*. freshwater. The light intensity exponentially decreases with depth, but each component of the spectrum from blue to red decreases with a characteristic slope (Brunet *et al.*, 2014).

The blue light decreases almost linearly and has the highest penetration capacity, reaching hundreds of meters depth. The green component instead has a lower penetration capacity and decreases exponentially along the water column. The red and infrared (IR) wavebands are strongly absorbed by water, disappearing after few meters in the water column, thus determining a dominance of blue and green light (400-500 nm) at deep (Fig. 1.9).

The blue:red ratio drastically varies in the water column, being the red wavelength present only in the surface layer together with high blue intensities. By consequence, this ratio could be used by microalgae as a signal to determine their position in the water column, and activate acclimative or protective processes (Brunet *et al*., 2014, see below).

The thermal stratification of the aquatic ecosystem is also a function of the light, since the heat energy provided by IR is absorbed in the first few meters; only 1% of it can penetrate beyond two meters depth (Gibson, 2000).

Due to the Earth's rotation, the solar insolation changes over a day scale following a sinusoidal light course: it increases gradually from dawn to midday, and then decreases progressively till the dusk. The cloud cover that modifies the resulting light availability at the surface of the water hinders this regular cycle, resulting in potential high and unpredictable frequency variation.

Water masses are naturally subject to currents, tides and vertical mixing, by consequence phytoplanktonic species experience a high temporal variability of the light climate at short time scales. Indeed, microalgae developed efficient mechanisms that allow them to rapidly adjust to the light environment in order to optimize the light harvesting to fuel the photosynthetic machinery minimizing the photodamage caused by excessive light. These processes are reviewed in the following sections.

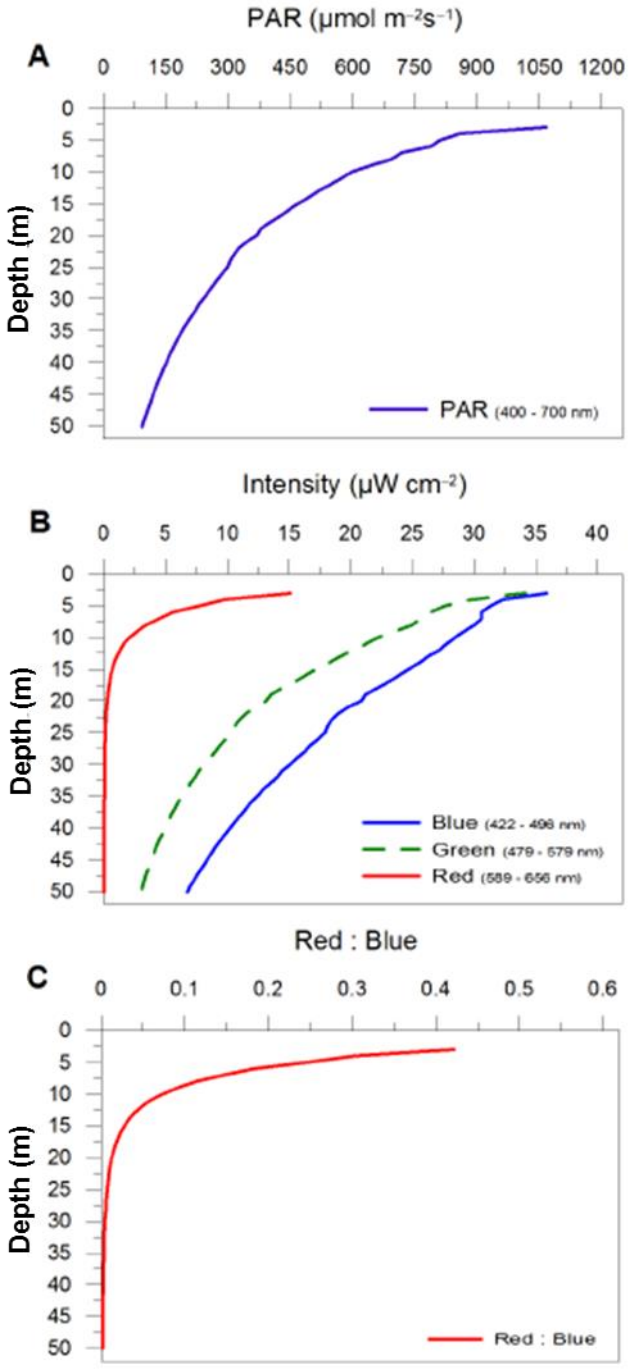

Figure 1.9: ***In situ*** **light profile** ***vs.*** **depth. (A) PAR (mol photons µm^{-2}s^{-1}) distribution along the water column, (B) blue, red and green radiation distribution along the water column (µW cm^{-2}; blue –422 to 496 nm, green –479 to 579 nm and red –589 to 656 nm), and (C) distribution of red : blue ratio along the water column. Data are mean of profiles done on 5 stations in the Mediterranean Sea in June–July 2008 (From Brunet** ***et al.*****, 2014).**

1.3.1.1 Light sensing in diatoms

Light is the essential energy which drives the photosynthetic process and carries crucial information for autotrophic organisms (Lepetit & Dietzel, 2015). Microalgae can cope with variable light conditions, they can perceive light, adjust their physiology accordingly and could even anticipate these variations following a putative internal circadian clock (Depauw *et al.*, 2012, Fortunato *et al.*, 2016).
The light sensing can be either direct so mediated by photoreceptors, or indirect, mediated by the sensing of the photosynthesis related parameters.

1.3.1.1.1 Photoreceptors

Although the information regarding photoreceptors in the red plastid lineage is scarce with respect on what we know in green lineage, it has been demonstrated that they can perceive most of the visible light spectrum through their known photoreceptors (Depauw *et al.*, 2012, Schellenberger Costa *et al.*, 2013b, Rockwell *et al.*, 2014, Lepetit & Dietzel, 2015, Fortunato *et al.*, 2016). As stated by Ashworth *et al.* (2013), more of these sensing proteins will be discovered in the next future.
The general mechanism through which the photoreceptors work is the light sensing mediated by a non-protein chromophore binding the photosensory proteic module, which undergoes structural reorganization and physicochemical changes propagating the signal (Depauw *et al.*, 2012).

Diatoms can directly perceive blue light through cryptochromes (CRYs) and aureochromes. The former are flavoproteins with a flavin adenine dinucleotide (FAD) and sometimes a methenyltetrahydrofolate (MTHF) not covalently bound at the N-terminus as chromophores (Lin & Todo, 2005). They are present in all the kingdoms and are considered as a superfamily of proteins containing four sub-families: animal CRYs, plant CRYs, DASH CRYs (*Drosophila*, *Arabidopsis*, *Synechococcus*, *Homo*) and cyclobutane pyrimidine dimer (CPD) photolyases (Lin & Todo, 2005). Diatoms possess the animal CRYs and DASH CRYs (Coesel *et al.*, 2009). Generally, animal CRYs do not possess photolyase activity although showing structural similarity to DNA photolyases. Diatom's animal CRY

CPF1 instead, localized in the nucleus, does possess DNA-repair activity (Coesel *et al.*, 2009). This protein is involved in the circadian regulation and in the expression of genes related to pigment biosynthesis, photosynthesis, photoprotection, cell cycle, nitrogen metabolism (Coesel *et al.*, 2009, Depauw *et al.*, 2012, Lepetit & Dietzel, 2015). Also the other CRYs analyzed in *Phaeodactylum tricornutum* show rhythmic expression profile, hinting a probable role in the regulation of the circadian clock (Oliveri *et al.*, 2014).

The others blue light photoreceptors are the aureochromes, which, in contrast to CRYs, are characteristic of photosynthetic *Stramenopiles*. The light sensor in this case is a LOV-domain (light, oxygen, voltage) at the C-terminus, which is constituted by a short polypeptide linked to the chromophore flavin mononucleotide (FMN). At the N-terminus a DNA binding basic region leucine zipper (bZIP) is present (Lepetit & Dietzel, 2015). The bZIP can bind DNA only when the aureochromes dimerize, but the signal which induces the dimerization is still unknown (Lepetit & Dietzel, 2015). Apart from their role in the regulation of diatom's cell cycle, studies on *Phaeodactylum tricornutum* demonstrated the role of these photoreceptors in photoacclimation processes (Schellenberger Costa *et al.*, 2013b). They seem to interact also with red light photoreceptors (Schellenberger Costa *et al.*, 2013b).

Recently, also another class of photoreceptor has been found in diatoms, the photorodopsins (Marchetti *et al.*, 2012), which absorbs in the green-blue region of the spectrum. Their chromophore is a retinal bound to a lysine residue inside seven transmembrane residues, whose protonation state determines the signal transduction. In the eukaryotic phytoplankton this light sensor is involved in phototaxis, but it can also act as light-driven proton pump for the ATP synthesis and import of small molecules. In diatoms, they seem to be involved in the ATP generation in low iron concentration (Marchetti *et al.*, 2012).

As regards the red light sensing, diatoms possess phytochromes, present also in plants, fungi and bacteria. The chromophore is a heme-derived tetrapyrrole covalently attached to the N-terminus of the apoprotein. At the C-terminus, a histidine kinase catalyzes the

phosphorylation of serine and threonine residues after the protein conformational change upon irradiation. In terrestrial plants these photoreceptors control developmental processes and shade avoidance response, and exist in two forms: an inactive one that is converted in its activated form when absorbing red light; while the latter is inactivated by the absorption of far red light. In phytoplankton, this photoreceptor is able to sense also other colors such as green, orange and blue light (Rockwell *et al.*, 2014). Recent findings showed that in diatoms these photoreceptors sense red/far red light, like higher plants (Fortunato *et al.*, 2016). They could act as a surface layer detector, or drive the photoperiodic responses, or even perceive the red autofluorescence of Chl *a*. This last feature would allow diatoms to perceive algal density in their surrounding or even function as retrograde signaling, activating nuclear gene expression (Fortunato *et al.*, 2016). The discovery of the genes controlled by these photoreceptors will unveil their function and so the prevailing mechanism of activation, if driven by external or internal signals (Fortunato *et al.*, 2016).

1.3.1.1.2 Indirect light signaling

Being the light environment extremely variable within short time scales, the photosynthetic apparatus generates, transmits, and responds to the signal generated during the light reactions. These signals are the redox state of the electron transport chain and the reactive oxygen species (ROS) and antioxidants concentration, which can induce short and long term photoprotective responses (Lepetit & Dietzel, 2015).

Change in irradiance determines the change in the redox state of the electron transport chain in chloroplast, thus, photosynthetic components such as plastoquinones and thiols induce a signal transduction leading to conformational changes of proteins, modification of gene expression, and enzyme regulation.

The redox poise in diatoms regulates the activity of some enzymes in a different way with respect to higher plants: those regulated by thioredoxins in higher plants are not redox regulated in diatoms, probably for the absence of key-cysteines or for a shift in the redox midpoint potential (Wilhelm *et al.*, 2014). In diatoms anyway, the regulated enzymes are mostly related to the Calvin cycle, so to the carbon metabolism (Wilhelm *et al.*, 2014).

The redox state of the plastoquinones also controls the photoacclimation process *via* the control of the photoprotective proteins Lhcx, the xanthophyll cycle pigments synthesis, and

the activation of alternative electron pathways (see below) (Lepetit *et al.*, 2013, Lepetit *et al.*, 2017).

Another mechanism through which photosynthetic cells perceive and respond to light is *via* the signaling dependent upon the byproducts of the photosynthetic process, the radical oxygen species (ROS), and low molecular weight antioxidants (Foyer & Noctor, 2009). These metabolites are a key component of the cellular system which controls the cell fate, addressing it towards a programmed cell death or towards the survival by the enhancement of the defense strategies (Foyer & Shigeoka, 2011). The different ROS induce retrograde signaling increasing the transcription of genes encoding for antioxidant enzymes in higher plants (Foyer & Noctor, 2009) as in diatoms (Waring *et al.*, 2010). The pattern of ROS-responsive genes in a transcriptomic study carried out on the terrestrial plant model *Arabidopsis* showed the specificity of response dependent upon the type of ROS produced, underlining the signal specificity of a given ROS and thus, its importance as signaling molecules, not only as a cause of cell disruption *via* oxidative stress (Gadjev *et al.*, 2006). Unfortunately, the knowledge on light dependent ROS signaling in diatoms, and in general in red-plastid derived organism, up to now is little. In *Phaeodactylum tricornutum* the treatment with 3-(3,4-dichlorophenyl)-1,1-dimethylurea (DCMU), which induces the production of $^1O_2$, in high light induces the transcription of genes controlled also by the redox state of the plastoquinones and by the blue light perception mediated by CRYs photoreceptors (Coesel *et al.*, 2009, Lepetit *et al.*, 2013). This feature underlines the complex and interactive regulation systems of these cells, able to face the environmental cue acclimating dynamically and adjusting their physiology.

1.3.2 Photosynthesis

Photosynthesis is the process through which the energy of light is converted into the chemical energy of the organic compounds. It's constituted by two major groups of reactions: the light dependent and the light independent ones (Fig. 1.10).

The first group of reactions is responsible for the light capture and its conversion into another form of energy, the nicotinamide adenine dinucleotide phosphate (NADPH) and adenosine triphosphate (ATP) that are sub-sequentially consumed by the second group of

reactions to fix and reduce inorganic carbon in triose phosphates. In other words, the light energy is converted into electrical energy and then into chemical energy.

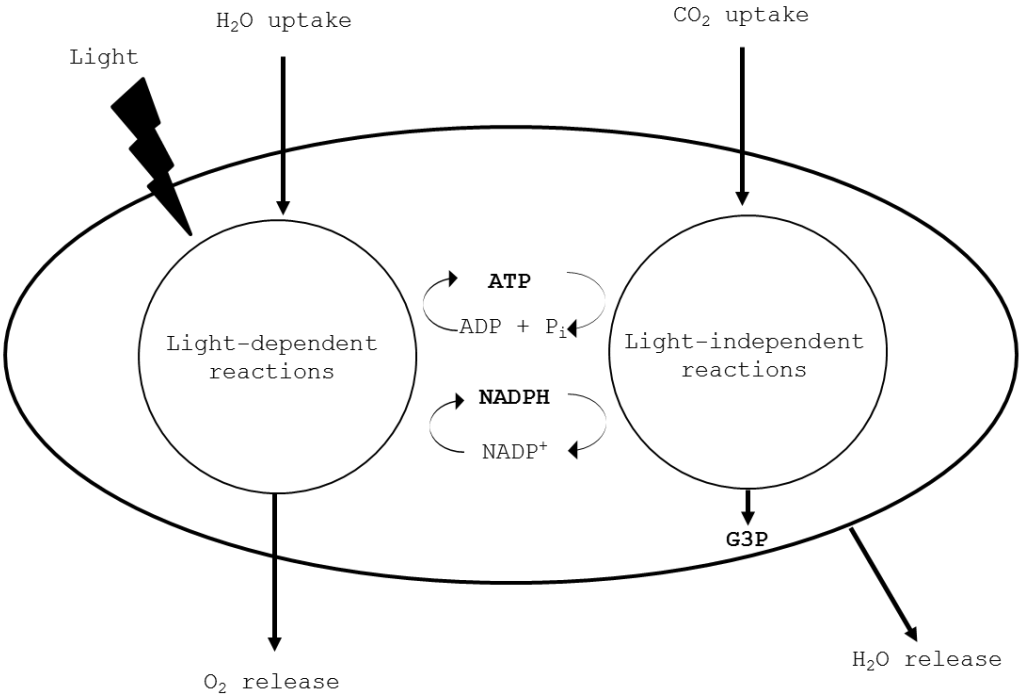

Figure 1.10: Schematic view of the photosynthetic machinery.

1.3.2.1 The light-dependent reactions

The light-dependent reactions occur in thylakoid membrane inside the chloroplast, a dynamic structure where the photosynthetic pigment-proteins complexes and the components of the photosynthetic electron transport chain are bounded.

The main components of the photosynthetic electron transport chain are the photosystem II (PSII), the cytochrome b_6/f (cyt b_6/f), the photosystem I (PSI) and the ATP-synthase. The mobile plastoquinone serves as electron carrier between PSII and cyt b_6/f (Fig. 1.11).

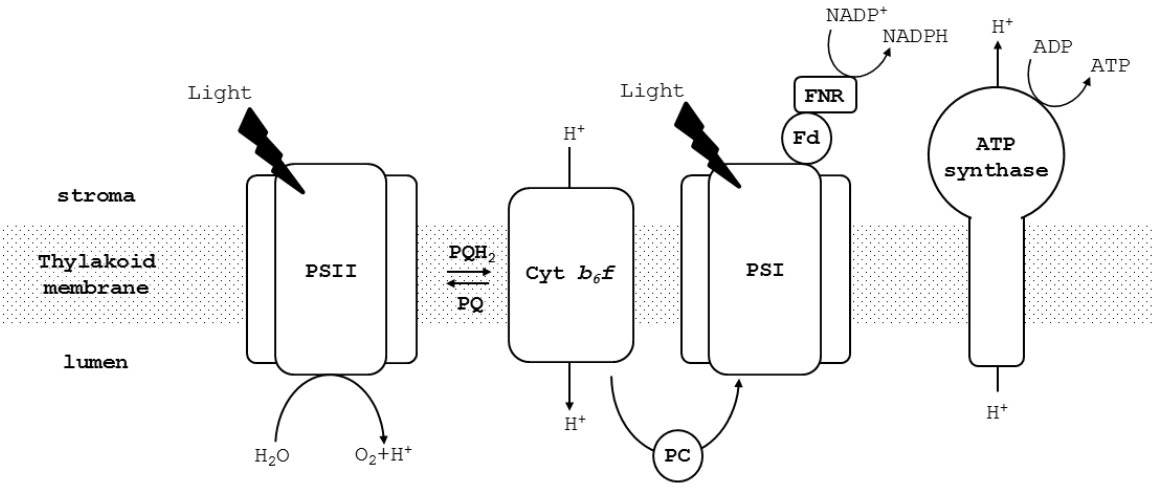

Figure 1.11: Schematic view of the photosynthetic electron transport chain.

Pigments and chlorophylls are essential for harvesting light and converting it into chemical energy. In diatoms chlorophyll a (Chl *a*), chlorophyll c (Chl *c*) and the carotenoid fucoxanthin (Fx) are components of the fucoxanthin-chlorophyll *a*/*c*-binding proteins (FCP) complex - an analogue of the light harvesting complexes (LHC) present in higher plants and performing the light harvesting function. The FCP serves the PSII and PSI, which are composed of an internal antenna proteins and a central core domain, named reaction center (RC), where the biochemical reactions occur. The RC of the PSII is composed of two similar polypeptides, the D1 and D2 proteins, associated with pigments and cofactors: 4 chlorophylls, 2 pheophytins, 2 plastoquinones and a non-heme iron (Xiong *et al.*, 1996). All these components are needed for the light-induced charge separation that initiates the transport of electrons across the thylakoid membrane (Diner & Babcock, 1996). To D1 and D2 is associated the internal or core antenna, composed by the Chl *a* binding proteins CP43 and CP47 (CP stands for chlorophyll-protein complex), which absorb energy from the FCP transferring it directly to the RC (Vermaas, 1993, Van Amerongen & Dekker, 2003).

During the photosynthetic process, photons are absorbed by the antenna pigments of the FCP associated with the PSII, which transfer the energy towards the core antenna CP43 and CP47 or directly to D1/D2. In the green lineage the photons reach the RC passing through the minor light-harvesting complexes CP24, CP26 and CP29 (Nelson & Ben-Shem, 2004), which serve as linkers and stabilizers of the LHCII trimers. These minor antenna complexes are absent in red algae and *Stramenopiles*. Therefore, the structure of PSII supercomplex is

different and seems to consist of only PSII dimeric cores and free antennas (Grouneva *et al.*, 2011, Litvín *et al.*, 2016). The first electron donor of the PSII is a dimer of Chl *a* absorbing at 680 nm linked to D1 and D2 proteins, the P680 (Telfer, 2002), facing the luminal surface of the thylakoid. The electron is then quickly transferred towards the stromal surface to the final electron acceptor, a plastoquinone, *via* a pheophytin. After accepting two electrons and undergoing protonation, plastoquinone is reduced to plastoquinol and released from the PSII into the membrane matrix. The cation $P680^+$ is re-reduced by a redox active tyrosine located in the D1 protein, which is reduced in turn by a Mn ion within a cluster of four. When the $(Mn)_4$ cluster accumulates four oxidizing equivalents (electrons), two water molecules are oxidized producing one molecule of O_2 and four protons.

The electron passes through the chain of electron carriers of the thylakoid membrane following their redox potential: from plastoquinone, to cyt b_6/f, to plastocyanin (PC) or a soluble cytochrome *c* (cyt *c*) depending on the diatom species (Marchetti *et al.*, 2012, Raven, 2013), reaching finally the PSI. The PSI is composed by PsaA and PsaB proteins, which show homologies with PSII: to D1 and D2 at the C-terminal part, and to CP43 and CP47 at the N-terminal part. These two proteins PsaA and PsaB are the reaction center of the PSI and are connected to most of the pigments, donor and acceptors of electrons (Nelson & Ben-Shem, 2004).

In PSI the first electron donor is a dimer of Chl *a* absorbing at 700 nm (P700). The electron passes along an electron transport chain consisting in another Chl *a*, a phylloquinone, and the Fe_4S_4 cluster. At the stromal side, the electron is donated by Fe_4S_4, the Rieske iron-sulfur protein, to ferredoxin and then transferred to $NADP^+$ by ferredoxin- $NADP^+$ oxidoreductase (FNR) reducing it to NADPH. The reaction cycle is closed by another re-reduction of $P700^+$ by PC or cyt *c*, at the luminal side of the membrane. The electron carried by PC or cyt *c* is provided by PSII by way of the pool of plastoquinone and cyt b_6/f complex.

A graphical representation of this process is the Z-scheme, an energy diagram of the electron transfer from water to $NADP^+$ in the light dependent reactions of photosynthesis (Fig. 1.12).

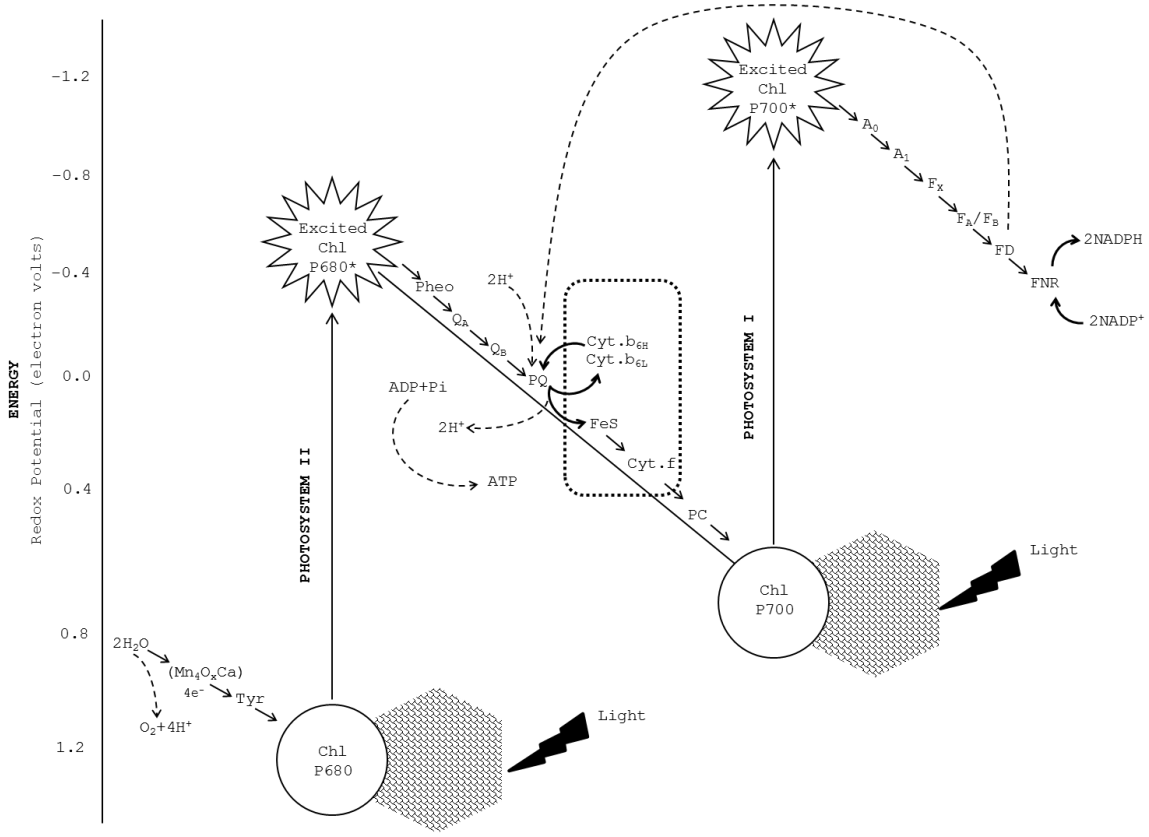

Figure 1.12: Z-Scheme of electron transport in photosynthesis, modified from Govindjee and Wilbert Veit, 2010 (gov@illinois.edu). The electron transport from H_2O to nicotinamide adenine dinucleotide ($NADP^+$) is traced from left to right on the diagram that uses two Photosystems (I and II). This process is initiated by the simultaneous absorption of light by two antenna complexes, represented by patterned hexagons. The absorbed energy is then transferred to the reaction center chlorophylls (Chl) P680 and P700 and this powers the entire process. (Mn_40_xCa) is the manganese center, a complex containing 4 manganese atoms, which participates in the splitting of two water molecules into 4 protons ($4H^+$), 4 electrons ($4e^-$) and one oxygen molecule (O_2). Tyr is a redox active tyrosine molecule which acts as an intermediate between the manganese center and reaction center of Photosystem II, PSII (P680), a chlorophyll (Chl) complex. Excited P680* has the energy of the photon, that was captured by and transferred to it from its light-gathering antenna complex (patterned hexagon). Pheo is pheophytin, a chlorophyll with its central magnesium ion (Mg^{2+}) replaced by two protons; it is the primary electron acceptor of PSII, whereas P680* is the primary electron donor. Q_A is a plastoquinone, which is tightly bound and immovable. It is also known as the primary stable electron acceptor of PSII, and it accepts and transfers one electron at a time. Q_B is a loosely bound plastoquinone molecule which accepts two electrons and two protons. Q_BH_2, reduced Q_B, then detaches, and becomes mobile, shuttling the 2 electrons and 2 protons within the hydrophobic core of the thylakoid membrane to the cytochrome b_6/f complex (rectangle). FeS is the Rieske iron-sulfur protein. Cyt *f* is cytochrome *f*. Cyt.b_6L and Cyt.b_6H are two cytochrome b_6 molecules (of lower and higher potentials) which participate in the Q cycle. PC is plastocyanin, a highly mobile copper protein. P700 and Excited P700* are Chls in the reaction center of Photosystem I in the ground and excited energy state, respectively. A_0 is a special chlorophyll a molecule that is the primary electron acceptor of PSI, whereas P700* is the primary electron donor of PSI. A_1 is a phylloquinone (vitamin K) molecule. F_X, F_A and F_B are three separate immobile iron sulfur protein centers. F_D is ferredoxin, a mobile iron sulfur protein, which can participate, along with other iron sulfur centers, in cyclic transport (dashed

line). FNR is the enzyme ferredoxin-NADP oxidoreductase, which enables $NADP^+$ to accept two electrons and a proton and become NADPH, the reduced form of $NADP^+$. The overall process concentrates protons into the thylakoid lumen, producing an energy gradient that is used in the production of ATP from ADP and inorganic phosphate (Pi) *via* ATP synthase.

The interplay of PSII and PSI leads to the transfer of electrons from water to NADPH, generating simultaneously a proton gradient across the thylakoid membrane, producing free energy for the ATP synthesis. The generation of these protons follows two routes: the photolysis of two water molecules that release four protons together with one oxygen molecule, and the transport of four electrons through the cyt b_6/f that leads to the translocation of eight protons from the stroma to the lumen. By consequence, the lumen becomes markedly acidic, and this proton gradient (ΔpH) is exploited for ATP synthesis.

1.3.2.2 The light-independent reactions

In all the oxygenic photoautotrophs, NADPH and ATP are used in the photosynthetic light independent reactions to fix CO_2 in organic compounds. This primary metabolic pathway responsible for carbon reduction occurs in the stroma of chloroplast and is called Calvin-Benson-Bassham cycle or Calvin cycle (Benson, 2002, Bassham, 2003). The first metabolite produced in this cycle is a 3-carbon organic acid, the 3-phosphoglycerate (G3P), from the fixation of a CO_2 molecule on a C5 compound, the ribulose 1,5-bisphosphate (RuBP), catalyzed by Ribulose-1,5-bisphosphate carboxylase oxygenase (Rubisco). For this reason the pathway of carbon fixation is called C3 photosynthesis. Briefly, the reactions of the Calvin cycle can be divided in three phases: the carboxylation through which CO_2 is fixed into a stable organic intermediate, the reduction of this intermediate to the level of carbohydrate and the regeneration of the CO_2 acceptor.

The fixed carbon serves for the biosynthesis of all the carbonic compounds of cells such as carbohydrates, lipids, proteins and nucleic acids. Anyway, the fate of the photosynthetically fixed carbon strongly depends on the environmental conditions. Under most of the growth conditions, intermediates metabolites for cell anabolic pathways such as amino acids are formed (Guerra *et al.*, 2013). However, under peculiar condition such as high nutrient concentration or high light, diatoms can redirect the fixed carbon towards the accumulation of large lipids and polysaccharides (Falkowski & Raven, 2013).

1.3.3 Photoprotection

1.3.3.1 Photocclimation

The light reactions of photosynthesis are driven by light availability and light capture. Since the light climate differs on a temporal and spatial scale, all algae are able to modulate photosynthesis and therefore their growth rate through the process of photoacclimation (Anning *et al.*, 2000). It relies on the light-dependent regulation of the gene expression and transcription downstream processes, from which depends the change in the macromolecular composition (MacIntyre *et al.*, 2002).

When the phytoplanktonic species move down in the photic zone, insufficient photon availability may impair the photosynthetic process, so in order to improve the photosynthetic yield algae may increase the size of the light harvesting complex, a strategy called σ-type photoacclimation, or changing the stoichiometry of the reaction centers, a strategy called *n*-type photoacclimation (Falkowski & Owens, 1980, Six *et al.*, 2008).

By contrast, in the marine upper layer, phytoplankton may be exposed to excessive light, which can cause the over-excitation of the photosynthetic apparatus, impairing the equilibrium between energy absorption and energy utilization, reducing the primary productivity (Lavaud & Goss, 2014). This impairing leads to the production of reactive oxygen species (ROS), eventually causing cell death if not appropriately scavenged (see section 1.4 Oxidative stress and antioxidants). In order to reduce the excess of income energy towards photosystems, photosynthetic organism evolved different mechanisms that operate at different time scales, from a few seconds to hours or days.

A long-term photoacclimation process is the change in the photosynthetic pigment content. At high irradiance diatoms lower their concentration of Chl *a*, Chl *c* and Fuco resulting in a reduction of the excitation energy hitting the reaction center (Anning *et al.*, 2000, Brunet *et al.*, 2014). It has been observed a down-regulation of genes involved in their biosynthesis, so the change is not ascribable to an active degradation of these pigments, but is due to a reduction of their synthesis, also controlled by cell division (Anning *et al.*, 2000, Nymark *et al.*, 2009), for this reason this change is the result of the light history experienced by cells.

While the photosynthetic pigments lower their content, in high light condition is observed an increase of the photoprotective pigments of the xanthophyll cycle (XC) diadinoxanthin (Dd) and diatoxanthin (Dt) (Lepetit *et al.*, 2010, Chandrasekaran *et al.*, 2014).
Other studies showed that also the antenna protein composition is altered in favor of a higher content of Lhcx proteins that possess a photoprotective function, and lower content of Lhcf and Lhcr, functional in the light harvesting (Nymark *et al.*, 2009, Bailleul *et al.*, 2010, Lepetit *et al.*, 2017).

1.3.3.2 Photoregulation

All the aforementioned mechanisms are efficient in the high light photoacclimation process, but are not fast enough to photoprotect cells suddenly exposed to higher irradiance. Planktonic species are passively transported within the water masses, therefore can pass in a few minutes from limiting light climate to high light environment (MacIntyre *et al.*, 2000).
For this reason, photosynthetic cells evolved mechanisms with a very fast activation timing, from seconds to minutes, which are crucial for surviving in a highly fluctuating light environment.

1.3.3.2.1 Non-photochemical quenching of chlorophyll *a* fluorescence (NPQ)

One of the most important regulation mechanisms is the dissipation of excessive excitation energy as heat, the so-called non-photochemical quenching of chlorophyll *a* fluorescence (NPQ)(Ruban, 2016).
In diatoms the extent of NPQ is way higher than most plants and other algae (Ruban *et al.*, 2004, Lavaud *et al.*, 2007).
Different components form the NPQ, each one with different relaxation kinetic: qE, the energy-dependent quenching, with a relaxation time of seconds/minutes; qT, the state transition quenching, in which the major light harvesting complex separates from PSII, with a relaxation time of tens of minutes; qI, the photoinhibitory quenching, caused by the photoinhibition, with the slowest relaxation kinetics (hours) (Müller *et al.*, 2001, Ruban & Murchie, 2012).

qT seems less important for photoprotection (Niyogi, 1999) and absent in diatoms (Goss & Lepetit, 2015). qI is poorly characterized and seems to be caused by a mix of photoprotection and photodamage. It is associated with the PSII core degradation in prolonged stressful conditions, and is mainly described in overwintering and evergreen plants (Demmig-Adams & Adams III, 2006). In a context of rapid response to sudden light increase, the qE is the most important actor. Therefore, from now on in this thesis the description of the NPQ process will refer only to the qE component.

The base of the photoprotective role of NPQ is the conformational change that causes the formation of energy traps at different quenching sites preventing the transfer of the excitation energy towards the reaction centers (Horton & Ruban, 1992).

This process is activated by three different components: the ΔpH across the thylakoid membrane, the xanthophyll cycle (XC) that involves the conversion of epoxy-xanthophyll into its de-epoxidated form (i.e. Dd into Dt), and the antenna proteins Lhcx (Goss & Lepetit, 2015).

1.3.3.2.1.1 The proton gradient

The ΔpH activates the de-epoxidation reaction that converts Dd into Dt and determines the protonation of the antenna proteins resulting in a conformational change into a quenching arrangement.

While in higher plants the ΔpH alone can induce significant NPQ through the conversion of violaxanthin (Vx) into zeaxanthin (Zeax), in diatoms without the presence of pre-existing Dt no NPQ is observed (Lavaud *et al.*, 2002a, Lavaud *et al.*, 2002b, Ruban & Murchie, 2012). Furthermore, in contrast with higher plants, the disappearance of the proton gradient is not sufficient for the relaxation of the NPQ, that needs the epoxidation of Dt back to its precursor Dd (Goss *et al.*, 2006). Anyway, the proton gradient is able to enhance the extent of the NPQ (Grouneva *et al.*, 2008).

1.3.3.2.1.2 The xanthophyll cycle (XC) enzymes and the lipid phase

The enzymes involved in the XC are violaxanthin de-epoxidase (VDE), which catalyzes the de-epoxidation of the epoxy-xanthophyll, from violaxanthin (Vx) into antheraxanthin (Ax)

and then into zeaxanthin (Zeax) in the green plastid lineage (Fig. 1.13a) and additionally from diadinoxanthin (Dd) into diatoxanthin (Dt) in diatoms (Fig. 1.13b), and zeaxanthin epoxidase (ZEP), which catalyzes the backward epoxidation reactions.

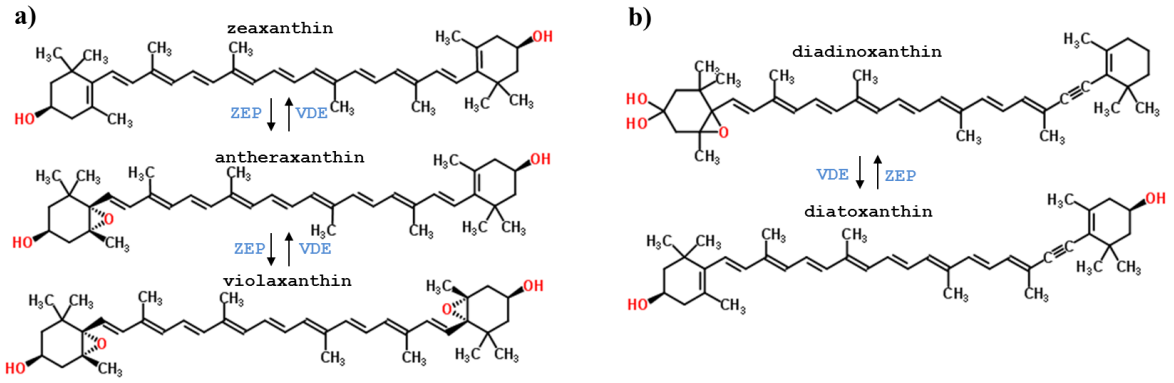

Figure 1.13: a) Xanthophyll cycle in green plastid lineage; b) Additional xanthophyll cycle in diatoms.

VDE is located in the thylakoid lumen and uses ascorbic acid (AsA) as electron donor for the reduction of the epoxy group. It's activated by high light (Goss & Jakob, 2010). ZEP instead is located in the stromal side of the thylakoid membrane and utilizes O_2, flavin adenine dinucleotide (FAD) and NADPH as co-substrates. It is activated in dark or low light conditions (Goss & Jakob, 2010).

Diatom's enzymes show differences with respect to those of the green algae and higher plants. First of all, in the genomes of the sequenced diatoms species (*Phaeodactylum tricornutum* and *Thalassiosira pseudonana*) more copies of the genes encoding for VDE and ZEP are present, each one more or less related to those of higher plants (Depauw *et al.*, 2012). The different derived protein structure may determine different localizations and dynamics of activation/deactivation (Coesel *et al.*, 2008, Depauw *et al.*, 2012).

Dt accumulation is also observed in dark/low light condition (Brunet *et al.*, 2006), driven probably by a different sensitivity to pH variations and so by the proton gradient created by the chlororespiration (Goss & Jakob, 2010, Goss & Lepetit, 2015). Green lineage VDE is active at acidic pH, showing an optimum at 5.2. Diatom's VDE instead, is active also at more neutral conditions, and possesses a higher pH optimum range. The maximal activity is recorded between pH 5 and 6, at pH 6.5 its activity is higher than 50% and it is still slightly active at pH 7 (Goss & Lepetit, 2015). The enzymatic activity span over a broader pH range

may depend on the higher affinity to the substrate AsA (Grouneva *et al.*, 2006), so that at high AsA concentration diatom's VDE optimum can shift towards more neutral pH.

Diatom's ZEP may be localized in the thylakoid lumen rather than at the stromal side, or may possess a pH sensitive residue in the lumen although facing the stromal side (Coesel *et al.*, 2008). It may explain its strong pH regulation, unlike higher plants, being inactive as soon as the proton gradient is established (Goss *et al.*, 2006).

Another important actor in the process of NPQ is the thylakoid membrane neutral lipid monogalactosyldiacylglycerol (MGDG). It solubilizes the lipophilic epoxy-xanthophylls released from their protein binding sites, and provides the three-dimensional structure necessary for the accessibility of the enzyme VDE to its substrate: the inverted hexagonal phase (H_{II} phase) (Schaller *et al.*, 2010). In diatoms, Dd has a higher solubilization rate than Vx in MGDG, and this feature explains why thylakoid membranes in diatoms may contain a larger amount of xanthophyll per Chl *a* than higher plants (Lepetit *et al.*, 2010). The MGDG and the Dd/Dt dissolved in it are tightly connected to the diatom antenna complex FPC in the inner membranes of the stacks of three membranes of the diatom's chloroplast (Lepetit *et al.*, 2012).

By contrast, the negatively charged lipid sulfoquinovosyldiacylglycerol (SQDG) inhibits the de-epoxidation reaction and forms domains separated from the antenna complexes. Probably, it interacts with ATP synthase participating in the ATP synthesis through the generation of the electrochemical gradient (Lepetit *et al.*, 2012).

1.3.3.2.1.3 The antenna proteins

Diatom's NPQ is modulated also by the light-harvesting complex stress related proteins Lhcx (Bailleul *et al.*, 2010, Taddei *et al.*, 2016). There are more isoforms of these proteins and most of them show a higher content and gene expression in high light condition (Bailleul *et al.*, 2010, Büchel, 2015, Lepetit *et al.*, 2017). Their involvement is probably due to the pigments binding, in particular the XC ones, that seems pH dependent (Büchel, 2015, Ballottari *et al.*, 2016). Following another model, the Lhcx may be analogs of PsbS in higher plants, being involved in NPQ through the induction of the conformational change of the FCPs and not through the binding of the XC pigments (Lepetit *et al.*, 2012), but there is no experimental evidence of this theory (Büchel, 2015). A better understanding

of the role of this protein family will be reached studying their associations with pigments and photosynthetic complexes (Taddei *et al.*, 2016).

1.3.3.2.1.4 The NPQ mechanism in diatoms

The mechanism through which the NPQ exerts its photoprotective role relies on conformational changes at the PSII antenna level, able to quench the excess of income energy. Following the most recent model of NPQ in diatoms, through this conformational rearrangements two quenching sites are formed, Q2 and Q1 (Goss & Lepetit, 2015).

Q2 is Dt dependent, specifically to the Dt pool bounded to the FCP antenna proteins, allegedly Lhcx. The other pools of Dt found in thylakoids i.e. those dissolved in the thylakoid lipid MDGD and those bounded to PSI antenna proteins, seem not to be involved in this Dt-dependent NPQ (Lepetit *et al.*, 2010, Grouneva *et al.*, 2011, Goss & Lepetit, 2015).

The prominent role of Dt is thought to depend on its direct quenching ability of the excess energy of the excited Chl *a*, *via* a direct transfer of the excitation energy from Chl *a* and a subsequent dissipation as heat, or *via* the excitation energy transfer, followed by the electron transfer from the Chl and a successive dissipation as heat.

Q1 instead is formed by the detachment of oligomeric antenna complex from the PSII. The quenching may be based on Chl *a* – Chl *a* interactions (Miloslavina *et al.*, 2009). The detachment may depend on the conformational changes induced by the conversion of Dd into Dt linked to Lhcx or on pH changes influencing the protonation of Lhc proteins (Goss & Lepetit, 2015, Ballottari *et al.*, 2016).

However, recently Giovagnetti and Ruban (2017) demonstrated that the detachment of the FCP antenna from the PSII only plays a minor role in photoprotection, showing that the increase of the NPQ was not paralleled by a diminished cross-section of the PSII.

Anyway, the pre-acclimation condition determines the extent of these phenomenon, since controls the amount of the XC pigments and Lhcx proteins, together with the structural organization of the thylakoid membranes (Goss & Lepetit, 2015, Giovagnetti & Ruban, 2017) (Fig. 1.14).

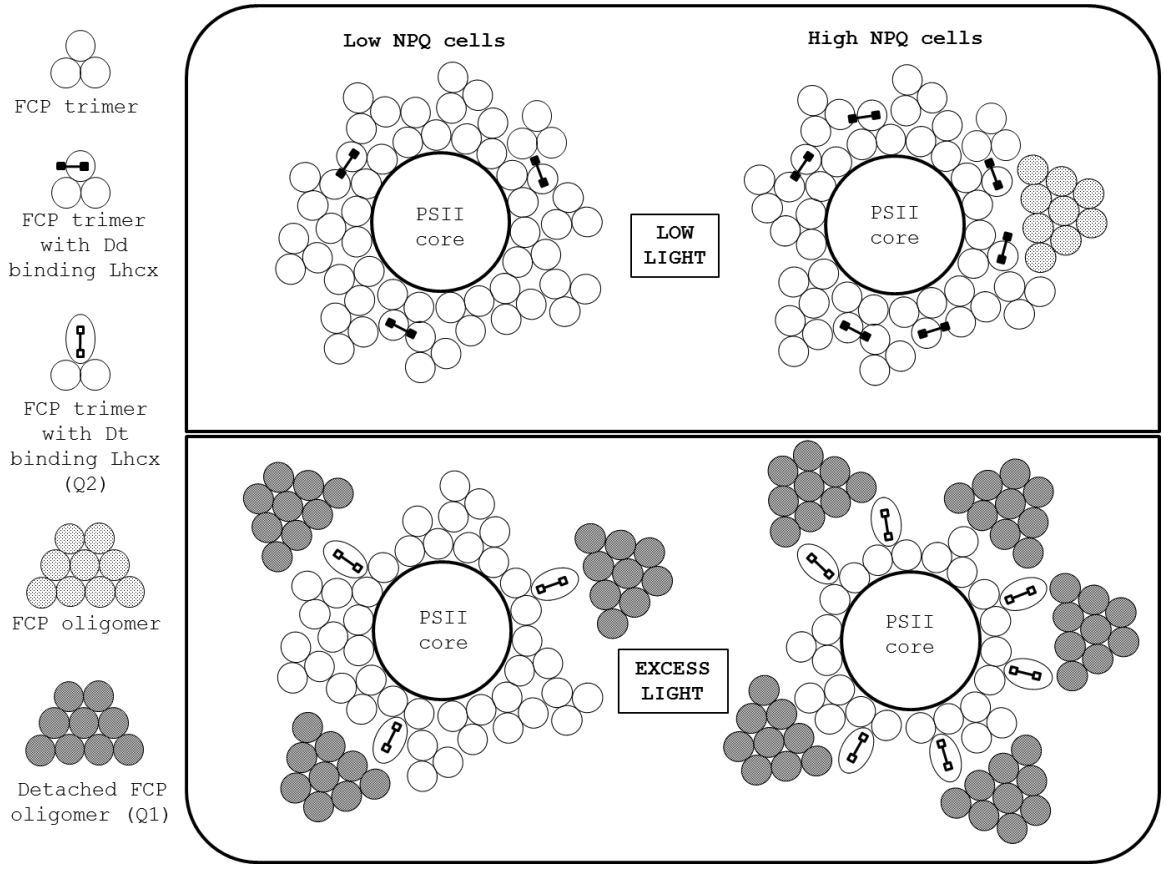

Figure 1.14: Model of the diatom NPQ conformational changes in low light and high light adapted cells (Modified from Goss & Lepetit 2015).

1.3.3.2.2 Other regulation mechanisms

1.3.3.2.2.1 Photorespiration and regulation of Rubisco

Apart from NPQ, diatoms possess other regulation mechanisms involved in the photoprotection.

One of them is the light sensitive activation/deactivation of Rubisco (MacIntyre & Geider, 1996). This level of regulation does not depend on the size of the enzyme pool, but on the activity of this enzyme.

The Rubisco is also involved in another regulation mechanism, the photorespiration, which has the double role of recovery energy and carbon potentially lost by cells and dissipate the excess of energy in high light and high O_2 concentration (Beardall *et al.*, 2003). The photorespiration relies on the oxygenase activity of Rubisco, which produces one molecule

of 3-phosphoglycerate (G3P) and one of 2-phosphoglycolate through the oxygenation of ribulose 1,5-bisphosphate (RuBP). The 2-phosphoglycolate, which cannot enter into the Calvin cycle, can be dephosphorylated and excreted by cells or it can be metabolized, allowing a partial recovery of the energy through the production of NADH and ATP, and of the fixed carbon in the tricarboxylic acid cycle in the mitochondrion (Beardall *et al.*, 2003). This process is energy- and oxygen-consuming since it needs NADPH, which in high light can be over-reduced, exceeding the Calvin cycle demand for reducing power (Peterhansel *et al.*, 2010). This is the reason why the photorespiration protects cells from photoinhibition, acting as electron sink under stressful conditions.
In diatoms it has been demonstrated that the genes involved in this pathway follow a diel cycle, increasing their expression during the day and being down-regulated in anticipation of the night (Parker *et al.*, 2004).

1.3.3.2.2.2 The cyclic electron flow around PSII and PSI

Another way to dissipate the excess energy is through alternative electron-cycling pathways.
In diatoms, these pathways include the cyclic electron transport around PSII (CET PSII) (Lavaud *et al.*, 2002b, Lavaud, 2007, Wagner *et al.*, 2016) and the cyclic electron transport around PSI (CET PSI) (Grouneva *et al.*, 2009).

The CET PSII avoids the over-saturation of the plastoquinones (PQ), electron carriers after the PSII, and competes with the oxidation of water from which O_2 evolves, reducing the probability of ROS generation and PSII damage; basically it functions as an additional electron sink activated under high light (Lavaud, 2007). It has been demonstrated that this process is activated even faster than NPQ in diatoms, and at lower light intensities (Lavaud, 2007). Apparently, the CET PSII in diatoms is similar to the green algal one, in which the redox state of the PQ pool is able to switch on and off this process. When activated, the electrons are diverted from the linear pathway starting from the Q_B towards the cytochrome b559 and then again towards the PSII (Onno Feikema *et al.*, 2006).

In the CET PSI the electrons produced at PSI are diverted back towards the cyt b_6/f *via* ferredoxin and NADPH passing through the PQ (Munekage *et al.*, 2004). This cyclic electron flow contributes to the generation of the proton gradient needed for the ATP synthesis and the induction of the NPQ process, preventing the over-reduction of the acceptor side of the PSI (Munekage *et al.*, 2004, Grouneva *et al.*, 2009, Miyake, 2010).

1.3.3.2.2.3 The water-water cycle

The water-water cycle (WWC) was firstly discovered by Mehler (1951), who realized that chloroplasts were able to reduce O_2 apart from evolving it through water oxidation. This process leads to the production of the reactive oxygen species (ROS) progressively neutralized by different enzymes. The molecular mechanism starts with the oxidation of water at PSII and the electrons are used to reduce O_2, which is oxidized back to water by means of different enzymes.

Asada (1999) proposed that the most important physiological function of this cycle was the immediate scavenging of ROS at their generation sites, before their interaction with target molecules. Anyway, it has been demonstrated that WWC is not able to fully scavenge ROS produced in the chloroplast (Miyake, 2010). Therefore other functions of this cycle have been hypothesized. It can actually operate as electron sink hindering the photoinhibition of PSII. Another photoprotective role of this cycle is ascribable to the induction of NPQ by means of an increased trans-thylakoidal ΔpH produced by a reduced stromal acidification due to AsA regeneration (Hormann *et al.*, 1994). The proton gradient is used also for the production of ATP. It has been demonstrated that in diatoms, similarly to green algae and higher plants, an increased irradiance induces the activation of this pathway (Claquin *et al.*, 2004).

1.3.3.2.2.4 The chlororespiration

The chlororespiration is a respiratory electron transport chain at the thylakoid membrane level. It is based on the non-photochemical reduction of the plastoquinone (PQ) pool and its subsequent re-oxidation at expense of O_2 (Peltier & Cournac, 2002). In this pathway a plastidal NAD(P)H dehydrogenase complex (NDH) oxidizes stromal NAD(P)H and

transfers the electrons to PQ. Then a plastid terminal oxidase (PTOX) takes the electrons from PQ and reduces O_2 to H_2O. The photoprotective role of this cycle is due to the removal of stromal reductants, lowering the excitation pressure on PSI, and to the creation of the proton gradient across the thylakoid membrane that contributes to ATP synthesis and the instauration of NPQ (Grouneva *et al.*, 2009). In diatoms it has been demonstrated that the excess of light is used for the accumulation of reducing equivalents, subsequently used to fuel the chlororespiratory ATP synthesis at dark (Lavaud *et al.*, 2002b).

1.4. Oxidative stress and antioxidants

The acclimation and regulation processes that cell displays in high light condition are crucial in order to avoid or at least diminish the production of chemical intermediates and by-products, the reactive oxygen species (ROS). When the production of ROS exceeds cell's ability to detoxify them, occurs the onset of oxidative stress.

ROS are able to damage the PSII and PSI, causing photoinhibition, and attack lipids, proteins and nucleic acids, causing their oxidation and thus mutation, fragmentation and loss of function (Erickson *et al.*, 2015).

1.4.1 Production of ROS in chloroplasts

Chloroplasts are a rich source of ROS, unavoidable consequence of the aerobic metabolism. The radical species can be formed following different routes, *via* energy transfer from chlorophyll or *via* electron transfer.

When a chlorophyll molecule absorbs light, its energy increases, passing from the ground state to its singlet excited state ($^1Chl^*$). To come back to the ground state, this energy can be transferred towards the reaction centers driving the photochemical reactions, or it can be re-emitted as fluorescence, or dissipated as thermal energy through NPQ (Müller *et al.*, 2001). If not dissipated through the aforementioned mechanisms, this energy may decay *via* intersystem crossing generating the chlorophyll triplet excited state ($^3Chl^*$), a photosensitizer of molecular oxygen. This chlorophyll has a longer half-life than its singlet state, increasing the chance of transferring its energy directly to oxygen, resulting in the formation the singlet oxygen ($^1O_2$)(Triantaphylides *et al.*, 2008)(Fig. 1.15).

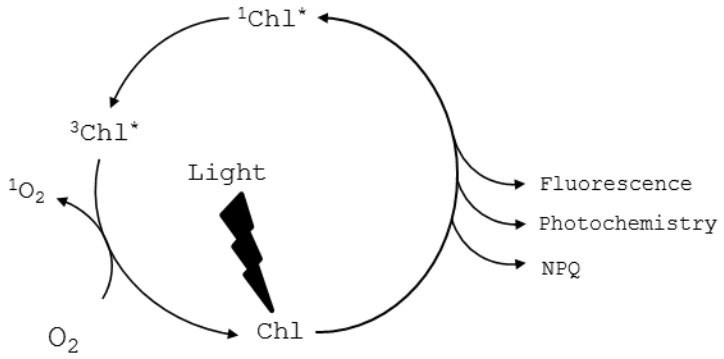

Figure 1.15: Possible fates of excited Chl. Modified from Müller *et al*., 2001.

This species is highly reactive due to the opposite spin of its two unpaired electrons, so it can participate in reactions transferring simultaneously two electrons (divalent reduction) (Sharma *et al.*, 2012). It is considered the main ROS responsible for the photo-oxidative damage in plants, and is mostly produced at the reaction centers of the PSII and in the antennae (Triantaphylides *et al.*, 2008, Krieger-Liszkay, 2006).

Under high light condition, the over-excitation of the electron transport chain induces the over-reduction of the NADP and ferredoxin, so the unused electrons are transferred to molecular oxygen, causing a stepwise monovalent reduction of O_2, sequentially reduced to superoxide ($O_2^{\bullet-}$), hydrogen peroxide (H_2O_2), and hydroxyl radical ($OH^{\bullet}$). These ROS are mostly formed at the acceptor side of the PSI (Erickson *et al.*, 2015)(Fig. 1.16).

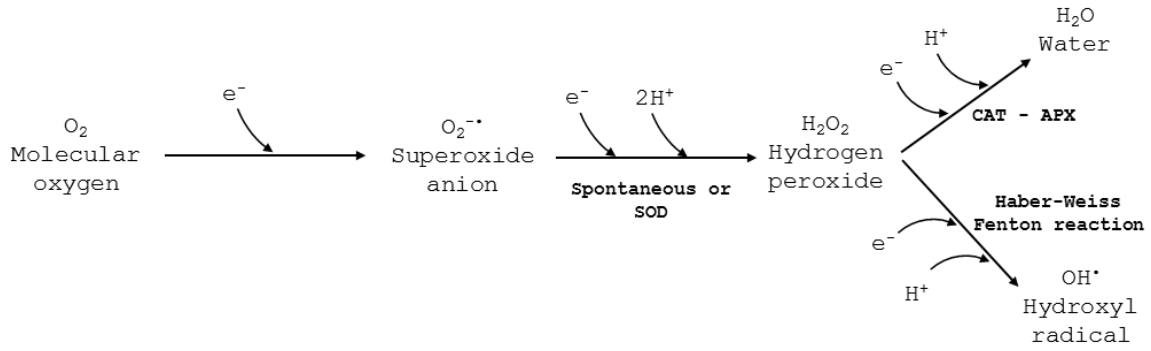

Figure 1.16: ROS formation at PSI.

$O_2^{\bullet-}$ is the primary, short-lived, moderately reactive ROS. It reacts with iron-containing proteins such as ferritin and Fe-S clusters, determining the release of iron (Paul, 2000, Imlay, 2008). All the other ROS are generated from this one, both directly and *via* enzyme or metal catalysis. $O_2^{\bullet-}$ can be converted into H_2O_2 accepting one electron and two protons

through a spontaneous reaction or by means of the enzyme superoxide dismutase (SOD). H_2O_2 is able to oxidize cysteine and methionine residues, inactivating, for example, the thiol-modulated enzymes of the Calvin cycle reducing drastically the CO_2 fixation, so even at low concentration it is a hazardous inhibitor of the photosynthetic process (Foyer & Shigeoka, 2011). Despite its toxicity towards the photosynthesis, H_2O_2 is generated under normal and stressful conditions in numerous cell compartments and is the most stable ROS. It is able to cross biological membranes, diffusing through aquaporin (Bienert *et al.*, 2007), so it can be found far from its generation site. H_2O_2 is less reactive than $OH^{\bullet}$, a strong oxidant whose formation depends on both H_2O_2 and $O_2^{\bullet-}$ *via* the Haber-Weiss and the Fenton reactions, which utilize a metal catalysis. In the first reaction, ferric ion (Fe^{3+}) is reduced by $O_2^{\bullet-}$, producing a ferrous ion (Fe^{2+}) and O_2. Then Fe^{2+} is oxidized by H_2O_2 producing Fe^{3+}, hydroxyl ion (OH^-) and $OH^{\bullet}$. H_2O_2 can also react directly with $O_2^{\bullet-}$ producing $OH^{\bullet}$, OH^- and O_2. $OH^{\bullet}$ is the most reactive ROS and is able to fragment macromolecules such as lipids, proteins and DNA, oxidizing and therefore degrading key enzymes such as Rubisco, and decomposing the PSI complex (Miyake, 2010).

1.4.2 Production of ROS in other cell compartments

In mitochondria, the respiratory electron transport chain also produces ROS in different sites. The monovalent reduction of molecular oxygen occurs mostly by means of redox-active prosthetic groups within proteins and produces $O_2^{\bullet-}$ (Murphy, 2009).

The photorespiration, a mechanism used to reduce the excitation pressure and therefore preventing ROS formation in the chloroplast, is a ROS source in peroxisome. In fact, the glycolate metabolism implies the formation of H_2O_2 (Suzuki *et al.*, 1991, Beardall *et al.*, 2003). In these organelles also the β-oxidation of fatty acids produces H_2O_2 (Cirulis *et al.*, 2013).

Both the endoplasmic reticulum, which in diatoms has a key role in the biomineralization of silica frustule (Sheppard *et al.*, 2010), and the plasma membrane can be a source of ROS, being the site where the enzyme NADPH oxidase (NOX) exerts its function. This enzyme produces $O_2^{\bullet-}$ by transferring electrons from NADPH to molecular oxygen. NOX has been found in different algal species and seems important for the response to different

environmental cues, such as grazing or iron availability. In diatoms the activity of this enzyme is light regulated (Laohavisit *et al.*, 2015).

In both cellular and organelle membranes the reaction of ROS with lipids determines the initiation of a process known as lipid peroxidation, which enhances the oxidative stress through the production of other radicals. This is a chain reaction mechanism where firstly lipids (LH) are oxidized by ROS producing fatty acid radicals ($L^{\bullet}$), highly unstable. By turns, they react with oxygen resulting in the formation of peroxyl-fatty acid radicals ($LOO^{\bullet}$), also unstable, which can combine with each other attacking membrane proteins, or can steal a hydrogen from adjacent fatty acid side chains in membrane propagating the chain reaction of lipid peroxidation, generating fatty acid radicals and lipid hydroperoxides (LOOH). The extent of the phenomenon depends on the protein/lipid composition of the membrane and the presence of chain-breaking antioxidants (Gutteridge & Halliwell, 1990).

1.4.3 Scavenging of ROS

Aerobic life brings the inevitable consequence of the production of ROS, harmful to living organisms due to the high reactivity towards all classes of biomolecules. Millions of years of evolution led to the adaptation of aerobic organisms, enabling them to minimize the detrimental actions of ROS and even use them as secondary messengers by means of an efficient antioxidant system.

Their concentration gives important information on the cell status, controlling, for example, PSII activity and therefore photosynthesis and the expression of genes involved in acclimation and defense strategies (Foyer & Shigeoka, 2011).

Due to the double role of ROS both as toxic species and as signaling molecules, photosynthetic cells developed different mechanisms to scavenge them, finely tuning their concentration for signaling purposes and detoxify them when in excess (Mittler, 2002, Foyer & Noctor, 2005a, b).

The antioxidant network is composed by antioxidant molecules and enzymes, located in the various cell compartments.

1.4.3.1 The non-enzymatic antioxidants

The non-enzymatic components of the antioxidant network include carotenoids, ascorbic acid (AsA), glutathione (GSH), tocopherols, and phenolic compounds.

The lipophilic carotenoids can be found in the chloroplast membrane phase, where they can exert their antioxidant role in the sites where photosynthetic ROS are produced. They are efficient quencher of $^1O_2$ and peroxyl radicals, besides their role in the electronic de-excitation of Chl, thus in the prevention of ROS formation (Stahl & Sies, 2003, Boon *et al.*, 2010, Snoeijs *et al.*, 2012, Kuczynska *et al.*, 2015). The mechanism through which carotenoids quench $^1O_2$ is mostly physical: $^1O_2$ reacts with carotenoids producing triplet excited state carotenoids ($^3Car^*$) and ground state O_2. $^3Car^*$ can return to the ground state by releasing energy by rotational and vibrational interactions with the surrounding solvent (Stahl & Sies, 2003). In this process carotenoids remain intact, so can be reused several times in these quenching cycles. The reason of their efficacy in the physical quenching relies on the conjugated double bonds which stabilize the triplet energy level. The quenching of peroxyl radicals by carotenoids instead depends on the formation of a resonance stabilized carbon centered radical adducts (Stahl & Sies, 2003, Nimse & Pal, 2015).

Tocopherols, or vitamin E, are lipophilic antioxidants synthesized exclusively by photosynthetic organisms. They exist in different forms, all characterized by the presence of a chromane ring with different number and position of methyl groups. The most abundant form in nature is α-tocopherol, which shows three methyl substituents on the aromatic ring (Li *et al.*, 2008). As carotenoids, α-tocopherol is a chain breaker during lipid peroxidation: it reacts with lipid peroxyl radicals ($LOO^\bullet$) generating a lipid hydroperoxyde (LOOH) and a tocopheroxyl radical (α-tocopherol-$O^\bullet$). This radical is quite stable and thus not enough reactive to progress the lipid peroxidation (Nimse & Pal, 2015). The regeneration of tocopherol from its radical form depends on β-carotene and subsequently the carotenoid radical cation is repaired by AsA (Stahl & Sies, 2003). Tocopherols have also the key role of $^1O_2$ physical scavenging by resonance energy transfer, protecting the PSII structure and function (Krieger-Liszkay, 2006).

Phenolic compounds are secondary metabolites produced from the shikimate-phenylpropanoids-flavonoids pathways, and constitute one of the most common and widespread groups of substances in plants (Cheynier *et al.*, 2013).

Among phenolic compounds, flavonoids act as potent antioxidant thanks to their ability to donate electrons or hydrogen atoms directly to reactive species (Pietta, 2000). They have the capacity to inhibit lipoxygenase (Pietta, 2000), the enzyme which catalyzes the formation of lipid hydroperoxides, and to chelate metals, inhibiting important sources of ROS such as the Haber-Weiss and Fenton reactions (Sharma *et al.*, 2012).

The diversity and role of phenolic compounds in microalgae is far less studied than in higher plants, but it has been shown that microalgae and cyanobacteria can contain several classes of flavonoids (Klejdus *et al.*, 2010).

Ascorbic acid (AsA), or vitamin C, is a six carbon compound related to glucose. It is a major hydrophilic component of cell plasma, and possesses a strong antioxidant activity (Snoeijs *et al.*, 2012). It can directly reduce $O_2^{\bullet-}$ and neutralize ROS such as hydroxyl and lipid peroxyl radicals, turning itself into a very stable radical due to the delocalization of the spare electron (Noctor & Foyer, 1998, Lü *et al.*, 2010). It is also a substrate of antioxidant enzymes peroxidase (see below) and VDE, thus contributing in the dissipation of the excess energy (Smirnoff & Wheeler, 2000).

Reduced glutathione (GSH) is a tripeptide (L-γ-glutamyl-L-cysteinyl-glycine), which is the major low-molecular-mass thiol compound in living organisms. It acts as a cellular thiol redox buffer, maintaining a given thiol/disulfide redox potential. It can directly quench free radicals donating one electron. As electrons are lost, two oxidized molecules dimerize by a sulfide bridge forming a molecule of glutathione disulfide, also known as oxidized glutathione (GSSG). Apart from its scavenging activity, it is an essential cofactor of many enzymes, of which some of them with antioxidant activity (Marí *et al.*, 2009).

1.4.3.2 The antioxidant enzymes

All the living organisms possess several antioxidant enzymes located in various cell compartments. They are catalase (CAT), superoxide dismutase (SOD), peroxidases, which utilize different substrates such as AsA (APX) or GSH (GPX) to detoxify ROS, and the various enzymes involved in the recycling of the antioxidant substrates, such as

monodehydroascorbate reductase (MDHAR), dehydroascorbate reductase (DHAR), and glutathione reductase (GR).

SOD is found in almost all the cellular compartments: cytosol, chloroplast, mitochondria, apoplast and peroxisomes (Mittler, 2002). It catalyzes the disproportionation of $O_2^{\bullet-}$ into molecular oxygen and H_2O_2 using metal cofactors (Wolfe-Simon *et al.*, 2005).

CAT converts H_2O_2 to water and molecular oxygen and possesses different isoforms. It is absent in chloroplast and mainly found in the peroxisomes (Noctor & Foyer, 1998, Mhamdi *et al.*, 2012) where H_2O_2 is produced by different processes (see section 1.4.2 Production of ROS in other cell compartments) or can arrive from cytosol under high ROS production condition (Mittler, 2002).

Also the peroxidases convert H_2O_2 to water and molecular oxygen, but they need a reductant. They can be found in all the cellular compartments and have a higher affinity for H_2O_2 than CAT (Noctor & Foyer, 1998). This feature suggests that CAT may be involved in the removal of excess ROS during stress, while peroxidases, mostly APX, might be in charge of the fine modulation of ROS for signaling (Mittler, 2002). In plant tissues, APX has a higher activity in detoxifying H_2O_2, but GPX seems to have the additional role of neutralize lipid hydroperoxides (Noctor *et al.*, 2000).

1.4.3.3 The antioxidant network

All the antioxidants, both molecules and enzymes act in concert in cells for the detoxification of ROS (Fig. 1.17). They are directly linked in the water-water cycle which operates in the chloroplast (Asada, 1999), including the AsA-GSH cycle, which is active in all the cellular compartments (Foyer & Noctor, 2011). In the water-water cycle the electrons coming from the oxidation of water at PSII reduce O_2 at PSI generating $O_2^{\bullet-}$ which is subsequently disproportionated by SOD in H_2O_2 and O_2. H_2O_2 is then scavenged by the AsA-GSH cycle: firstly it is reduced to water by APX using AsA as electron donor, generating monodehydroascorbate (MDHA). AsA is subsequently regenerated through different routes: a direct reduction of MDHA by ferredoxin (Fd), or *via* MDHA reductase (MDHAR), which uses NADPH as electron donor, or *via* the disproportionation of MDHA into dehydroascorbate (DHA) and AsA. DHA is then reduced to AsA by DHA reductase (DHAR), which uses GSH as electron donor. The oxidized glutathione (GSSG) is reduced

back to GSH by GSH reductase (GR), which uses NAPDH as electron donor. NADPH is regenerated by ferredoxin- $NADP^+$ oxidoreductase (FNR) and the reduced Fd is regenerated by the PSI (Noctor & Foyer, 1998, Miyake, 2010).

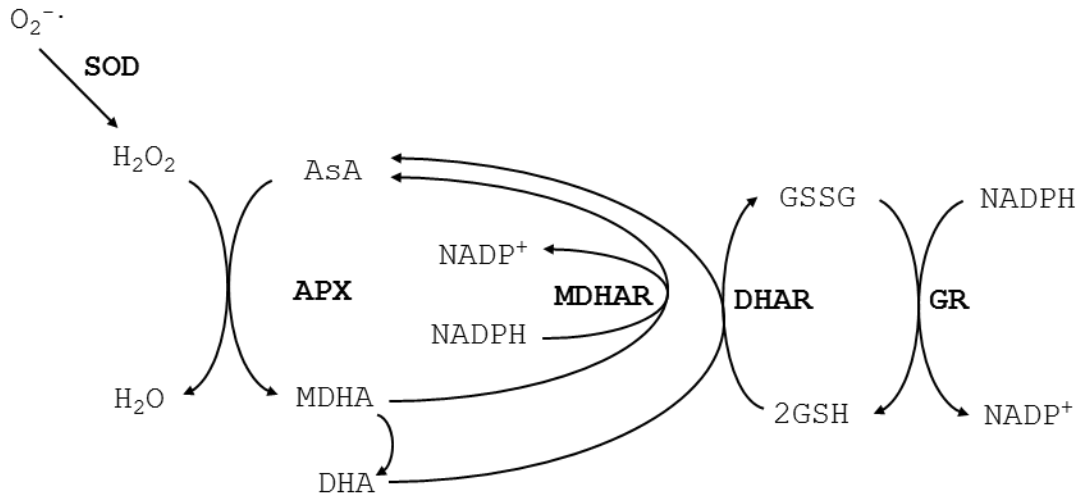

Figure 1.17: Antioxidant network - AsA-GSH cycle.

1.5 Aims of the study

Diatoms constitute one of the most abundant and diversified groups among the phytoplankton species, prevailing in the seas and oceans and thriving in turbulent and nutrient-rich waters. Among the various reasons explaining the astonishing ecological success of these organisms, their ability to hastily acclimate to the fickle light environment through the modification of their light harvesting apparatus and photoprotective capacity is surely one of the most accredited (Wagner *et al.*, 2006, Lavaud *et al.*, 2007).

Being light a crucial ecological axis in ruling the metabolism of photosynthetic organisms, the general aim of my thesis was to decipher the role of the various light properties such as intensity, spectral composition, and distribution over time on the activation of the photophysiological responses, in particular the photoprotective mechanisms and antioxidant network functioning in diatoms, and their role on the modulation of growth. While the photoprotective mechanisms in diatoms are currently studied (Lavaud *et al.*, 2004, Lavaud, 2007, Ruban *et al.*, 2004, Derks *et al.*, 2015, Goss & Lepetit, 2015), the role of the antioxidant network as a second line defense able to reduce the light stress, although described (Waring *et al.*, 2010, Cartaxana *et al.*, 2013), is far less explored in diatoms. The relationships between photoprotective mechanisms and antioxidant network, which are supposed to be regulated in concert to avoid the consequence of the photoinhibition, are poorly understood.

Therefore, the aim of my PhD project is to fill this gap of knowledge and pave the way for a deeper understanding of the photophysiological defense mechanisms developed in diatoms.

This study has important spillover on the biotechnological field. In fact, microalgal great potential as a source of bioproducts is now limited by their high cost of production, which could be considerably reduced optimizing the growth condition. The role of light in ruling microalgal physiology should be taken into consideration for the designing of enclosed photobioreactors for large scale production of specific products.

The various light properties were analyzed separately.

The role of light distribution in shaping the photophysiology and the metabolism of cells was the first objective. The aim was to assess if the exposure to a fluctuating light regime, similar to what happen in natural conditions, stimulates the photoprotective mechanisms without causing the insurgence of photodamage, and how the macromolecular content of cells was modulated by the acclimation to the different light environments. In parallel, we compared the effects of a sudden exposure to light (square-wave light course: on/off system) with a gradual light intensity increase to test our hypothesis that a sudden light increase might be able to impair the normal cell functioning by not allowing the progressive acclimation to increasing light.

The results of these experiments are presented in chapter 3.

Briefly, *Skeletonema marinoi* was long term acclimated to four different light climates, one mimicking a natural 40 meters depth sea environment, so a sinusoidal blue light distribution with a midday peak equal to 150 µmol photons m^{-2} s^{-1}; then two others where to this sinusoidal light, different peaks of red light (3 and 9) were superimposed. These two conditions simulate a sudden up- and down-welling along the water column happening with a more or less stressful fashion (9 peaks and 3 peaks, respectively). These light treatments were then compared with the most used light distribution in indoor microalgal cultivation, which is a square-wave course (on/off system) with the same maximal photon flux density (PFD) as the blue sinusoidal condition.

Another objective of my thesis was to explore the connection between the photoprotective and defense strategies and their short-term regulation in response to change in light spectrum, intensity and velocity of increase, hypothesizing a key role of the spectral light in ruling these processes through photoreceptors activation.

Compared to the previous chapter, the study of the antioxidant network was implemented by the quantification of antioxidant molecules, as well as enzymatic and antioxidant activities.

The results of this set of experiments are presented in chapter 4.

Briefly, *S. marinoi* was pre-acclimated to a sinusoidal blue light distribution with a midday peak ≈ 150 µmol photons m^{-2} s^{-1} and then switched to different light climates characterized by the presence of only blue light, only red light, and blue and red together, at different intensity and velocity of increase.

A third objective was the investigation of the role of the growth phase on the regulation of the photoprotective mechanisms and antioxidant network in *S. marinoi*. Indeed, along the different growth phases, the physiology of batch cultured cells is expected to change in order to counteract and delay the cell culture death. These modifications should lead to an altered photophysiology and by consequence cell metabolism, notwithstanding the exposure to the same light climate. From a biotechnological perspective, the harvesting of cells in their different growth phases may change the yield of the product of interest.
The results of this study are presented in chapter 5.
Briefly, *S. marinoi* was cultivated in batch exposed to a natural-like light mimicking a coastal 5/10 meters depth environment, composed by blue, red and green spectrum. The growth curve was followed and sampled during exponential, late exponential and stationary phases.

Another objective of my PhD was to investigate the long-term (i.e., after a complete diel biological cycle, 24-36 hours) acclimative responses and the photoprotective and antioxidant network functioning activated to cope with high light. The effects of instantaneous and integrated light intensity variations were investigated.
The results of this study are presented in chapter 6.
Briefly, *S. marinoi* cells pre-acclimated to the same light climate used in chapter 5 were switched to three different high light conditions, characterized by high intensity sinusoidal light distribution, and two square-wave light distributions characterized by different integrated daily light dose.

Complementary to the previous study, another objective was to investigate the role of very low light or dark environment on the photoregulative system in diatoms. This study was also conceived for investigating the infradiel trend of defense mechanisms in *S. marinoi*. Indeed, the results obtained in chapter 5 showed the daily cyclic nature of some photosynthetic and photoprotective parameters, and antioxidant and carotenoid synthesis. Therefore a question roused: are these infradiel fluctuations strictly dependent on light stimulus or is there the influence of an internal circadian clock?
The results of this set of experiments are presented in chapter 7.

Briefly, we compared the effects of complete darkness experimental condition with two very low light intensity conditions, with light following a sinusoidal distribution or a continuous distribution.

A further objective of my work was to explore the antioxidant molecules network activation in a natural microalgal community in real oceanographic conditions. Indeed, after having verified that *S. marinoi* has a powerful photoprotective and antioxidant network, modulated with the different light properties, we wanted to investigate the presence of such molecules and the activation of such defense network in the pelagic ecosystem.

The information obtained from laboratory experiments was therefore compared to the results of this study, presented in chapter 8.

Briefly, in June 2016 in the Gulf of Naples a mesocosm experiment was carried out aiming to investigate the pelagic ecosystem functioning, from molecules to ecosystem, during a phytoplankton outburst. The tools (mesocosms) deployed at sea allowed the study of the ecosystem and its biotic and abiotic properties in controlled conditions.

This project offered the unique opportunity to study the photosynthetic acclimation, the antioxidant production and their link during the different phases of the bloom in a natural context.

The last objective of my thesis was to explore the antioxidant role of the pigments involved into the photoprotective xanthophyll cycle activated in *S. marinoi*. Indeed, the hypothesis of antioxidant activity of these pigments has been reported by some studies, but it still has to be demonstrated. Also, the results obtained in the previous chapters often reported a link between photoprotection and antioxidant molecules and/or activity.

The results of this experiment are reported in chapter 9

Briefly, *S. marinoi* cells were cultured under a light condition which maximized both the growth and the synthesis of xanthophyll cycle involved pigments. Pigment fractions were then separated and purified and the antioxidant activity of those fractions was tested.

2. Materials and methods

2.1 The model species *Skeletonema marinoi*: biology and cultivation

Experiments were conducted on a non-axenic strain of *Skeletonema marinoi* Sarno & Zingone (CCMP 2092), which was used as a model species for its high capability of growth and potential relevant role in biotechnological applications (Chandrasekaran *et al.*, 2014), as well as for all the information already available on the biology and photophysiology of this species (Vidoudez & Pohnert, 2012, Chandrasekaran *et al.*, 2014, Di Dato *et al.*, 2017)
The mitotic generation time is short, approximately one division per day, making this species a suitable organism for the study of phenotypic responses. Yet, this species is easy to collect, isolate and maintain in culture. The survival of monoclonal culture after single cell isolation is almost 100%. Furthermore, the transcriptome of this species is available, while genome is under study (Godhe, 2017)
S. marinoi is a cosmopolitan centric diatom, very abundant during spring bloom in temperate waters when its concentration can reach millions of cells per litre in the photic zone. It forms chains and its main propagation system is through vegetative division, although sexual reproduction and formation of auxospores have also been documented (Godhe *et al.*, 2014). It possesses a benthic resting stage, and in the sediments can be found up to 50k propagules per gram (McQuoid *et al.*, 2002).
The strain CCMP 2092 used in this work was collected from the surface waters of the northern Adriatic Sea, where this diatom is known to be the major contributor to the late-winter blooms (Miralto *et al.*, 1999) and is found in very shallow waters (Brunet, personal communication).
S. marinoi was cultivated at 20°C in autoclaved seawater, pre-filtered through a 0.7 µm GF/F glass-fiber filter (Whatman™, Whatman International Ltd, Maidstone, UK) and enriched with F/2 medium nutrients (Guillard, 1975). Depending on the experiment, cells were grown in 1 L plastic flasks, 2 L polycarbonate bottles with air bubbling or in 4.5 L glass flasks with air bubbling.
S. marinoi was maintained under sinusoidal light distribution with a midday peak of 150 µmol photons s^{-1} m^{-2} and with a photoperiod equal to 12:12 dark:light. The spectral light used for the cell's maintaining was blue or white composed by red:green:blue 10:40:50. The light was provided by a custom-built LED illumination system (see next paragraph).

2.2 Light system

Light was provided by a custom-built LED illumination system (European patent registration number: EP13196793.7) allowing to modulate the spectral composition and light intensity (Brunet *et al.*, 2014)).

The light system is a computing system based on a series of Z-POWER LED – RGB (Red-Blue-Green) allowing the monitoring and regulation of the intensity and/or the spectral composition of light. The three colors were provided at wavelengths of 460 nm (± 36 nm, blue), 530 nm (± 50 nm, green) and 626 nm (± 36 nm, red).

Light intensity (Photosynthetically Active Radiation PAR) was measured inside each flask by using a laboratory PAR 4 π sensor (QSL 2101, Biospherical Instruments Inc., San Diego, CA, USA), while spectral composition (PAR(λ)) were measured by using a radiometer (Hyper OCR I, Satlantic, Halifax, CA).

2.3 Cell density and growth rate

To assess cell density, 2 mL of cell suspension were collected from each flask, and fixed with Lugol's iodine solution (1.5% v/v). 1 mL of this solution was used to fill a Sedgewick Rafter counting cell chamber. Cells were then counted using a Zeiss Axioskop 2 Plus light microscope (Carl Zeiss, Göttingen, Germany).

The growth rate was estimated from cell concentration measurements using the following equation:

$$\mu\ (day^{-1}) = \frac{\ln\ (X_1/X_0)}{t_1 - t_0}$$

where μ is the growth rate, X_0 and X_1 are cell densities at the beginning (t_0) and end (t_1) of a selected time interval (generally 24 hours).

2.4 Determination of the photochemical efficiency of the photosystem II

To assess the photosynthetic capacities and the photophysiological state of phytoplankton cells, measurements of active chlorophyll a fluorescence were performed using a DUAL-PAM fluorometer (Heinz Walz GmbH, Effeltrich, Germany). The pulse amplitude modulation (PAM) measurement is based on the selective amplification of the fluorescence signal emitted by the Chl *a* after excitation by an intense and very short light pulse. At room temperature, most of the fluorescence measured comes from the photosystem II (PSII), whilst in microalgae PSI contributes to only 1 to 5 % to the signal fluorescence (Kirk, 1994).

Measurements of the photosystem II (PSII) photochemical efficiency were performed on samples submitted to two kinds of treatment: 15-minutes dark-acclimated or light-acclimated algal samples. After dark-acclimation, all the energy has been removed from the photosynthetic electron transport chain. The reaction centers are "open" and the limiting step for energy transfer is the oxidation/reduction reactions regarding the electron acceptors in the photosynthetic pathway, downstream of PSII, notably the plastoquinone pool, particularly QA (Consalvey *et al.*, 2005). When all reaction centers are "open", QA is completely oxidized and the level of fluorescence is minimal (F_o):

$$F_0 = K\left(E\frac{k_f}{k_f + k_p + k_d}\right)$$

where K is the proportionality constant, k_f, k_p and k_d are the rate constants of chlorophyll fluorescence, photochemistry, and constitutive thermal energy dissipation, respectively; E is the light received by the PSII. The measurement of F_o was done using light of low intensity (1 µmol photon m^{-2} s^{-1}) and low frequency (approximately 25 Hz).

F_m was measured by applying a short and intense flash of actinic light which completely reduces QA. In our case, the saturation flash of bright red light (655 nm) were applied at an intensity of 2400 µmol photons m^{-2} s^{-1} for a duration of 450 ms. Once all reaction centers are "closed", QA is reduced (QA^-) and the fluorescence level is maximal (F_m):

$$F_m = K\left(E\ \frac{k_f}{k_f + k_d}\right)$$

The photochemical efficiency of the PSII (F_v/F_m) defined as the quantum yield of photochemistry (ϕ_p), corresponds to the quantum yield of electron transfer from the PSII (P680) to the plastoquinone pool (QA). It is estimated by:

$$\phi_p = \frac{F_m - F_0}{F_m} = \frac{F_v}{F_m}$$

where F_v is the variable fluorescence ($F_v = F_m - F_o$).

For the dark-acclimated cells, F_v/F_m corresponds to the maximal photochemical efficiency of the PSII (or the maximal light utilization efficiency of PSII) and 15 minutes of dark acclimation is enough to relax the photosystems II and thus to get reliable measurements of F_o (Brunet *et al.*, 2014).

When cells were not previously exposed to 15 min dark period, some of the reaction centers are closed due to the photosynthetic activity. The PSII photochemical efficiency depends on the proportion of open reaction centers but also on their efficiency to transmit energy (Consalvey *et al.*, 2005). In case of non-dark acclimated cells, the light utilization efficiency of the PSII was calculated by:

$$\Delta\phi = \frac{F_v'}{F_m'} = \frac{F_m' - F'}{F_m'}$$

where F_v'/F_m' is the PSII operating efficiency with $F_v' = F_m' - F'$.

F_m' is the maximum fluorescence in the light-acclimated state and F' is the steady-state fluorescence level in the light obtained with the measuring light. With increasing light, F_v'/F_m' decreases due to the progressive closure of the reaction centers. The more light-acclimated is the sample, the slower is the decrease of the F_v'/F_m'.

2.5 Determination of the non-photochemical fluorescence quenching

Under excess light, a part of the incident light is diverted away from the reaction centers and dissipated as heat. This phenomenon is known as non-photochemical chlorophyll *a* fluorescence quenching (NPQ). The dissipation of light energy as heat induces a fluorescence down-regulation and the yield (F_v/F_m or F_v'/F_m') decreases due to lower F_m or F_m' (White & Critchley, 1999).

Estimation of the non-photochemical quenching is given by the qN coefficient, calculated as follows:

$$qN = 1 - \left(\frac{F_m' - F_0'}{F_m - F_0}\right)$$

Since the determination of F_o' (minimum light-acclimated fluorescence level) is difficult, a proxy for NPQ is calculated by the Stern-Volmer expression (Bilger *et al.*, 1989):

$$NPQ = \frac{F_m - F_m'}{F_m'} = \frac{F_m}{F_m'} - 1$$

This equation derives a parameter proportional to the level of NPQ developed by the cells at any particular light level. Indeed, the decrease of F_m to F_m' is proportional to the level of NPQ when expressed as a fraction of the maximum fluorescence at a certain light level (Consalvey *et al.*, 2005).

The estimation of NPQ consisted in measuring F_o and F_m on 15 min dark-acclimated samples and then measuring F_m' and F_0' every minute on the same sample illuminated by an actinic light (setup at 399 µmol photon m^{-2} s^{-1}) for 10 minutes.

2.6 Determination of the electron transport rate-light curves

The photosynthetic capacity of cells was estimated by studying the relationship between irradiance and photosynthesis. The electron transport rate (ETR) *vs.* irradiance (E) curves were determined on 15-minutes dark-acclimated samples by applying a series of 10

increasing intensity actinic lights (composed by 2/3 of blue and 1/3 of red light, lasting 1.5 minute each, ranging from from 1 to 1222 μmol photon m^{-2} s^{-1}).

The photochemical efficiency of the PSII was measured on the 15-min dark-acclimated sample, while the light utilization efficiency of the PSII ($\Delta\phi$) was measured after each actinic light level.

The relative ETR, taking into account the part of incident light energy effectively absorbed by the photosystem (Genty *et al.*, 1989, Kolber & Falkowski, 1993), was calculated as follows:

$$relETR = \frac{F_{v'}}{F_{m'}} \cdot E \cdot 0.5 \cdot a^*$$

where E is irradiance, and a^* is the cell specific absorption coefficient expressed in m^2 $cell^{-1}$ (see paragraph 2.7). A factor of 0.5 was applied since it is assumed that half of the incident light is absorbed by the PSI and half by the PSII.

The relative ETR is expressed in nmol e^- h^{-1} $cell^{-1}$.

Determination of photosynthetic parameters was based on the electron transport rate (ETR) measurements. From the $_{rel}$ETR *vs.* E curve, the photosynthetic parameters (α, $_{rel}ETR_{max}$ and E_k) are retrieved according to the equation of Eilers and Peeters (1988):

$$relETR = \frac{E}{(a*E^2)+(b*E)+c}$$

where a, b, and c are three constants.

The three photosynthetic parameters are determined as follow:

$\alpha = \frac{1}{c}$; $r\text{elETRmax} = \frac{1}{b+2\,ac}$; and $E_k = \frac{c}{b+2ac}$

The α parameter represents the slope of the initial linear increase of the $_{rel}$ETR *vs.* E curve (Fig. 2.1).

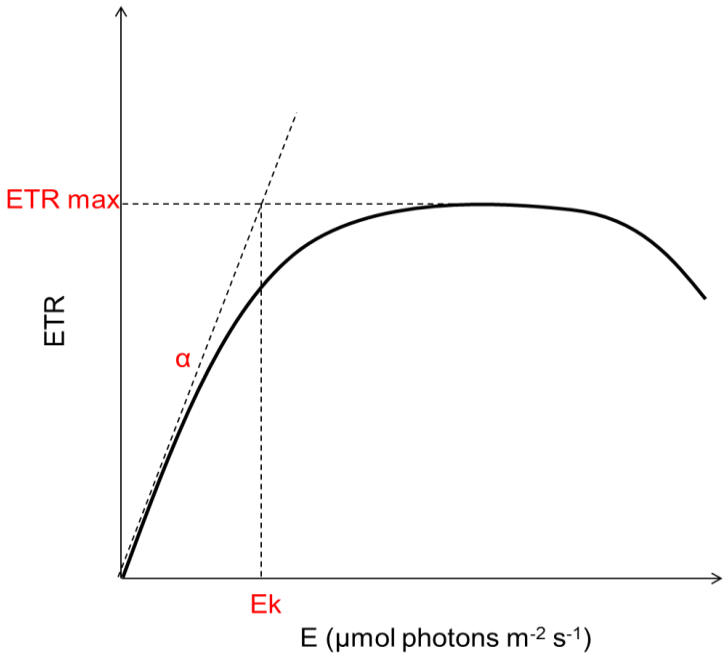

Figure 2.1: Electron transport rate (ETR) *vs.* Light (E) curve

The $_{rel}ETR_{max}$ is the saturated electron transfer rate and E_k represents the light intensity value at which photosynthesis becomes saturated (Fig. 2.1)

2.7 *S. marinoi* absorption spectrum analysis

The analysis of the cells' absorption spectrum was performed on a spectrophotometer Hewlett Packard HP-8453E equipped with an inverted Labsphere integrating sphere (RSA-HP-53 Reflectance Spectroscopy Accessory). 30 mL samples of algal culture were filtered on 25-mm GF/F glass-fiber filter (Whatman™, Buckinghamshire, UK) and the filters were immediately stored in cell culture plates (Corning Inc., NY, USA) in the dark at −20° C. Filters were thawed just prior to analysis and moistened with filtered sea water (FSW), together with a Whatman GF/F blank filter used as blank reference. The filters were then placed on a glass slide and scanned for 4 seconds between 400 and 800 nm with a 1-nm slit

width. The filter absorption, estimated from the spectrum done on the blank Whatman GF/F filter, was removed from the phytoplankton spectrum.

A correction factor of 0.72 was applied on the absorbance values due to the use of Hewlett Packard diodes (as recommended by the Ocean Optics Protocol Version 2.0 - 2000). Before calculating the absorption coefficient, all particulate absorption spectra were corrected for scattering by subtracting the average absorption between 790 and 800 nm from the entire spectrum. Since the strong diffusivity of the filter, the measurements of absorption spectrum need to be corrected by applying a β-correction. To convert the absorption obtained for phytoplankton particles on the filter (A_s) to particles in suspension (A_{sus}), the Tassan and Ferrari equation was applied (Tassan & Ferrari, 1995):

$$A_{sus}(\lambda) = 0.406 \cdot A_s(\lambda) + 0.519 \cdot A^2_s(\lambda)$$

The absorption of particles in suspension was then converted to an absorption coefficient using the relationship of Cleveland and Weidemann (1993).

$$a(\lambda) = 2.3 \cdot A_{sus} \cdot (\lambda) / (V / A)$$

where $a(\lambda)$ is the absorption coefficient (m^{-1}) of particulate organic material at a fixed wavelength, V is the volume of culture filtered (in m^3) and A is the clearance area of the filter (m^2, "clearance rate").

The absorption coefficient $a(\lambda)$ was then transformed to the total absorption coefficient of cells *in vivo* (a) by calculating the mean integrated absorption between 400 and 700 nm (the photosynthetically active radiation, PAR) with the following equation:

$$a = [\Sigma\, a(\lambda_i)] / (700 - 400)$$

Finally, a was divided by cell concentration to obtain the cell-specific absorption coefficient, a^*, expressed in m^2 $cell^{-1}$.

The photosynthetically usable radiation (PUR) was then calculated from the $a(\lambda)$PAR values using the following equation (Morel *et al.*, 1987):

$$PUR = \int_{400}^{700} PAR(\lambda)a(\lambda)d\lambda$$

where, PAR is the photosynthetically active radiation and $a(\lambda)$ is described as the probability that a photon of a given wavelength will be absorbed by the cells, which is derived from the absorption spectrum at the given wavelength (λ).

2.8 Pigments analysis

Pigment analysis was conducted by HPLC (High Performance Liquid Chromatography). An aliquot of algal culture (10 mL) was filtered on GF/F glass-fiber filter (25 mm, Whatman, Maidstone, UK) and immediately stored in liquid nitrogen until further analysis. Pigments were extracted by mechanical grounding during 3 minutes in 1.5 mL of absolut methanol. The homogenate was then filtered onto Whatman 25-mm GF/F filters and the volume of the extract accurately measured.

Prior to injection into the HPLC, 250 µL of an Ion Pairing Agent (ammonium acetate 1 mol L^{-1}, final concentration 0.33 mol L^{-1}) were added to 500 µL of the pigment extract and incubated for 5 minutes in darkness at 4° C. The ion pairing agent was used to increase pigments hydrophobicity in order to obtain a better retainment on the column improving the peaks quality (Mantoura & Llewellyn, 1983).

This extract was then injected in the 50 µL loop of the Hewlett Packard series 1100 HPLC (Hewlett-Packard, Wilmington, NC, USA). The reversed-phase column (2.6 mm diameter C8 Kinetex column; 50 mm × 4.6 mm; Phenomenex®, USA) corresponded to an apolar stationary phase composed of silica beads possessing aliphatic chains of 8 carbon atoms (C8).

The temperature of the column was steadily maintained at 20° C and the flow rate of the mobile phase was set up at 1.7 mL min^{-1}.

The mobile phase was composed of two solvents mixture: A, methanol:aqueous ammonium acetate (70:30, v/v) and B, absolute methanol. During the 12-minutes elution, the gradient between the solvents was programmed: 75% A (0 min), 50% A (1 min), 0% A (8 min), 0% A (11 min), 75% A (12 min).

Pigments were detected at 440 nm using a Hewlett Packard photodiode array detector model DAD series 1100 which gives the 400-700 nm spectrum for each detected pigment. A fluorometer (Hewlett Packard standard FLD cell series 1100) with excitation at 407 nm and emission at 665 nm allowed the detection of fluorescent molecules (chlorophylls and their degraded products). Identification of pigments was carried out according to their retention time and by comparing the on-line-collected pigment spectra with the database established with standards from the D.H.I. Water & Environment (Hørsholm, Denmark). These standards allowed the quantification of the chlorophylls and carotenoids of our interest.

2.9 Cell pellet preparation

Depending on the subsequent analysis, different cells pellet preparations were carried out.

The volume sampled for the antioxidant properties analysis was centrifuged at 3600 g for 15 min at 4°C (DR15P centrifuge, B. Braun Biotech International, Melsungen, Germany); the supernatant was discarded, the pellets were pooled together and centrifuged again in the same conditions. The final pellet was weighed, frozen in liquid nitrogen and then stored at -20°C.

For transcriptional expression analysis cells were centrifuged at 3900 g for 30 min at 4°C. The pellet was subsequently transferred in a 2 mL Eppendorf tubes and centrifuged at 20817 g for 15 minutes at 4 °C (5417R centrifuge, Eppendorf, Hamburg, Germany). TRIzol® Reagent was then added according to the manufacturer's protocol.

For the amino acids, lipids and carbohydrate analysis cells were centrifuged at 3900 g for 30 min at 4°C. For lipids and carbohydrates, the pellets obtained after the centrifugation were pooled together and centrifuged again as previously mentioned and weighed.

For amino acid analysis the pellet was transferred to a 2 mL Eppendorf tube and centrifuged at 20817 g for 15 minutes at 4 °C.

2.10 Ascorbic acid content determination

To assess the ascorbic acid (AsA) content in cells, a modified method from Running *et al.* (2002) was used. In this method the ferric ion is reduced to ferrous ion by AsA. The ferrous ion forms a complex with 2,2'-dipyridyl, producing a red-orange color. The o-phosphoric acid at pH 1-2 was added in order to inhibit other reducing or interfering material, such as glutathione, cysteine, α-tocopherol (Omaye *et al.*, 1979).

Cells were resuspended in 5% trichloroacetic acid (TCA) and sonicated for 1 minute with a micro tip at 20% output on ice (S-250A Branson Ultrasonic). Cell debris were precipitated by centrifugation at 5000 g for 5 min at 4°C and the supernatant was used for the colorimetric analysis.

The color reagent was composed by 4 parts of 0.5% 2,2'-dipyridyl and 1 part of 8.3 mM ferric ammonium sulfate in 15% (v/v) o-phosphoric acid. The two components were mixed immediately before use. Then, one part of cell extract and five parts of the color reagent were mixed. After one hour the absorbance was read at 520 nm. AsA concentration was calculated by comparison with AsA standards.

2.11 Preparation of the methanolic extracts

Cells were re-suspended in methanol and sonicated for 1 minute with a micro tip at 20% output on ice (S-250A Branson Ultrasonic). The suspension was left 30 min at room temperature in the dark, and then was centrifuged at 3060 g for 10 min at 4°C. Supernatant was collected and the pellet was re-suspended in an equal volume of methanol and left other 30 min at room temperature in the dark. The suspension was centrifuged again in the same conditions, and the two supernatants were combined.

Depending on the experiments, the methanolic extract was directly used for the analysis, otherwise the solvent was removed from the extract through a rotary evaporation and the air in the vial was replaced by nitrogen gas to avoid subsequent oxidation processes, weighted and stored at -20°C.

These samples were used for the determination of 2,2'-azino-bis (3-ethylbenzothiazoline-6-sulphonic acid) (ABTS) radical scavenging activity, 2,2-diphenyl-1-picrylhydrazyl (DPPH) radical scavenging activity, total phenolic content (TPC) and total flavonoid content (TFC) (see below).

2.12 Total phenolic content

Total phenolic content (TPC) was estimated by the Folin-Ciocalteu method (Singleton & Rossi, 1965).

Polyphenols in plant extracts react with specific redox reagents (Folin-Ciocalteu reagent) to form a blue complex that can be quantified by visible-light spectrophotometry.

The reaction forms a blue chromophore constituted by phosphotungstic-phosphomolybdenum complex where the maximum absorption of the chromophores depends on the alkaline solution and the concentration of phenolic compounds.

The total phenolic content was evaluated following the method by Li and collaborators (Li *et al.*, 2007). Briefly, 200 µL of the sample was mixed with 1 mL of Folin-Ciocalteu's phenol reagent, pre-diluted in distilled water 1:10 v/v. After 4 minutes, 800 µL of Na_2CO_3 75 g/L were added to the mixture, shacked vigorously and left 2 hours at room temperature. The absorbance was read at 765 nm. Gallic acid was used for the standard calibration curve. The results were expressed in fg of gallic acid equivalents (GAEq) $cell^{-1}$.

Even though this classic method is largely used for phenolic compounds quantification (the procedure developed by Singleton & Rossi (1965) has being cited in scientific papers more than 5500 times) (Sanchez-Rangel *et al.*, 2013), the reactivity of Folin-Ciocalteu reagent towards other antioxidants common in plants, such as vitamins and thiols might be a bias (Everette *et al.*, 2010). Yet, it has been shown that ascorbic and dehydroascorbic acids have the highest impact on hampering the accuracy of the assay (Sanchez-Rangel *et al.*, 2013). Therefore, the lack of exclusive specificity of this assay towards phenolic compounds has to take into consideration when interpreting the results.

2.13 Total flavonoid content

The total flavonoid content was estimated by aluminium chloride ($AlCl_3$) colorimetric method (Lamaison & Carnet, 1990). $AlCl_3$ forms acid stable complexes with the C-4 keto groups and either the C-3 or C-5 hydroxyl group of flavones and flavonols. It also forms acid labile complexes with the orthodihydroxyl groups in the A- or B-ring of flavonoids.

Briefly, 600 µl of sample pre-diluted1:2 v/v in methanol 80% v/v, were mixed with an equal volume of $AlCl_3$ 2%. The mix was shaken and left 1 hour at room temperature. The absorbance was read at 410 nm. Quercetin was used for the standard calibration curve. The results were expressed in fg of quercetin equivalents (QEq) $cell^{-1}$.

2.14 ABTS radical scavenging activity

The antioxidant activity was assessed by the 2,2'-azino-bis (3-ethylbenzothiazoline-6-sulphonic acid) (ABTS) radical scavenging activity assay. The assay relies on the antioxidant capability of the samples to reduce the blue/green $ABTS^{\bullet+}$ chromophore, a stable radical cation, to ABTS.

The scavenging activity of ABTS radical was measured following Xia *et al.* (2013). The ABTS free radical was generated by mixing 7 mM ABTS diammonium salt with 2.45 mM potassium persulphate and left it overnight at room temperature. The solution was diluted with methanol till the absorbance at 734 nm reached 0.70 ± 0.01 units.

Then one part of sample was mixed with three parts of ABTS radical solution. The mix was shaken and left 1 hour at room temperature in the dark. The absorbance was read at 734 nm. Ascorbic acid was used for the standard calibration curve. The results were expressed in fg of ascorbic acid equivalents (AEq) $cell^{-1}$.

2.15 DPPH radical scavenging activity

This method is based on the antioxidant capability of the sample to reduce the stable free radical α, α-diphenyl-β-picrylhydrazyl (DPPH). The odd electron of nitrogen atom in

DPPH is reduced by receiving a hydrogen atom from the antioxidant to the corresponding hydrazine (Kedare & Singh, 2011). Thanks to the delocalization of the spare electron all over the molecule, the radical form has a deep violet color with a maximum absorption at 517 nm. Its reduced form instead loses this color. The resulting de-colorization is stoichiometric with respect to number of electrons captured.

Briefly, 0.16 mM of methanolic DPPH solution was added to the sample (1:1 v/v). The mix was shaken vigorously and left 1 hour at room temperature in the dark. The absorbance was measured at 517 nm. Ascorbic acid was used for the standard calibration curve. The ability to scavenge the DPPH radical was expressed in fg of ascorbic acid equivalents (AEq) $cell^{-1}$.

2.16 Antioxidant enzyme activity and protein content determination

Frozen microalgal pellets were resuspended in extraction buffer (50 mM potassium phosphate buffer pH 7.8, 0.1 mM EDTA, 150 mM NaCl, 2 µg/mL Leupeptin, 0.1 mM PMSF) and sonicated for 1 minute with a micro tip at 20% output on ice (S-250A Branson Ultrasonic). Cell debris was precipitated by centrifugation at 3060 g for 15 min at 4°C. The supernatant was transferred to a new tube and used in antioxidant enzyme activity assays and proteins quantification.

2.16.1 Protein content

The protein content was determined according to Lowry *et al.* (1951). The sample was pre-treated with copper ion in alkali solution. The aromatic amino acids in the treated sample reduce the phosphotungstic-phosphomolybdate acid present in the Folin Reagent. The end product of this reaction has a blue colour.

Briefly, 100 volumes of an alkaline solution of Na_2CO_3 2% in NaOH 0.1 N were mixed with 1 volume of $CuSO_4$ $5H_2O$ 0.5% and 1 volume of potassium tartrate 1%. The sample and the working solution were mixed (1:10 v/v) and left 10 minutes at room temperature in the dark. The Folin-Ciocalteu's phenol reagent pre-diluted in sterile water (50% v/v) was

then added to the reaction mixture (1:12 v/v). After 30 min at dark, the absorbance was read at 700 nm. Bovine serum albumin (BSA) was used for the standard calibration curve.

2.16.2 Catalase activity

The catalase (CAT) activity was assayed according to the procedure described by Aebi (1984). This method is based on the spectrophotometric measurement of the rate of disappearance of H_2O_2.

Briefly, the sample was mixed with 50 mM potassium phosphate buffer pH 7.0, then 10 mM H_2O_2 was added in the cuvette and the absorbance was read at 240 nm (ε = 46,6 M^{-1}). cm^{-1}) for 180 s at 25°C. Results were expressed as µmol H_2O_2 consumed per minute per mg of proteins.

2.16.3 Ascorbate peroxidase activity

Ascorbate peroxidase (APX) activity was evaluated according to Janknegt *et al.* (2009), by tracking the changes in absorbance at 290 nm for 180 s at 25°C of the ascorbate substrate (ε = 2.8 mM^{-1} cm^{-1}) in a reaction mixture composed of 50 mM potassium phosphate buffer (pH 7.0), 0.5 mM ascorbate , 0.2 mM H_2O_2 and the sample. APX activity was expressed as µmol of ascorbic acid consumed per minute per mg of protein.

2.16.4 Superoxide dismutase activity

Superoxide dismutase (SOD) activity assay was performed according to McCord and Fridovich (1968). In this method the enzyme xanthine oxidase (XOD) reacts with its substrate, the hypoxanthine, producing xanthine and subsequently uric acid, generating a superoxide anion (O^{2-}). This species reduces the cytochrome c that, in the reduced form, absorbs energy at 550 nm. The SOD competes with cytochrome c for O^{2-}, lowering the amount of reduced cytochrome c.

The blank reaction mixture was composed of 0.1 M potassium phosphate buffer (pH 7.8), 100 µM hypoxanthine, and 20 µM cytochrome c.

For activity determination of the diatoms extract, different volumes of the sample (V_{sample}) were added to the reaction mixture till an inhibition (I) between 45% and 65% of

cytochrome c reduction was reached (Janknegt *et al.*, 2007). The volume needed to obtain 50% inhibition (V_{50}) was calculated as follow:

$$V_{50} = V_{sample} * \frac{50\%}{I}$$

Specific activity (SA) was then calculated using the following equation:

$$SA = \frac{1}{V_{50} * [protein]}$$

2.16.5 Glutathione reductase activity

The glutathione reductase (GR) activity assay was performed following Janknegt *et al.* (2009). The assay is based on the catalytic property of GR to convert the oxidized GSSG into its reduced form GSH, using NADPH as a reducing agent. NADPH consumption is measured at 340 nm (ε = 6.22 mM^{-1} cm^{-1}) for 180 sec at 25°C. The reaction mixture was composed of 50 mM potassium phosphate buffer (pH 7.0), 1 mM GSSG, 83 µM NADPH, and the sample. GR activity was expressed as µmol of NADPH consumed per minute per mg protein.

2.17 Gene expression analysis

The molecular analysis was done in collaboration with Dr. Ida Orefice, post-doctoral student in our research group. I collaborated with her in the analysis and interpretation of the results obtained.

2.17.1 RNA extraction and reverse transcription

The total RNA has been extracted from the pellet following the procedure described in Barra *et al.* (2013). DNase treatment was carried out using DNase I recombinant, RNase-free (Roche, Basel, Switzerland) according to the manufacturer's protocol to eliminate potential genomic DNA contamination. Total RNA sample was purified and concentrated using RNeasy MinElute Cleanup Kit (Qiagen, Venlo, Netherlands) and eluted in 20 µL RNase-free water. Concentration of the resulting RNA samples was assessed by absorbance at 260 nm (ND-1000 Spectrophotometer; NanoDrop Technologies, Wilmington, DE, USA). The integrity of total RNA was checked by agarose gel electrophoresis. From each RNA sample, 1 µg were retro-transcribed in complementary DNA (cDNA) with the iScriptTM cDNA synthesis kit (Bio-Rad Laboratories, Hercules, CA, USA), following the manufacturer's instructions, using the T100 Thermal cycler (Bio-Rad Laboratories, Hercules, CA, USA).

2.17.2 Best reference genes assessment

In order to analyse expression levels of specific genes of interest, a panel of putative reference genes, previously tested in Orefice *et al.* (2015), was first analysed to find the most stable genes in our conditions. The candidate reference genes where histone 4 (*H4*), α- and β-tubulin (*TUB A* and *TUB B*), TATA-binding protein (*TBP*), elongation factor 1α (*EF1a*), glyceraldehyde-3-phosphate dehydrogenase (*GAPDH*), cyclin dependent kinase (*CDK*), ribosomal protein small subunit 30S (*RPS*), actin (*ACT*) and ubiquitin (*UB*).
Three different algorithms were utilized to identify the best reference genes in our experimental design: BestKeeper (Pfaffl *et al.*, 2004); NormFinder (Andersen *et al.*, 2004) and geNorm (Vandesompele *et al.*, 2002).

2.17.3 Primer design and reverse transcription-quantitative PCR (RT-qPCR)

Primers were designed using Primer3 program V. 0.4.0 considering the putative sequences reported in the *S. marinoi* transcriptome (Cod MMETSP1039) deposited in the public database iMicrobe (http://data.imicrobe.us/project/view/104). RT-qPCR was performed in

MicroAmp Optical 384-Well reaction plate (Applied Biosystems, Foster City, CA, USA) with Optical Adhesive Covers (Applied Biosystems, Foster City, CA, USA) in a Viia7 Real Time PCR System (Applied Biosystem, Foster City, CA, USA). Serial dilutions of cDNA were used to determine primer reaction efficiency (E) and correlation factor. Standard curves were generated with five dilution points by using the cycle threshold (Ct) value versus the logarithm of each dilution factor and the equation $E=10^{-1/slope}$. The PCR volume for each sample was 10 µL, with 5 µL of Fast Start SYBR Green Master Mix with ROX (Roche, Basel, Switzerland), 1 µL of cDNA template (1:50 template dilution) and 0.7 pmol/µL for each primer. The RT-qPCR thermal profile was obtained using the following procedure: 95 °C for 20 seconds, 40 cycles of 95 °C for 1 second and 60 °C for 20 seconds. The program was set to reveal the melting curve of each amplicon from 60 °C to 95 °C, and read every 0.5 °C. Single peaks for all genes confirmed gene-specific amplification and the absence of primer-dimers. All RT-qPCR reactions were carried out in triplicate to capture intra-assay variability. Each assay included three no-template negative controls for each primer pair. To study the expression levels for each gene of interest relative to the most stable reference genes, the REST tool (Relative Expression Software Tool, (Pfaffl *et al.*, 2002) was used. Statistical analysis was performed using the Pair Wise Fixed Reallocation Randomisation test by REST.

2.18 Nutrients concentration determination

The nutrient concentrations in culture media were determined using a Technicon AutoAnalyzer following classical methods (Grasshoff *et al.*, 2009).
Aliquots (10 mL) of cell culture were collected, filtered on GF/F glass-fiber filter (25 mm, Whatman, Maidstone, UK) and the media stored in polyethylene vials immediately frozen and stored at -20°C.

Ammonium, nitrate, nitrite, silicic acid and phosphate concentration analysed from the morning sample (dawn) of each experiment was used to estimate the daily uptake of nutrients per cell calculated using the following equation:

$$Nu = \frac{(N_2 - N_1)}{(C_2 - C_1)}$$

where, Nu is the nutrient uptake expressed in nmol cell^{-1} day^{-1}, C_n is the cell concentration at day n and N_n is the nutrient concentration at day n.

2.19 Macromolecular composition analysis

The macromolecular composition analysis was performed in the first experiment on light-induced changes in the photosynthetic physiology and biochemistry (see Chapter 3). All the following assays were done by external collaborators. I participated in the interpreation of the results obtained.

2.19.1 Amino acids analysis

The analysis of the amino acid content was done by Dr. Fabrizio Dal Piaz, from the University of Salerno (Italy).

The total proteins from the pellet was extracted by sonication for 2.4 minutes in 600 µL of sterile water and centrifuged at 13000 rpm (17949 g) for 20 minutes at 4 °C. Then the supernatant was collected and the pellet was re-extracted with 500 µL of 0.1 N NaOH and 0.5% β-mercaptoethanol (v/v). The mixture was kept at RT for 1 hour (with occasional shaking) and centrifuged at 13000 rpm (17949 g) for 20 minutes at 21 °C. The supernatant was mixed and the pellet was discarded. Proteins were then purified with trichloroacetic acid (TCA) before acid hydrolysis for amino acids analysis, according to Barbarino & Lourenço (2005) and the crude extract has been quantified with Folin-Ciocalteu's phenol reagent.

Samples containing 50 µg of protein were acid hydrolysed with 1 mL of 6 N HCl in vacuum-sealed hydrolysis vials at 110 °C for 22 hours. Norleucine was added to the HCl as an internal standard. Although tryptophan was completely lost with acid hydrolysis and methionine and cysteine + cystine could be destroyed to varying degrees by this procedure, the hydrolysates were suitable for analysis of all other amino acids. The tubes were cooled

after hydrolysis, opened, and placed in a dessicator containing NaOH pellets under vacuum until dry (5–6 days). The residue was then dissolved in a suitable volume of dilution Na–S R buffer (pH 2.2; Beckman Instr.), filtered through a Millipore membrane (0.22 µm pore size) and analysed for amino acids by ion-exchange chromatography in a Beckman, model 7300 instrument equipped with an automatic integrator.

2.19.2 Lipid and fatty acids analysis

The lipid and fatty acids analysis was done by Dr. Tonino Caruso, from the University of Salerno (Italy).

Each wet pellet was sonicated for 15 minutes at 25 °C in 10 mL of acetic acid / chloroform (1 / 9), or acetone / methanol (9 / 1) or pure methanol in order to get respectively triglyceride, glycolipid or phospholipid fraction. The extracted solution is passed through cartridges Supelclean™ ENVI-Florisil® SPE Tubes (by Aldrich), pre-conditioned with 30 mL of chloroform (Popovich *et al.*, 2012). The samples were subsequently concentrated under N_2 flux to reach a final volume of 1 mL and esterified with 2M KOH in methanol according to Graziani *et al.* (2013). 1 µL was directly injected in a Thermo Finnigan TRACE gas chromatograph equipped with a fused silica capillary column (FAMEWAX Restek, 30 m × 0.25 mm i.d., 0.25 µm film thickness) and a FID detector. The calibration has been performed using a standard PUFA's (by Supelco) as internal standard.

The degree of unsaturation (DU) is calculated using the following formula as reported in Ramos *et al.* (2009):

DU = (monounsaturated Cn : 1, wt%) + 2 × (polyunsaturated Cn : 2, 3, wt%)

2.19.3 Carbohydrate analysis

The carbohydrate analysis was done by Dr. Maria Michela Corsaro, from the University of Naples Federico II (Italy)

The pellets obtained for carbohydrate analysis were sonicated for 5 minutes in 5 mL of F/2 culture medium and centrifuged. The supernatant and the cellular debris pellet are stored separately for the analysis. Total carbohydrates content, calculated on both supernatant and pellet of each sample, is determined by microphenol assay as reported in Kobata (1972).

2.20 Statistical analysis

All the experiments were conducted in triplicate in order to capture random biological variation. For some analysis, technical replicates were performed in order to establish the variability of the analysis technique.

Calculations of mean, standard deviation, variance, coefficient of variation (CV), Student's t-test for mean comparison, Pearson linear correlation, Spearman rank correlation, analysis of variance (ANOVA), Tukey test for multiple comparisons, and principal component analysis (PCA) on correlation matrix were performed using the PAST software package, version 3.10 (Hammer *et al.*, 2001).

3. Light-induced changes in the photosynthetic physiology and biochemistry in the diatom *Skeletonema marinoi*

3.1 Introduction

In this chapter, I present a study aiming to investigate the effects of light distribution, together with spectral light composition variations, on cell growth, physiology and metabolic performances.

Chandrasekaran *et al.* (2014) demonstrated that the optimal light condition for growth of the coastal diatom *Skeletonema marinoi* was a blue sinusoidal light course with a midday peak of 130 µmol photons m^{-2} s^{-1}. This condition also provided the best physiological state and synthesis of primary metabolites such as carbohydrates, lipids and proteins.

The un-stressful nature of this light condition was demonstrated also by the low content of the xanthophyll cycle pigments, key players of the short-term photoprotective response to light stress (see chapter 1). In a pelagic ecosystem this light regime corresponds approximately to 40 meters depth, but diatoms, for their planktonic nature, constantly move along the vertical gradient due to the mixing to which the water column is subject (see chapter 1). They can rapidly reach the surface layer characterized by the presence of red light and suddenly sink again to the blue dominant deeper layer.

Indeed, microalgae are naturally adapted to the highly fluctuating light regime activating photodefence mechanisms such as the non-photochemical quenching (NPQ) and xanthophyll cycle (XC), adjusting their metabolism accordingly (Su *et al.*, 2012).

Being the light responsible for the change in the carbon allocation patterns (Jakob *et al.*, 2007, Jungandreas *et al.*, 2014), also the macromolecular content is expected to change in response to the different light regime to which the cells are acclimated to. This feature is particularly important since diatoms can be employed in many industrial applications for the production of high added value products such as polyunsaturated fatty acids, polysaccharides, vitamins (Pulz & Gross, 2004, Borowitzka, 2013, Barra *et al.*, 2014).

In order to support a cost effective production of diatoms' derived products, there is the need to understand the physiology and growth characteristic of these organisms in response to the different environmental stimuli. This knowledge can finally lead to an optimization of their cultivation and thus to a sustainable production of microalgal-derived products.

The hypothesis behind this study is that a fluctuating light regime constituted by a sinusoidal blue light course with the superimposition of red-blue light peaks determines an increased activation of the xanthophyll cycle pigment synthesis, and a change in the macromolecular composition of the cells.

Two different fluctuating light profiles were compared to the sinusoidal blue light course (with a peak of 150 µmol photons m^{-2} s^{-1}): three and nine superimposed red light peaks. The red wavelength was selected in order to investigate the biological effects of the mixed red + blue light compared to the monochromatic blue. Furthermore, the red light is less energetic than blue light being less absorbed, by consequence the superimposition of red light allows the study of a fluctuating light regime preventing the photoinhibition caused by an excess of instantaneous light experienced by cells.

Currently, the most used illumination system for indoor microalgal cultivation is an on/off system, so a square-wave light course: from the dark, light is suddenly turned on and kept constant during the diurnal phase, so cells are exposed to the maximal photon flux density (PFD) all day long. This condition is far from the natural one, where the cells experience a gradual light increase from dawn to midday, and then a decrease from midday to sunset.

Thus, in this study, we wanted to test the hypothesis that a sinusoidal light course that mimics the natural environment allows cells to efficiently cope with PFD variation with a probable match between physiological processes induced by light increase and the light increase itself. Microalgae should progressively acclimate to the increasing light regulating their photosynthetic machinery. The square-wave light course instead should represent a stressful condition that causes an impairment of the daily-regulated cell processes for coping with light climate in an efficient way. As consequence of the impairment of the normal cell functioning, part of the biochemical energy from the photosynthetic reactions is diverted in repairing processes and activation of defense mechanisms against oxidative stress (Snoeijs *et al.*, 2012). For this reason we compared the sinusoidal blue light *vs.* the square-wave blue light course, both with a maximal PFD equal to 150 µmol photons m^{-2} s^{-1}, but a different integrated daily light dose caused by the different daily distribution.

The results obtained from this experiment correspond to a paper published in 2016 (Orefice, I., Chandrasekaran, R., Smerilli, A., Corato, F., Caruso, T., Casillo, A., Corsaro,

M. M., Dal Piaz, F., Ruban, A. V. & Brunet, C. 2016. Light-induced changes in the photosynthetic physiology and biochemistry in the diatom *Skeletonema marinoi*. Algal Research 17:1-13).

3.2 Materials and methods

3.2.1 Experimental strategy and sampling

Experiments were conducted on *Skeletonema marinoi*, cultured in 4.5 L glass flasks with air bubbling (see chapter 2). All the experiments were performed in triplicate and lasted one day during the exponential growth phase on cells pre-acclimated to each experimental condition for at least two weeks before the experiment.

Four light conditions were tested, each with a 12:12 h light:dark photoperiod. The control condition (Con) corresponded to a sinusoidal blue light course with a midday peak equal to 150 µmol photons m^{-2} s^{-1} (Fig. 3.1 a).

To this condition, fluctuating red light peaks were superimposed with two procedures: 3 Red Peaks and 9 Red Peaks (Fig. 3.1 b, c). Each superimposed red peak lasted 40 minutes and was setup with a red:blue ratio of 1.

The fourth condition was a blue square-wave light course (Quad; Fig. 3.1 d). Sampling was done three times during the day: dawn (0h, before the light phase), midday (6h after the start of the light phase), and afternoon (9h after the start of the light phase).

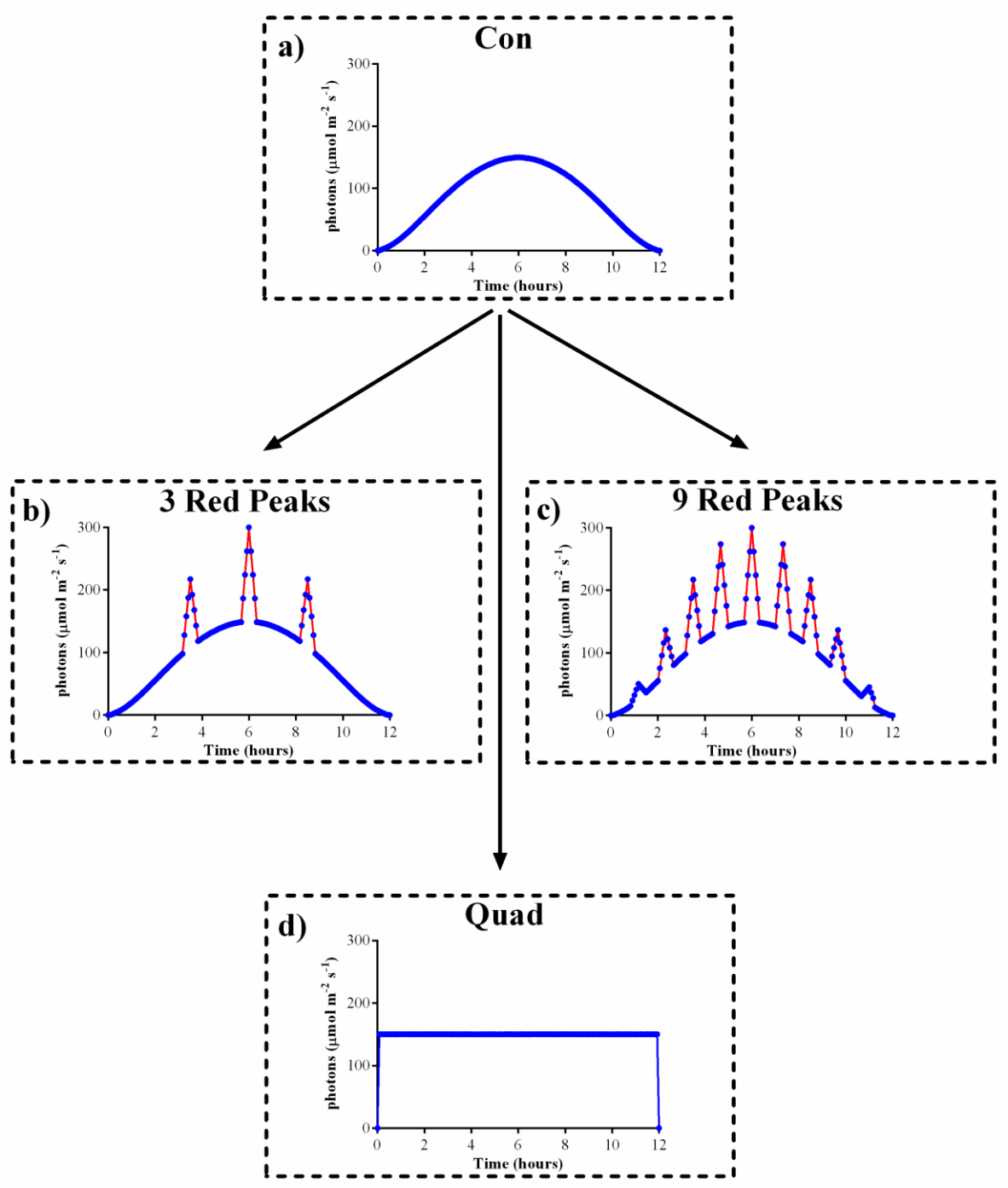

Figure 3.1: Experimental light conditions: a) the blue sinusoidal light course peaking at a photon flux density of 150 µmol m^{-2} s^{-1} (Con); b) the 3 fluctuating red light peaks superimposed upon the control light (3 Red Peaks); c) the 9 fluctuating red peaks superimposed upon the control light (9 Red Peaks); d) the blue square-wave light course (Quad, photon flux density = 150 µmol m^{-2} s^{-1}).

3.2.2 Parameters analyzed

The following parameters were tested:

- Cell concentration
- Photochemical efficiency of the photosystem II
- Electron transport rate (ETR)-light curves
- Non-photochemical quenching (NPQ)
- Pigments
- Absorption spectra
- Gene expression analysis of antioxidant enzymes:
  - Glutathione peroxidase (*GPX*)
  - Glutathione reductase (*GR*)
  - Catalase (*CAT*)
  - Superoxide dismutase (*SOD*)
  - Ascorbate peroxidase (*APX*)
- Gene expression analysis of genes related to carotenogenesis:
  - Phytoene desaturase (*PDS*)
  - Lycopene β-cyclase (*LCYB*)
  - Lutein deficient protein (*LUT*)
  - Zeaxanthin epoxidase 1 and 2 (*ZEP1* and *ZEP2*)
  - Violaxanthin de-epoxidase (*VDE*)
- Protein and amino acid analysis[§]
- Lipid and fatty acid analysis[§]
- Carbohydrate analysis
- Statistical analysis

The experimental procedures for each of these parameters are described in the chapter 2.

[§]Data on amino acids and lipids are missing for the dawn sampling time in the sinusoidal blue light course.

3.3 Results

3.3.1 Growth properties and integrated daily light dose

The daily light dose was different between the experiments: 3.66 mol $m^{-2}d^{-1}$ for the control condition (Con), 4.10 mol $m^{-2}d^{-1}$ for the 3 red peaks condition, 4.65 mol $m^{-2}d^{-1}$ for the 9 red peaks condition and 6.95 mol $m^{-2}d^{-1}$ for the square-wave light course (Quad; Tab. 3.1).

Table 3.1 Photosynthetic properties and growth rate of *Skeletonema marinoi* under the four light conditions. At the exception of light, data represent means ±SD of the three sampling times (dawn, midday and afternoon, n=9). Daily light dose (mol $m^{-2}d^{-1}$); mean daily light dose (=mean instantaneous irradiance averaged over 12 hours illumination period, mmol $m^{-2}s^{-1}$); daily red light dose (mol $m^{-2}d^{-1}$); growth rate (μ, d^{-1}); $a^* \times 10^{-11}$ (cell-specific absorption coefficient, m^2 $cell^{-1}$); PUR × 10^{-6} (photosynthetically usable radiation, μW $cell^{-1}$); $_{rel}ETR_{max} \times 10^{-6}$, (maximal relative rate of linear electron transport, pmol e^{-1} h^{-1} $cell^{-1}$); α [maximum light use efficiency, pmol e^{-1} h^{-1} $cell^{-1}$ (μmol photon m^{-2} s^{-1}) $^{-1}$]; Ek (light saturation index for photosynthesis, μmol photon m^{-2} s^{-1}); Fv/Fm (maximum quantum yield of PSII); NPQ (non-photochemical quenching); DES [de-epoxidation state = Dt/(Dd + Dt)].

Light Condition	Con	3 Red Peaks	9 Red Peaks	Quad
Daily Light dose	3.66	4.10	4.65	6.95
Mean light intensity	0.08	0.09	0.11	0.16
Daily Red dose	0	0.44	0.99	0
μ	0.45 ± 0.04	0.47 ± 0.06	0.50 ± 0.05	0.65 ± 0.08
*a**	3.52 ± 0.17	2.88 ± 0.07	1.72 ± 0.18	2.00 ± 0.60
PUR	1.90 ± 0.18	1.80 ± 0.15	1.85 ± 0.14	1.30 ± 0.22
$_{rel}ETR_{max}$	20.40 ± 3.71	18.77 ± 5.04	13.93 ± 4.71	15.03 ± 6.57
α	0.046 ± 0.004	0.036 ± 0.003	0.014 ± 0.004	0.028 ± 0.006
Ek	254 ± 15	363 ± 56	464 ± 17	457 ± 56
Fv/Fm	0.64 ± 0.01	0.71 ± 0.02	0.76 ± 0.05	0.67 ± 0.06
NPQ	0.11 ± 0.03	0.19 ± 0.03	0.51 ± 0.11	0.13 ± 0.05
DES	0.096 ± 0.001	0.210 ± 0.005	0.270 ± 0.005	0.360 ± 0.004

During the exponential phase, the growth rate measured increased linearly with the daily light dose, independently on how the light was provided (sinusoidal, fluctuating, or square wave distribution; $p<0.01$; Fig. 3.2 a).

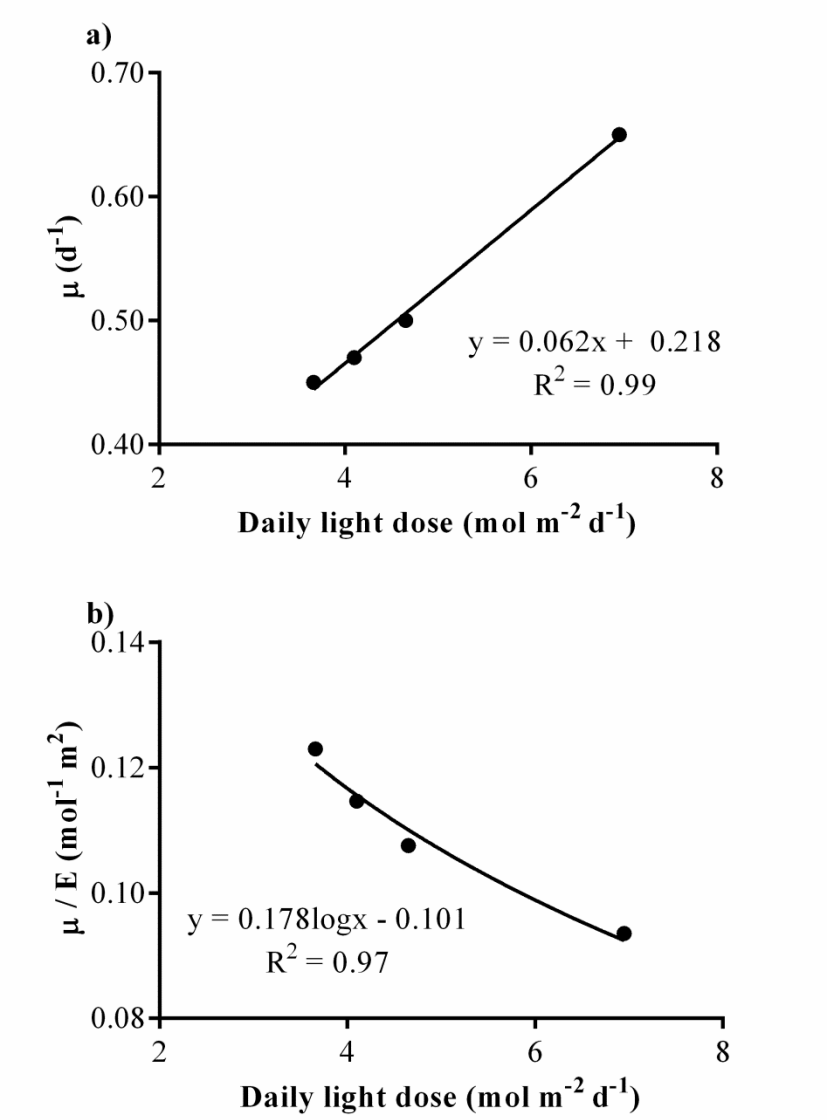

Figure 3.2: Growth – light relationships. a) Correlation between growth rate during the exponential phase (μ, d^{-1}) and the daily light dose (mol m^{-2} d^{-1}); b) Correlation between the quantum yield of growth (μ/E, in mol^{-1} m^{-2}) and the daily light dose (mol m^{-2} d^{-1})

By contrast, the quantum yield of growth (μ/E) was inversely correlated with the daily light dose ($p < 0.01$; Fig 3.2b), revealing a higher efficiency of biomass increase rate per mol of photons in lower daily light dose conditions.

3.3.2 Biological responses to fluctuating red light superimposed upon sinusoidal blue light

In this section, I report the data comparison between the three sinusoidal-based light courses with the aim to investigate the effects on fluctuating red light superimposed upon blue light on the algae performance and metabolic state.

3.3.2.1 Physiological parameters

The maximum quantum yield of PSII in the dark (Fv/Fm) was high in all the conditions (>0.65; Tab. 3.1), but to the increase of the daily light dose corresponded a decrease of the PSII electron transport rate (ETR; $p<0.01$), the cell-specific absorption capacity (*a**; $p<0.01$) and the quantum yield of growth ($p<0.01$; Tab. 3.1).

Intriguingly, ETR followed an inverse trend compared to the growth rate ($p<0.01$).

To an increase of the maximum light use efficiency (α) between the three experimental conditions, corresponded a decrease of the photosynthetic light saturation index (E_k) (Tab. 3.1).

The photosynthetic usable radiation (PUR) did not change between the different experimental conditions, meaning that cells were able to finely regulate the absorption of energy.

Both the Chl.*a* and Chl.*c* contents were almost unaffected under the 3 Red Peaks with respect of control, even though Chl.*c* showed a slight decrease (Fig. 3.3 a, b). Under the 9 Red Peaks instead the two pigments showed a significant decrease (Fig. 3.3 a, b). The main accessory pigment fucoxanthin (Fuco) did not vary among the experiments (Fig. 3.3 c).

Only in the control condition a significant correlation was found between Chl.*c* content and non-photochemical quenching (NPQ, $p<0.01$, $n=9$) as already reported for a different diatom by Brunet *et al.* (2014). Fluctuating red lights superimposed upon sinusoidal blue light induced an increase in NPQ (Tab. 3.1).

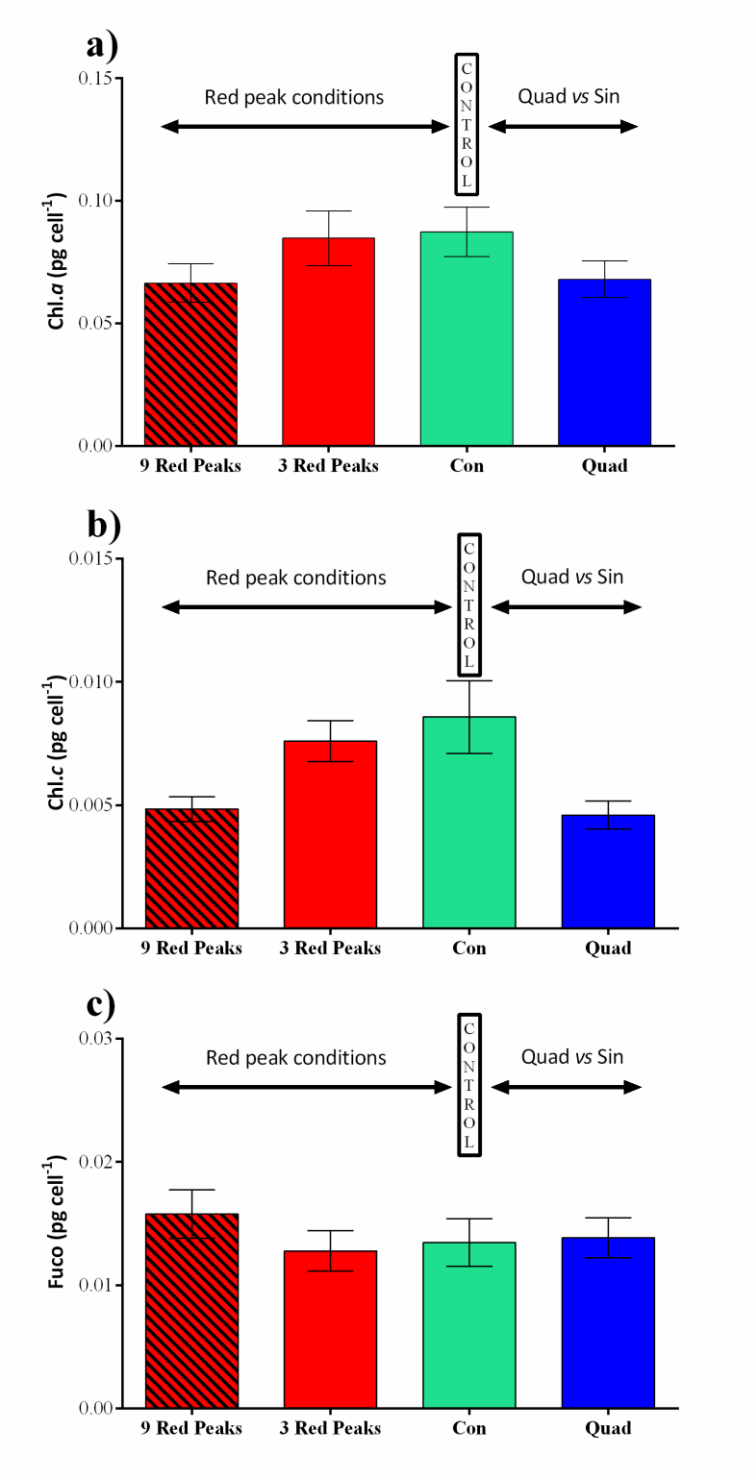

Figure 3.3: Photosynthetic pigment content. a) chlorophyll a content (Chl.*a*, pg cell^{-1}), b) chlorophyll c content (Chl.*c*, pg cell^{-1}) and c) fucoxanthin content (Fuco, pg cell^{-1}) under the four light conditions: Con, 3 Red Peaks, 9 Red Peaks and Quad. Data represent means ±SD of the three sampling times (dawn, midday and afternoon, n=9).

NPQ was significantly correlated with the activation of the xanthophyll cycle: it showed a positive relation both with Dt ($p<0.01$, $n=9$) and the de-epoxidation state (DES, $p<0.01$, $n=9$).

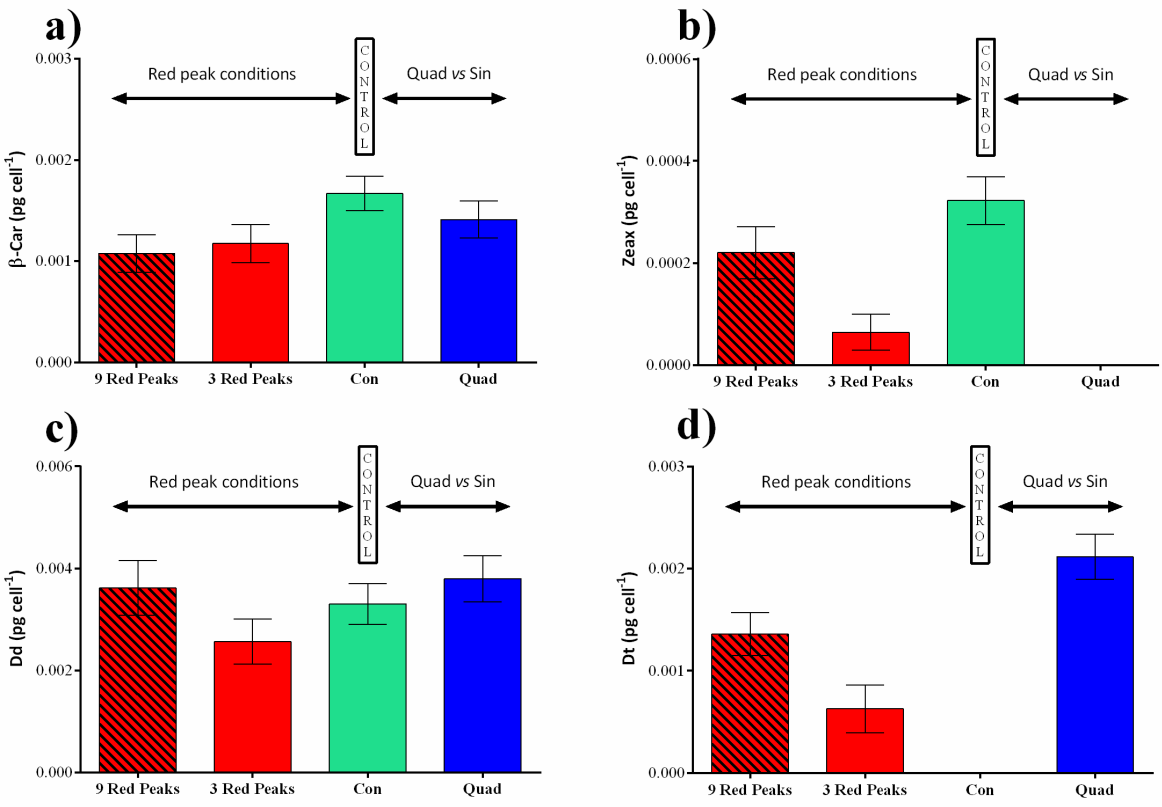

Figure 3.4 Xanthophyll cycle and precursors' pigments content: a) β-carotene content (β-Car, pg cell^{-1}), b) zeaxanthin content (Zeax, pg cell^{-1}), c) diadinoxanthin content (Dd, pg cell^{-1}) and d) diatoxanthin content (Dt, pg cell^{-1}) under the four light conditions: Con, 3 Red Peaks, 9 Red Peaks and Quad. Data represent means ±SD of the three sampling times (dawn, midday and afternoon, n=9).

The sum of Dt and Dd was similar between Con and 3 Red Peaks (0.0032 ± 0.0003 pg cell^{-1}), while it increased in 9 Red Peaks. The Dt was not detected in Con, and its concentration increased linearly with the daily light dose (Fig. 3.4 d). The Dd concentration was almost stable; only in 3 Red Peaks is observed a slight decreased in favor of its conversion into Dt (Fig. 3.4 c). The *de-novo* synthesis of Dd in 9 Red Peaks was responsible for the increased sum (Dt + Dd).

The precursors of the XC pigments, β-carotene (β-Car) and zeaxanthin (Zeax), were higher in Con relatively to the other sinusoidal light conditions (Fig. 3.4 a, b), suggesting a significant effect of red light on the synthesis or use of these pigments. The β-Car per cell

showed a significant decrease when red light was superimposed upon blue light compared to the Con condition (Fig. 3.4 a), suggesting a red light effect on the modulation of the β-Car content. Indeed, β-Car cell^{-1} decreased only a little between 3 and 9 Red Peaks although the relevant difference in daily light dose. Interestingly, the sum (β-Car + Zeax) was constant between the 3 and 9 Red Peaks condition with the increase of Zeax compensating for the decrease of β-Car under the 9 Red Peaks.

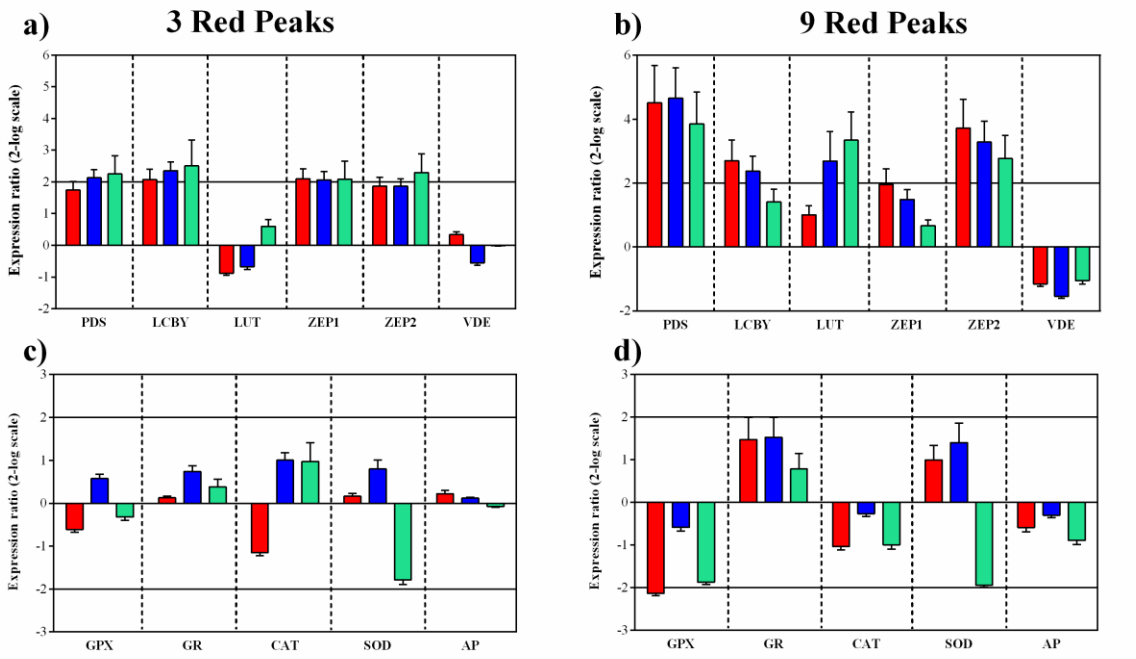

Figure 3.5 Transcriptional expression analysis of carotenoid or antioxidant genes in the red+blue light conditions: a) carotenoid genes under 3 Red Peaks, b) carotenoid genes under 9 Red Peaks, c) antioxidant genes under 3 Red Peaks, d) antioxidant genes under 9 Red Peaks. Samples were collected at dawn (red bar), midday (blue bar) and afternoon (green bar). Data are reported as fold difference (mean ±SD, n=3) compared to control (blue sinusoidal light with PFD peaking at 150 µmol m^{-2} s^{-1}). Fold differences greater than ±2 (see horizontal guidelines at values of 2 and -2) were considered significant. Phytoene desaturase (PDS), lycopene beta cyclase (LCYB), lutein deficient protein (LUT), zeaxanthin epoxidase 1 and 2 (ZEP1 and ZEP2), violaxanthin de-epoxidase (VDE), glutathione peroxidase (GPX), glutathione reductase (GR), catalase (CAT), superoxide dismutase (SOD) and ascorbate peroxidase (APX) are shown.

The transcriptional expression levels of some putative genes related to carotenoid biosynthesis confirmed the previous results. The gene encoding the phytoene desaturase (*PDS*), which catalyzes the first two desaturation reactions of the conversion from phytoene to lycopene was up-regulated when red light was superimposed upon blue light (2.0-fold at midday and 2.2.-fold at afternoon under 3 Red Peaks, 4.5-fold at dawn, 4.7-fold at midday

and 3.9-fold at afternoon under 9 Red Peaks), compared to only blue light condition (Fig. 3.5 a, b). The gene for the synthesis of lycopene β-cyclase (*LCYB*), which catalyzes the formation of the β-ionone rings at both ends of the linear lycopene molecules yielding the formation of β-Car, was also up-regulated under red + blue light, although it showed a different daily rhythm (Fig. 3.5 a, b). Under 9 Red Peaks condition the up-regulation level decreased along the day (2.7-fold and 2.4-fold at dawn and midday, respectively), until being non-significantly up-regulated in the afternoon (Fig. 3.5 b). By contrast, in 3 Red Peaks condition the expression of *LCBY* gene increased a little along the day (2.1-fold, 2.4-fold and 2.5-fold at dawn, midday and afternoon, respectively; Fig. 3.5 a). The lutein-like protein (*LUT*) gene involved in the hydroxylation of β-Car was up-regulated exclusively under 9 Red Peaks condition, especially under the high light period of the day (2.7-fold and 3.3-fold at midday and afternoon, respectively; Fig. 3.5 b). The zeaxanthin epoxidase (*ZEP*) and violaxanthin de-epoxidase (*VDE*), present in different copies in diatoms (Coesel *et al.*, 2008), convert Zeax to violaxanthin (Vx) and Vx back to Zeax respectively, and might be involved in the Dd – Dt cycle (Kuczynska *et al.*, 2015). While the *VDE* gene did not present any significant variation in expression in the red + blue light conditions compared to Con, the expression of the genes encoding for ZEP1 and ZEP2 presented significant changes. Under the 3 Red Peaks condition, *ZEP1* gene was slightly up-regulated (2.1-fold at each sampling time), while in 9 Red Peaks condition this gene did not display any significant variation in expression (Fig. 3.5 a, b). On the contrary, *ZEP2* gene was up-regulated in the 9 Red Peaks condition throughout the day (3.7-fold at dawn, 3.2-fold at midday and 2.8-fold at afternoon), while in the 3 Red Peaks condition (2.3-fold) it was up-regulated only in the afternoon (Fig. 3.5 a, b).

Among the genes involved in the antioxidant system investigated in our study only the one encoding for the glutathione peroxidase enzyme (*GPX*), that detoxifies H_2O_2 to H_2O using glutathione as reducing agent, was down-regulated at dawn in the 9 Red Peaks condition (-2.1-fold, Fig. 3.5 d) compared to the Con condition. This feature hypothetically reveals a decrease of the GPX system activation in the chloroplast at night (Foyer & Shigeoka, 2011).

Genes encoding antioxidant enzymes like catalase (*CAT*), superoxide dismutase (*SOD*), ascorbate peroxidase (*APX*) and glutathione reductase (*GR*) were unaffected. This observation is in accordance with the results reported on the diatom *Phaeodactylum*

tricornutum (Nymark *et al.*, 2009), in which *CAT*, *SOD*, *GPX* gene expressions were stable under high light on the opposite to genes encoding of other antioxidants (e.g., peroxiredoxin Q).

3.3.2.2 Macromolecular composition

The cellular carbohydrate pool was strongly increased in the presence of fluctuating red light, relatively to Con (Tab. 3.2) with concentration of 26- and 30-fold compared to Con, under 3 and 9 Red Peaks conditions, respectively.

Table 3.2: Biochemical properties of *Skeletonema marinoi* under the four light conditions at dawn (0 h) and midday (6 h). Data represent mean and standard deviation (n=3). Carbohydrates and lipids data are lacking in the control condition at dawn.

		Light Condition			
	Time point	**Con**	**3 Red Peaks**	**9 Red Peaks**	**Quad**
Total Carotenoids (pg/cell)	0h	0.020 ± 0.002	0.019 ± 0.002	0.019 ± 0.003	0.016 ± 0.004
	6h	0.021 ± 0.001	0.016 ± 0.002	0.021 ± 0.001	0.021 ± 0.003
Total Carbohydrates (pg/cell)	0h	-	14.23 ± 2.81	26.73 ± 4.79	8.11 ± 1.79
	6h	0.79 ± 0.24	26.61 ± 4.91	30.24 ± 10.72	9.25 ± 2.64
Total Lipids (pg/cell)	0h	-	1.44 ± 0.04	2.37 ± 0.01	1.85 ± 0.07
	6h	2.60 ± 0.25	2.34 ± 0.24	1.66 ± 0.35	2.02 ± 0.28
Total Proteins (pg/cell)	0h	26.57 ± 4.81	22.27 ± 0.65	30.11 ± 5.62	27.76 ± 0.66
	6h	31.70 ± 5.71	35.55 ± 1.64	41.28 ± 0.86	33.44 ± 3.41

By contrast, the lipid content per cell was not affected by the presence/absence of red wavelengths but, pooling together the three sinusoidal-based light courses, it was correlated to daily light dose ($p<0.01$) and growth rate ($p<0.01$). Indeed, lipid concentration was similar between Con and 3 Red Peaks condition, while it decreased in 9 Red Peaks (Tab. 3.2). Moreover, the intraday dynamics of lipid content was reversed between 3 Red Peaks and 9 Red Peaks with an increase and a decrease from dawn to midday, respectively (Tab. 3.2).

Among the lipid classes, only the phospholipids showed a significant trend with the daily light dose ($p<0.01$) or growth rate ($p<0.05$). However, differences in lipid classes between Con and red conditions were low. At midday, for all the three conditions tested, the contribution of phospholipids, neutral lipids and glycolipids was homogeneous (27-37% phospholipids; 30-35% neutral lipids and 28-41% glycolipids; Fig. 3.6). At dawn, for the two red conditions, neutral lipids dominated over the other classes (85-68%) followed by phospholipids (10-28%), while glycolipid contribution was drastically decreased (4-5%).

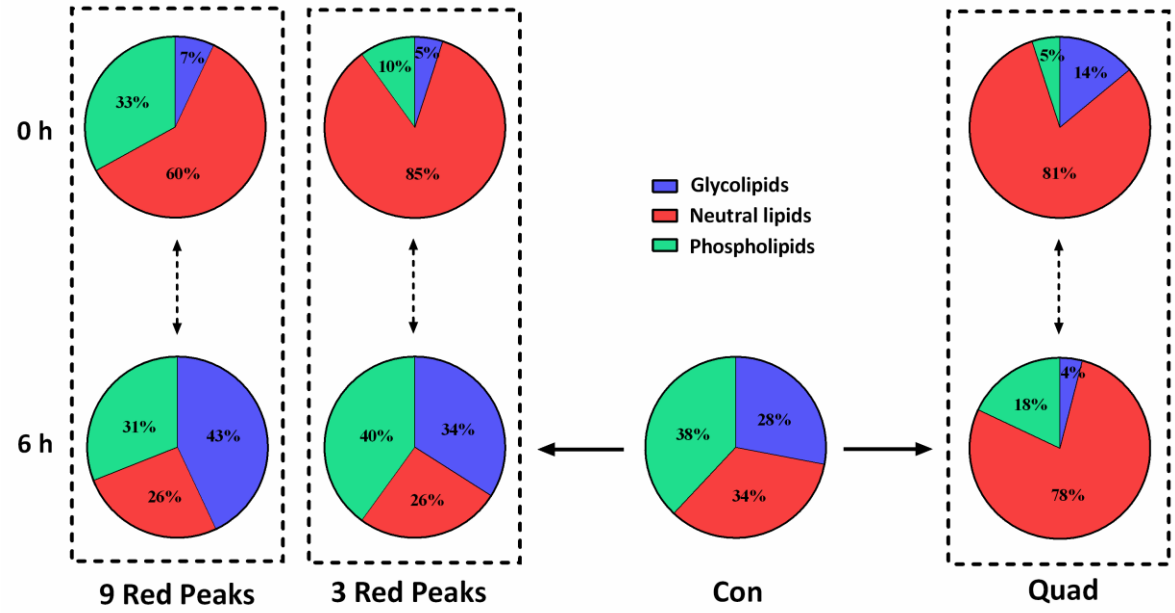

Figure 3.6: Distribution of lipid classes. Glycolipids, neutral lipids and phospholipids contribution under the four light conditions at dawn (0 h) and midday (6 h) are shown. Data represent means of the relative contribution (n=3).

The presence of red light lowered the percentage of monounsaturated lipids (3-6%) compared to Con (25%; Fig. 3.7). Saturated lipids dominated the lipid composition (49-53%), except for 3 Red Peaks condition at dawn, for which the composition of lipids was ≈ 64% of polyunsaturated lipids and ≈ 25% of saturated lipids (Fig. 3.7). As consequence, the degree of unsaturation (DU) in the 3 and 9 Red Peaks conditions strongly varied, decreasing during the day from 144 at dawn to 93 at midday in 3 Red Peaks, while being constant during the day (88-89) in 9 Red Peaks.

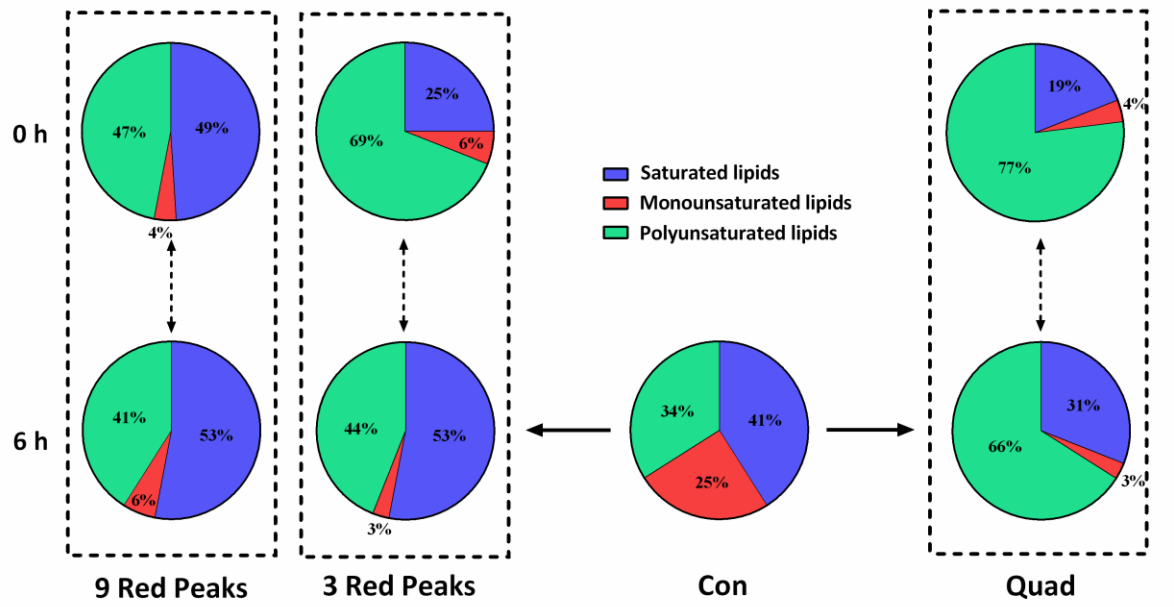

Figure 3.7: Distribution of fatty acids classes. Saturated, monounsaturated and polyunsaturated contribution under the four light conditions at dawn (0 h) and midday (6 h) are shown. Data represent means of the relative contribution (n=3).

The protein content per cell was similar between Con and 3 Red Peaks condition (Tab. 3.2), while it increased significantly in 9 Red Peaks during the day, revealing an effect of (red) light intensity on the protein synthesis (Tab. 3.2), and an opposite trend between lipids and proteins (Tab. 3.2).

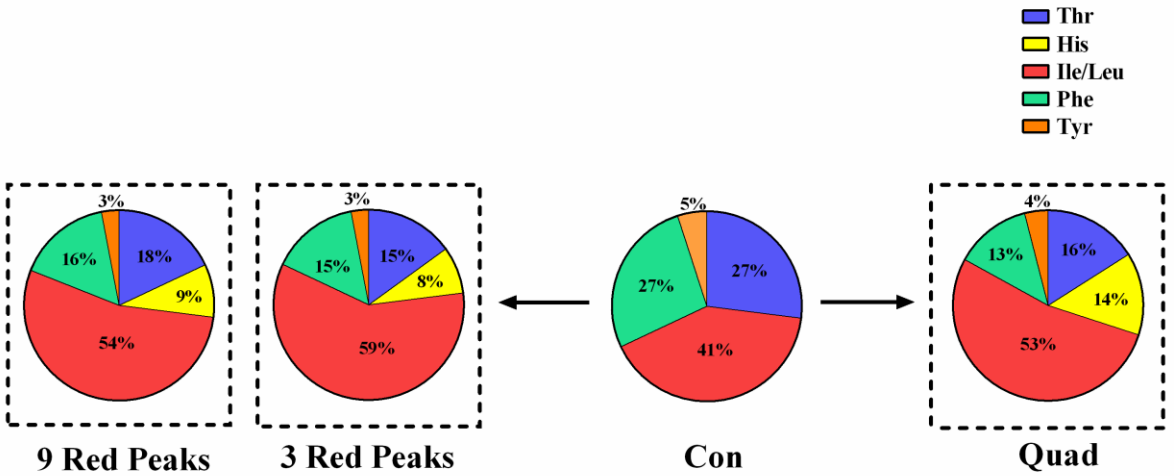

Figure 3.8: Distribution of the main amino acids concentration under the four light conditions. Data represent means of the dawn and midday samples (n=6). Threonine (Thr), histidine (His), isoleucine (Ile), leucine (Leu), phenylalanine (Phe) and tyrosine (Tyr) are shown.

The analysis of the essential amino acids profile revealed the higher contribution of histidine (His) in presence of red light, which was very low or under the detection threshold in Con (Fig. 3.8).

3.3.3 Biological responses to square-wave blue light course

Here I compare the results obtained from the square-wave light course (Quad) with the sinusoidal light course (Con). Both have similar blue light spectrum, although in Quad the daily light dose and the mean instantaneous irradiance averaged over the 12 h illumination period are almost 2-fold higher than Con (Tab. 3.1).

3.3.3.1 Physiological parameters

In the square-wave light course (Quad) cells displayed different photosynthetic rate and regulation compared with the control condition (Con; Tab. 3.1). The ETR decreased in agreement with the decrease of a^* and α, while E_k increased (Tab. 3.1). The high value of Fv/Fm revealed that cells did not undertake any photoinhibition process (Tab. 3.1), but the NPQ was too low considering the high income energy (Tab. 3.1). Indeed, PUR was the lowest among all the light conditions (Tab. 3.1).

Chl.*a* concentration as well as Chl.*c* decreased under Quad (Fig. 3.3 a, b) compared to Con highlighting the re-arrangement of the composition of the light-harvesting complexes under Quad. While Fuco concentration was similar under Quad and Con (Fig. 3.3 c), an activation of the carotenogenesis pathway, mainly related to the XC operation, was revealed. Indeed, the sum (Dd + Dt) was almost doubled compared to Con (0.0032 pg cell^{-1} ± 0.0003 pg cell^{-1} *vs.* 0.0060 ± 0.0003 pg cell^{-1} under Con and Quad, respectively), revealing a strong activation of the XC.

A high increase of Dt concentration was reported under Quad (Fig. 3.4 d), while Dd showed a slight increase (Fig. 3.4 c). β-Car and Zeax followed a decreasing trend under Quad, with Zeax not detected anymore (Fig. 3.4 d).

The transcriptional level of *LUT* and *ZEP2* genes showed a constant increase during the day (Fig. 3.5), reaching a significant up-regulation both at midday and at afternoon (2.2 and 4.0-fold respectively for *LUT* and 2.9 and 3.0-fold respectively for *ZEP2*). The other genes, *PDS*, *LCBY*, *ZEP1* and *VDE*, did not display significant transcriptional variation during the experiment. Under this condition, down-regulation of *GPX*, *CAT* and *AP* were shown at dawn (-2.1, -3.1; and -2.2-fold change respectively, Fig. 3.9), while the only gene which

was down-regulated in the other light conditions was *GPX* at dawn under 9 Red Peaks (see previous section).

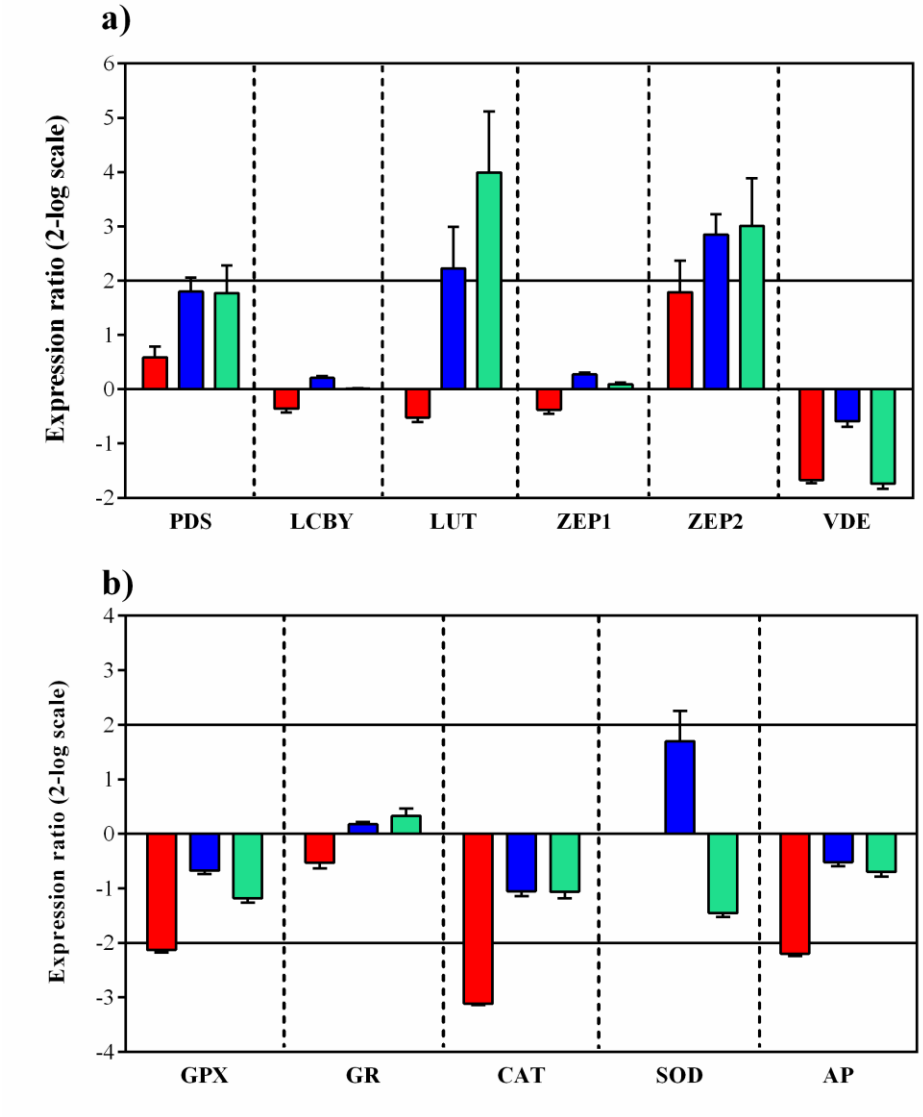

Figure 3.9: Transcriptional expression analysis of carotenoid or antioxidant genes under the Quad condition: a) carotenoid genes and b) antioxidant genes. Samples were collected at dawn (red bar), midday (blue bar) and afternoon (green bar). Data are reported as fold difference (mean ±SD, n=3) compared to control (blue sinusoidal light with PFD peaking at 150 µmol m^{-2} s^{-1}). Fold differences greater than ±2 (see horizontal guidelines at values of 2 and -2) were considered significant. Phytoene desaturase (PDS), lycopene beta cyclase (LCYB), lutein deficient protein (LUT), zeaxanthin epoxidase 1 and 2 (ZEP1 and ZEP2), violaxanthin de-epoxidase (VDE), glutathione peroxidase (GPX), glutathione reductase (GR), catalase (CAT), superoxide dismutase (SOD) and ascorbate peroxidase (APX) are shown.

3.3.3.2 Macromolecular composition

The Quad condition strongly modified the biochemical profile and the carbon allocation of the cells compared to the condition with a more natural distribution of light.

Although the carbohydrate content per cell increased under Quad condition compared to Con (Tab. 3.2), the lipid content was lowered (Tab. 3.2), as already described under high light in many studies [e.g., Rivkin (1989)].

Interestingly, among the lipids, the neutral ones strongly dominated under Quad (about 78-81%, Fig. 3.6) allowing the storage of a large quantity of chemical energy (Falkowski & Raven, 1997).

Phospholipid content ($p<0.01$) accounted for 5-18% of total lipids (Fig. 3.6), while under Con the lipid classes were more homogeneously distributed (37% phospholipids; 35% neutral lipids and 28% glycolipids; Fig. 3.6).

Interestingly, in the Quad condition, the relative abundance of phospholipids and glycolipids showed an opposite trend from dawn to midday. At dawn, glycolipids contributed to 14% of the total lipids, and the phospholipid content was very low (5%) while, at midday, the percentages were reversed (glycolipids 4% and phospholipids 18%, Fig. 3.6).

The Quad condition also induced a re-distribution of the composition of fatty acids (FAs) comparatively to the Con condition. The polyunsaturated fatty acids (PUFAs) dominated (67-76%), followed by saturated (20-30%) and monounsaturated (3-4%), while these classes were homogeneously distributed under Con (41% saturated; 34% polyunsaturated and 25% monounsaturated; Fig. 3.7). The DU therefore increased from 92 (Con) to 137 (Quad). Only the saturated fatty acid content was correlated to the daily light dose ($p<0.01$) or growth rate ($p<0.05$) and phospholipid content ($p<0.01$).

In parallel to the carbohydrates/lipids shift from Con to Quad, and the similar protein content (Table 3.2), the distribution of amino acids changed (Fig. 3.8), revealing a remodeling of the proteome in response to constant light distribution or high daily light

dose. Under Quad, threonine (Thr) and phenylalanine (Phe) contribution decreased while His increased, comparatively to Con (Fig. 3.8).

3.4 Discussion

In order to support microalgae as sources of biomass and molecules of interest in a biotechnological perspective, the optimization of diatoms cultivation is mandatory.

Indeed light, and its multiple properties such as the intensity, spectral composition and daily distribution, are key players in driving growth, photosynthesis and carbon allocation in cells.

We based our study on the hypothesis that the addition of red fluence rate to a sinusoidal blue light course, resulting in an overall fluctuating light regime, is able to induce the activation of photoprotective mechanisms such as the increase of XC pigment content without the insurgence of photodamages. The rationale behind this hypothesis is based on the observation of what happens in nature to fluctuating particles at sea such as phytoplankton: they are constantly moved along the water column, and so they must show adaptive traits that allow them to promptly acclimate to the variable light environments. Also the macromolecular content is expected to change in response to different light milieu.

Due to the biotechnological application of this study, the comparison with the indoor light climate generally used for microalgal cultivation was necessary. We wanted to test the hypothesis that the traditional on/off system, so a square-wave light course is harmful for cells, impairing the photophysiology and therefore altering the downstream biological events from light capturing to carbon allocation in cells.

Indeed, we found that the growth rate was clearly dependent on the daily light dose experienced by cells, as already reported for other species (Dimier *et al.*, 2009). Other studies instead reported variations of growth rate related to fluctuating light (Rivkin, 1989, Litchman, 2000, Litchman & Klausmeier, 2001, Van Leeuwe *et al.*, 2005, Wagner *et al.*, 2006, van de Poll *et al.*, 2007, Grobbelaar, 2013). The discrepancies between these results can be attributed to the pre-acclimation condition and/or to the species-specificity of response to light environment (Litchman, 2000, Litchman & Klausmeier, 2001, van de Poll *et al.*, 2007).

Even though the growth rate of *S. marinoi* was significantly dependent upon the integrated daily light dose, the photosynthesis, the light harvesting properties and the metabolic state were more affected by light course and/or spectrum, confirming what expected: the growth rate is a longer term process (day) dependent upon the integrated light energy harvested by cells, while the other parameters depend on the light variations occurring at shorter term (minutes, hours).

Considering the photosynthesis, differences between the sinusoidal light treatments and the square wave light course were noticeable. The ETR in the sinusoidal conditions decreases with the increase of the daily light dose together with the specific absorption coefficient (*a**) and the quantum yield of growth, indicating the dependence of ETR upon the light harvesting absorption properties and its role in governing the biomass light increase per mol of photons. The inverse trend between the ETR and the growth rate indicates modulations in the cells' energy flow, implying an unbalanced growth and so a modification of the cell state. Indeed, cells showed effective photoacclimation: the higher the daily light dose the lower the capacity of cells to harvest light (i.e. inverse correlation between *a** and daily light dose). The shift from the low light- to the high light-adapted state was confirmed by the opposite trend between the maximum light use efficiency (α) and the photosynthetic light saturation index (E_k), indicating a fine regulation of the income energy, confirmed by the same values of PUR recorded among the experimental conditions. The increased NPQ under fluctuating lights confirms what already observed on the diatom *Pseudo-nitzschia multistriata* (Brunet *et al.*, 2014): the NPQ does not respond to the daily light dose *per se* but requires red light to be enhanced, while its amplitude depends upon the blue fluence rate.

By contrast, under the square wave light course all these significant relationships between the physiological parameters were no longer valid. Indeed, the lowest PUR value indicates that cells were not able to finely tune the metabolic energy flow under this light climate as they did in the other sinusoidal light treatments. The lack of NPQ enhancement revealed that cells went under an impaired dissipation of excess of income energy, probably due to the absence of red light. Anyway cells showed high light acclimation features (i.e. lower ETR, *a** and α, and higher E_k with respect of control) and absence of photoinhibition (i.e. high Fv/Fm value).

As regards the photosynthetic pigments, different behavior between Chl.*a*, Chl.*c* and Fuco indicates the rearrangement in the light harvesting antenna composition and/or size. A decrease in the Chl.*a* and Chl.*c* content is observed both in presence of red as under the square wave light course. The lower content in Chl.*c* under fluctuating lights could be explained by the fact that this pigment is able to absorb red wavelengths, as opposed to carotenoids, and thus must be more sensitive to this type of light (Brunet *et al.*, 2014). In the Quad condition instead the lower content of Chl.*a* and Chl.*c* pigments can be caused by the rearrangement of the photosystems as a result of the higher light energy received.

In all the experimental conditions a strong activation of the XC is recorded: the photoprotective pigment Dt was always higher with respect of the control condition, were was not detected at all. Also its precursors in the biosynthetic pathway resulted affected by the light regime: both the β-Car and the Zeax were lower with respect of the control, but in a different way among the experimental conditions. The increase of Dt and the missing Zeax in the Quad condition led us to hypothesize that the Zeax pool present in the cell were depleted in favor of a strong enhancement of Dt, following the sudden increase of light experienced by cells.

All the results on the photoprotection behavior indicate that the square wave light course causes an impairment of the “healthy” daily-regulated cell processes for coping with light variations in an efficient way.

The impairment of the cell physiology is also reflected by the results obtained by the gene expression analysis. Under the square wave light course the only genes activated were the ones involved into the transformation of intermediary pigments of the photoprotective biosynthetic pathway. The absence of significant regulation of the genes involved upstream in the biosynthetic pathway, on the opposite to what observed in the 3 or 9 Red Peaks conditions, might be related to the absence of red light or to the sudden light increase which prevents any gradual acclimation from the photo-biosynthetic point of view.

All these results highlight the role of red + blue light, compared to blue light, on shaping the photobiological responses in diatoms. The carotenogenesis was affected by the addition of red together with blue light, both at a transcriptional and molecular level. This is probably related to the role of red (together with blue) on the photoprotective behavior as revealed by NPQ results (Depauw *et al.*, 2012).

As regards the antioxidant enzymes, differences between the light treatments in terms of gene expression were noticeable: while in the sinusoidal conditions the only gene that changed its relative expression with respect of control were *GPX* at dawn under 9 Red Peaks, in Quad also *CAT* and *APX* were down-regulated. So it seems that the down-regulations are higher under the most stressful conditions. Since dawn sampling has been performed before the start of the light phase, this result underlines that the light history, i.e. the light energy perceived during the previous day with its repertoire of downstream mechanisms, strongly affects the regulative processes of the metabolic energy in the chloroplast.

The macromolecular content was notably different among the experimental conditions, where it's observed a strong modification of the biochemical profile and the carbon allocation of cells with respect of the control condition.

The great increase of carbohydrates in presence of red light confirms what already observed in other microalgae: providing only blue light induces a breakdown of the carbohydrate reserves in the cells (Marchetti *et al.*, 2013, Jungandreas *et al.*, 2014).

By contrast, a slight decrease of the lipid content is observed in all the experimental condition with respect of control. Indeed, the decrease of lipid concentration in high light conditions has already been observed (Chandrasekaran *et al.*, 2014, Chen *et al.*, 2015). Interestingly, while the lipid classes were homogenously distributed in the sinusoidal light conditions, under square wave-light course a shift towards the accumulation of neutral lipids is observed. This class of lipids serves primarily as a storage form of energy and carbon fixed in excess during photosynthesis. Also the degree of unsaturation of fatty acids showed alteration, with a higher relative content of saturated fatty acids in presence of red (more stable against oxidation), in contrast to a higher relative content of polyunsaturated fatty acids (PUFA) under the square-wave light course. Generally at higher intensity a decrease in PUFA is observed (Meiser *et al.*, 2004, Hu *et al.*, 2008, Li *et al.*, 2014), while our results show the opposite. Probably this difference depends on the shape of light

distribution (quadratic *vs.* sinusoidal) that influences this feature, rather than the light intensity *per se*. This class of fatty acids has two main functions: they are essential components of cell membranes, regulating their phase transition and permeability, and they act as precursor of many metabolites, such as oxylipins, prostaglandins, eicosanoids and hydroxyl-FAs, that regulate many critical biological functions. It has been demonstrated that oxylipin content in diatoms is strongly enhanced in conditions of physiological stress (Ribalet *et al.*, 2007b, Ribalet *et al.*, 2009), and that they take part in the chemical defense system (Pohnert, 2005) being involved in signaling to determine cell fate and death of the population (Casotti *et al.*, 2005, Vardi *et al.*, 2006, Vardi *et al.*, 2008). In this context, we can hypothesize that this increase of PUFAs was due to an enhanced need of precursors for the *de novo* synthesis of signaling molecules involved in stress responses.

As regards the amino acid profile, their changed distribution between the treatments with respect of control revealed a remodeling of the proteome in response to changed light spectrum, distribution and daily light dose. The higher content of histidine (His), absent in the control condition, let suppose its enhancement when higher light energy is provided to cells.

This study demonstrates that the manipulation of light condition is a valuable tool for modifying and optimizing diatom's cell state and macromolecular composition, providing more efficient quantum yield of growth.

The red superimposed upon blue light provokes an almost 30-fold increase of the carbohydrate pool, without determining a substantial alteration of the carbon allocation into lipid and protein cellular pools, nor a great alteration of the other physiological parameters.

The square-wave light course instead, although the increased growth rate, affects in negative way many biological processes subsequent to the light capture, therefore should be avoided for diatoms cultivation.

4. Photoprotective and antioxidant responses to light spectrum and intensity variations in the coastal diatom *Skeletonema marinoi*

4.1 Introduction

The results obtained in the previous series of experiments (Orefice *et al.*, 2016) demonstrated that the photophysiological state, the light harvesting properties, the metabolic state of the cells and the carbon allocation are hugely affected by the irradiance, in terms of intensity, velocity of increase and spectral composition.

This study, opened new questions on the light modulation of the defense and regulative processes in diatoms. It is known that an excess of light may lead to photoinhibition; the excitation energy accumulates in the chloroplasts increasing the chance of singlet oxygen formation and generating other reactive oxygen species (ROS) in the donor side of the photosystem I (PSI). The oxidative stress derived from an excess of reactive species is able to impair the normal cell functioning. While it is known that photosynthetic cells possess different mechanisms contrasting the oxidative stress (see chapter 1), a full comprehension of the activation of the antioxidant network in diatoms is still lacking.

Since the different properties of light are able to modulate the photophysiology and metabolic state of cells, our hypothesis was that the antioxidant network also respond to these environmental cues (light colors and intensities).

The regulation of the antioxidant network could be mediated by photoreceptors that directly sense the different type of light (Depauw *et al.*, 2012), or by the presence of ROS itself. It is known that the production of ROS and their scavenging must be finely tuned, since they play a key role as signaling molecules involved in growth and acclimation of environmental stress (Foyer & Noctor, 2005a, b).

In the previous study (Orefice *et al.*, 2016) a first attempt was made to fill the gap of knowledge on the antioxidant network, measuring the expression level of genes encoding for some antioxidant enzymes. Although the gene expression analysis is a proxy commonly used to estimate the concentration and thus the activity of the corresponding proteins, the transcription downstream processes have also a large influence on the protein concentration, and the correlation between the gene expression and the protein level may be not so strong (Vogel & Marcotte, 2012). For this reason, in this new set of experiments (see below), we implemented the information of the defense processes with other protocols. Indeed, I developed measurements of the enzymatic activity, the total antioxidant capacity

of cells that relies on antioxidant molecules (i.e. the DPPH radical scavenging activity), ascorbic acid (the major water-soluble antioxidant in cell plasma), and phenolic compounds (one of the most important classes of antioxidants)(Pietta, 2000, Sharma *et al.*, 2012).
A better understanding of the quantity, role and synthesis modulation of the antioxidant molecules from diatoms can improve microalgal culturing for a subsequent exploitation in the field of biotechnology. In fact, diatoms are a sound source of high added value products that can be used in many industrial applications: in nutraceutic, pharmaceutic and cosmetic industries (Pulz & Gross, 2004, Barra *et al.*, 2014).

The purpose of this study was to extricate the short term (4 h) modulation and potential connection of the photoprotective and defense strategies to spectral composition and intensity of light variations.
At the start of the experiment, cells were shifted to different light climates that correspond to four different "scenarios": the marine upper layer (high light with the presence of red wavelengths), the marine deeper layer (low light without red), and two unnatural situations (high light without red and low light with red).
In order to decipher the role of the light spectrum and intensity in driving the studied processes, cells were firstly exposed to a gradual photon flux density (PFD) increase, reaching the plateau of light intensity in two hours. Gradual light increase allows cells to regulate the photosynthetic machinery and so to cope better with the enhancing light compared with a sudden light increase (i.e. a traditional on/off system; (Giovagnetti *et al.*, 2014, Orefice *et al.*, 2016), whilst the velocity of light increase modulates the on-going photoprotective mechanisms (Giovagnetti *et al.*, 2014). In this way it is possible to decipher the role of the color, intensity and velocity in changing the cell physiology without the stress related to the on/off system and its undesirable effects on cell functioning.
After the gradual light increase, two hours of constant light were provided, to better compare the effects of the different PFDs and spectra, independently from the light enhancement-dependent processes.

The results obtained from this experiment correspond to a paper published in 2017.

(Smerilli A., Orefice I., Corato F., Gavalás Olea A., Ruban A. V. and Brunet C., 2017. Photoprotective and antioxidant responses to light spectrum and intensity variations in the coastal diatom *Skeletonema marinoi*. *Environmental microbiology* **19**:611-627).

4.2 Materials and methods

4.2.1 Experimental strategy and sampling

The experiments were conducted on the centric diatom *Skeletonema marinoi*, grown at 20°C in 1 L flasks.

The cells were pre-acclimated to a photoperiod of 12:12h light:dark, and the diurnal phase consisted in a sinusoidal blue light course, characterized by a gradual light intensity increase from dawn to midday (6 hours) peaking at 150 µmol photons s^{-1} m^{-2}, and then a gradual light decrease from midday to sunset (6 hours). This pre-acclimation setup has been selected following the results obtained by Chandrasekaran *et al.* (2014) and Orefice *et al.* (2016).

The experiments, lasting 4 hours, were conducted in triplicate during the exponential growth phase (growth rate ≈ 0.82 d^{-1}) in order to investigate the first-hours photoresponses developed by cells to cope with the new light conditions.

The experimental light setups were (Fig. 4.1a, b, c):

- Blue light peaking at 150 µmol photons m^{-2} s^{-1} (B150),
- Blue light peaking at 300 µmol photons m^{-2} s^{-1} (B300),
- Blue light peaking at 500 µmol photons m^{-2} s^{-1} (B500),
- Blue light peaking at 800 µmol photons m^{-2} s^{-1} (B800),
- Red light peaking at 300 µmol photons m^{-2} s^{-1} (R300),
- Blue+Red lights peaking at 300 µmol photons m^{-2} s^{-1} (BR300),
- Blue+Red lights peaking at 500 µmol photons m^{-2} s^{-1} (BR500),
- Blue+Red lights peaking at 800 µmol photons m^{-2} s^{-1} (BR800).

In the blue+red light conditions, the red:blue ratio was setup at 1 (half light intensity of blue and half light intensity of red).

Two successive light courses were applied in each of the 8 conditions: 2 h of gradual light increase (from dawn) followed by a 2 h constant light period (Fig. 4.1 a, b, c).

Sampling was carried out at dawn, at the end of the gradual light increase (2 h) and at the end of the constant light period (4 h).

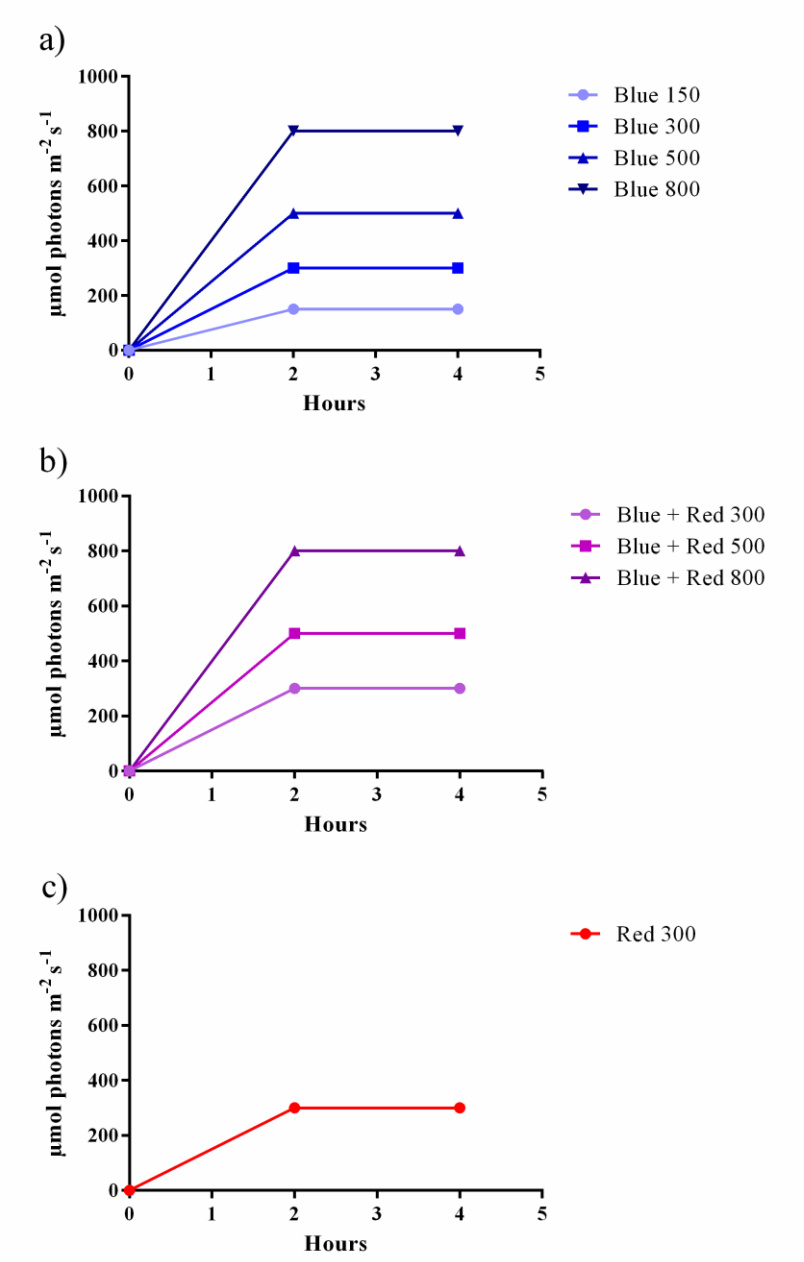

Figure 4.1: Experimental light setup (in µmol photons $m^{-2}s^{-1}$): a) blue conditions: B150, B300, B500, B800; b) blue + red conditions: BR300, BR500, BR800; c) red condition: R300.

4.2.2 Parameters analyzed

The subsequent parameters were followed during the experiments:

- Cell concentration
- Photochemical efficiency of the photosystem II
- Electron transport rate (ETR)-light curves
- Non-photochemical quenching (NPQ)
- Pigments
- Absorption spectra
- Gene expression analysis of antioxidant enzymes:
  - Glutathione reductase (*GR*)
  - Catalase (*CAT*)
  - Superoxide dismutase (*SOD*)
  - Ascorbate peroxidase (*APX*)
- Gene expression analysis of genes related to carotenogenesis:
  - Phytoene desaturase 1 and 2 (*PDS1* and *PDS2*)
  - Lycopene β-cyclase (*LCYB*)
  - Lutein deficient protein (*LUT*)
  - Zeaxanthin epoxidase 1 and 2 (*ZEP1* and *ZEP2*)
  - Violaxanthin de-epoxidase (*VDE*)
- Total phenolic content
- Ascorbic acid content
- DPPH radical scavenging activity
- Antioxidant enzyme activities
  - Catalase (CAT)
  - Glutathione reductase (GR)
  - Ascorbate peroxidase (APX)
  - Superoxide dismutase (SOD)
- Protein quantification
- Statistical analysis

All the experimental procedures for each of these parameters are described in the chapter 2.

4.3 Results

4.3.1 Photoprotection and carotenoids

Pooling all data together, the amounts of three pigments, diadinoxanthin (Dd) ,diatoxanthin (Dt) and β-carotene (β-Car) were significantly correlated with the light intensity experienced by cells ($p<0.01$, $p<0.001$, and $p<0.001$, respectively; $n=48$). However, the sum of these protective molecules differed between Blue (B) and Blue+Red (BR) conditions (Tab. 4.1). This feature revealed that the concentration of these pigments was affected by the spectral quality of light combined to the PFD. At Dark, the sum (Dd+Dt+β-Car) was 20 fg $cell^{-1}$ (Tab. 4.1). After the gradual light increase period, this sum was stable under BR (23-26 fg $cell^{-1}$) and higher under B conditions (27-33 fg $cell^{-1}$), with the only exception of B150. During the constant light period, this sum increased in parallel with the photon flux density (PFD) provided by the BR conditions, reaching the highest value under BR800. On the contrary, (Dd+Dt+β-Car) decreased with the PFD provided by the B conditions.

Differences between B and BR conditions were noticeable. At Dark the Dt concentration was 2 fg $cell^{-1}$ (Fig. 4.2 a). Under blue (without red) this pigment increased reaching a plateau (17-19 fg $cell^{-1}$) from PFD ≥ 300 µmol photons m^{-2} s^{-1}, despite the large range of PFD values (from 300 to 800 µmol photons m^{-2} s^{-1}; Fig. 4.2 a). By contrast, under BR conditions Dt concentration linearly increased with the PFD experienced by cells. The Dt concentration reached in BR800 coincided with the value obtained under PFD ≥ 300 µmol photons m^{-2} s^{-1} in the B conditions. This feature highlighted the main role of blue fluence rate on Dt synthesis since BR800 was composed by 400 µmol photons s^{-1} m^{-2} of blue, i.e. a value belonging to the range of blue PFD for which Dt reached a plateau. This might be due to the cells' major absorption capacity of blue compared to red, or/and to the higher energy brought by blue wavelengths relatively to red.

Although the de-epoxidation of Dd into Dt is fast, Dt increased with time of high light exposure. Indeed, in all conditions Dt concentration was significantly higher after the constant light period (4h) than after the gradual light increase (2h; $p<0.01$; Fig. 4.2 a). Since Dd did not decrease between 2 and 4h (Fig. 4.2 b), the increase of Dt during the constant

light period was due to a *de novo* synthesis of the XC pigment pool, with a replenishment of the Dd pool when used to form Dt (Fig. 4.2 b).

Table 4.1: Pigment content and photophysiological characteristics of *S. marinoi* after the gradual light increase (2 hours) and the stable light period (4 hours). Dt+Dd+β-Car = sum of diatoxanthin, diadinoxanthin and β-carotene (fg/cell); DES = de-epoxidation state (Dt/(Dt+Dd)); Chl.*a* = chlorophyll *a* (fg/cell); Fuco = fucoxanthin (fg/cell); Fv/Fm = maximum quantum yield of the PS II; NPQ = non-photochemical quenching. Data are reported as mean ±SD of three biological replicates (n=3), with the exception of Dark condition (n=27). Dark, Blue light at 150 µmol photons m^{-2} s^{-1} (B150), Blue light at 300 µmol photons m^{-2} s^{-1} (B300), Blue light at 500 µmol photons m^{-2} s^{-1} (B500), Blue light at 800 µmol photons m^{-2} s^{-1} (B800), Red light at 300 µmol photons m^{-2} s^{-1} (R300), Blue+Red lights at 300 µmol photons m^{-2} s^{-1} (BR300), Blue+Red lights at 500 µmol photons m^{-2} s^{-1} (BR500), and Blue+Red lights at 800 µmol photons m^{-2} s^{-1} (BR800) are shown.

		Dt+Dd+βCar	DES	Chl.*a*	Fuco	F_v/F_m	NPQ
Dark		20 ± 4	0.14 ± 0.07	210 ± 60	90 ± 20	0.79 ± 0.09	0.56 ± 0.10
B150	2 hours	9 ± 1	0	201 ± 60	70 ± 20	0.74 ± 0.05	0.20 ± 0.06
	4 hours	10 ± 2	0.62 ± 0.09	190 ± 10	70 ± 10	0.72 ± 0.16	0.86 ± 0.24
B300	2 hours	27 ± 4	0.26 ± 0.08	280 ± 40	90 ± 40	0.70 ± 0.03	0.63 ± 0.07
	4 hours	45 ± 2	0.58 ± 0.06	330 ± 40	110 ±10	0.76 ± 0.17	1.15 ± 0.35
B500	2 hours	31 ± 1	0.46 ± 0.05	290 ± 20	100 ± 20	0.71 ± 0.02	0.84 ± 0.10
	4 hours	42 ± 2	0.65 ± 0.08	310 ± 40	110 ± 10	0.57 ± 0.03	0.47 ± 0.39
B800	2 hours	33 ± 3	0.21 ± 0.09	280 ± 60	110 ± 10	0.71 ± 0.02	1.05 ± 0.20
	4 hours	39 ± 1	0.62 ± 0.09	190 ± 70	90 ± 30	0.46 ± 0.01	0.64 ± 0.31
R300	2 hours	20 ± 1	0.17 ± 0.02	220 ± 30	90 ± 10	0.77 ± 0.03	0.49 ± 0.01
	4 hours	26 ± 3	0.47 ± 0.05	260 ± 60	110 ± 10	0.77 ± 0.03	0.40 ± 0.10
BR300	2 hours	23 ± 2	0.24 ± 0.04	280 ± 10	120 ± 10	0.70 ± 0.04	0.64 ± 0.10
	4 hours	30 ± 2	0.46 ± 0.09	250 ± 40	100 ± 10	0.62 ± 0.06	0.66 ± 0.05
BR500	2 hours	26 ± 1	0.51 ± 0.06	230 ± 30	100 ± 10	0.73 ± 0.03	0.64 ± 0.01
	4 hours	38 ± 4	0.61 ± 0.07	270 ± 100	90 ± 30	0.60 ± 0.09	0.50 ± 0.07
BR800	2 hours	23 ± 2	0	340 ± 40	140 ± 30	0.61 ± 0.03	0.53 ± 0.08
	4 hours	52 ± 4	0.60 ± 0.10	290 ± 60	110 ± 20	0.68 ± 0.06	0.49 ± 0.07

By contrast, upstream in the biosynthetic pathway of the XC pigments, β-Car was enhanced when PFD was ≥ 300 µmol photons s^{-1} m^{-2}, so in high light conditions, reaching the highest

concentrations after the constant light period (Fig. 4.1 c). Under B800 at 4h β-Car strongly decreased, probably to be used for Dd and Dt synthesis (see below).

Intriguingly, after the gradual light increase (2h), the low De-epoxidation state (DES, Dt/(Dt+Dd)) at dark (0.14) reached its highest values under PFD = 500 µmol photons s^{-1} m^{-2} (0.46 in B500 and 0.51 in BR500, respectively), compared to all the other conditions (<0.26), even those with a higher PFD (B800 or BR800; Tab. 4.1). These highest DES values in B/BR500 are due to the lower concentration of Dd compared to B/BR300 and B/BR800 (Fig. 4.2 a, b). This increased DES up to 500 µmol photons s^{-1} m^{-2} and its following decrease under higher light intensity revealed that the Dd consumption required for Dt formation was not fully replenished. We can thus hypothesize that photoprotective mechanisms developed by cells differed depending on the light stress magnitude.

Indeed, the highest excess energy dissipation through non photochemical quenching (NPQ) was recorded during the gradual light increase period (2h, Tab. 4.1) under B800 while DES was very low. These features revealed that cells coped with a rapid increase to high PFD by an enhancement of NPQ and low XC while the same rapid increase to moderate PFD activated more XC and less NPQ. This is in agreement with previous results obtained on the coastal diatom *Pseudo-nitzschia multistriata* (Giovagnetti *et al.*, 2014).

The mismatch between XC and NPQ was confirmed by the divergence between the enhancement of Dt during the constant light period and the NPQ development (Tab. 4.1). For instance, NPQ decreased under the two highest blue light conditions (B500 and B800), meaning that the supplementary Dt synthesized was not involved into mechanisms of excess energy dissipation as heat.

This low capacity of NPQ development under the constant high light period in B500 and B800 might be responsible for the decrease of Fv/Fm recorded in these two conditions (Tab. 4.1), revealing that cells underwent photoinhibition. Moreover, changes in the light harvesting complexes *vs.* reaction center ratio occurred under B800, as noticed by the lowering of Chl.*a* content between 2 and 4h (Tab. 4.1), while fucoxanthin concentration stayed the same (Tab. 4.1).

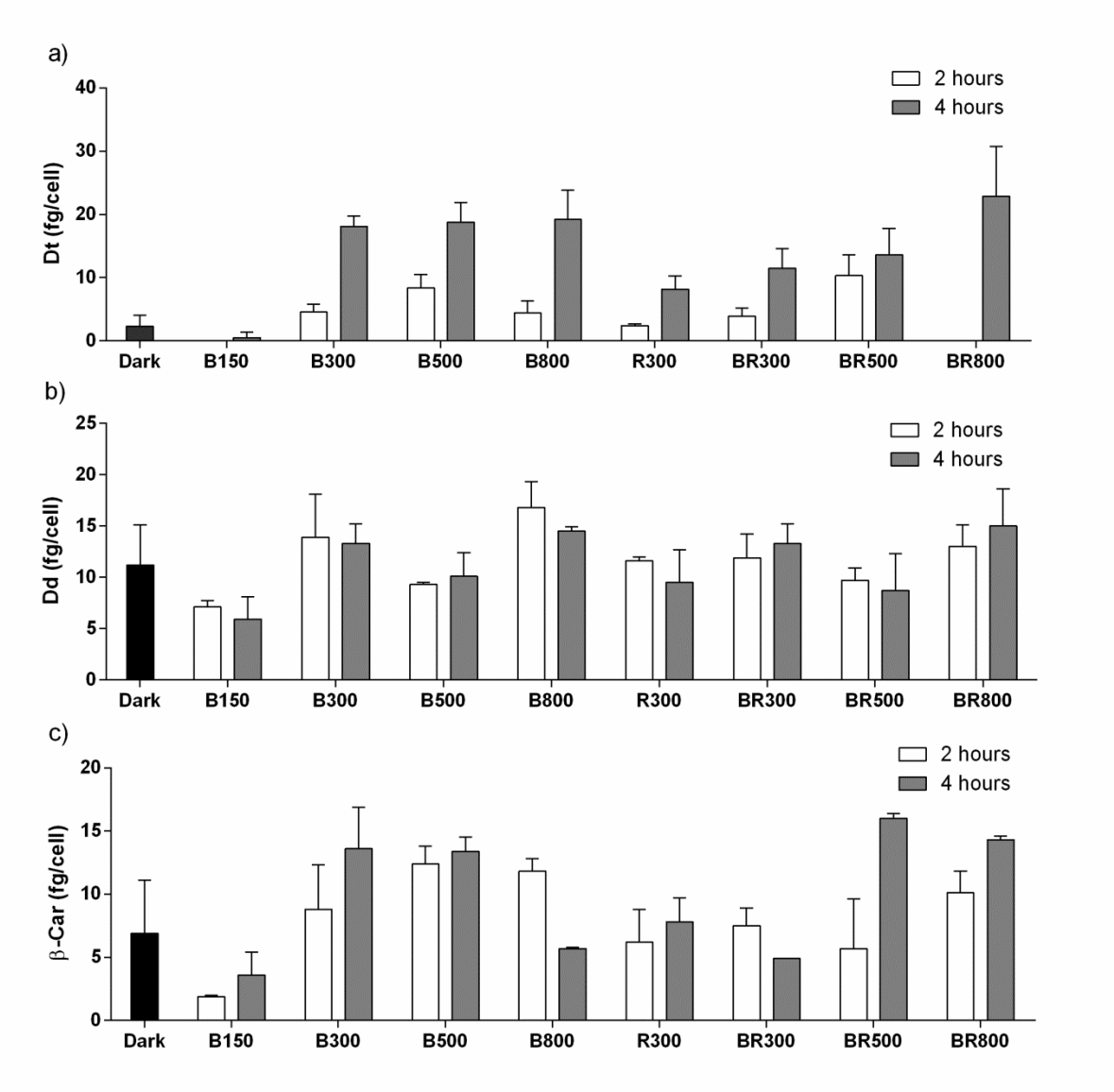

Figure 4.2: Pigment content. a) diatoxanthin (Dt, fg cell^{-1}), b) diadinoxanthin (Dd, fg cell^{-1}) and c) β-carotene (β-Car, fg cell^{-1}). Samples were collected at Dark (black bar), at the end of the gradual light increase (2 hours, white bars) and at the end of the constant light period (4 hours, grey bars). Data are reported as mean ±SD of three biological replicates (n=3). Blue light at 150 µmol photons m^{-2} s^{-1} (B150), Blue light at 300 µmol photons m^{-2} s^{-1} (B300), Blue light at 500 µmol photons m^{-2} s^{-1} (B500), Blue light at 800 µmol photons m^{-2} s^{-1} (B800), Red light at 300 µmol photons m^{-2} s^{-1} (R300), Blue+Red lights at 300 µmol photons m^{-2} s^{-1} (BR300), Blue+Red lights at 500 µmol photons m^{-2} s^{-1} (BR500), and Blue+Red lights at 800 µmol photons m^{-2} s^{-1} (BR800) are shown.

4.3.2 Carotenoid gene expression

The transcriptional expression levels of putative genes related to carotenoid biosynthesis confirmed that the gradual light increase did not require an activation of XC (Fig. 4.3 a). By contrast, an up-regulation of genes encoding zeaxanthin epoxidase (*ZEP*) enzymes was revealed after the constant light period. In higher plants *ZEP* converts zeaxanthin to violaxanthin. In diatoms there are more copies of this gene which encode for different isoforms of ZEP (Coesel *et al.*, 2008). In these organisms, this enzyme should be also responsible for the conversion of Dt back to Dd under low light, but the light-dependent (de)activation mechanism and its localization that depends on the different domains, is still poorly understood (Coesel *et al.*, 2008, Depauw *et al.*, 2012). It remains to be confirmed if these additional enzymes participate in the XC or if they are involved in other processes (Goss & Lepetit, 2015). The isoform 1, *ZEP1*, was up-regulated when the blue fluence rate was $\geq$ 300 µmol photons m^{-2} s^{-1} (B300, B500, B800 and BR800) while the isoform 2, *ZEP2*, was up-regulated only under BR800 (Fig. 4.3 b). Also the gene lycopene β-cyclase (*LCYB*), yielding to the formation of β-Car, was up-regulated only at 4h under BR800, revealing a probable same kind of modulation as *ZEP*2.

The gene encoding the phytoene desaturase 2 (*PDS2*), involved in the first two desaturation reactions of the conversion from phytoene to lycopene, is the only one to show a consistent up-regulation in the presence of blue light and not in presence of only red light (R300) after the gradual light increase (2h, Fig. 4.3 a). The situation was different after the constant light exposure period (4h). Indeed, *PDS2* gene expression did not change in B300 and B800, while it was up-regulated in all the other conditions, revealing a modulation of the transcriptional expression of this gene by the downstream photoacclimative processes induced by light sensing.

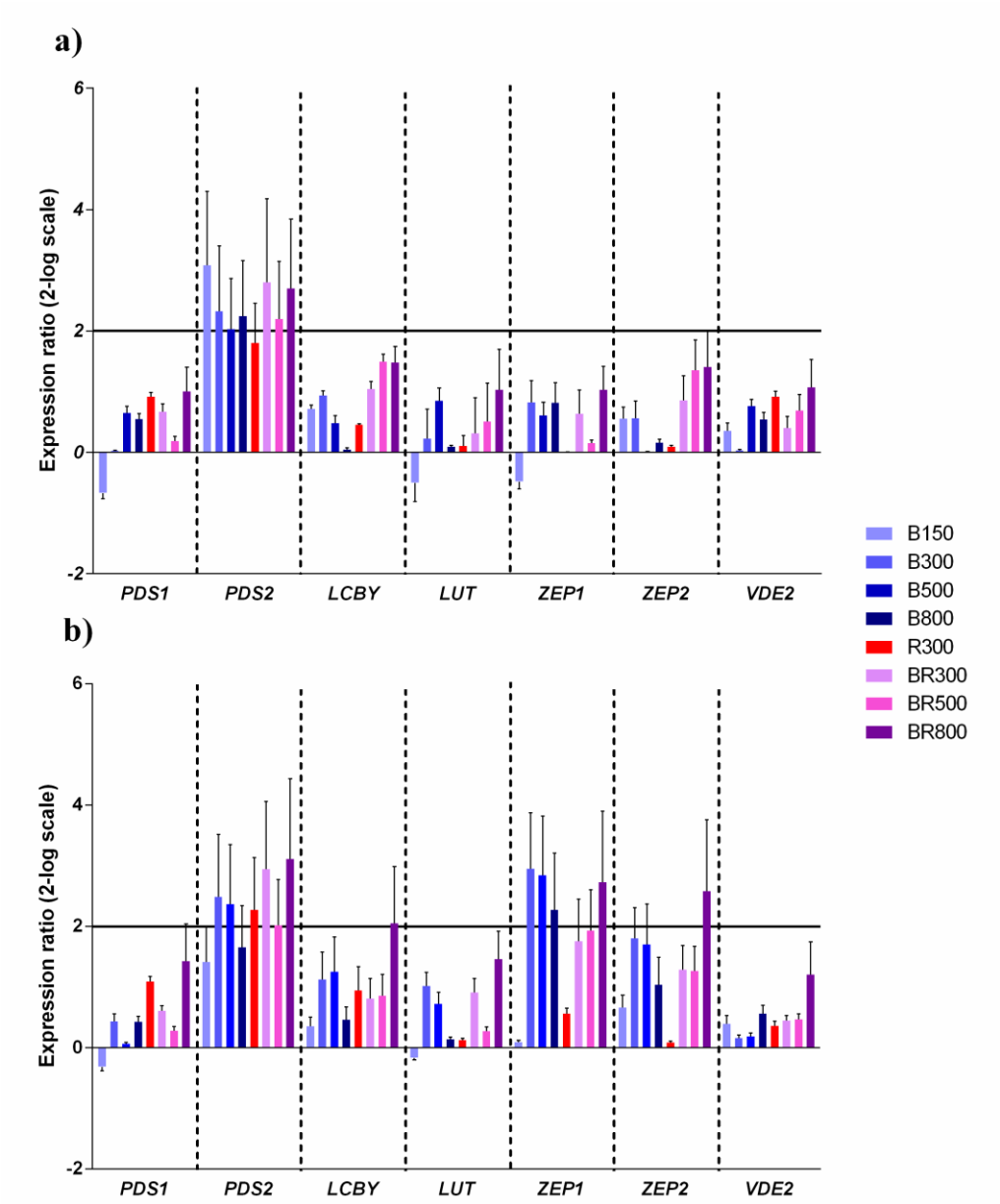

Figure 4.3: Transcriptional expression analysis of carotenoid genes. Samples were collected a) at the end of the gradual light increase (2 hours) and b) at the end of the constant light period (4 hours). Data are reported as fold difference (mean ±SD, n=3) compared to control (samples collected in the dark). Fold differences greater than ±2 (see horizontal guidelines at values of 2 and −2) were considered significant. Phytoene desaturase 1 and 2 (*PDS1* and *PDS2*), lycopene beta cyclase (*LCYB*), lutein deficient protein (*LUT*), zeaxanthin epoxidase 1 and 2 (*ZEP1* and *ZEP2*) and violaxanthin de-epoxidase (*VDE*) are shown.

4.3.3 Antioxidant molecules and activity: the Ascorbic Acid (AsA), the Total Phenolic Content and the DPPH radical scavenging activity

Although PFD did not directly modulate the content of antioxidant molecules ($p>0.05$, $n=48$), the ascorbic acid (AsA) and the total phenolic content (TPC) were correlated to Dt ($p<0.001$, $n=48$) and β-Car ($p<0.001$, $n=48$) suggesting a parallel time scale of response by those molecules and Dt or β-Car as well as an indirect role of light intensity on their synthesis.

AsA peaked at PFD = 500 µmol photons s^{-1} m^{-2}, with a maximal concentration in B500 (366±25 fg AsA $cell^{-1}$), both at 2 and 4h (Fig. 4.4 a). Under the highest PFD (800 µmol photons m^{-2} s^{-1}), AsA stayed low after the gradual light increase period while it increased after the constant light period in BR800 (Fig. 4.4 a). In B800, AsA stayed low at 4h, being thus not produced or quickly consumed. The time- or light increase shape- role on AsA concentration changes in the cells was also revealed by the significant correlation with DES ($p<0.01$, $n=18$) only found after the gradual light increase, i.e. not at 4h.

The total phenolic content increased under high intensity of blue light, especially at 4h (Fig. 4.4 b). Under high blue+red light the amount of phenols were comparable to those of the Dark condition at 2h, and increased only at 4h. The maximal TPC was found at B300 and in a lower way at B800 (686±114 fg Gallic Acid Equivalents (GAE) $cell^{-1}$ and 524±46 fg GAE $cell^{-1}$, respectively; Fig. 4.4 b). Moreover, the TPC was positively correlated to the blue fluence rate ($p<0.01$) while it followed the inverse trend in the red fluence rate ($p<0.01$), underlying the key role of light spectrum in the modulation of these molecules. Anyway, the presence of other reactive compounds in the extract could have hampered the specificity of the assay used to determine the TPC (Everette *et al.*, 2010).

The total antioxidant capacity measured with the DPPH radical scavenging activity did not changed significantly between the experimental conditions, although all the data measured after the gradual light increase were a bit lower with respect of dark, at the exception of B500 (Fig. 4.4 c). A weak trend was also perceptible during the light treatments with a higher activity revealed at 4h with respect of the 2 hours sampling point, even if it was not statistically significant. This result might confirm the dependence of this parameter to the integration of light received during time.

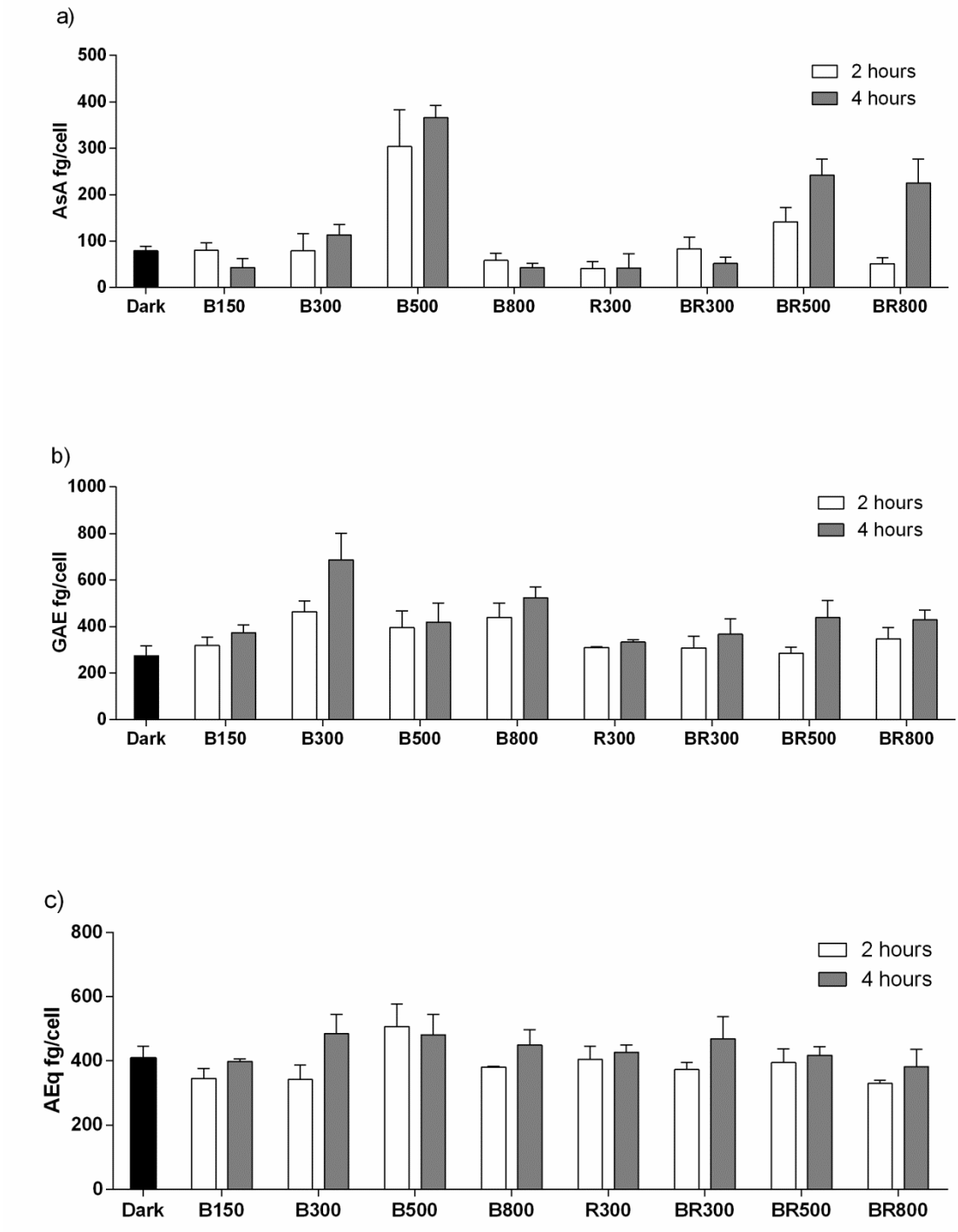

Figure 4.4: Antioxidant molecules content and antioxidant activity. a) ascorbic acid (AsA) expressed as fg per cell; b) total phenolic content (TPC) expressed as fg of gallic acid equivalents (GAE) per cell; c) DPPH radical scavenging activity expressed as fg of ascorbic acid equivalents (AEq) per cell. Samples were collected at Dark (black bars), at the end of the gradual light increase (2 hours, white bars) and at the end of the constant light period (4 hours, grey bars). Data are reported as mean ±SD of three biological replicates (n=9).

4.3.4 Antioxidant enzyme activities

The superoxide dismutase (SOD) catalyses the transformation of superoxide to molecular oxygen and hydrogen peroxide (H_2O_2, (Wolfe-Simon *et al.*, 2005). The SOD specific activity followed an opposite behaviour compared with that of Dt and β-Car ($p<0.01$, $p<0.05$, respectively; n=48), revealing an opposite behaviour with photoprotection and with the antioxidant molecules. The SOD activity was generally higher after the gradual light increase period than after the constant light period (Fig. 4.5 a), at the exception of B800 and BR300. Interestingly, under blue light SOD activity was decreasing with the PFD increase, with the exception of B800 (Fig. 4.5 a). By contrast, at 2h under blue+red, SOD activity was increasing with the PFD increase, showing an opposite trend compared to blue light conditions. A positive effect of the red fluence rate on the SOD activity could therefore be hypothesized, as suggested by its maximal activity recorded in BR800, and high values in R300 and BR500 (Fig. 4.5 a).

Another key enzyme in the antioxidant network is ascorbate peroxidase (APX) that catalyses the reduction of H_2O_2 to water using ascorbate as electron donor (Asada, 1999). The activity of APX (Fig. 4.5 b) was strongly affected by the spectral composition of light. APX was higher in the presence of red light (when provided together with blue) comparatively to the conditions with only blue light, except after the gradual light increase in the lowest light condition B150 (Fig. 4.5 b). As for the SOD activity, increasing blue fluence rate in the only blue light conditions led to a decrease of APX activity compared to the Dark, with the exception of B800. Catalase (CAT) catalyses the production of H_2O from the degradation of H_2O_2. Also CAT activity was affected by the spectral composition of light (Fig. 4.5 c). It was inhibited under monochromatic blue or red light with respect of Dark, while in BR conditions its activity was higher. Under BR conditions, greater the PFD, higher the CAT activity after the constant light period (4h), while at 2h is present an inverse trend (Fig. 4.5 c). Another enzyme, the glutathione reductase (GR) catalyses the reduction of glutathione (GSSG) to its reduced form (GSH) in presence of NADPH. The GR activity did not vary significantly among the different conditions (Fig. 4.5 d). Only in B500 and R300, a significant lowering of GR activity was recorded.

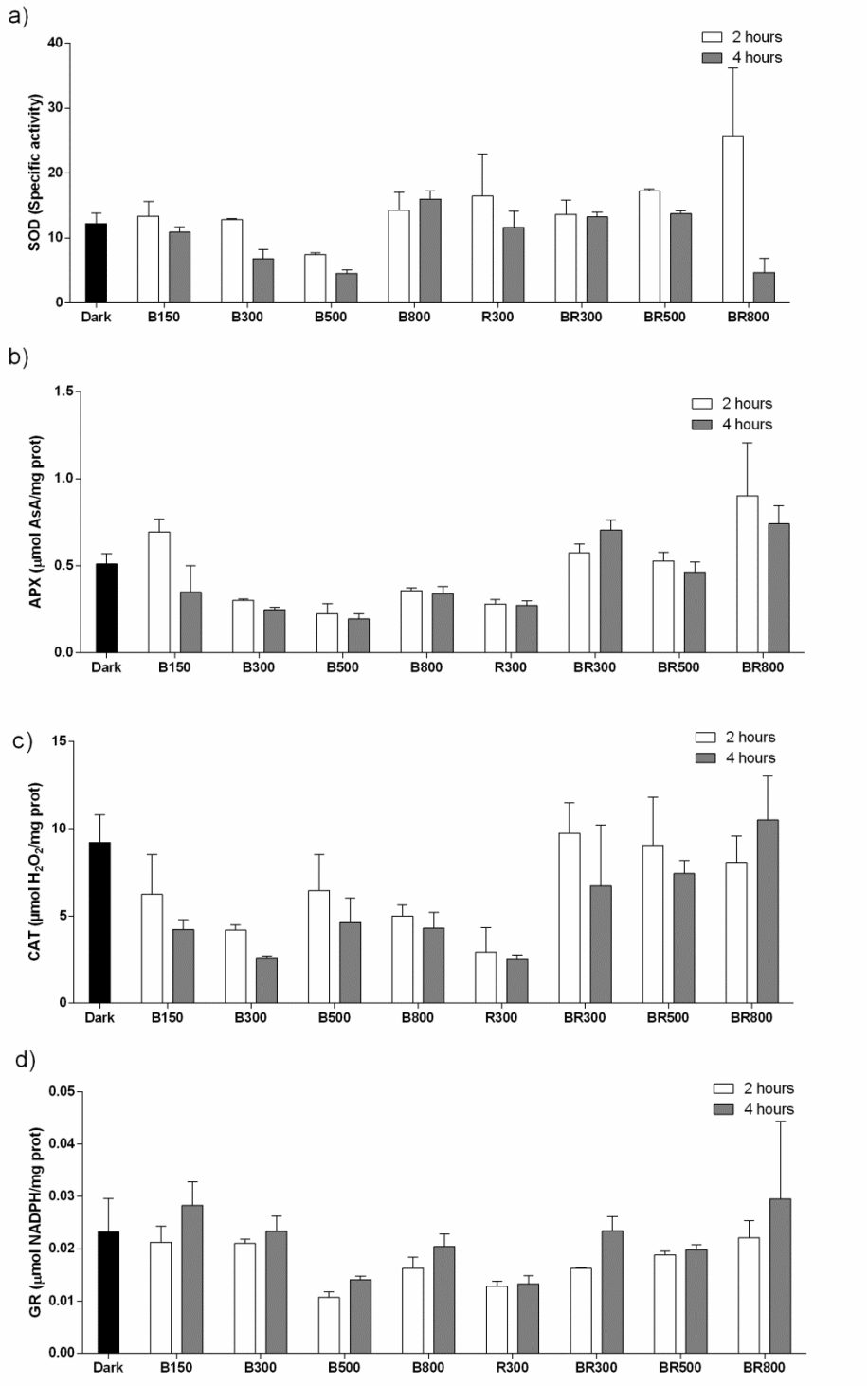

Figure 4.5: Antioxidant enzyme activities. a) superoxide dismutase (SOD) expressed as specific activity, b) ascorbate peroxidase (APX) expressed as µmol of ascorbic acid (AsA) consumed in one minute per mg of proteins, c) catalase (CAT) expressed as µmol of hydrogen peroxides (H_2O_2) consumed in one minute per mg of proteins and d) glutathione reductase (GR) expressed as µmol of nicotinamide adenine dinucleotide phosphate (NADPH) consumed in one minute per mg of proteins. Samples were collected at Dark (black bars), at the end of the gradual light increase (2 hours, white bars) and at the end of the constant light period (4 hours, grey bars). Data are reported as mean ±SD of three biological replicates (n=9).

4.3.5 Antioxidant gene expression

The transcriptional level of the *APX* gene was enhanced in all the conditions, revealing that the regulation of the expression of this gene was not controlled by light experienced by cells (Fig. 4.6 a, b), on the contrary to what observed for the APX enzyme activity (see above and Fig. 4.5 b).

On the opposite, no significant transcriptional variation of the glutathione reductase gene (*GR*) was shown (Fig. 4.6 a, b).

Gene expression for the catalase (*CAT*) was always up-regulated in BR conditions (Fig. 4.6 a). Interestingly, the transcriptional level of the *CAT* gene was up-regulated only at 4h under monochromatic blue or red light conditions (Fig. 4.6 b).

No significant difference in regulation of the transcriptional level of the *SOD* gene compared to the control was observed in BR conditions (Fig. 4.6 a, b). However, under R300 the SOD gene expression displayed an up-regulation at 4h, confirming a positive effect of the red fluence rate on *SOD* (Fig. 4.6 b). By contrast, the *SOD* gene expression was down-regulated under high monochromatic blue fluence rate (B500 and B800) after 2h (Fig. 4.6 a).

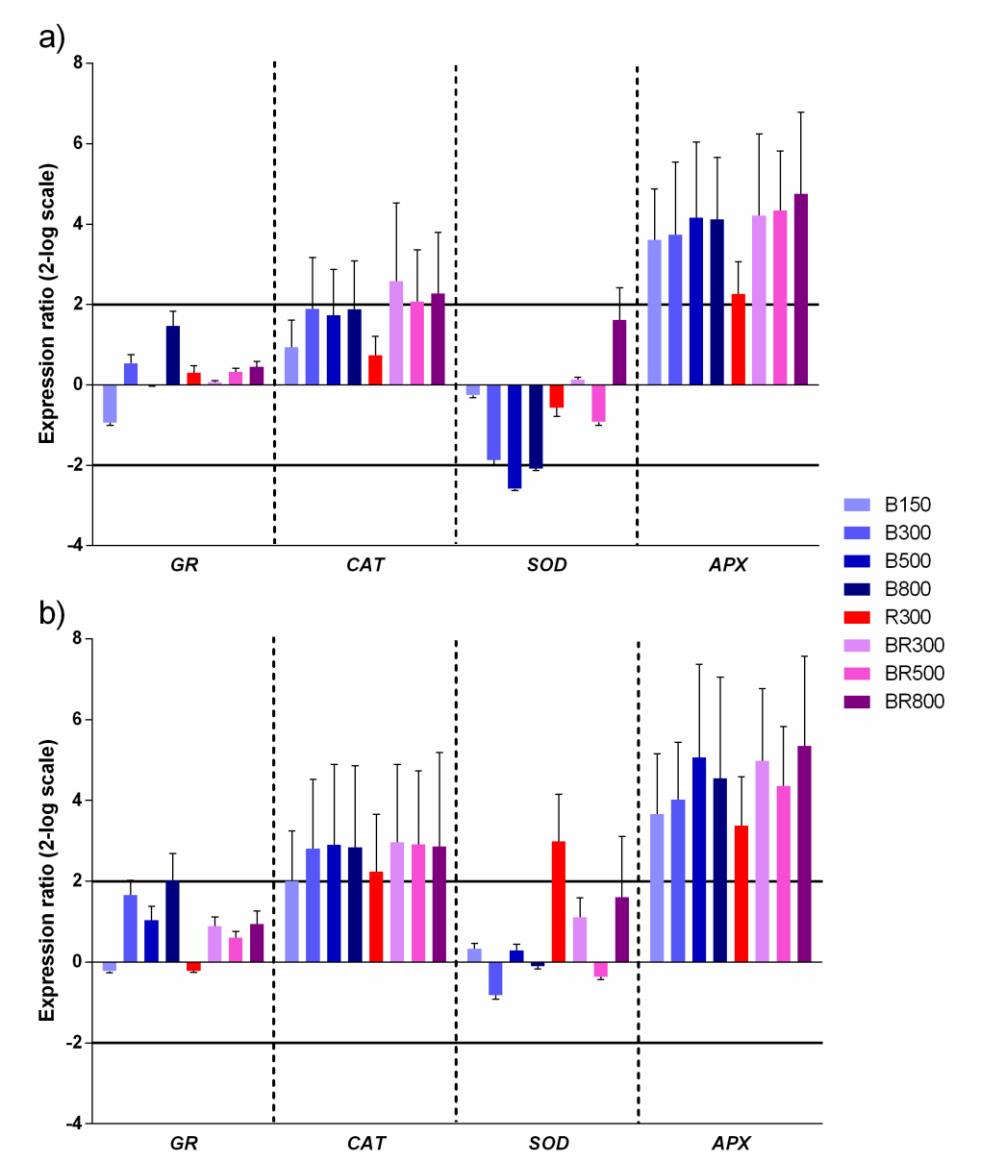

Figure 4.6: Transcriptional expression analysis of antioxidant genes. Samples were collected a) at the end of the gradual light increase (2 hours) and b) at the end of the constant light period (4 hours). Data are reported as fold difference (mean ±SD, n=3) compared to control (samples collected in the dark). Fold differences greater than ±2 (see horizontal guidelines at values of 2 and −2) were considered significant. Glutathione reductase (*GR*), catalase (*CAT*), superoxide dismutase (*SOD*) and ascorbate peroxidase (*APX*) are shown.

4.3.6 Integrative photoprotective and antioxidant responses to spectral and intensity light changes

The diversity of responses developed by cells to cope with the effects of light composition and intensity was noticeable, as also revealed by the principal components analysis (PCA)

performed using all the physiological and biochemical data. The first plot (Fig. 4.7 a) corresponded to the gradual light increase period, with the first two axes of the PCA explaining 57% of the total variability. Two main groups, i.e. monochromatic blue (B) and blue+red (BR) lights were segregated independently on the PFD reached after the 2h progressive light increase from dawn. The spectral composition of light explained the highest variability observed in the data set (axis 1 of the plot Fig. 4.7 a, 37%). Interestingly, the activity of the four enzymes pulled the BR group segregation, with BR800 mainly drawn by SOD, APX and GR activity while CAT was related to BR300 and BR500. The blue conditions were separated into two subgroups, the first one composed by B500 which was relied to an enhancement of Dt and AsA, while the B300 and B800 group was explained by the XC precursors and TPC.

The second plot (Fig. 4.7 b) corresponded to the constant light data set; the first two axes of the PCA explained 62% of the total variability, with the first accounting for 42% and the second for 20% (Fig. 4.7 b). The two main clusters of light conditions, i.e. monochromatic blue and blue+red lights were still segregated, but relevant changes compared to the gradual light increase were noticeable. Enzymes activity mainly accounted for BR300, while BR500 and BR800 were more related to the XC dynamics (Dd $cell^{-1}$, (Dd+Dt) $cell^{-1}$). This BR group showed a higher heterogeneity than the B group, which was drawn by AsA, TPC, Dt and β-Car.

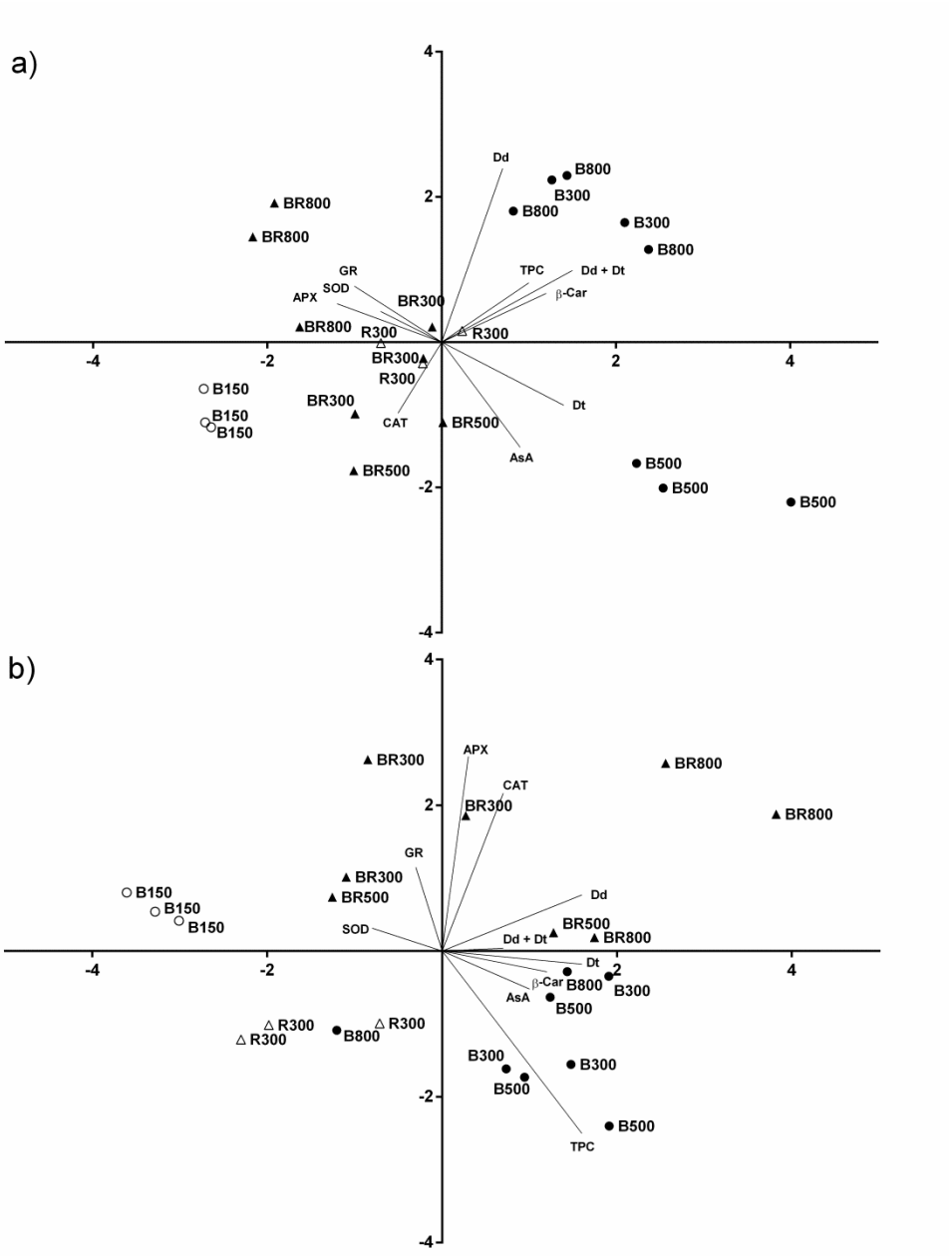

Figure 4.7: Principal components analysis (PCA). Data set consisted in the photoprotective and antioxidant network parameters, i.e. xanthophyll cycle pigments (Dt, Dd, Dd + Dt), β-carotene (β-Car), total phenolic content (TPC), ascorbic acid (AsA) and the activity of glutathione reductase (GR), catalase (CAT), ascorbate peroxidase (APX) and superoxide dismutase enzyme (SOD). The analysis was performed on data collected a) at the end of the gradual light increase (2 hours) and b) at the end of the constant light period (4 hours).

4.4 Discussion

In the marine environment dramatic changes of light spectrum occur together with variations of the photon flux density (PFD) along the water column (Depauw *et al.*, 2012, Brunet *et al.*, 2014). Among wavelengths ranging in the visible region (400-700 nm), blue and red mostly affect microalgal life traits (Depauw *et al.*, 2012). From a bio-optical point of view, two main conditions exist in the water column: the absence of red and a low light intensity regime in the deeper water layers, beneath the moderate to high light superficial layer characterized by the presence of red together with the other wavelengths in the range 400-700 nm. In this layer, a large decrease of fluence rate occurs, different for the diverse wavelengths, inducing changes in the blue:red ratio. For instance, in the sunny Mediterranean sea basin, this ratio varies from 0 to ≈ 0.50 (Brunet *et al.*, 2014), corresponding to PFD of 300 to 1000 µmol photons s^{-1} m^{-2} (see Fig. 1 in Brunet *et al.* (2014)).

While blue is the wavelength with the highest level of energy and red with a lowest, both are harvested by pigments fuelling the photosynthetic machinery and are sensed by photoreceptors (Depauw *et al.*, 2012) inducing downstream cascades of metabolic and physiological reactions (Depauw *et al.*, 2012, Schellenberger Costa *et al.*, 2013a, Schellenberger Costa *et al.*, 2013b, Brunet *et al.*, 2014).

The study is based on the hypothesis that different combinations of colours (blue, red or mixed blue+red) and PFD affect the capacity of cells to photoacclimate and photoprotect coping with light variations. The aim was to investigate how the short term response relied on antioxidant and photoprotective network system is modulated by spectral variations (presence *vs.* absence of red at different light intensities). The light conditions applied were: high light with red (natural), high light without red (unnatural), low light with red (unnatural) and low light without red (natural).

It was found that PFD directly drives the pigment photoprotection mechanism and it does affect the antioxidant network system. This suggests that the different mechanisms involved into the photodefence network are activated by different light properties. Waring *et al.* (2010) showed that in the diatom *Thalassiosira pseudonana* the activity of the enzymes superoxide dismutase (SOD) and ascorbate peroxidase (APX) is driven by the light

experienced by cells and modulated by the light history. After a high light stress period, cells pre-acclimated to high light showed a higher enzymatic activities than cells pre-acclimated to low light.

The results show that the presence of red together with blue light fosters the antioxidant enzyme activities of APX, SOD and catalase (CAT) compared to monochromatic blue light, that on the contrary inhibit these activities. Since the red+blue light conditions mimic the natural upper layer environment, the results reported here highlight the key role of the adaptive traits of microalgae to the natural environment in inducing physiological protective mechanisms. Since the fluence rate is similar between blue and blue+red for each PFD condition, the heterogeneity of responses is probably under the control of photoreceptor signalling and do not only depend upon sensing mechanisms such as the change in the redox state or the production of reactive oxygen species (Li *et al.*, 2009, Foyer & Shigeoka, 2011). Recent studies on diatoms reveal that some photoacclimative patterns may be directly promoted by photoreceptor-mediated light sensing (Depauw *et al.*, 2012, Schellenberger Costa *et al.*, 2013a). Also, in another diatom it has been shown that the presence of red together with low blue light activates the photoprotective xanthophyll cycle (XC) operation compared to the same PFD provided by monochromatic blue light (Brunet *et al.*, 2014). Schellenberger Costa *et al.* (2013a) hypothesized that the energy dissipation under monochromatic red light is linked to an increased mitochondrial respiration, that in turn can induce oxidative stress (Tiwari *et al.*, 2002). We thus hypothesize that the presence of red in addition of blue light directly enhances the formation of ROS and therefore the "first line defence" such as the antioxidant enzymatic activity.

CAT catalyses the disproportionation of H_2O_2 to H_2O and O_2 and possesses different isoforms. It's mainly found in the peroxisomes (Mhamdi *et al.*, 2012) where H_2O_2 can arrive from cytosol in condition of high levels of ROS production (Mittler, 2002). Surprisingly, after the constant monochromatic blue light period a discrepancy between gene expression and enzymatic activity is reported, being the gene upregulated while the activity is inhibited with respect of the dark condition. This feature confirms the inactivation of CAT by high monochromatic blue light as described in higher plants (Shang & Feierabend, 1999). In the same way, while transcriptional expression of *APX* is always upregulated, its activity is limited under high monochromatic blue light. This uncoupling

can be caused by post-translational modifications, for example those mediated by nitric oxide-derived molecules that are able to both enhance or inhibit this enzymatic activity (Begara-Morales *et al.*, 2014). The variability of the APX enzyme activity indicates different physiological mechanisms of photodefence in blue+red compared to blue light, since this enzyme is involved in the water-water cycle in chloroplasts and in the ascorbate-glutathione cycle (Mittler, 2002). APX reduces H_2O_2 to H_2O using ascorbic acid as substrate, producing monodehydroascorbate (MDHA) and then dehydroascorbate (DHA) (Mittler, 2002). It is found in different isoforms specific for the three compartments: thylakoid bound, stromal and cytosolic (Mittler & Zilinskas, 1993). The discrepancy between *SOD* transcriptional expression (never upregulated except under monochromatic red light) and SOD enzymatic activity (higher under blue+red, B800 and monochromatic red) might be due to the fact that the gene expression of only one isoform of this enzyme has been analysed. In fact there are multiple isoforms of SOD with different intracellular localization: FeSOD, which is the form analysed by real time qPCR, is typically localized in the chloroplast and cytoplasm, while MnSOD is associated with the lumen side of photosystems and mitochondria, the major sites of superoxide formation (Wolfe-Simon *et al.*, 2005); Cu/ZnSOD seems to be absent in most eukaryotic microalgae even though this statement needs to be confirmed (Janknegt *et al.*, 2009). Probably, an increase in *FeSOD* gene expression might be paralleled to a decrease in the other isoforms, resulting in an overall lower enzymatic activity, and *vice-versa*.

While the presence of red light enhances the antioxidant enzyme activities, its absence - i.e. the monochromatic blue light conditions - induces different photoresponses compared to blue+red, such as an increase of the antioxidant molecules, ascorbic acid (AsA) and total phenolic content (TPC). The correlation of AsA with TPC and the photoprotective pigment diatoxanthin (Dt) as well as its precursor along the biosynthetic pathway (β-Car) confirms the role of high light in their synthesis. This behaviour suggests a similar use of environmental cues of the analysed processes: the XC-photoprotection mechanism and the antioxidants synthesis (AsA and TPC). Anyway, being AsA reactive towards the reagent used to determine TPC (Everette *et al.*, 2010), these correlation could be caused by a lack of specificity of the assay. Segregating the different spectral conditions, the positive correlation between TPC and blue fluence rate together with the negative relationship between TPC and the red fluence rate reveals an inhibition of TPC synthesis induced by

red. Indeed, we exclude as cause of this feature the role of the high energy level brought by blue compared to red on the TPC modulation, since we should have high TPC under BR500 or BR800 (blue fluence rate of 250 and 400 µmol photons m^{-2} s^{-1}, respectively) as under B300 or B500 (blue fluence rate of 300 and 500 µmol photons m^{-2} s^{-1}, respectively).

Although the different antioxidant molecules concentration, the DPPH radical scavenging activity did not showed significant changes, probably because this assay is strongly dependent upon the solvent used (i.e. some antioxidants may precipitate), the pH, and the reaction times of the different molecules (Sharma & Bhat, 2009, Nicklisch & Waite, 2014).

However, high monochromatic blue light, which does not exist in nature, induces some peculiar photoresponses. The activation of the XC occurred when the blue fluence rate was ≥ 300 µmol photons m^{-2} s^{-1} and interestingly the Dt concentration was comparable between the treatments, although the PFD were significantly different, ranging from 300 to 800 µmol photons m^{-2} s^{-1}. This result is paralleled with the upregulation of the expression of *ZEP1*, so probably this isoform is involved in the conversion from zeaxanthin to violaxanthin, precursor of diadinoxanthin (Dd) and Dt, rather than in the conversion from Dt back to Dd. The violaxanthin de-epoxidase (VDE) is one of the putative enzymes that converts Dd in Dt (Depauw *et al.*, 2012) and requires AsA as substrate (Grouneva *et al.*, 2006). However, among the different functions of this molecule AsA is also a substrate for APX, and is able to scavenge ROS directly as an electron donor for hydroxyl radicals. The latter function might explain its increase under B300 and especially B500 that would decrease its availability for Dd to Dt conversion. The peculiar and damaging effect of high monochromatic blue light is strengthened by the results obtained in B800. The protective mechanisms developed by cells in B800 are not enough to fully protect the photosystems, as shown by the lowering of Fv/Fm and chlorophyll *a* (Chl.*a*). The unvaried fucoxanthin concentration compared to the other light conditions indicates changes at the level of the reaction centres and probably not in the antennae. Also, relevant biochemical changes occur in the cells, such as the opposed trend between AsA and Dt or TPC, on the opposite to what is obtained under the other high light conditions (B500, BR500 and BR800).

Our study reveals the noticeable production of TPC in the diatom *Skeletonema marinoi*, especially under unnatural high monochromatic blue light. In higher plants, many compounds belong to the TPC group, such as simple phenols, phenolic acids, flavonoids, tannins and lignin. They are secondary metabolites produced from the shikimate-

phenylpropanoids-flavonoids pathways, and constitute one of the most common and widespread groups of substances in plants (Cheynier *et al.*, 2013). Many functions of these compounds have been highlighted, such as UV sunscreen, allelochemichals, as pigment responsible for fruit and flower colour and as internal physiological regulators (Lattanzio *et al.*, 2006). Studies on higher plants demonstrated the role of UV light in enhancing the phenolic content in a dose-dependent manner and in increasing the total antioxidant activity of plant extracts (Wilson *et al.*, 2001, Wang *et al.*, 2009). Among phenolic compounds, flavonoids act as potent antioxidant thanks to their ability to donate electrons or hydrogen atoms directly to reactive species (Pietta, 2000). They have the capacity to inhibit lipoxygenase (Pietta, 2000) and to chelate metals inhibiting important sources of ROS, i.e. the Haber-Weiss and Fenton reactions (Sharma *et al.*, 2012).

The phenolic content in diatoms and other microalgae is less known and few studies explored the change in its concentration in response to light and other environmental stressors (Duval *et al.*, 2000, Kovacik *et al.*, 2010, Goiris *et al.*, 2015). UV-C radiations determined an increase in phenolics in the green alga *Chlamydomonas nivalis* (Duval *et al.*, 2000). In another green alga, *Scenedesmus quadricauda*, UV-A exposure did not determine changes in TPC, but caused a decrease of some flavonols and an increase of benzoic acid, while UV-C induced the breakdown of flavonols and a decrease in cinnamic acid (Kovacik *et al.*, 2010). Differences in these studies might be due to the different UV radiations (A or C) applied and to different combination between light intensity and UV-dose. Indeed, it has been reported that the photoprotective responses to UV are narrowly dependent on the PAR intensity applied in combination with UV (Brunet *et al.*, 2011).

The TPC in *S. marinoi* (this study) is in the higher range of values reported from microalgae (Li *et al.*, 2007, Hajimahmoodi *et al.*, 2010, Goiris *et al.*, 2012). In average, values ranged from 2.11 mg GAE g^{-1} dry weight (DW) to 10.8 mg GAE g^{-1} DW (Li *et al.*, 2007, Hajimahmoodi *et al.*, 2010, Goiris *et al.*, 2012). In *Phaeodactylum tricornutum* it has been found a value of 3.5 mg GAE g^{-1} DW (Goiris *et al.* (2012). Assuming a dry weight per cell equivalent to 55 pg as in *S. costatum* (FAO, 1996), we estimate an average TPC ≈ 6.6 mg GAE g^{-1} DW, with values of 12.4 and 9.5 mg GAE g^{-1} DW under B300 and B800, respectively.

Hajimahmoodi *et al.* (2010) and Goiris *et al.* (2012) demonstrated that phenolic compounds are the main contributor to microalgal antioxidant capacity, highlighting that microalgae

can be used as a source of natural antioxidants. In *P. tricornutum*, Goiris *et al.* (2012) measured a Trolox Equivalent Antioxidant Capacity (TEAC) ≈ 19 µmol trolox eq. g^{-1} DW in correspondence to a sum of 3.5 mg GAE g^{-1} DW and 3.6 mg carotenoid g^{-1} DW. Therefore, we roughly estimate that in our samples with TPC and carotenoid content ≈ 6.6 mg GAE g^{-1} DW and 2.4 mg g^{-1} DW respectively, the estimated TEAC would be ≈ 25 µmol trolox eq. g^{-1} DW. Moreover, by light manipulation (B300), the TPC ≈ 12,4 mg GAE g^{-1} DW with a carotenoid content ≈ 2.9 mg g^{-1} DW, we might expect an increase of TEAC to 41 µmol trolox eq. g^{-1} DW. Mean values of 9 and 0.9 µmol trolox eq. g^{-1} DW were obtained from medicinal plants and edible fruit or vegetables, respectively (Cai *et al.*, 2004), while it is known that a sample with a TEAC value above 10 µmol trolox eq. g^{-1} DW is considered rich in antioxidants (Cai *et al.*, 2004).

In conclusion, our study demonstrates that the photodefence strategies adopted by cells are modulated by the combination of light intensity and spectral composition. The high monochromatic blue light fosters the synthesis of bioactive molecules such as AsA, phenolics and XC pigments. The presence of red together with high blue light, that mimics the natural marine upper layer environment, enhances the activation of the antioxidant enzymes CAT, SOD and APX.

Our study provides insights into the great potential of microalgae as source of antioxidant molecules, and on the role of light manipulation of diatom's cultivation as a tool for enhancing the production of bio-molecules.

5. Growth phase dependent activation/functioning/performance/ efficiency of protective and antioxidant network in *Skeletonema marinoi*

5.1 Introduction

Microalgal cells cultivated in batch cultures in nutrient-replete conditions follow successive steps during growth (Fig 5.1). After the lag phase, i.e. acclimation to the new culture condition, cells grow rapidly during the exponential growth phase. When the nutrients begin to run low, cells enter into the stationary phase, a stage also known as conditional senescence (McLean, 1968, Humby *et al.*, 2013), characterized by a block of cell division with further decrease in the cell concentration. During this phase, microalgae are subject to metabolic and structural changes leading to cell death. It has been observed that in stationary phase pigment content changes, photosynthetic capacity decreases, and an accumulation of cytosolic lipid bodies enriched of carotenoids occurs (Hu *et al.*, 2008, Vidoudez & Pohnert, 2012, McLean, 1968). These lipid bodies may have a role in photoprotection, functioning as a sink for the electrons generated in the photosystems. They can also absorb the excess light, "shading" the chloroplasts, and so reducing the oxidative stress (Hu *et al.*, 2008). Therefore, the change in the ultrastructure during cell senescence may alter the light perception and thus the activation of the photoprotective mechanisms. The lower ability to fix carbon during cell aging may increase the chance of ROS generation through the transfer of the excitation energy to oxygen, caused by the over-reduction of the NADP pool.

The biological and physiological changes occurring in cells entering into the senescence phase have been deeply studied in higher plants (Noodén (2003) and bibliography therein), while the knowledge in microalgae is still little (Ribalet *et al.*, 2007a, Barofsky *et al.*, 2010, Vidoudez & Pohnert, 2012, Humby *et al.*, 2013). In order to fill this gap, the activation of protective and antioxidant network in *Skeletonema marinoi* was investigated during active and stationary growth phase. Our hypothesis is that the defence network related to photoprotection and antioxidant activity increases during senescence. The questions we address are:

- What is the extent of the defence network changes?
- Do cells invest into antioxidant molecules synthesis?
- Do these changes affect the infradiel responses to light variations?

The general objective of this study is to investigate if cells entered in stationary phase display a higher content of bioactive molecules, such as the antioxidant ones, therefore enabling their enhanced extraction from algal biomass for biotechnological purposes.

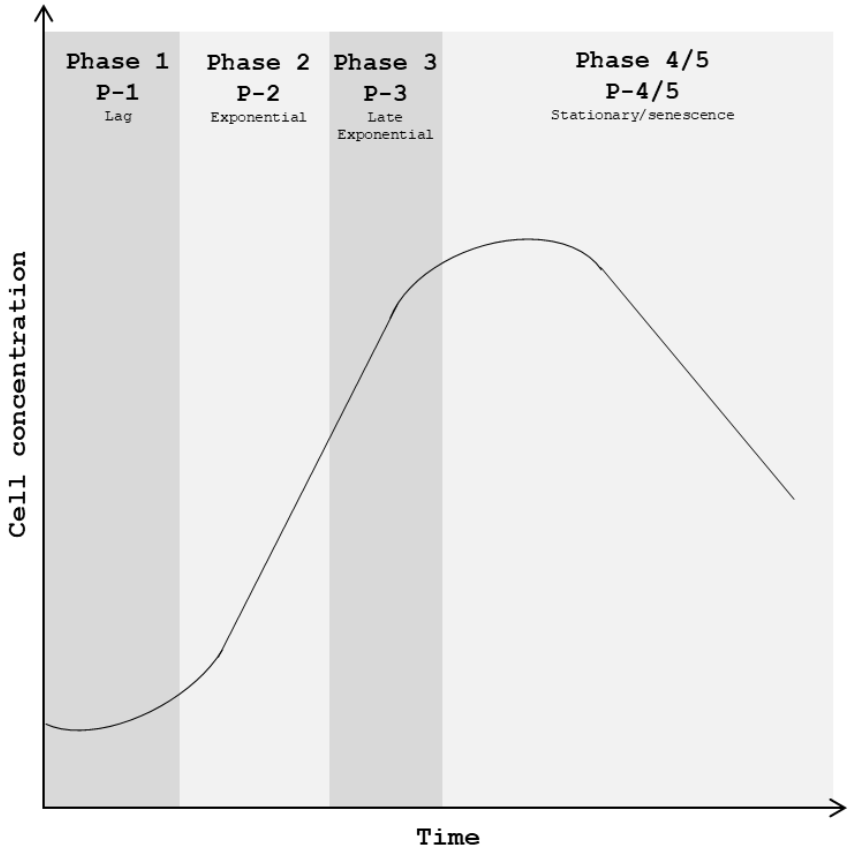

Figure 5.1: Growth phases of microalgal cultures according to Humby *et al.*, 2013. Phase 1 (P-1) Lag; Phase 2 (P-2) Exponential; Phase 3 (P-3) Late exponential; Phase 4/5 (P-4/5) Stationary/senescent

Cultures were provided with a light that mimics what microalgae can perceive at sea between 5 and 10 meters depth (depending on the season) in coastal waters: a sinusoidal white light composed by Red:Green:Blue (RGB) with a ratio of 10:40:50. The mixture of these three colors allows the overall stimulation of the intracellular responses controlled by the different photoreceptors. In fact, as previously observed, the spectral light quality is a key activator of photophysiological responses (Schellenberger Costa *et al.*, 2013a, Brunet *et al.*, 2014, Jungandreas *et al.*, 2014, Orefice *et al.*, 2016, Smerilli *et al.*, 2017), together with light intensity. It is known that monospectral light induces specific photophysiological responses due to photoreceptor deactivation and the consequent lack of cell signaling (Schellenberger Costa *et al.*, 2013a, Brunet *et al.*, 2014, Smerilli *et al.*, 2017).

5.2 Materials and methods

5.2.1 Culture conditions

The experiments were conducted on the centric diatom *Skeletonema marinoi*, grown at 20°C in 4.5 L glass tanks with air bubbling.

The cells were long term acclimated to a sinusoidal light distribution with a midday peak of 150 µmol photons s^{-1} m^{-2} and with a photoperiod equal to 12:12 dark:light, following the results obtained by Chandrasekaran *et al.* (2014), Orefice *et al.* (2016) and Smerilli *et al.* (2017).

The white light was composed by Red:Green:Blue (RGB) with a ratio of 10:40:50.

The optimization of growth conditions due to the light provided and the water mixing allowed reaching a very high growth of cells in the pre-acclimation condition (growth rate >1 d^{-1}). Indeed, in this experiment – and in the following ones (see successive chapters 6, and 7) - we used a new device for water movement in the flasks compared to the one used for the previous experiments (an electric rotor instead of airstones). By consequence, to avoid a too fast nutrient depletion, we enriched the culture medium doubling the content of the essential nutrients (phosphate, silicates, metals and vitamins).

5.2.2 Experimental strategy and parameters analyzed

During the experiment, the three cultures were sampled twice a day (at pre-dawn, just before the switch on of the light, and at the midday light peak reached after 6 hours) during the exponential (phase 2; P-2), late exponential (phase 3; P-3) and stationary/senescent growth phases (phase 4/5; P-4/5), according to (Humby *et al.*, 2013)(Fig. 5.1). The lag phase (phase 1) was not considered in this experiment.

The subsequent parameters were followed during the experiment:

- Cell concentration
- Photochemical efficiency of the photosystem II
- Electron transport rate (ETR)-light curves
- Non-photochemical quenching (NPQ)
- Photosynthetic and photoprotective pigments

- Absorption spectrum of the cells
- Total phenolic content
- Total flavonoid content
- Ascorbic acid content
- ABTS radical scavenging activity

The experimental procedures for the analysis of these parameters are described in the chapter 2.

5.3 Results

5.3.1. Growth rate and photosynthesis

The growth capacity of the cells during the three different growth phases is reported in the Table 5.1. As it can be observed from these values, a little decrease of μ occurred between exponential (P-2) and late exponential (P-3) growth phases, while in the last day of the experiment μ became negative (stationary/senescent phase, P-4/5), i.e. the death exceeded the division rate.

Table 5.1: Growth properties of the cultures. Cell concentration expressed as cell mL^{-1}, and growth rate expressed as μ, d^{-1}, during the exponential phase (P-2), late exponential phase (P-3), and stationary/senescent phase (P-4/5) Data are reported as mean ±SD of three biological replicates (n=3).

	Exponential phase P-2	Late exponential phase P-3	Stationary/senescent phase P-4/5
Cell concentration Cells mL^{-1}	285'380 ± 42'807	815'517 ± 125'337	527'932 ± 67'219
Growth rate μ, d^{-1}	1.24 ± 0.11	1.05 ± 0.16	-0.43 ± 0.28

Photosynthetic electron transport rate (ETR, Fig 5.2) followed the growth rate trend with a decrease between P-2 and P-3. However, no difference was noticeable between the late exponential and stationary phase, on the contrary to what observed for the growth rate.

The main difference in ETR between P-2 and the two other phases was observed in the pre-dawn sampling, which resulted statistically significant with P-4/5 ($p<0.05$).

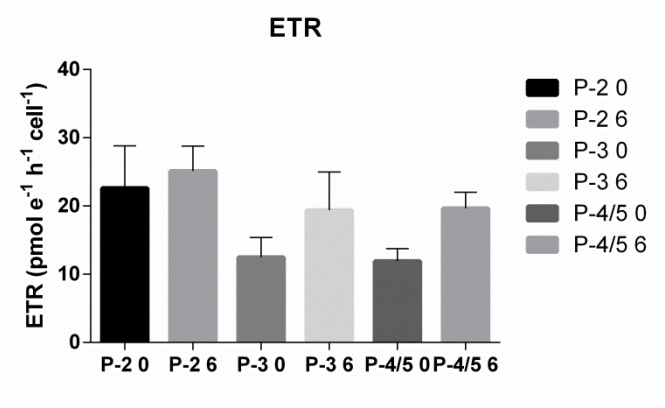

Figure 5.2: Electron Transport Rate (ETR, pmol e^- $cell^{-1}$ h^{-1}). Samples were collected at pre-dawn (0) and midday (6) during the exponential (P-2), late exponential (P-3), and stationary/senescent (P4/5) phases. Data are reported as mean ±SD of three biological replicates (n=3)

5.3.2 Photosynthetic acclimation and pigments

The photochemical efficiency of the photosystem II (Fv/Fm) did not vary significantly with cell aging, ranging between 0.79 ± 0.01 and 0.70 ± 0.05 (Fig. 5.3 a), revealing that cells were able to maintain high Fv/Fm even when passing through different growth phases.

The light use efficiency (α, Fig. 5.3 b) lowered with time, starting from 0.050 ± 0.007 and stabilizing around 0.029 ± 0.004 in the late exponential and stationary/senescent phases. Interestingly, α enhanced with the midday light increase during the exponential phase, while this infradiel acclimation disappeared in the successive growth phases.

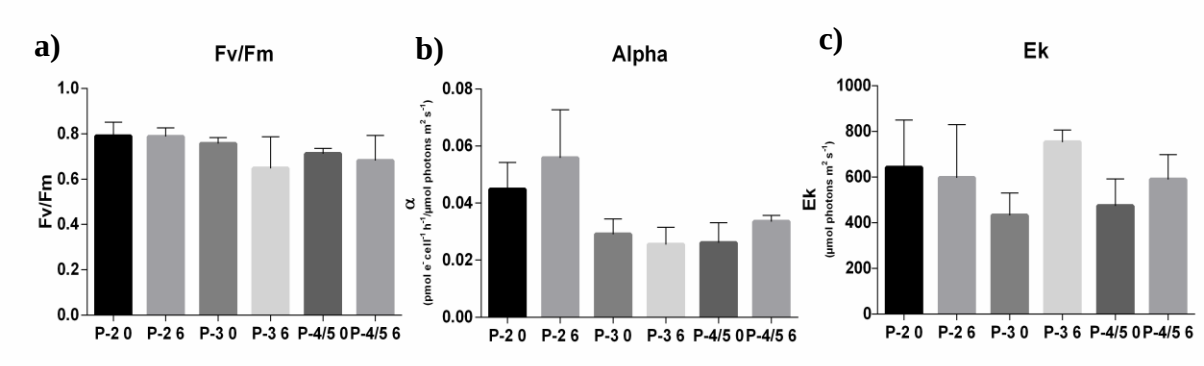

Figure 5.3: Photosynthetic parameters. a) Fv/Fm (maximum quantum yield of the PSII); b) α (maximum light use efficiency in pmol e^- $cell^{-1}$ h^{-1}/µmol photons m^{-2} s^-1); c) Ek (light saturation index for photosynthesis, in µmol photons m^{-2} s^{-1}). Samples were collected at pre-dawn (0) and midday (6) during the exponential (P-2), late exponential (P-3), and stationary/senescent (P4/5) phases. Data are reported as mean ±SD of three biological replicates (n=3).

The light saturation index for photosynthesis (Ek, Fig. 5.3 c) was relatively stable in the three growth phases. Interestingly, it followed an opposite trend compared to α (Fig. 5.3 b): Ek did not change during the day in the exponential phase, although it followed an increase at midday compared to pre-dawn in the two successive growth phases. This might indicate a modulation of the infradiel acclimation strategy between the different growth phases.

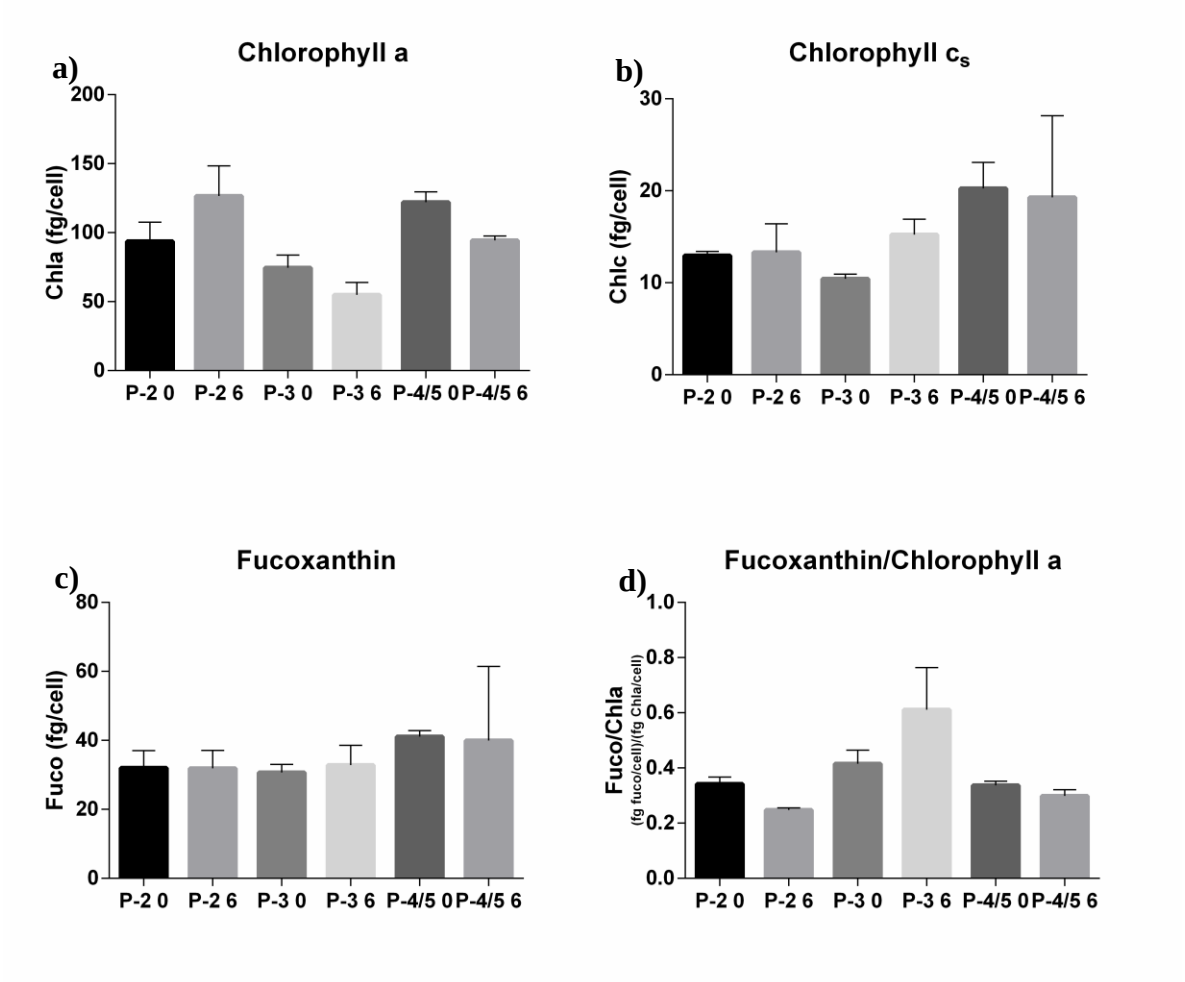

Figure 5.4: Photosynthetic pigments. a) Chlorophyll a (Chla in fg/cell); b) Chlorophyll c_s (Chlc in fg/cell); c) Fucoxanthin (Fuco in fg/cell); d) Fucoxanthin/Chlorophyll a ratio. Samples were collected at pre-dawn (0) and midday (6) during the exponential (P-2), late exponential (P-3), and stationary/senescent (P4/5) phases. Data are reported as mean ±SD of three biological replicates (n=3).

The chlorophyll a (Chla) content per cell varied with cell aging (Fig. 5.4 a). Firstly, it decreased from exponential to late exponential phase, with also an inverted trend between pre-dawn and midday. The increase in Chla content per cell at midday in the exponential phase was probably relied to the cell cycle progression, and the relative increase of molecules in preparation of cell division. The slow-down of growth in P-3 probably

masked this feature. At pre-dawn, Chla during the stationary/senescent phase was significantly higher compared to both exponential and late exponential phases ($p<0.05$ and $p<0.01$, respectively). This enrichment in Chla might be related to the stop of division.

Interestingly, chlorophyll c (Chlc) per cell did not follow the same trend as Chla. It was stable between the exponential phase and in the late exponential phase (Fig. 5.4 b), while an increase was observed in the stationary/senescent phase.

Fucoxanthin (Fuco) per cell followed the same trend as Chlc, with similar values in the exponential and late exponential phase, and a significant increase during the stationary/senescent phase ($p<0.05$).

The Fuco/Chla ratio changed along the experiment revealing a change in the antenna/reaction center dynamical acclimation between the growth phases. It lowered between pre-dawn and midday of the exponential phase ($p<0.01$), inverting this trend during the late exponential phase when the highest values of this ratio were recorded, and reestablishing the initial values in the stationary/senescent phase.

5.3.3 Non-photochemical quenching and xanthophyll cycle

During the exponential and late exponential phases the non-photochemical quenching (NPQ) significantly decreased ($p<0.05$) at midday compared to pre-dawn (Fig. 5.5 a). This feature denoted an infradiel acclimation of the photoprotective behavior during the day. By contrast, when cells stopped to grow, this infradiel acclimation disappeared, with high values of NPQ measured both at pre-dawn and midday.

The higher NPQ in P-4/5 was accompanied by a higher content of the photoprotective pigment diatoxathin (Dt), which increased progressively from 0.5 fg/cell to a concentration of almost 2.5 fg/cell at midday of the last sampling day (Fig. 5.5 b). Also its precursor diadinoxanthin (Dd) was enhanced in the stationary/senescence compared to the previous phases (Fig. 5.5 c). An infradiel variation of Dd with an increase at midday compared to pre-dawn, also present in Dt, was noticeable except in the stationary phase, where Dd decreased probably due to its conversion into Dt.

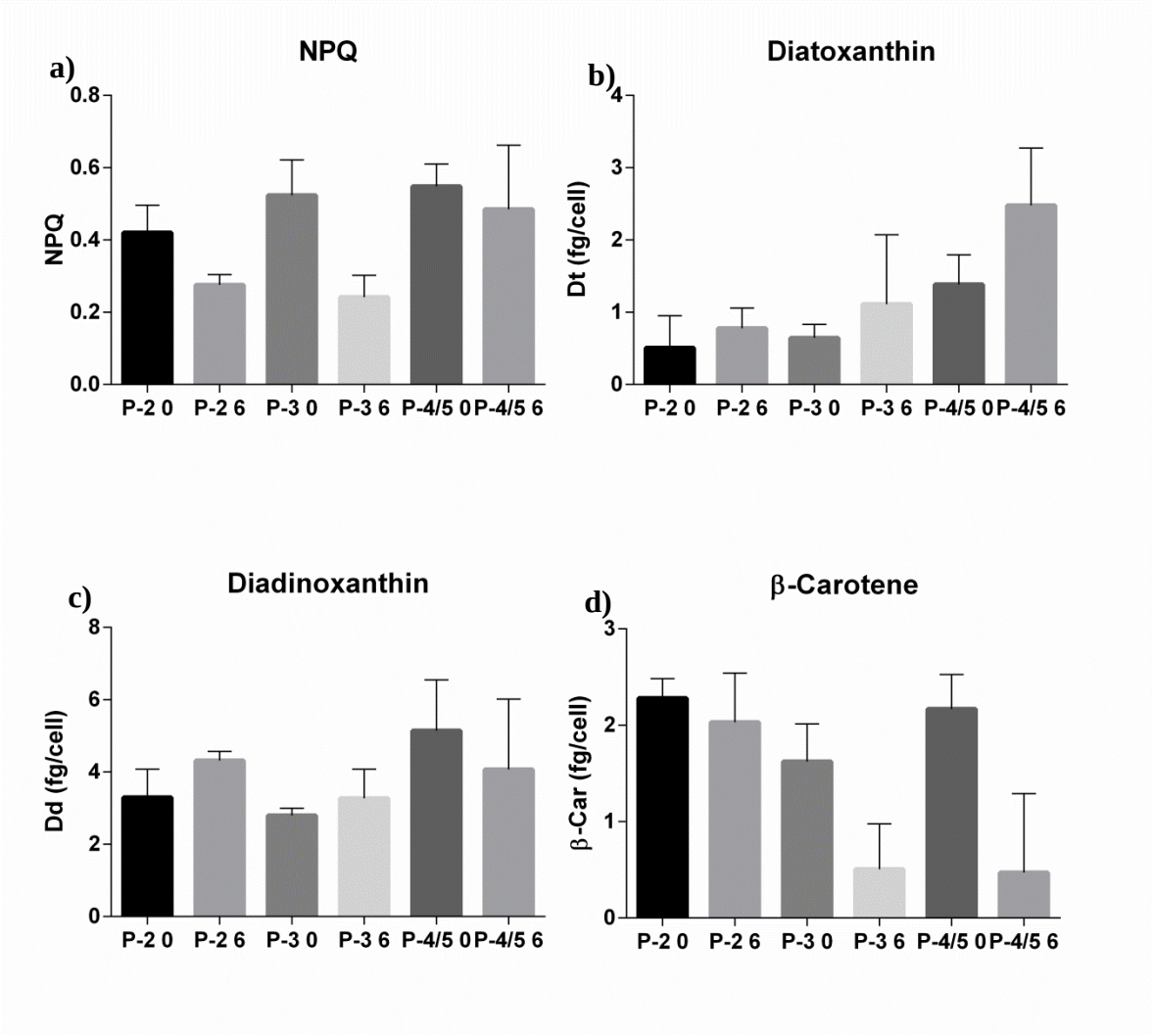

Figure 5.5: Photoprotection. a) non-photochemical quenching (NPQ); b) Diatoxanthin (Dt in fg/cell); c) Diadinoxanthin (Dd in fg/cell); d) β-carotene (β-car in fg/cell). Samples were collected at pre-dawn (0) and midday (6) during the exponential (P-2), late exponential (P-3), and stationary/senescent (P4/5) phases. Data are reported as mean ±SD of three biological replicates (n=3).

The precursor of these pigments, β-carotene (β-car), was higher at pre-dawn respect to midday (Fig. 5.5 d), probably being used for Dd synthesis during the day. With cell aging, its content tended to decrease, except at pre-dawn of the stationary phase, where β-car strongly increased.

Intriguingly, the NPQ and the concentration of the photoprotective pigment Dt were not correlated, as previously observed (Giovagnetti *et al.*, 2014, Smerilli *et al.*, 2017). Instead,

NPQ showed a positive correlation with Dd ($p<0.05$, $r=0.48$). The β-car consumption in favor of XC pigments (Dd and Dt) synthesis was confirmed by the negative correlation between β-car and Dt ($p<0.05$, $r=0.47$).

The XC pigment Dd was correlated to the photosynthetic pigments Chla, Fuco and Chlc ($p<0.001$, $r=0.76$; $p<0.0001$, $r=0.84$; $p<0.00001$, $r=0.87$, respectively). The same happened for the other photoprotective pigment Dt, positively correlated to Chla, Fuco and Chlc, but in a less pronounced way ($p<0.05$, $r=0.51$; $p<0.05$, $r=0.48$; $p<0.0001$, $r=0.64$, respectively). These features suggest that the structural reorganization of the antennae was paralleled by the modification of the photoprotective pigment content.

5.3.4 Antioxidants

In the three growth phases, ascorbic acid (AsA) concentration strongly increased from pre-dawn to midday (Fig. 5.6 a). Interestingly, stationary phase induced an increase of AsA concentration in both the time points, with a more accentuated increase at pre-dawn respect to the previous phases, as observed for β-car.

The phenolic content followed the same trend, with a conserved infradiel variations with higher values found at midday compared to pre-dawn and enhanced concentration during the stationary/senescence phase (Fig. 5.6 b). The same behavior displayed by AsA and phenolic compounds could be caused by the reagent used for the phenolics determination, which has been showed to be reactive also towards the former molecule (Everette *et al.*, 2010).

As AsA and phenolic contents, flavonoids increased at midday compared to pre-dawn (Fig. 5.6 c). When cells entered into stationary phase, these variations disappeared and the flavonoids' concentration hugely increased.

The proportion between phenolic content and flavonoids concentrations, despite the fluctuations, did not change consistently in none of the sampling times (data not shown).

The ABTS test reflected the trend observed for the antioxidant molecules, following infradiel variations, being enhanced at midday compared to pre-dawn, and increasing during the stationary/senescence phase, as a result of the antioxidant molecules accumulation (Fig. 5.6 d).

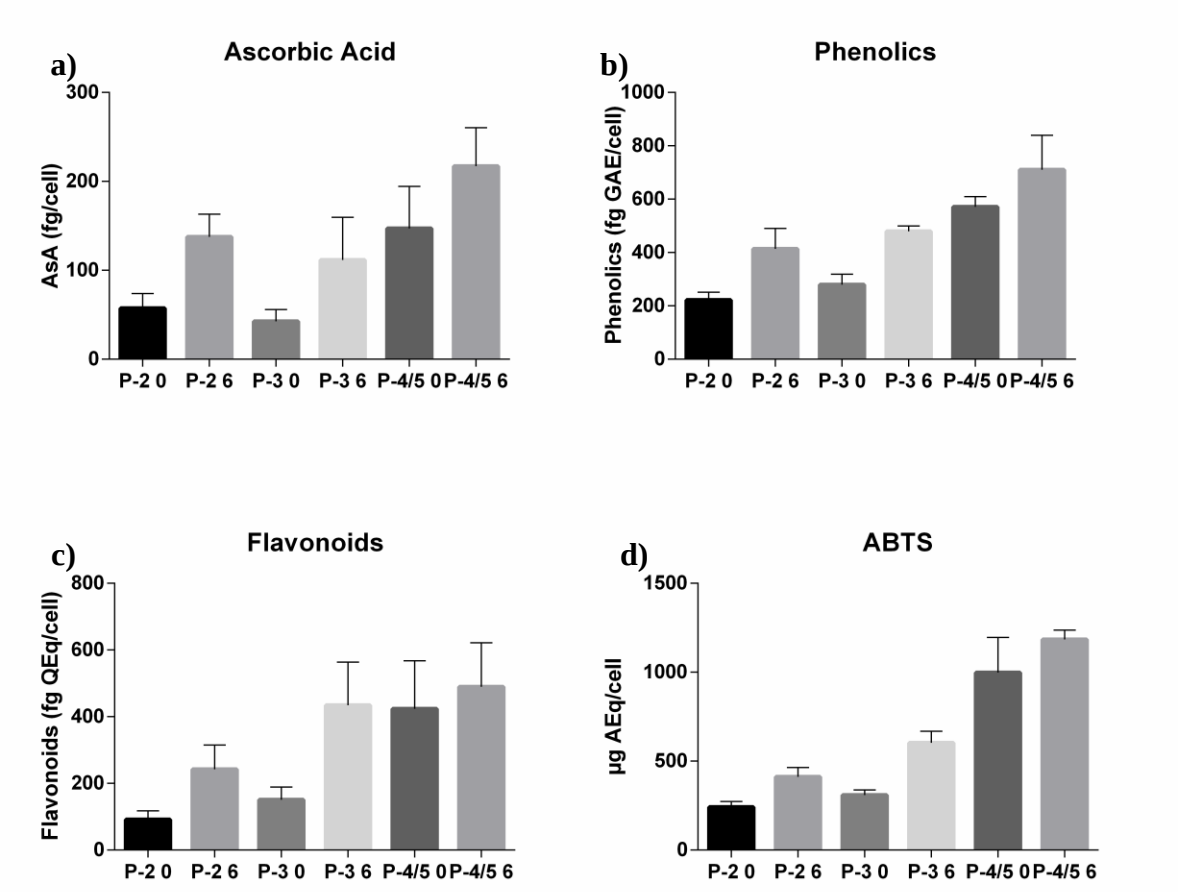

Figure 5.6: Antioxidant molecules and antioxidant activity. a) Ascorbic acid (AsA in fg/cell); b) Phenolics (in fg GAEq/cell); c) Flavonoids (in fg QEq/cell); d) ABTS test (in fg AEQ/cell). Samples were collected at pre-dawn (0) and midday (6) during the exponential (P-2), late exponential (P-3), and stationary/senescent (P4/5) phases. Data are reported as mean ±SD of three biological replicates (n=3).

The antioxidant molecules showed a number of correlations among each other and with the photoprotective pigments. All the correlations are summarized in Table 5.2. As expected, the antioxidant molecules were linked to the total antioxidant capacity, and the variation of the phenolic content was paralleled by the variation of the flavonoid content. Also AsA content was related to the phenolic and flavonoid content, due to the same infradiel trend and the accumulation in senescent cells. Interestingly, the photoprotective pigments Dt and

Dd were positively correlated with the antioxidant activity and molecules, suggesting a parallel time scale of response and a possible antioxidant activity of these pigments.

Table 5.2: Correlations between the antioxidant capacity and molecules among each other and with the photoprotective pigments. The values are the Pierson's correlation coefficients, and in parenthesis are reported the asterisks which stand for the significance values (p), where *=p<0.05; **=p<0.01; ***=p<0.001; ****=p<0.0001; *****:p<0.00001. NS means absence of correlation.

	ABTS	AsA	Phenolics	Flavonoids	Dd	Dt
ABTS	-	0.79 (***)	0.94 (*****)	0.80 (****)	0.72 (***)	0.56 (*)
AsA	0.79 (***)	-	0.82 (***)	0.70 (**)	NS	NS
Phenolics	0.94 (*****)	0.82 (***)	-	0.86 (***)	0.70 (**)	0.56 (*)
Flavonoids	0.80 (****)	0.70 (**)	0.86 (***)	-	0.64 (**)	0.51 (*)
Dd	0.72 (***)	NS	0.70 (**)	0.64 (**)	-	NS
Dt	0.56 (*)	NS	0.56 (*)	0.51 (*)	NS	-

5.4 Discussion

During the exponential phase, cells were highly performing, as shown by the high growth rate, photosynthetic rate and photochemical efficiency.

The infradiel variations between pre-dawn and midday revealed the acclimation to the sinusoidal light environment. Cells showed an increase in α at midday, a low light acclimation feature. This variation could be due to the increased concentration of Chla, which induced a self-shading effect lowering the incident light reaching the photosystems.

The slight increase in Chla was probably due to a *de-novo* synthesis in preparation for the cell division (Bowler *et al.*, 2010a). The latter, a process dependent on light-dark periodicity, was performed in the afternoon and/or during the night, as observed in many microalgal species, and among them in diatoms (Vaulot *et al.*, 1986, Bowler *et al.*, 2010a).

The XC pigments concentration was not strictly linked to the NPQ development, the former showing a slight increase at midday at contrary to the latter. This feature is in agreement with previous results (Giovagnetti *et al.*, 2014, Smerilli *et al.*, 2017), confirming that a progressive increase to moderate PFD does not stimulate a high NPQ development, which by contrast is higher in cells coming from dark. Probably, the additional Dt observed at midday belonged to the thylakoid pool, and thus was not involved in the NPQ mechanism (Lepetit *et al.*, 2010, Grouneva *et al.*, 2011, Goss & Lepetit, 2015). The increase of the XC pigments at midday was paralleled by the slight decrease of β-car, being their precursor in

the biosynthetic pathway. The low stimulation of the Dt synthesis was due to the moderate light environment cells were exposed to, guaranteeing the permanence of the photosystems in their light harvesting state, and not in a heat dissipating state.

The fact that the concentration of Dd and Dt was linked to the antioxidants, might reveal that they are active players of the antioxidant network. The latter is clearly a light acclimation response. Indeed, the antioxidant molecules and activity displayed an infradiel cycle with higher values recorded at midday. The increase in antioxidants at midday confirms the light control of the synthesis of these molecules as already observed in higher plants (Massot *et al.*, 2012, Wang *et al.*, 2013). This increase could counteract the detrimental excess of light energy, contrasting the ROS formation.

Overall, the cells during the exponential growth phase were highly performing and showed a daily periodicity of their photophysiology, suggesting the efficacy of their metabolism in responding to the light environment experienced.

The late exponential phase is characterized by slightly lower growth and photosynthetic rate, mainly at pre-dawn, respect to the exponential phase. Nevertheless, cells were still highly performing, showing high values of photochemical efficiency. The values of α lowered respect to the exponential phase, a high light acclimation feature, in spite of the unvaried light regime cells were exposed to, suggesting a reorganization of the photosynthetic apparatus. Also Ek underwent some fluctuations, lowering at pre-dawn; being always higher than the maximal PFD supplied. The modification of the photosynthetic apparatus was visible through the measurement of the pigment concentration. Chla decreased while the antenna pigments Chlc and Fuco were stable, determining a different antenna/reaction center ratio. As regards the photoprotection, the behavior of the NPQ and the XC pigments Dd and Dt was similar to the exponential phase, with a slight increased pigment concentration at midday paralleled by a decreased NPQ. By contrast, β-car was strongly reduced mainly at midday, suggesting an alteration of the carotenoid biosynthetic pathway. Also the antioxidant molecules and activity conserved a similar trend respect to the exponential phase, with increased values at midday.

Overall, during the late exponential phase the cells displayed photophysiological characteristics halfway between the exponential and the stationary phase. The latter was characterized by similar photosynthetic properties of the late exponential phase, i.e. lower

α, Ek, and ETR at pre-dawn, but with different pigment concentration, both photosynthetic and photoprotective, and antioxidant content. Aged cells lowered the growth rate and the photosynthetic performance, even though Fv/Fm remained high. This is in line with what observed on *Chlamydomonas reinhardtii*, who showed a significant decrease of the maximum quantum yield of photochemistry only during the death phase (Humby *et al.*, 2013).

The three photosynthetic pigments Chla, Chlc and Fuco were enhanced during this phase, an accumulation probably due to a block of the cell division. Also Dd and Dt increased, determining a high NPQ at midday. The high β-car present at pre-dawn was lately converted into the XC pigments. All the antioxidant molecules measured showed the same accumulation observed on the photoprotective pigment. The enlargement of the AsA pool has been already observed in the senescent diatom *Skeletonema costatum* (Brown & Miller, 1992).

The infradiel cycle observed during the active growth phase were disrupted during the stationary/senescent phase, vouching for the drastic changes cells were subjected to. This is in line with previous observation from (Vidoudez & Pohnert, 2012). In fact, culture age changes dramatically the transcriptome and metabolome of cells, being predominant the catabolic process, showing a lower amino acid production, being absent the cell division, a greater biosynthesis of storage lipids, different sugar profile, increased free putrescin levels (Barofsky *et al.*, 2010, Vidoudez & Pohnert, 2012, Ashworth *et al.*, 2013).

In higher plants, the early event of cell senescence is the inactivation of the enzyme Rubisco (Grover, 1993, Mae *et al.*, 1993). This is not paralleled by a loss of the thylakoid proteins, which happens at a later time (Mae *et al.*, 1993). These circumstances lead to a potential exposure to an excess of excitation energy, which must be appropriately scavenged. The first line defense is represented by the NPQ mechanism, which prevents the transformation of the light energy into electric energy, lowering the redox potential. Subsequently, the antioxidant network is involved into the scavenging of the radical species produced by the accumulation of electrons from the photosynthetic process.

Therefore we can assert that the higher NPQ and antioxidant capacity found in senescent cells are the key component used to counteract the photoinhibition and the consequent oxidative stress.

These events hinder or at least postpone the induction of the programmed cell death (PCD), a phenomenon activated during starvation, oxidative stress or culture age (Vardi *et al.*, 1999, Bidle & Falkowski, 2004, Bidle & Bender, 2008, Luo *et al.*, 2014).

Our findings describe the light regulation functioning in diatoms during the exponential growth phase. The defense and protection mechanisms are activated at midday, even under a moderate light (150 µmol photons m^{-2} s^{-1}). The antioxidant molecules, such as AsA, phenolics and flavonoids, are normally synthesized by cells to cope with light increase.

Cells aging modify these normal infradiel regulative processes. It appears that many of these infradiel variations disappear, cells keeping high their defense and photoprotective "barriers", such as Dt, NPQ and antioxidant molecules. This mechanism is not anymore relied to light, but to physiological stress-induced senescence.

These results highlight the importance to know the growth phase of the cells when performing experiments on them.

At a biotechnological perspective point of view, harvesting aged cells might be a way to improve the yield of antioxidant molecules from cultivated microalgal biomass. However, being the death rate higher than the growth rate, this strategy is risky since the culture is collapsing, a state which might also induce an increase in bacterial or viral activity (Bidle & Vardi, 2011, Segev *et al.*, 2016).

6. High light acclimation of protective and antioxidant network in *Skeletonema marinoi*

6.1 Introduction

The results obtained in a previous set of experiments (Chapter 4) showed the dependency of the short-term photoprotective and defense strategies adopted by diatoms to different light climate (Smerilli *et al.*, 2017). The photoprotective and antioxidant network appeared strongly controlled by light spectral composition and intensity, resulting in a complex regulation system which allows planktonic diatoms to survive in the highly fluctuating light environment they inhabit.

Once assessed the short-term responses modulation, we focused here on longer temporal scales. The aims of these new experiments were to unveil the functioning of acclimative strategies relied to the photoprotective and antioxidant network over a daily scale and its role on the biology and fundamental living processes (photosynthesis, growth) of diatoms. Since the impressive lack of knowledge on the functioning of photoprotective and antioxidant network in diatoms, we decided to focus on the light intensity and distribution effect, and to keep constant the spectrum of the light provided during the experiment. In order to do so, we investigated biological and physiological responses developed by cells to different light shifts, taking into account the variations in instantaneous photon flux density (PDF), integrated daily light dose, and light distribution over time.

Different studies which aimed to understand the photophysiological responses of diatoms used completely unnatural light pre-acclimation and experimental conditions, such as continuous light distribution or a square-wave light course, and frequently the light spectrum, which is known to play a major role in photoacclimation and photoregulation processes (Depauw *et al.*, 2012, Schellenberger Costa *et al.*, 2013a, Brunet *et al.*, 2014, Jungandreas *et al.*, 2014, Orefice *et al.*, 2016, Smerilli *et al.*, 2017), is not considered (Lepetit *et al.*, 2013, Dong *et al.*, 2016, Li *et al.*, 2017).

At the contrary, previous results showed that a square-wave light course is stressful to cells, impairing the photophysiology and therefore altering the downstream biological events from light capturing to carbon allocation in cells (Orefice *et al.*, 2016). These findings are important to take into account since the light environment provided for microalgal production into enclosed photobioreactors generally has a square-wave distribution.

Also, the integrated daily light dose, which depends on both the intensity and the distribution, affects diatoms growth (Dimier *et al.*, 2009, Orefice *et al.*, 2016).

Here we wanted to understand what happen to cells acclimated to a natural light climate when they are exposed to a higher light environment, taking into consideration both the light distribution and the integrated daily light dose. The hypothesis behind this experiment is that cells should be able to cope with natural-like situations such as a shift to high light with a sinusoidal distribution, better than completely unnatural ones such as a shift to high light with a square-wave distribution.

The spectral light provided during pre-acclimation and all the experimental conditions was the same than in the previous chapter (Chapter 5), i.e. a condition that mimics the spectrum found between 5 and 10 meters depth in coastal waters: a white light composed by Red:Green:Blue (RGB) with a ratio of 10:40:50. This choice was made in order to avoid specific biological responses related to monospectral light environment, being the photophysiology of cells dependent upon the sensing and consequent signaling photoreceptor related (Depauw *et al.*, 2012, Schellenberger Costa *et al.*, 2013, Brunet *et al.*, 2014, Jungandreas *et al.*, 2014, Orefice *et al.*, 2016, Smerilli *et al.*, 2017).

The questions we address were:

- Do the photoprotective and antioxidant networks respond to the same light triggers?
- Is there a functional/dependent/complementary link between these two responses?
- How does the light history affect the acclimative state of the cells?

High light effects were explored providing different light climates and temporal light distribution.

The first one corresponded to the same natural light course distribution than the pre-acclimation condition (sinusoidal light course) peaking at midday at a PFD of 600 µmol photons s^{-1} m^{-2}. Furthermore, we explored the effects of a square wave light courses setup at 600 and 300 µmol photons s^{-1} m^{-2}. It is known that for the same PFD provided at the

midday peak, the ratio of the integrated daily light between sinusoidal light course and square wave light course is 1.8 (Orefice *et al.*, 2016). Both the square-waves shared one aspect with the sinusoidal distribution: the first one had the same peak of light intensity (600 µmol photons s^{-1} m^{-2}), while the second one provided the same integrated daily light dose (12.96 mol photons m^{-2} d^{-1}). These two experimental conditions allowed to explore the effects of (i) light course distribution (sinusoidal *vs* square wave) with the same integrated daily light value, (ii) different integrated daily light and (iii) the physiological stress induced by a light off/on system setup at different light intensities.

6.2 Materials and methods

6.2.1 Experimental strategy and sampling

The experiments were conducted on the centric diatom *Skeletonema marinoi*, grown at 20°C in 4.5 L glass tanks with air bubbling.

The pre-acclimation condition, similar to the one used in the previous set of experiment (Chapter 5), was a white (R:G:B: 10:40:50) sinusoidal light distribution with a midday peak of 150 µmol photons s^{-1} m^{-2} and with a photoperiod equal to 12:12 dark:light.
The experiments were conducted in triplicate during the exponential growth phase.
The experimental light setups are summarized in the Table 6.1.
The first sampling occurred in the dark, just before dawn, and then the other samplings were performed after 2, 6, 24 hours and additionally after 10 and 30 minutes after the light on in the square wave light courses experiments (0.17 and 0.5 hour, respectively).
The results were compared with the results obtained on cells grown under the control condition: sinusoidal light distribution with a midday peak of 150 µmol photons s^{-1} m^{-2} and with a photoperiod equal to 12:12 dark:light (see Chapter 5).

Table 6.1: Experimental light conditions.

Pre-acclimation	Name	Light switch	Experimental "sketch"	Sampling points (hours after the beginning of the experiment)
Ctrl Sin 150 **White sinusoidal light distribution peaking at 150 µmol photons s^{-1} m^{-2}** **12:12 dark:light photoperiod** **R:G:B 10:40:50**	Sin 600	Sinusoidal 600	High PFD same distribution as pre-acclimation condition	0, 2, 6, 24
	Quad 600	Quadratic 600	High PFD High daily light dose Different distribution respect pre-acclimation	0, 0.17, 0.5, 2, 6, 24
	Quad 300	Quadratic 300	Same daily light dose as sinusoidal 600 Different distribution respect pre-acclimation	0, 0.17, 0.5, 2, 6, 24

6.2.2 Parameters analyzed

The subsequent parameters were followed during the experiments:

- Cell concentration
- Photochemical efficiency of the photosystem II
- Electron transport rate (ETR)-light curves[§]
- Non-photochemical quenching (NPQ)
- Pigments
- Absorption spectra
- Total phenolic content[#]
- Total flavonoid content[#]
- Ascorbic acid content[#]
- ABTS radical scavenging activity[#]

All the experimental procedures for each of these parameters are described in Chapter 2.

[§]Data on ETR, Ek, and α are missing for the 10 minute sampling (0.17 hour) in the Quadratic 300 condition

[#]Samples for the antioxidant molecules and activity are missing for the 30 minute sampling (0.5 hours) in both the quadratic conditions.

6.3 Results

6.3.1 General trends

Pooling together all the results, it has been possible to understand some general trend regarding the growth as well as the links between the photoprotective and antioxidant network. First of all, no significant correlation between the growth rate and the photosynthetic rate was found ($p>0.05$, data not shown), meaning that the photochemical energy was not strictly used for the biomass enlargement.

The correlations between photoprotection parameters and antioxidant molecules and activity were many, underlining the parallel time-scale of responses of the photoprotective and antioxidant networks (Table 6.2). The antioxidant parameters resulted strongly correlated among each other and with the xanthophyll-cycle pigments diadinoxanthin (Dd) diatoxanthin (Dt) as well as β-carotene (β-car). Interestingly, the non-photochemical quenching (NPQ) had an opposite trend with Dt, the total antioxidant capacity (ABTS), the ascorbic acid (AsA) and the phenolic content.

Table 6.2 Correlations between the antioxidant capacity and molecules among each other and with the photoprotective parameters pooling together the three high light conditions. Significance values (p) and Pierson's correlation coefficients (r).

		p	r
ABTS	AsA	<0.00001	0.67
	Phenolics	<0.00001	0.95
	Flavonoids	<0.00001	0.71
	NPQ	<0.01	-0.40
	Dd	<0.001	0.44
	Dt	<0.01	0.32
	β-car	<0.001	0.43
AsA	Phenolics	<0.00001	0.82
	Flavonoids	<0.00001	0.55
	NPQ	<0.05	-0.32
	Dd	<0.001	0.47
	Dt	<0.0001	0.48
	β-car	<0.01	0.36
Phenolics	Flavonoids	<0.00001	0.73
	NPQ	<0.01	-0.36
	Dd	<0.001	0.44
	Dt	<0.01	0.40
	β-car	<0.001	0.44
Flavonoids	Dd	<0.0001	0.48
	Dt	<0.00001	0.54
	β-car	<0.01	0.35
NPQ	Dt	<0.05	-0.25
Dd	Dt	<0.00001	0.86
	β-car	0	0.96
Dt	β-car	<0.00001	0.85

6.3.2 Sinusoidal 600

6.3.2.1 Growth rate and photosynthesis

The growth rate (μ) measured at 24 hours in Sin 600 was equal to 0.1 d^{-1}, meaning that the cell concentration only slightly increased, suggesting a physiological stress during the day of the light shift (Table 6.3).

Table 6.3: Growth properties of the cultures. Cell concentration expressed as cell mL^{-1}, and growth rate expressed as μ, d^{-1}at 0 (pre-dawn) and 24 hours later

	0	24
Cell concentration Cells mL^{-1}	719'907 ± 35'679	804'398 ± 214'481
Growth rate μ, d^{-1}	1.1 ± 0.1	0.1 ± 0.2

Photosynthetic rate (ETR, Fig. 6.1) increased after two hours, although the absence of a statistical significance, and came back to the previous values after 6 hours, as in the exponential phase of the control condition. At 24 hours instead, this parameter was higher respect to time 0 ($p<0.05$).

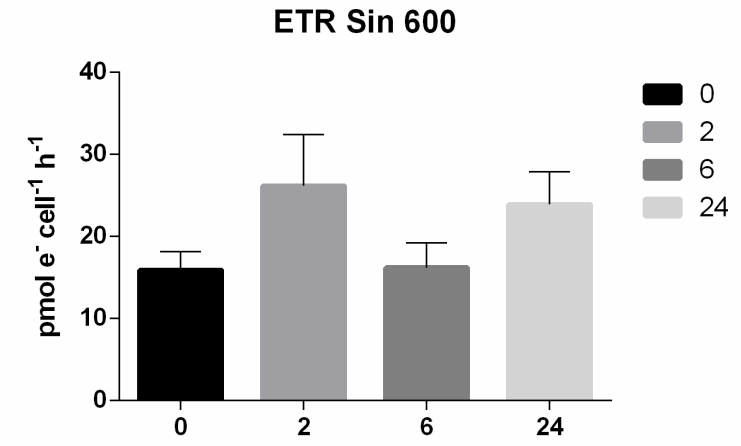

Figure 6.1: Electron Transport Rate (ETR, pmol e^- $cell^{-1}$ h^{-1}) of Sinusoidal 600. Samples were collected at pre-dawn (0), and after 2, 6, and 24 hours. Data are reported as mean ±SD of three biological replicates (n=3).

6.3.2.2 Photosynthetic acclimation and pigments

The quantum yield of photochemistry (Fv/Fm) in all the time points was high (mean value between the four time points equal to 0.80 ± 0.06, Fig. 6.2 a). Also the other photosynthetic parameters α (maximum light use efficiency, Fig. 6.2 b) and Ek (light saturation index for photosynthesis, Fig. 6.2 c) were both quite stable, showing only minimal oscillations.

As regards the photosynthetic pigments, the Sin 600 did not cause a significant change in their concentration (Fig. 6.3 a, b, c). Anyway there was a significant change in the Fucoxanthin/Chlorophyll a ratio, which decreased both at 6 and 24 hours ($p<0.05$, Fig. 6.3 d).

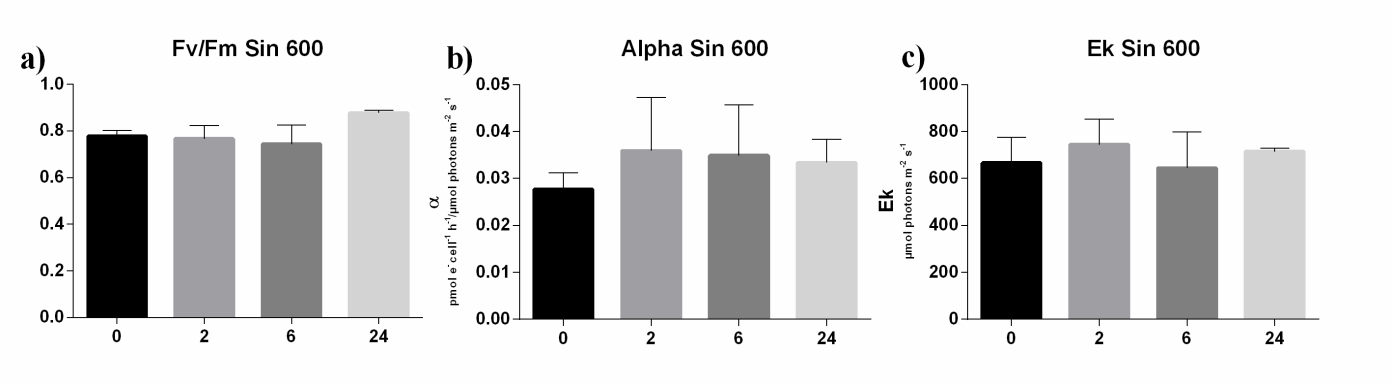

Figure 6.2: Photosynthetic parameters of Sinusoidal 600. a) Fv/Fm (maximum quantum yield of the PSII); b) α (maximum light use efficiency, in pmol e^- $cell^{-1}$ h^{-1}/µmol photons m^{-2} s^{-1}); c) Ek (light saturation index for photosynthesis, in µmol photons m^{-2} s^{-1}). Samples were collected at pre-dawn (0), and after 2, 6, and 24 hours. Data are reported as mean ±SD of three biological replicates (n=3).

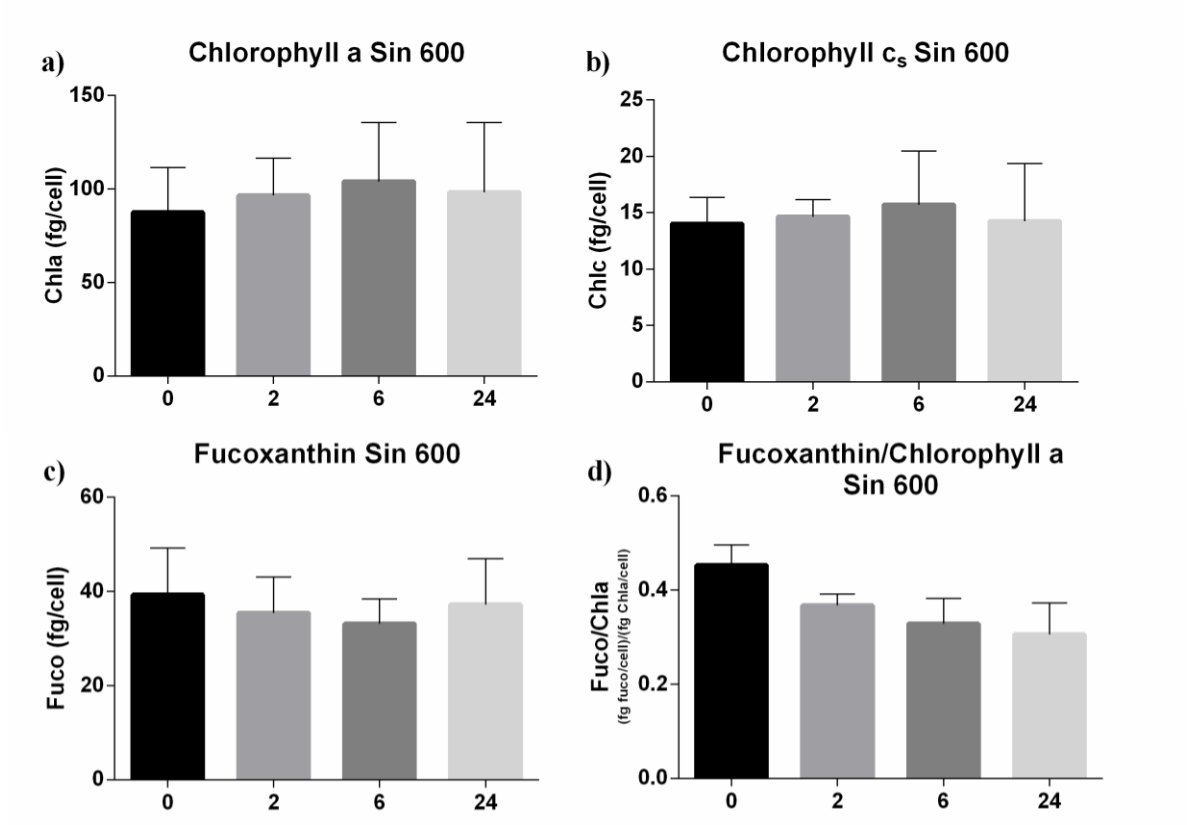

Figure 6.3: Photosynthetic pigments. a) Chlorophyll a (Chla in fg/cell); b) Chlorophyll c_s (Chlc in fg/cell); c) Fucoxanthin (Fuco in fg/cell); d) Fucoxanthin/Chlorophyll a ratio. Samples were collected at pre-dawn (0), and after 2, 6, and 24 hours. Data are reported as mean ±SD of three biological replicates (n=3).

6.3.2.3 Photoprotection

The non-photochemical quenching (NPQ, Fig. 6.4 a) increased rapidly in the first two hours ($p<0.05$), coming back to the pre-dawn values at midday. At 24 hours NPQ was significantly higher ($p<0.001$) with respect of the same time point of the previous day.

Diatoxanthin (Dt) in Sin 600 (Fig. 6.4 b) displayed a higher concentration both at 2 and 6 hours ($p<0.01$), peaking at 6 hours, where NPQ reached its minimum value. At 24 hours, the Dt concentration was not statistically different from the previous day.

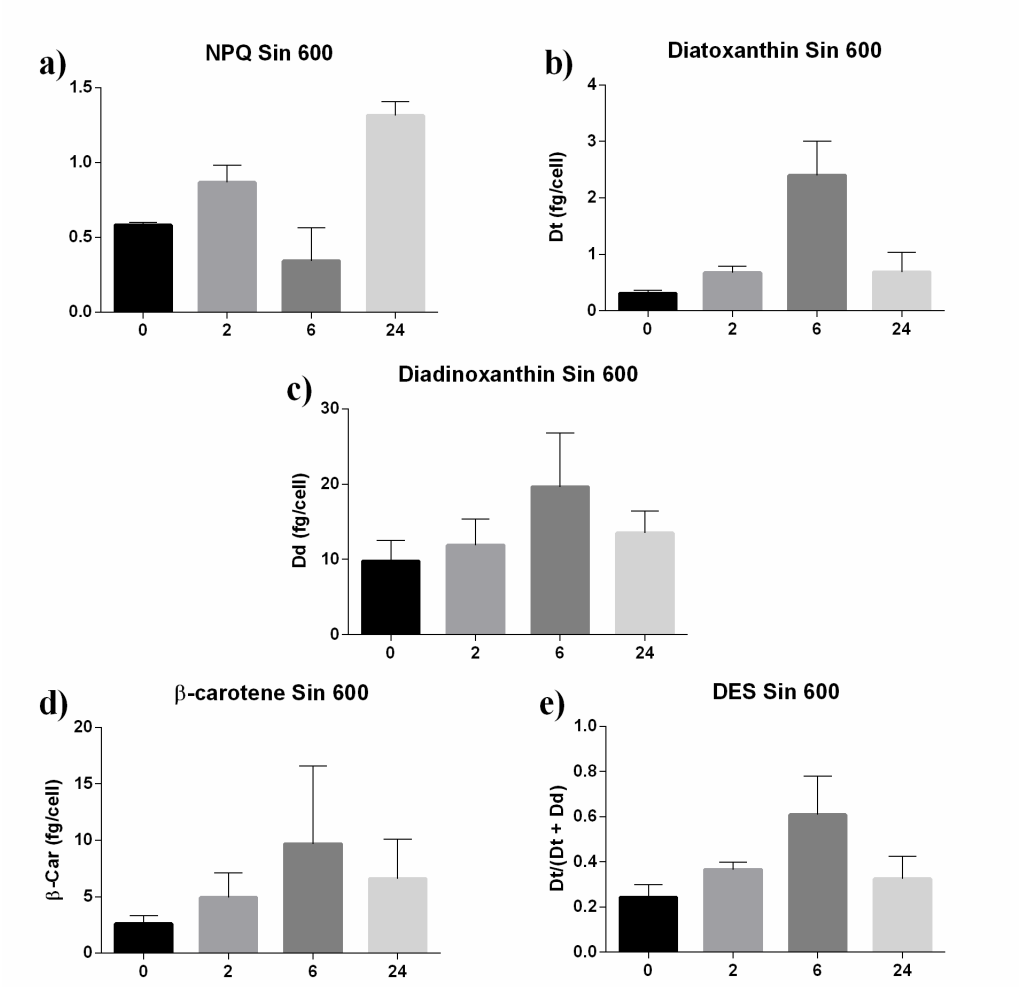

Figure 6.4: Photoprotection. a) non-photochemical quenching (NPQ); b) Diatoxanthin (Dt in fg/cell); c) Diadinoxanthin (Dd in fg/cell); d) β-carotene (β-car in fg/cell); e) De-epoxidation state [DES=Dt/(Dt+Dd)]. Samples were collected at pre-dawn (0), and after 2, 6, and 24 hours. Data are reported as mean ±SD of three biological replicates (n=3).

The precursors of Dt in the biosynthetic pathway, diadinoxanthin (Dd) and β-carotene (β-car), had the same trend as Dt, underlining the rapid *de-novo* synthesis of the photoprotective pigments (Fig. 6.4 c, d). The *de-novo* synthesis of Dd was paralleled by its conversion into Dt, as visible by the de-epoxidation state (DES), higher both at 2 and 6 hours ($p<0.05$, Fig. 6.4 e).

6.3.2.4 Antioxidant molecules and activity

The key antioxidant molecule ascorbic acid (AsA, Fig. 6.5 a) in Sin 600 doubled its content already at 2 hours, keeping constant its concentration at 6 hours ($p<0.01$ and $p<0.05$, respectively). At 24 hours it restored to the initial values, so the diel cycle trend observed in the control condition was preserved, although the increase between 0 and 6 hours in the control condition was slightly higher (2.4 times increase in Ctrl Sin 150 against a 1.8 times increase in Sin 600).

The total phenolic content followed the same trend (Fig. 6.5 b), being increased already at 2 hours, keeping high values at 6 hours, although showing a slightly lower increase with respect of control condition, and coming back to initial values at 24 hours. This feature could be caused by the lack of specificity of the assay used for phenolic determination, which is responsive also towards other antioxidants, such as AsA (Everette *et al.*, 2010).

Among the phenolic compounds, the photoprotective flavonoids (Fig. 6.5 c) increased with light, which reflected the exact trend of the phenolic compounds, accumulating at 2 and 6 hours, and restoring its initial concentration at 24 hours. The ratio between phenolic compounds and flavonoids in fact, results unvaried in all the time points (data not shown).

The lower increase of the antioxidant molecules with respect to the control condition was reflected by the unvaried values recorded for the antioxidant activity measured through the ABTS test (Fig. 6.5 d).

Under the sinusoidal high light, the hookup between the antioxidant and photoprotective network was visible (Table 6.4). Interestingly, AsA content was not linked to the antioxidant capacity but resulted positively correlated to the photoprotective pigment Dt (Table 6.4).

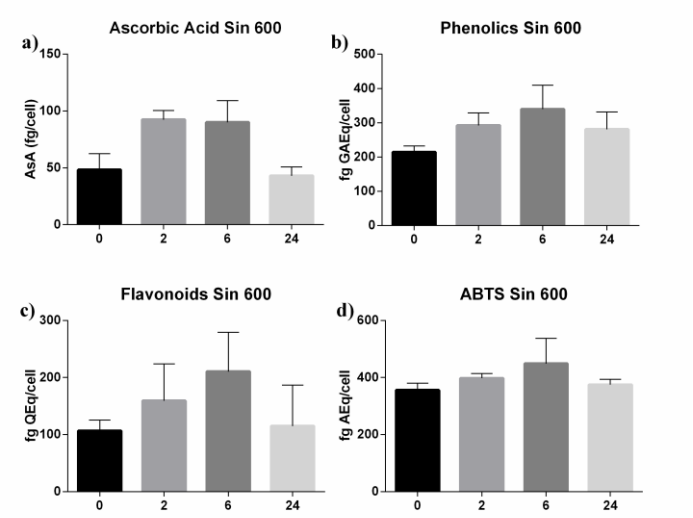

Figure 6.5: Antioxidant molecules and antioxidant activity. a) Ascorbic acid (AsA in fg/cell); b) Phenolics (in fg GAEq/cell); c) Flavonoids (in fg QEq/cell); d) ABTS test (in fg AEQ/cell). Samples were collected at pre-dawn (0), and after 2, 6, and 24 hours. Data are reported as mean ±SD of three biological replicates (n=3).

Table 6.4: Correlations between the antioxidant capacity and molecules among each other and with the photoprotective parameters measured under Sin 600. Significance values (P) and Pearson's correlation coefficients (r).

		P	r
ABTS	Phenolics	<0.01	0.79
	Flavonoids	<0.05	0.62
	Dd	<0.01	0.72
	β-car	<0.0001	0.90
AsA	Dt	<0.05	0.59
Phenolics	Flavonoids	<0.01	0.74
	Dt	<0.05	0.61
	β-car	<0.05	0.68
Dd	β-car	<0.01	0.81

6.3.3 Quadratic 600

6.3.3.1 Growth rate and photosynthesis

The exposure to a square wave light course with PFD equal to 600 µmol photons m^{-2} s^{-1} resulted in a dramatic decrease of cell concentration, which started already at the first time

point, 10 minutes after the light on (data not shown), culminating with a negative growth rate equal to -1.5 d^{-1} at 24 hours (Table 6.5).

Table 6.5: Growth properties of the cultures. Cell concentration expressed as cell mL^{-1}, and growth rate expressed as µ, d^{-1}at 0 (pre-dawn) and 24 hours later

	0	24
Cell concentration Cells mL^{-1}	588'752 ± 170'171	151'247 ± 104'095
Growth rate µ, d^{-1}	0.8 ± 0.2	-1.5 ± 0.4

As regards the photosynthetic rate (ETR, Fig. 6.6), it did not vary within the first 6 hours of experiment, but at 24 hours it was higher with respect to pre-dawn ($p<0.01$), as in Sin 600.

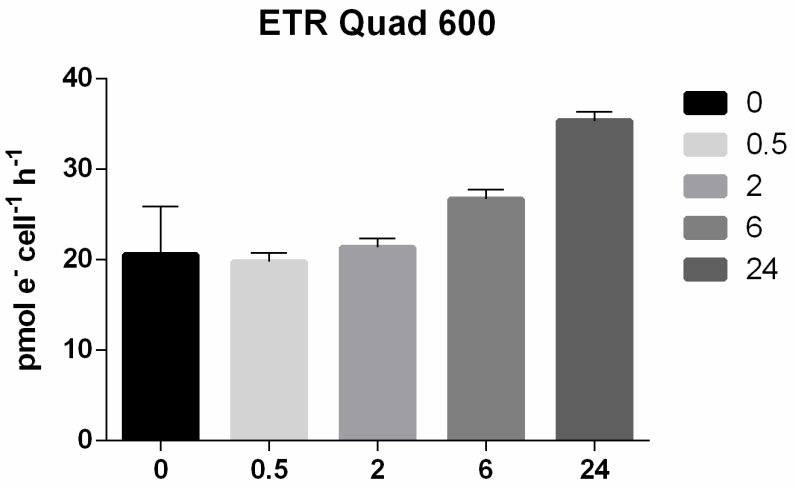

Figure 6.6: Electron Transport Rate (ETR, pmol e- cell-1 h-1) of Quadratic 600. Samples were collected at pre-dawn (0), after 30 minutes (0.5), 2, 6, and 24 hours. Data are reported as mean ±SD of three biological replicates (n=3).

6.3.3.2 Photosynthetic acclimation and pigments

In Quad 600, the cells were able to keep a high Fv/Fm until 6 hours, when this parameter decreased significantly with respect to the time 0 ($p<0.05$, Fig. 6.7 a).

At 24 hours the survived cells recovered, restoring the Fv/Fm to values comparable to those of the previous day.

The photosynthetic parameters Ek and α showed some fluctuations (Fig 6.7 b, c); at 6 hours α decreased significantly from pre-dawn ($p<0.05$), coupled with a slight increase of Ek, suggesting a reorganization of the photosynthetic apparatus. During night the cells recovered, as observable by the restoring the photosynthetic parameters of the previous day. As regards the photosynthetic pigments, their content did not change significantly from pre-dawn in no one of the time points (Fig. 6.8 a, b, c). The Fuco/Chla ratio slightly decreased at 6 hours ($p<0.05$), increasing again at 24 hours (Fig. 6.8 d).

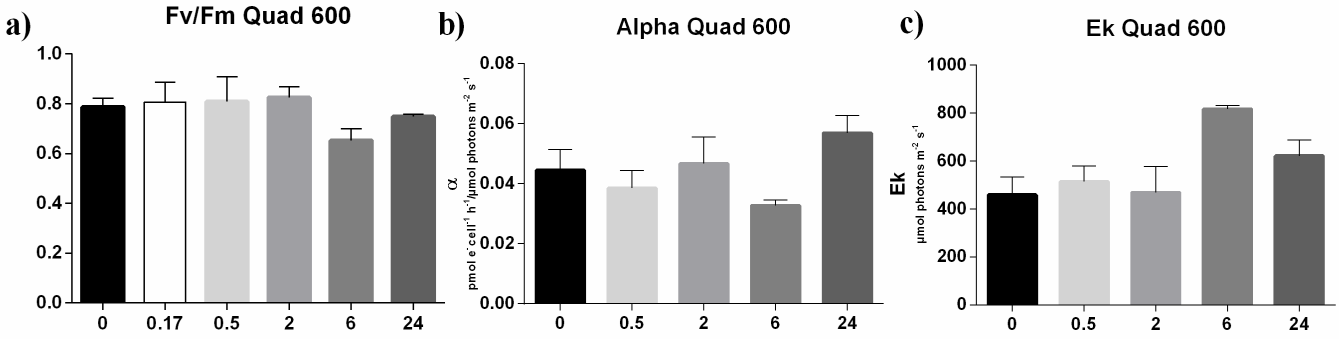

Figure 6.7: Photosynthetic parameters of Quadratic 600. a) Fv/Fm (maximum quantum yield of the PSII); b) α (maximum light use efficiency, in pmol e^- $cell^{-1}$ h^{-1}/µmol photons m^{-2} s^{-1}); c) Ek (light saturation index for photosynthesis, in µmol photons m^{-2} s^{-1}). Samples were collected at pre-dawn (0), after 10 minutes (0.17), 30 minutes (0.5), 2, 6, and 24 hours. Data are reported as mean ±SD of three biological replicates (n=3).

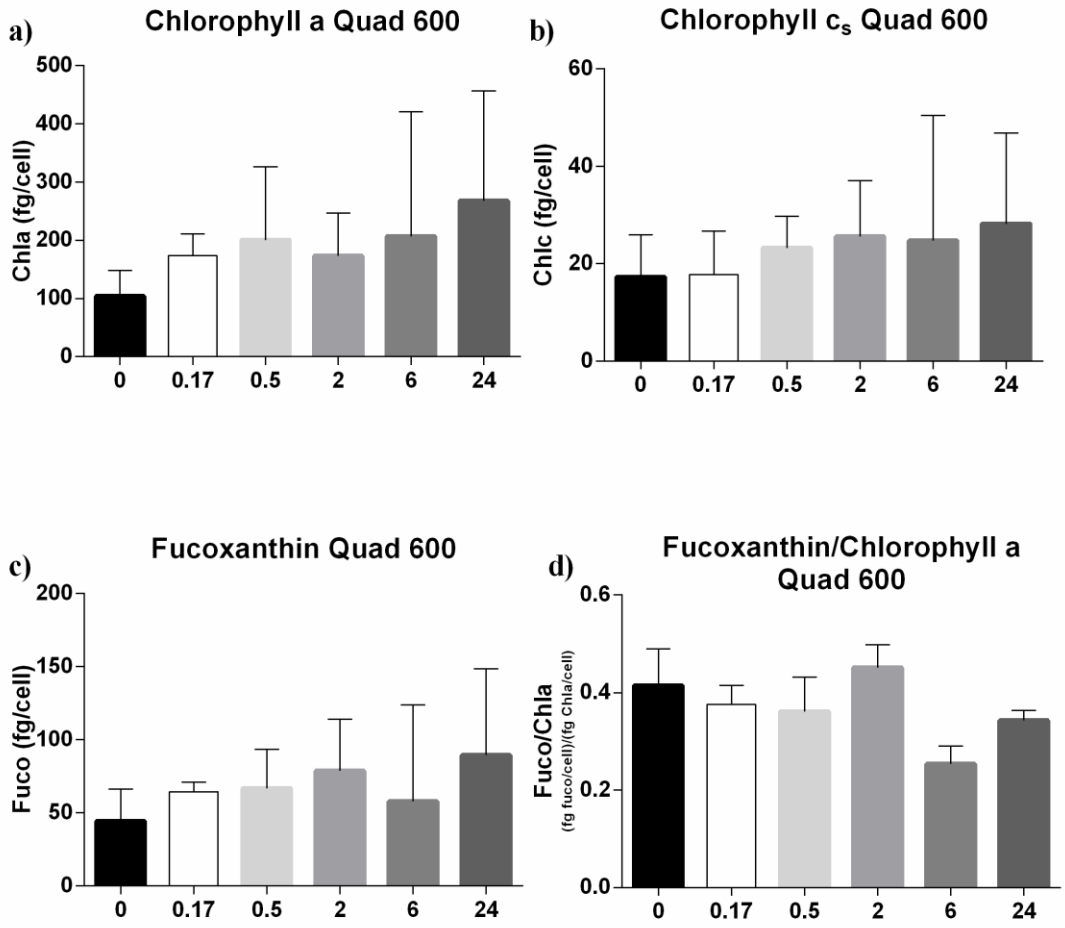

Figure 6.8: Photosynthetic pigments. a) Chlorophyll a (Chla in fg/cell); b) Chlorophyll c_s (Chlc in fg/cell); c) Fucoxanthin (Fuco in fg/cell); d) Fucoxanthin/Chlorophyll a ratio. Samples were collected at pre-dawn (0), after 10 minutes (0.17), 30 minutes (0.5), 2, 6, and 24 hours. Data are reported as mean ±SD of three biological replicates (n=3).

6.3.3.3 Photoprotection

The NPQ did not change within the first two hours of experiment (Fig. 6.9 a). At 6 hours instead, it decreased significantly ($p<0.05$). Anyway, the surviving cells at 24 hours exhibited values of NPQ similar to pre-dawn.

The increase of Dt reached its maximum at 2 hours ($p<0.01$, Fig. 6.9 b), not paralleled with an increase of NPQ, followed by a reduction of this pigment, which at 24 hours had the same concentration of the day before. Neither Dd nor β-car concentration (Fig, 6.9 c, d)

resulted in a significant deviation from the time 0, although showing some fluctuation. The DES was stable with time (Fig. 6.9 e).

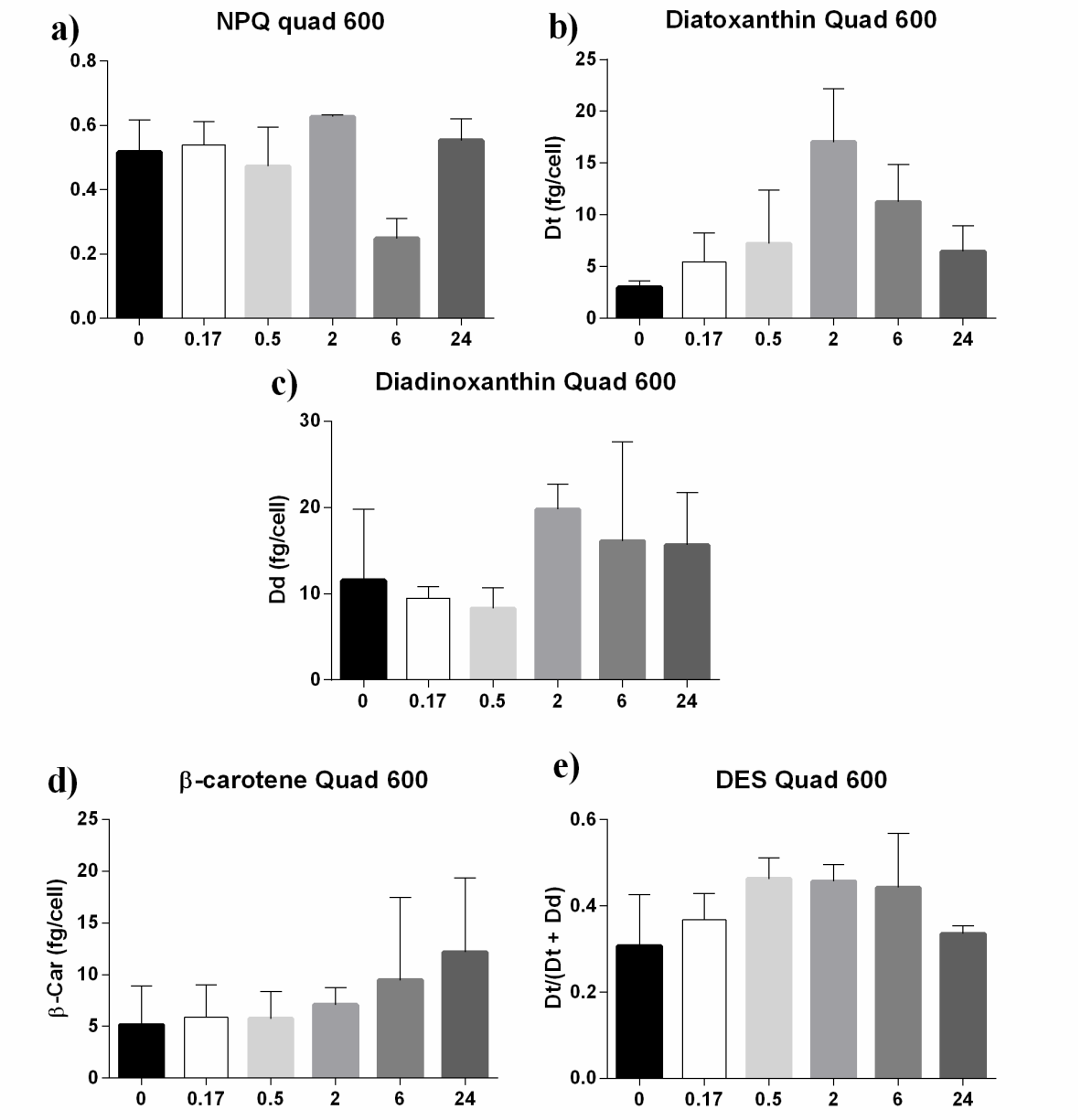

Figure 6.9: Photoprotection. a) non-photochemical quenching (NPQ); b) Diatoxanthin (Dt in fg/cell); c) Diadinoxanthin (Dd in fg/cell); d) β-carotene (β-car in fg/cell); e) De-epoxidation state [DES=Dt/(Dt+Dd)]. Samples were collected at pre-dawn (0), after 10 minutes (0.17), 30 minutes (0.5), 2, 6, and 24 hours. Data are reported as mean ±SD of three biological replicates (n=3).

6.3.3.4 Antioxidant molecules and activity

In Quad 600 the diel cycle trend of AsA observed in the control condition was still present (Fig., 6.10 a), but with some interesting peculiarities. The sampling performed 10 minutes after the light start revealed a very fast consumption of this molecule. It's concentration in fact was halved with respect to the time 0 ($p<0.05$). After that, AsA was recycled and newly synthesized, reaching the highest values at 2 and 6 hours ($p<0.05$ and $p<0.01$ respectively). The higher synthesis of this molecule in this particular light condition was reflected by the fact that the increase between the time 0 and 2 - 6 hours was higher with respect to the control condition, being of *circa* 3 times against 2.4 in Ctrl sin 150 and 1.8 in Sin 600.

In spite of the possible reactivity of AsA towards the reagent used for phenolics determination (Everette *et al.*, 2010), this class of compounds did not present the fast decrease at 10 minutes as AsA (Fig. 6.10 b). Anyway these molecules almost doubled their concentration at 2 and 6 hours ($p<0.05$), coming back to the starting values after 24 hours.

The flavonoids instead followed a bit different trend, not changing consistently in any of the sampling points (Fig. 6.10 c). Although not significantly, the ratio between flavonoids and phenolic compounds at 24 hour was slightly higher than in the other sampling points (Fig. 6.10 d).

The ABTS test reflected the increase of the antioxidants concentration already at 2 hours ($p<0.05$, Fig. 6.10 e), remaining high at 6 hours. Interestingly, after one day the antioxidant capacity was still higher than T0 ($p<0.01$), while the antioxidant molecules decreased or were stable with respect to the previous day.

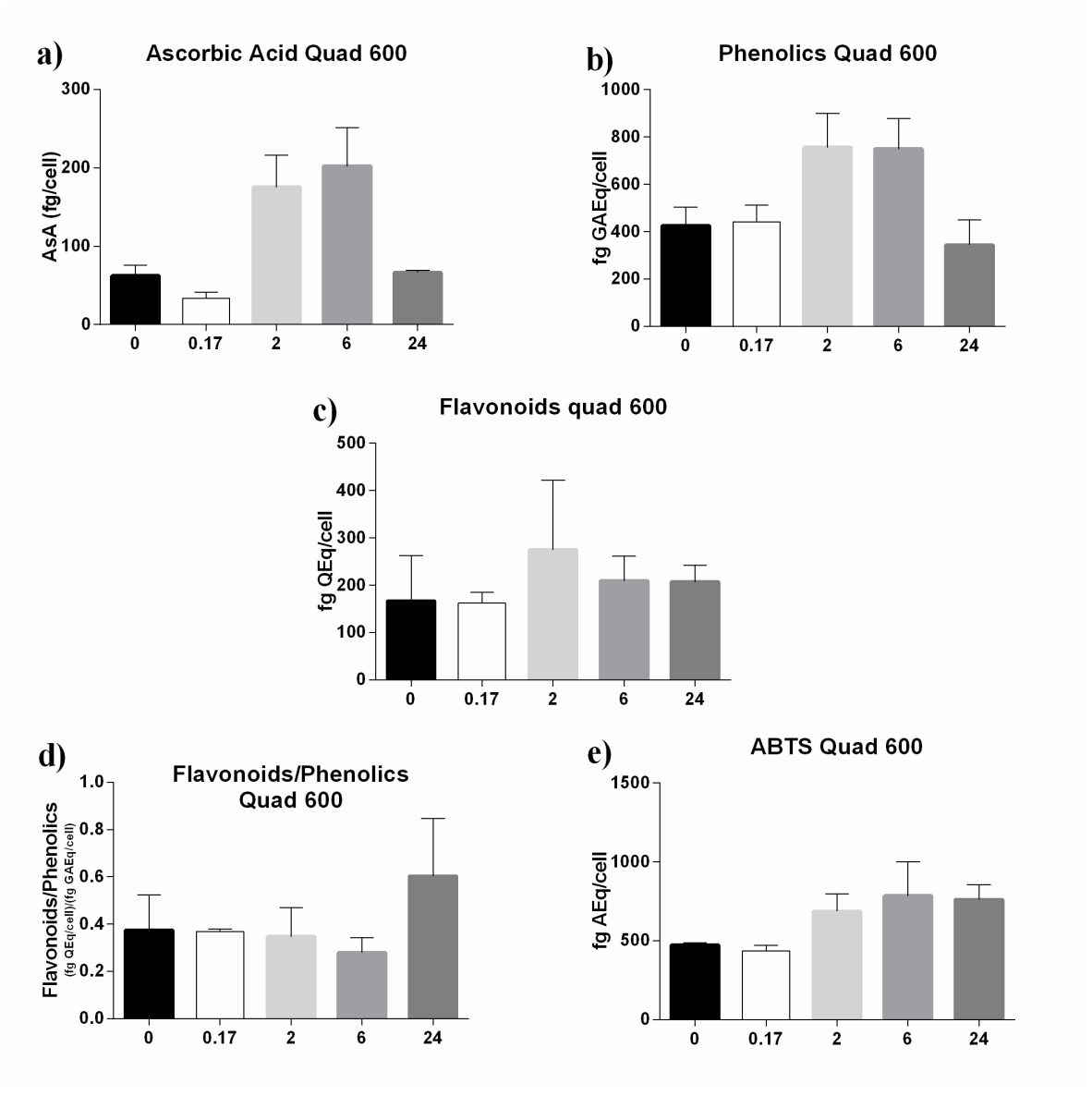

Figure 6.10: Antioxidant molecules and antioxidant activity. a) Ascorbic acid (AsA in fg/cell); b) Phenolics (in fg GAEq/cell); c) Flavonoids (in fg QEq/cell); d) Flavonoids/phenolics ratio; e) ABTS test (in fg AEQ/cell). Samples were collected at pre-dawn (0), 10 minutes (0.17), 2, 6, and 24 hours.Data are reported as mean ±SD of three biological replicates (n=3).

Positive correlation between the photoprotective and antioxidant network was found also under Quad 600, although there were some differences respect to Sin 600 (Table 6.6). The strong correlations between Dt, Dd and β-car suggest a stimulation upstream of the carotenoid biosynthetic pathway which involved all the photoprotective pigments.

Table 6.6: Correlations between the antioxidant capacity and molecules among each other and with the photoprotective parameters measured under Quad 600. Significance values (P) and Pierson's correlation coefficients (r).

		P	r
ABTS	Phenolics	<0.05	0.75
	Flavonoids	<0.01	0.81
AsA	Phenolics	<0.05	0.68
Phenolics	Flavonoids	<0.05	0.63
	Dt	<0.001	0.81
Flavonoids	Dt	<0.05	0.59
Dd	Dt	<0.001	0.75
	β-car	<0.0001	0.79
Dt	β-car	<0.05	0.50

6.3.4 Quadratic 300

6.3.4.1 Growth rate and photosynthesis

The switch to a square wave light course with PFD equal to 300 µmol photons m^{-2} s^{-1} determined a strong decrease of cells' concentration, resulting in a negative growth rate after one day (Table 6.7).

Table 6.7: Growth properties of the cultures. Cell concentration expressed as cell mL^{-1}, and growth rate expressed as µ, d^{-1}at 0 (pre-dawn) and 24 hours later

	0	24
Cell concentration Cells mL^{-1}	464'500 ± 96'874	177'000 ± 205'061
Growth rate µ, d^{-1}	0.5 ± 0.2	-1.5 ± 1.4

The photosynthetic rate (ETR, Fig. 6.11), slightly increased after two hours, although the absence of a statistical significance, and came back to the previous values after 6 hours, as in the control condition.

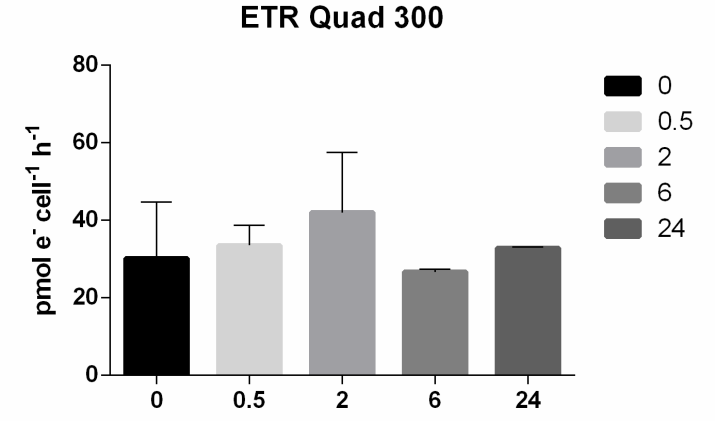

Figure 6.11: Electron Transport Rate (ETR, pmol e- cell^{-1} h^{-1}) of Quadratic 300. Samples were collected at pre-dawn (0), after 30 minutes (0.5), 2, 6, and 24 hours. Data are reported as mean ±SD of three biological replicates (n=3).

6.3.4.2 Photosynthetic acclimation and pigments

Also in Quad 300 the quantum yield of photochemistry showed a similar trend with respect of the other quadratic condition, decreasing significantly at 6 hours ($p<0.01$, Fig. 6.12 a). Interestingly, the overnight period was not sufficient to allow cells to recover, so at 24 hours the efficiency of PSII photochemistry was lower with respect to the time 0 ($p<0.001$). The maximum light use efficiency (α) decreased significantly at 6 hours ($p<0.01$, Fig. 6.12 b), but at 24 hours it was equal to the previous day, not showing any acclimation of the photosynthetic apparatus. Stable indeed was Ek, which showed comparable values in all the time points (Fig. 6.12 c).

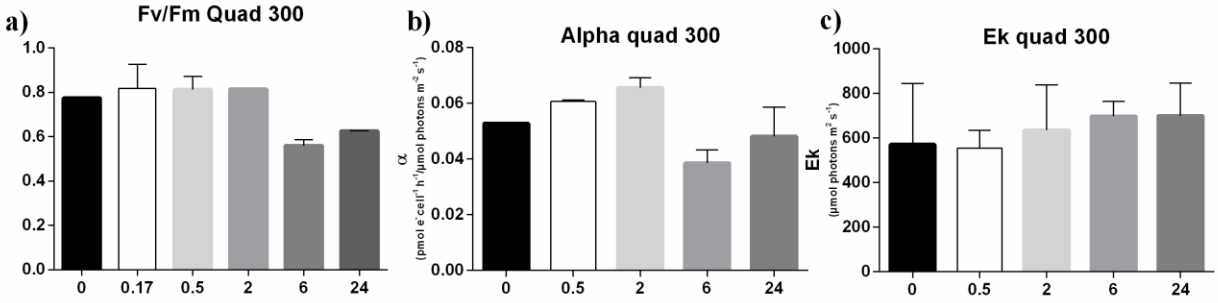

Figure 6.12: Photosynthetic parameters of Quadratic 300. a) Fv/Fm (maximum quantum yield of the PSII); b) α (maximum light use efficiency, in pmol e- cell-1 h-1/µmol photons m-2 s-1); c) Ek (light saturation index for photosynthesis, in µmol photons m-2 s-1). Samples were collected at pre-dawn (0), after 10 minutes (0.17), 30 minutes (0.5), 2, 6, and 24 hours. Data are reported as mean ±SD of three biological replicates (n=3).

In the Quad 300 no significant change of the photosynthetic pigments Chla, Chlc, and Fuco was noticed within the first 6 hours of experiment (Fig. 6.13). At 24 hours instead a strong increase in concentration of these pigments was recorded, probably synthesized in preparation of the cell division which did not occurred during the first day.

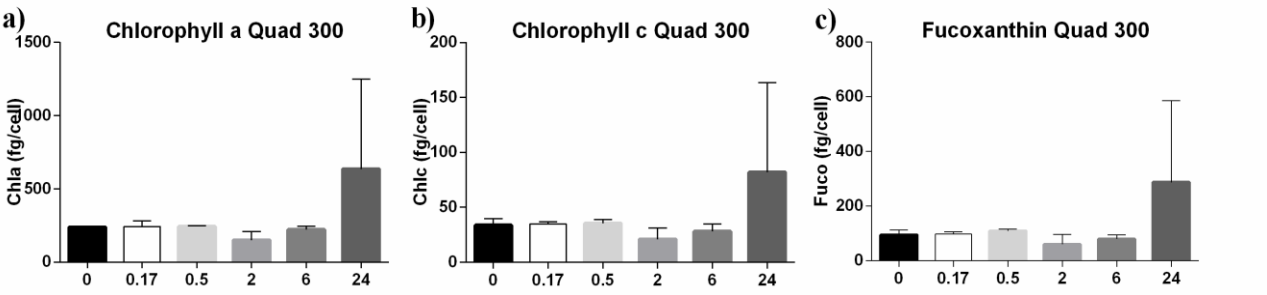

Figure 6.13: Photosynthetic pigments. a) Chlorophyll a (Chla in fg/cell); b) Chlorophyll c_s (Chlc in fg/cell); c) Fucoxanthin (Fuco in fg/cell). Samples were collected at pre-dawn (0), after 10 minutes (0.17), 30 minutes (0.5), 2, 6, and 24 hours. Data are reported as mean ±SD of three biological replicates (n=3).

6.3.4.3 Photoprotection

NPQ (Fig. 6.14 a) showed a slight increase after 10 minutes respect to time 0, but later on it decreased progressively, reaching the lowest value after 6 hours ($p<0.05$). The subsequent day this parameter was still lower ($p<0.05$).

Dt (Fig. 6.14 b) progressively increased reaching its maximal concentration at 6 hours ($p<0.05$), when NPQ reached its minimum. The precursors Dd and β-car (Fig. 6.14 c, d) did not change significantly within 6 hours. This result is also visible by the significant increase in the DES both at 30' and 6 hours ($p<0.05$, Fig 6.14 e). This feature suggested the *de-novo* synthesis of these pigments, converted into Dt.

At 24 hours these three pigments showed the same increase than the photosynthetic ones.

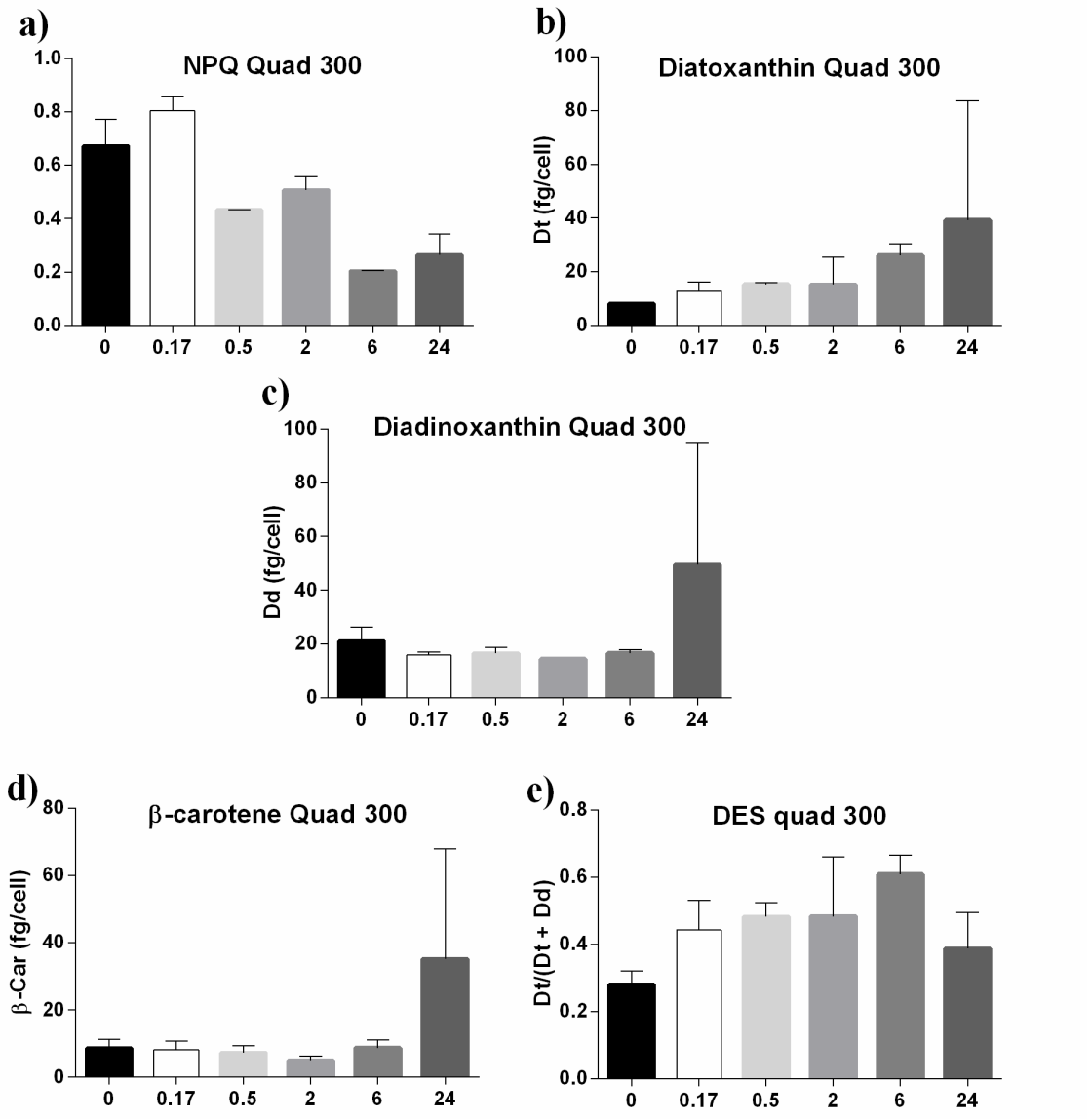

Figure 6.14: Photoprotection. a) non-photochemical quenching (NPQ); b) Diatoxanthin (Dt in fg/cell); c) Diadinoxanthin (Dd in fg/cell); d) β-carotene (β-car in fg/cell); e) De-epoxidation state [DES=Dt/(Dt+Dd)]. Samples were collected at pre-dawn (0), after 10 minutes (0.17), 30 minutes (0.5), 2, 6, and 24 hours. Data are reported as mean ±SD of three biological replicates (n=3).

6.3.4.4 Antioxidant molecules and activity

In Quad 300 AsA content (Fig. 6.15 a) did not change within the first minutes of the experiment. This molecule increased at 2 hours, keeping constant its concentration at 6

hours ($p<0.05$) and restoring the starting values after 24 hours. The lower stimulation of the *de-novo* synthesis of AsA with respect of Quad 600 was reflected by the lower relative increase between the time 0 and 2 - 6 hours, which in this case was only of *circa* 2 times, similarly to Sin 600.

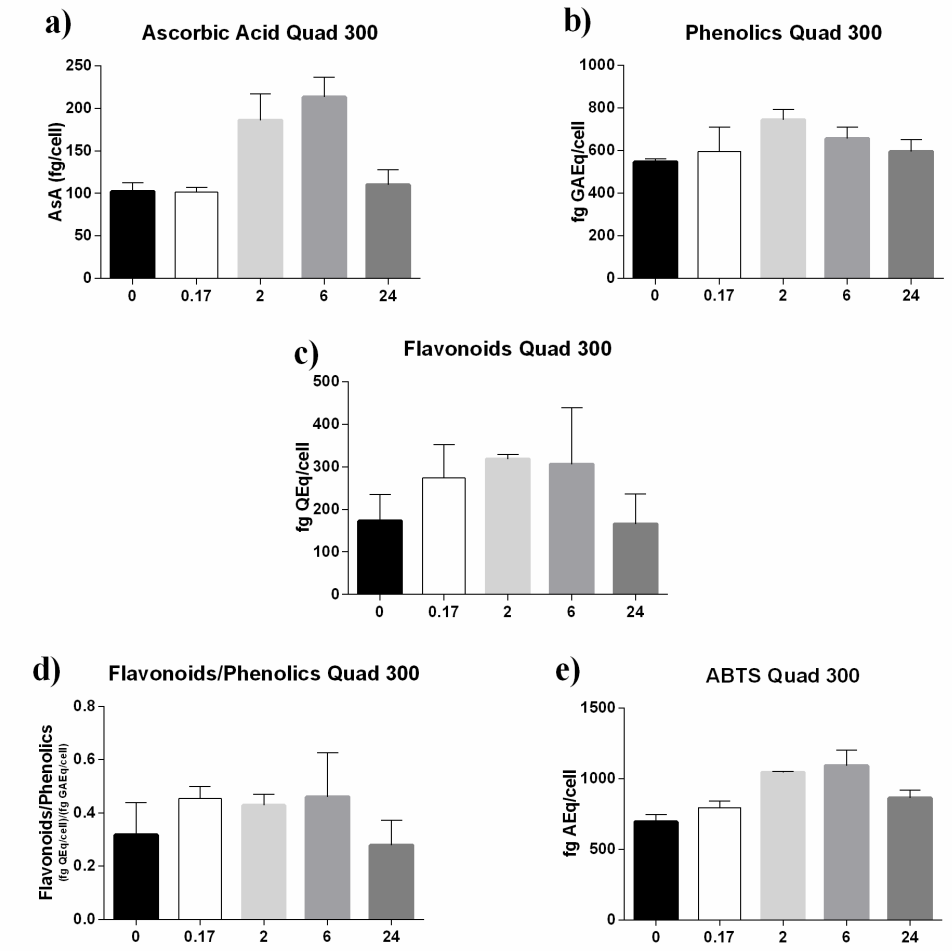

Figure 6.15 Antioxidant molecules and antioxidant activity. a) Ascorbic acid (AsA in fg/cell); b) Phenolics (in fg GAEq/cell); c) Flavonoids (in fg QEq/cell); d) Flavonoids/phenolics ratio; e) ABTS test (in fg AEQ/cell). Samples were collected at pre-dawn (0), 10 minutes (0.17), 2, 6, and 24 hours.Data are reported as mean ±SD of three biological replicates (n=3).

Differently from the other conditions, the phenolic content in Quad 300 peaked at 2 hours ($p<0.05$, Fig. 6.15 b), decreasing after that and restoring the initial values at 24 hours. Flavonoids (Fig. 6.15 c) did not show any significant change, although they increased a bit already at 10 minutes, keeping this concentration for 6 hours from the beginning of the experiment. The ratio between flavonoids and the phenolic compounds reflected this behavior (Fig. 6.15 d).

The ABTS followed the same trend of AsA, increasing at 2 hours and keeping high values at 6 hours ($p<0.05$, Fig. 6.15 e).

Also under the square-wave light condition Quad 300 significant relationships between photoprotection and antioxidant network were noticed (Table 6.8) despite some differences respect to the other two high light conditions. Interestingly, a negative correlation between NPQ and the total antioxidant capacity (ABTS) was revealed, suggesting an opposite stimulation of these two protective mechanisms.

Table 6.8: Correlations between the antioxidant capacity and molecules among each other and with the photoprotective parameters measured under Quad 300. Significance values (P) and Pierson's correlation coefficients (r).

		P	r
ABTS	AsA	<0.01	0.92
	NPQ	<0.05	-0.71
AsA	Dt	<0.01	0.80
Phenolics	Flavonoids	<0.05	0.75
Dd	Dt	<0.001	0.89
	β-car	<0.00001	0.99
Dt	β-car	<0.0001	0.90

6.3.5 Discussion

The exposure of cells to different high light climates presents repetitive features as well as induces different biological responses.

Overall, the uncoupling between growth and the photosynthetic rate suggests that the photochemical energy was used to perform biochemical adjustments in order to survive to the stressful light condition instead of biomass enlargement.

The photoprotective and antioxidant parameters were correlated between each other, suggesting a parallel time-scale of responses of the different networks. The correlation between the antioxidant capacity and the photoprotective pigments also suggest an additional antioxidant role of these pigments apart of their known role in photoprotection. The opposite trend observed between NPQ and Dt is intriguing, and this result brings once again to the hypothesis that the Dt thylakoid pool not directly involved in chlorophyll a

(Chla) quenching plays a major role in photoprotection *via* the ROS scavenging and/or lipid peroxidation avoidance rather than dissipation of excess energy as heat (previous chapters) (Lepetit *et al.*, 2010, Giovagnetti *et al.*, 2014)

The cells switched to a high sinusoidal light were still highly performing (high Fv/Fm and growth rate). The lower values of Fv/Fm measured in the two quadratic condition instead were probably caused by the closure or damage of the reaction centers, highlighting the stressful nature of this light distribution, which led to cell death. The same values of the photosynthetic parameters at 24 hours respect to those of the time 0 demonstrate the lack of acclimation to the high light regime experienced the day before.

Intriguingly, the photosynthetic rate at 24 hours stabilized on a mean value of 31 ± 6 pmol e^{-1} h^{-1} $cell^{-1}$ between the three light conditions, despite the difference of the light received.

The different Fuco/Chla ratio observed in Sin 600 suggests a reorganization of the antennae, in favor of a lower antenna/reaction center ratio, a high light acclimation feature (Ruban, 2009). This feature is absent under quadratic light distribution, revealing an impairment of the normal high light acclimation feature under high light sudden stress.

The different trend of NPQ measured in the two quadratic conditions compared to Sin 600 confirms this feature and demonstrates that cells were not able to promptly dissipate the excess of income energy, whose detrimental action culminated in a massive cell death. In Sin 600, the higher values of NPQ recorded at two hours and its subsequent decrease confirms the role of NPQ as early response mechanism used by microalgae in order to dissipate the excess of income energy. The higher NPQ revealed at 24 hours indicates that cells acclimated to the light environment experienced the day before. This high value not paralleled by an increase of Dt suggests that the higher NPQ is probably due to structural reorganization of the antennae ascribable to the proteic component, allegedly LHCXs (Giovagnetti & Ruban, 2017, Lepetit *et al.*, 2017).

The lack of any photoacclimative process under the highest quadratic condition is also visible by the unvaried DES values, which stayed the same despite the extremely stressful quantity of incident light the cells were exposed to.

Also the antioxidant molecules present differences between Sin 600 and the quadratic light distribution. The lower values recorded under Sin 600 compared to the two other conditions suggest their consumption in order to prevent the oxidative stress.

Also, the lower AsA recorded after 10 minutes in Quad 600 was probably due to its fast consumption to counteract the oxidative process induced by the abrupt high light exposure. The unvaried concentration of the phenolic compounds in the same time point may be due to the different nature of this class of molecules, less versatile than AsA, which by contrast is used by several enzymes in several pathways or scavenge the radical species directly (Foyer & Noctor, 2005b, Noctor & Foyer, 1998, Foyer & Noctor, 2011). While the phenolic compounds concentration increased under this light condition, the flavonoids didn't show any variation that might be due to their oxidation which prevents their detection (Agati & Tattini, 2010). Probably, the discrepancy between phenolics and flavonoids trends could be caused by the additional reactivity of the Folin-Ciocalteu reagent towards AsA (Everette *et al.*, 2010).

The lack of the AsA consumption at 10 minutes of the Quad 300 was probably due to lower level of incident light, less stressful in comparison with the other quadratic condition.

The discrepancy between the unvaried antioxidant molecules and the higher antioxidant capacity in both the quadratic conditions is intriguing. Some other molecule must have been responsible for the scavenging activity, supposedly tocopherol, whose synthesis is light controlled (Kobayashi & DellaPenna, 2008). It may also explain the high Fv/Fm recorded, having this molecule a protective role against PSII inactivation (Demmig-Adams *et al.*, 2014).

The light intensity and its distribution shape greatly affect the photophysiological state of cells. This result is confirmed by the principle component analysis (PCA) performed using a correlation matrix of the collected physiological and biochemical data. The first analysis (Fig. 6.16 a) corresponds to the data of the midday sampling for the control (Ctrl sin 150) and the three high light treatments (Sin 600, Quad 600 and Quad 300). The first two axes explain 74% of the total variability. Three main clusters are visible: Ctrl sin 150 (Fig., 6.16 a, solid ellipse), the two quadratic conditions (Fig. 6.16 a, dotted ellipse) and opposed to them the Sin 600 (Fig. 6.16 a, dashed ellipse). The separation of the Quad conditions from the Sin 600 is driven by the different antioxidant molecules and pigments. This result demonstrates that cells respond differently among the experiments, showing the strong influence of the light shape distribution, which determines the segregation of the two

quadratic conditions from the high sinusoidal one. The integrated daily light dose instead has low or even no influence at all, compared to the light distribution effect.

The same analysis performed with the 24 hours and time 0 sampling data shows two main clusters: one includes the two sinusoidal light distributions (Fig. 6.16 b, solid ellipse), mainly pulled by NPQ and Fv/Fm, and one more dispersed including the two quadratic conditions (Fig. 6.16 b, dotted ellipse). The two first axes explained the 67% of the variability.

The fact that cells exposed to high sinusoidal light after 24 hours are clustered with the time 0 means that cells acclimate very well to higher light climate, being able to respond to this type of fluctuation without drastically changing their photophysiological state or biochemical composition. In Quadratic light, however, a completely different situation is outlined.

Overall, my results highlight the key role of the light course distribution in shaping the photophysiological responses of diatoms. The high sinusoidal light, although slowing microalgal growth, is well tolerated. The switch to an unnatural light distribution consisted in an on/off system instead severely impaired the cell functioning.

The detrimental effect of high light with a square-wave distribution led probably to an oxidative stress to which cells were not able to counteract through the modulation of the antioxidant network.

a)

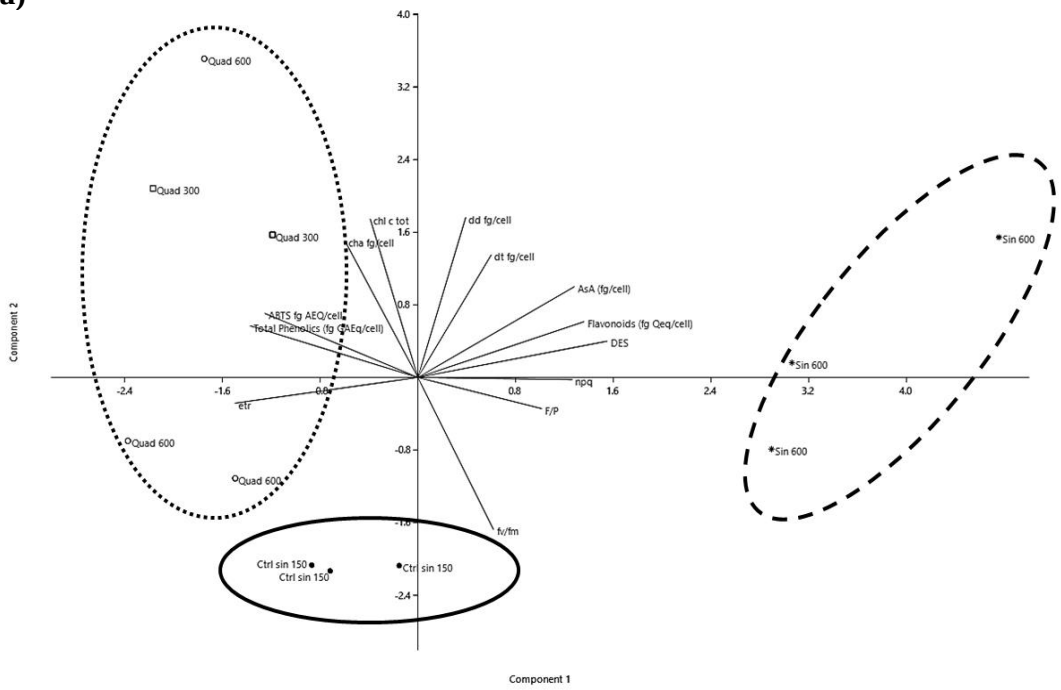

b)

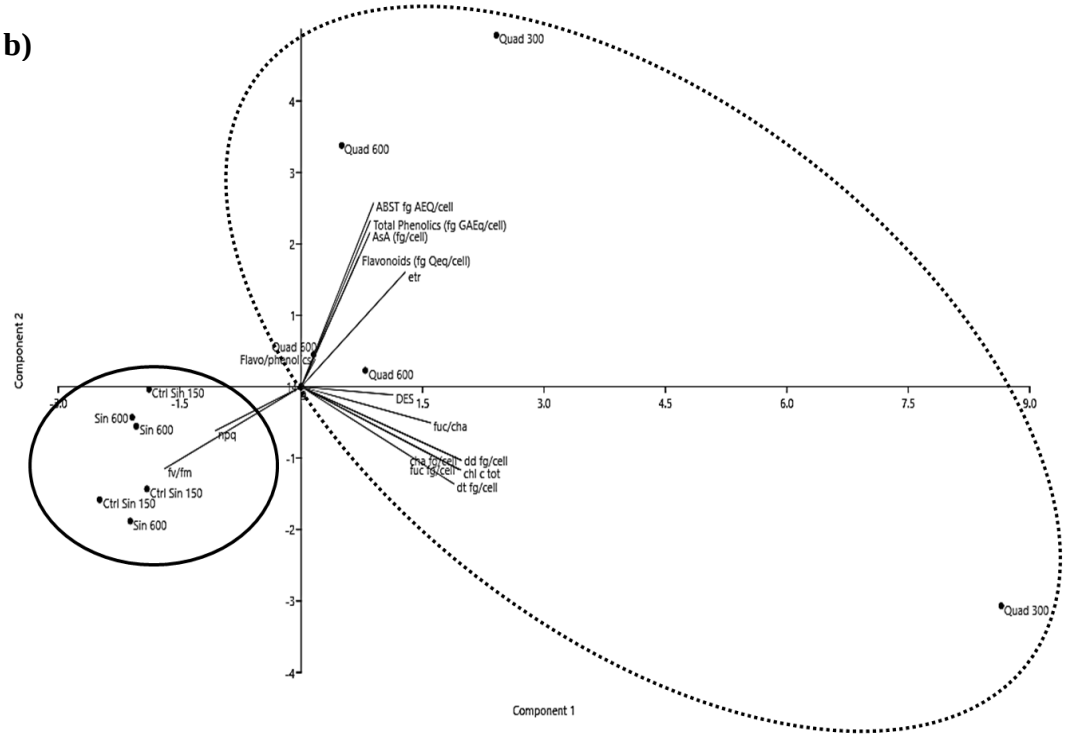

Figure 6.16: Principal components analysis (PCA). The analysis was performed on data collected a) at midday time point of the control (Ctrl sin 150) and the three high light treatments (Sin 600, Quad 600 and Quad 300) ; b) at time zero of the control (Ctrl sin 150) and the 24 hour time point of the three high light treatments (Sin 600, Quad 600 and Quad 300). Analysis was performed on correlation matrix of the data set, constituted by the photosynthetic, photoprotective and antioxidant network parameters such as ETR, Fv/Fm, Chla, Chlc, NPQ, Dt, Dd, DES, AsA, Phenolics, Flavonoids, Flavonoids/Phenolics (F/P), ABTS.

7. Dark and low light acclimation of protective and antioxidant network in *Skeletonema marinoi*

7.1 Introduction

In the previous chapters, it has been demonstrated the fundamental role of light and its multiple properties such as the spectral composition, the intensity, distribution shape, the velocity of increase, the integrated daily light dose, in ruling the photophysiological process of diatoms and shaping the responses of the photoprotective and antioxidant network.

One crucial aspect still unexplored is the investigation of the "other side of the coin": the role of absence of light.

It is known that microalgae, being passively transported along the water column by the turbulent mixing and currents, can be rapidly carried below the photic zone, where no solar energy can fuel the photosynthetic process (MacIntyre *et al.*, 2002).

It has been reported that Antarctic diatoms can survive up to 10 months in complete darkness and up to 3 months without consistent changes of their physiology (Peters, 1996b). By contrast, experiments carried out on some temperate water diatoms demonstrated that they have lower survival capability, but still after 20 days or more of prolonged darkness they were able to resume growth (Peters, 1996a).

The strategies that allow them to survive to the absence of light seem to be multiple and maybe species specific. Various long term acclimative physiological mechanisms have been described, such as a reduction of the metabolic rate (Jochem, 1999), the catabolism of the storage lipids as energy form to maintaining metabolism (Schaub *et al.*, 2017), the switch to heterotrophy as nutritional strategy (Tuchman *et al.*, 2006).

When exposed to prolonged darkness, diatoms stop growing because their division is light controlled. In fact, various cell cycle genes are light-regulated, and prolonged darkness determines the arrest in G_1 phase in the pennate diatom *Phaeodactylum tricornutum* and both in G_1 and G_2+M phases in the centric diatom *Thalassiosira weissflogii*, followed by a release of the cell cycle arrest upon re-illumination (Vaulot *et al.*, 1986, Huysman *et al.*, 2010). It has been found that cell cycle progression is under control of photoreceptors, which induce the transcription of cyclins controlling the activation of cyclin-dependent kinases (CDKs) (Coesel *et al.*, 2009, Huysman *et al.*, 2013).

The model diatom *P. tricornutum* exposed to prolonged darkness (48 hours) showed a huge transcriptional response, with a general down-regulation of the genes encoding for photosynthesis-associated proteins (Nymark *et al.*, 2013). Yet, the quantum yield of photochemistry, the photosynthetic and the maximum light use efficiencies decreased at dark, but, interestingly as soon as the cells were re-exposed to light they immediately recovered, restoring their photosynthetic ability (Nymark *et al.*, 2013). These findings indicate that photosynthetic apparatus can enter into a stand-by status which allows a fast recovery upon re-irradiation (Nymark *et al.*, 2013).

It has been demonstrated that under prolonged darkness (48-60 hours) transcriptional expression of one isoform of the light-harvesting complex stress related proteins, namely Lhcx4, is upregulated, in contrast to other isoforms (Lhcx1, Lhcx2, and Lhcx3) which are light-induced (Nymark *et al.*, 2013, Taddei *et al.*, 2016). Lhcx4 aminoacidic structure lacks in key protonatable residues present instead in the other isoforms, which are responsible of diminishing of the electrostatic repulsion upon protonation which allows an enhanced quenching capacity by rearranging the pigment orientation and the protein structure (Ballottari *et al.*, 2016). The higher presence of this isoform at dark should therefore be responsible for the lower NPQ capacity recorded in these cells by hampering the quenching site formation (Taddei *et al.*, 2016).

Dark is a condition that algae experience daily during night. During this phase, respiration is still active while the absence of light limits carbon fixation. By consequence, diatoms convert the excess of diurnal energy into storage products such as lipids and carbohydrates which are subsequently used to fuel cellular activity.

In higher plants as well as in (micro)algal and cyanobacterial species it has been demonstrated the presence of a circadian clock regulating photosynthesis, pigment content, growth as well as photo- and chemotaxis, cell-glass adherence, and cell division (Ouyang *et al.*, 1998, Mittag & Wagner, 2003, Dodd *et al.*, 2005, Mittag *et al.*, 2005, Noordally & Millar, 2015). This intrinsic rhythmicity determines anticipatory behaviors, being the organism able to foresee the daily environmental changes (Ouyang *et al.*, 1998). The synchronicity with external day-night cycles confers a selective advantage assuring the activation of cellular processes in the best time window such as the phototaxis happening during the day and the chemotaxis and light sensitive processes such as UV-sensitive DNA

synthesis during the night (Mittag & Wagner, 2003, Mittag *et al.*, 2005). By definition, a circadian rhythm is an endogenous near-24 hours long biological rhythm (circadian means *about a day* in Latin) regarding gene expression and consequent biological activity (Bell-Pedersen *et al.*, 2005). This rhythm is different from externally driven oscillation, being persistent even when the organism is isolated from daily environmental cycles (Ivleva *et al.*, 2005). It is controlled by an internal clock which is a 24-hours timing mechanism composed by molecular oscillators. The oscillators contain positive and negative elements forming an autoregulatory feedback loops used to generate 24-hours timing circuits (Bell-Pedersen *et al.*, 2005). The single circadian oscillator does not operate independently from other oscillators although being self-sustained, but needs to be driven by a specialized oscillator called pacemaker which is entrained by environmental cues and drives rhythmic outputs directly and/or through other oscillators (Bell-Pedersen *et al.*, 2005). The environmental cue synchronizing the oscillators is called zeitgeber (meaning *time giver* in German), which in most species is typically the light:dark cycle (Bell-Pedersen *et al.*, 2005). By consequence, the pacemaker, being light entrained, must be a photoreceptor (Bell-Pedersen *et al.*, 2005). In the cyanobacterium *Synechococcus elongates* additional pacemaker senses the redox state of the cell (Ivleva *et al.*, 2005).

An experiment carried out in outer space on the green alga *Chlamydomonas reinhardii* demonstrated the circadian rhythmicity of phototaxis, which was kept unvaried for six days despite the cells orbited the Earth every 90 minutes aboard a spacecraft, demonstrating also that its circadian clock works independently from magnetism, cosmic ray irradiation, gravity and so on (Mergenhagen & Mergenhagen, 1987).

In diatoms, although the daily regulation of some processes such as the photosynthesis, enzyme activity, cell division (chapter 5)(Sigaud-Kutner *et al.*, 2005, Bowler *et al.*, 2010a) the presence of an endogenous circadian clock has not been demonstrated.

The results reported in chapter 5 demonstrated a cyclical trend of some features such as the antioxidant molecules and pigment content synthesis, and by the consequent antioxidant activity, as well as the photoprotective mechanism of the non-photochemical quenching (NPQ) during the exponential phase.

The aims of the new experiments were:

- to assess if this periodicity was a consequence of the direct light stimulus or it was driven by a putative internal circadian clock,
- if assessed the absence of a circadian regulation, we wanted to explore the photoprotective and antioxidant network activation in response to prolonged darkness or limiting light intensity.

We setup three light treatments: a continuous dark and a very low light with sinusoidal course peaking at midday at a PFD of 10 µmol photons m^{-2} s^{-1} to simulate what happens in nature when photosynthetic cells sink below or at the limit of the euphotic zone. These two light conditions were then compared with another light treatment which represented a completely unnatural situation: a continuous low light (photoperiod 24:0 light:dark) setup at 10 µmol photons m^{-2} s^{-1}. In this way, comparing it with prolonged darkness, it has been possible to explore the role of light in terms of no photons *vs*. few photons, and the physiological consequence of the exposure to this peculiar light climate which foresaw the total absence of a dark phase.

7.2 Materials and methods

7.2.1 Experimental strategy and sampling

The experiments were conducted on the centric diatom *Skeletonema marinoi*, grown at 20°C in 4.5 L glass tanks with air bubbling.

The pre-acclimation condition, similar to the one used in the previous set of experiment (Chapters 5 and 6), was a white (R:G:B: 10:40:50) sinusoidal light distribution with a midday peak of 150 µmol photons s^{-1} m^{-2} and with a photoperiod equal to 12:12 dark:light (Ctrl sin 150).
The experiments were conducted in triplicate during the exponential growth phase.
The experimental light setups are summarized in the Table 7.1.

Table 7.1: Experimental light conditions

Pre-acclimation	Name	Light switch	Experimental "sketch"	Sampling points (hours after the beginning of the experiment)
Control Sinusoidal 150 (Ctrl sin 150)	Dark	Dark	Continuous absence of light	0, 6, 24, 30
	Con 10	Continuous 10	Very low and continuous light	0, 6, 24, 30
	Sin 10	Sinusoidal 10	Very low light (sinusoidal distribution)	0, 6, 24, 30

7.2.2 Parameters analyzed

The subsequent parameters were followed during the experiments:

- Cell concentration
- Photochemical efficiency of the photosystem II
- Electron transport rate (ETR)-light curves
- Non-photochemical quenching (NPQ)
- Pigments
- Absorption spectra
- Total phenolic content
- Total flavonoid content
- Ascorbic acid content
- ABTS radical scavenging activity

The experimental procedures for the analysis of these parameters are described in Chapter 2.

7.3 Results

7.3.1 General trends

Pooling together the results obtained from the three experiments, relationships between the photoprotective and antioxidant responses were revealed, indicating parallel time-scale of responses of these different networks. The correlations are summarized in Table 7.2.

Table 7.2 Correlations between the antioxidant capacity and molecules among each other and with the photoprotective parameters pooling together the three experiments (Dark, Con 10, Sin 10). Significance values (p) and Pierson's correlation coefficients (r).

		p	r
ABTS	AsA	<0.0001	0.71
	Phenolics	<0.0001	0.97
	Flavonoids	<0.001	0.64
	NPQ	<0.0001	-0.54
	Dd	<0.0001	0.93
	Dt	<0.0001	0.89
	β-car	<0.0001	0.90
AsA	Phenolics	<0.0001	0.91
	Flavonoids	<0.01	0.57
	Dd	<0.001	0.66
	Dt	<0.01	0.51
	β-car	<0.0001	0.68
Phenolics	Flavonoids	<0.001	0.65
	NPQ	<0.01	-0.53
	Dd	<0.0001	0.87
	Dt	<0.0001	0.94
	β-car	<0.0001	0.88
Flavonoids	Dd	<0.001	0.59
	Dt	<0.05	0.42
Dd	NPQ	<0.01	-0.52
	Dt	<0.0001	0.90
	β-car	<0.0001	0.88
Dt	β-car	<0.0001	0.90

Like in the previous set of experiments performed in high light, there was an absence of correlation between growth and photosynthetic rate (electron transport rate, ETR, $p>0.05$). The total antioxidant capacity measured with the ABTS radical scavenging activity was related to the antioxidant molecule concentrations (ascorbic acid (AsA), phenolics, flavonoids) as well as to the xanthophyll cycle pigments diadinoxanthin (Dd), diatoxanthin

(Dt), and their precursor β-carotene (β-car). Interestingly, this capacity was opposed to the non-photochemical quenching (NPQ).

The three antioxidant molecules were linked among each other and with the xanthophyll cycle pigments. Interestingly, no correlation was found between NPQ and the photoprotective pigment Dt, while Dd showed an opposite trend with NPQ.

7.3.2 Dark

7.3.2.1 Growth rate and photosynthesis

The growth rate (μ) calculated after 24 hours of absence of light was negative (Table 7.3), caused by a block of cell division, and cell death.

Table 7.3: Growth properties of the cultures. Cell concentration expressed as cell mL^{-1}, and growth rate expressed as μ, d^{-1}at 0 (pre-dawn) and 24 hours later

	0	**24**
Cell concentration Cells mL^{-1}	460'150 ± 45'130	399'990 ± 40'790
Growth rate μ, d^{-1}	1.0 ± 0.2	-0.1 ± 0.1

The photosynthetic rate (ETR, Fig. 7.1), although showing slightly lower values at 6, 24, and 30 hours, didn't change consistently.

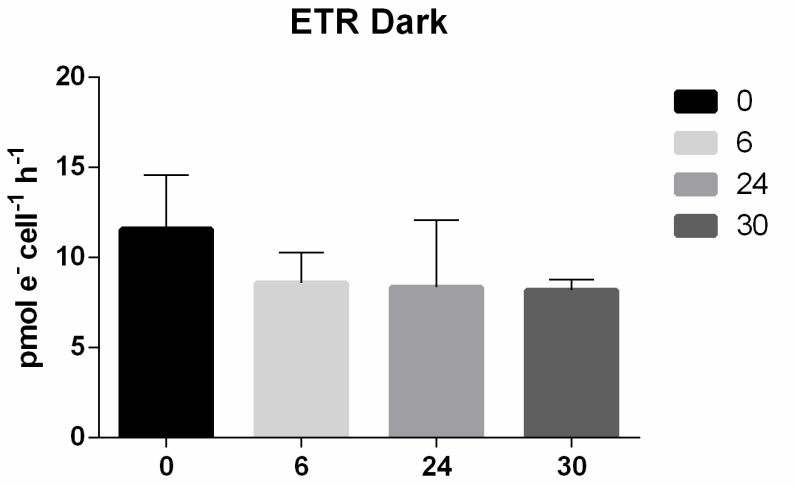

Figure 7.1: Electron Transport Rate (ETR, pmol e^- $cell^{-1}$ h^{-1}) of Dark. Samples were collected at pre-dawn (0), and after 6, 24, and 30 hours. Data are reported as mean ±SD of three biological replicates (n=3).

7.3.2.2 Photosynthetic acclimation and pigments

The quantum yield of photochemistry (Fv/Fm) under Dark did not change significantly (Fig. 7.2 a). The other photosynthetic parameters α (maximum light use efficiency, Fig. 7.2 b) and Ek (light saturation index for photosynthesis, Fig. 7.2 c) were also quite stable, although Ek showed a weak lowering, suggesting a low light acclimation feature.

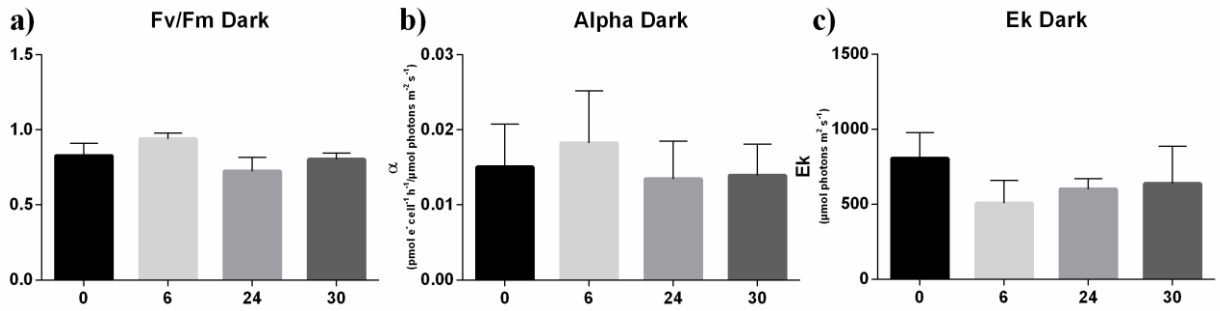

Figure 7.2: Photosynthetic parameters of Dark. a) Fv/Fm (maximum quantum yield of the PSII); b) α (maximum light use efficiency, in pmol e^- $cell^{-1}$ h^{-1}/µmol photons m^{-2} s^{-1}); c) Ek (light saturation index for photosynthesis, in µmol photons m^{-2} s^{-1}). Samples were collected at pre-dawn (0), and after 6, 24, and 30 hours. Data are reported as mean ±SD of three biological replicates (n=3).

Chlorophyll a (Chla) increased its concentration over time compared to Time 0 ($p<0.05$ at 6 hours and $p<0.01$ at 30 hours, Fig. 7.3 a). Chlorophyll c (Chlc) increased significantly at 30 hours ($p<0.05$, Fig. 7.3 b). Fucoxanthin (Fuco) didn't vary consistently (Fig. 7.3 c), determining a slight decrease - although not significant - of antennae/reaction center ratio (Fucoxanthin/Chlorophyll a ratio, Fig. 7.3 d).

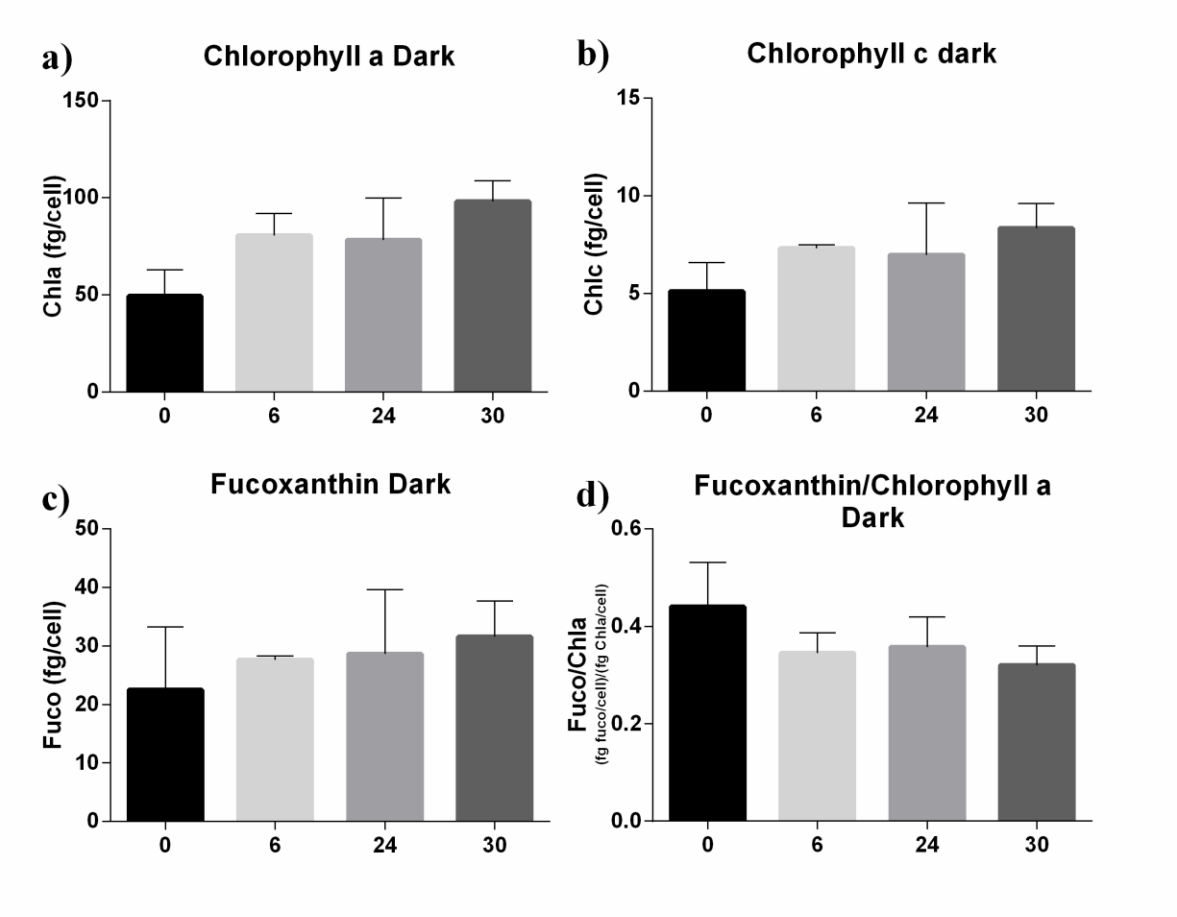

Figure 7.3: Photosynthetic pigments. a) Chlorophyll a (Chla in fg/cell); b) Chlorophyll c_s (Chlc in fg/cell); c) Fucoxanthin (Fuco in fg/cell); d) Fucoxanthin/Chlorophyll a ratio. Samples were collected at pre-dawn (0), and after 6, 24, and 30 hours. Data are reported as mean ±SD of three biological replicates (n=3).

7.3.2.3 Photoprotection

NPQ did not vary under Dark (Fig. 7.4 a), and the concentration of the photoprotective pigment diatoxanthin (Dt) slightly increased over time (Fig. 7.4 b). The same happened to the precursors diadinoxanthin (Dd) and β-carotene (β-car), who slightly increased (Fig. 7.4 c, d), revealing a weak induction of the photoprotective pigment synthesis.

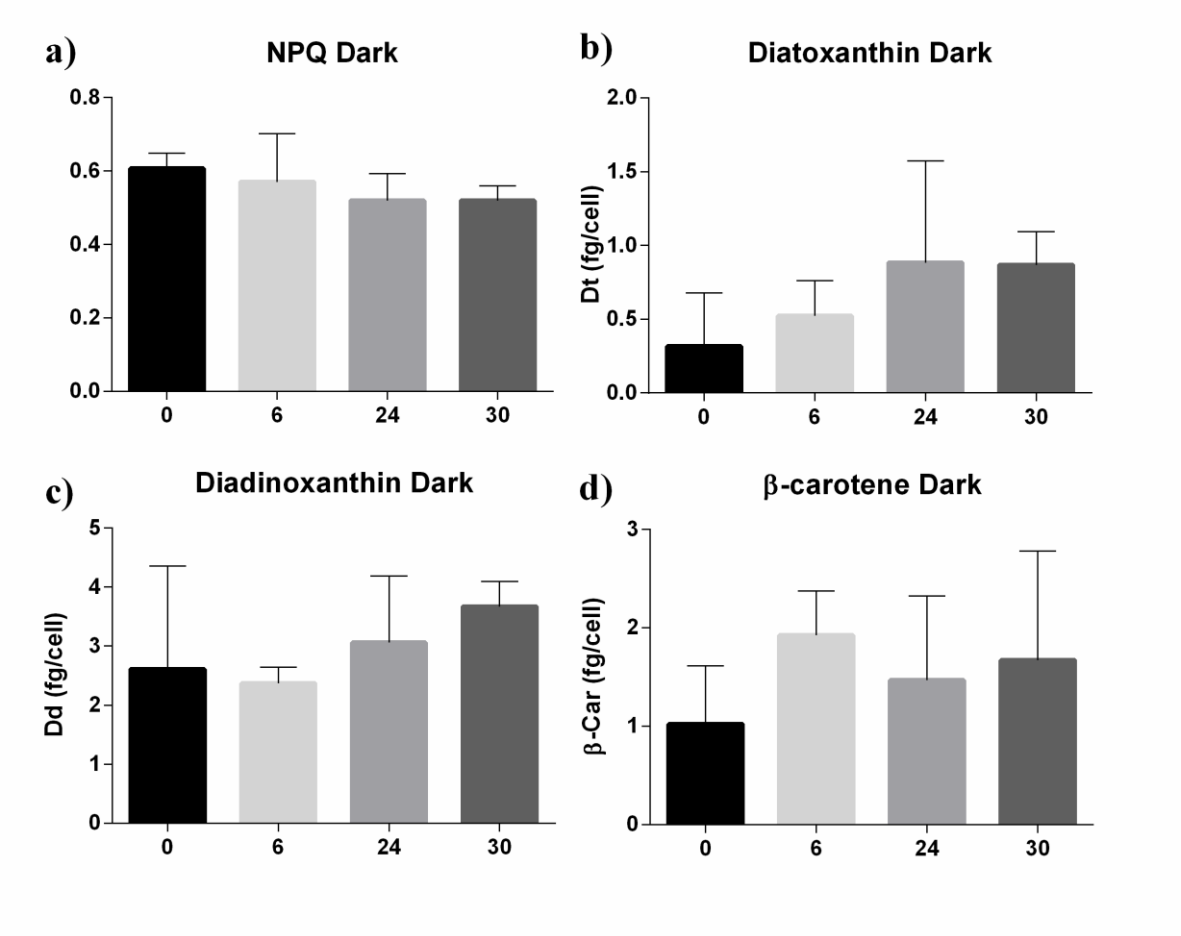

Figure 7.4: Photoprotection. a) non-photochemical quenching (NPQ); b) Diatoxanthin (Dt in fg/cell); c) Diadinoxanthin (Dd in fg/cell); d) β-carotene (β-car in fg/cell). Samples were collected at pre-dawn (0), and after 6, 24, and 30 hours. Data are reported as mean ±SD of three biological replicates (n=3).

7.3.2.4 Antioxidant molecules and activity

The concentration of ascorbic acid (AsA, Fig. 7.5 a) did not change a lot over time, decreasing a bit the second day of experiment. Also the total phenolics and total flavonoids content unvaried (Fig. 7.5 b, c), apart from a not statistically significant decrease of flavonoids at 6 hours. The same trend observed for AsA and phenolics might be due to the lack of specificity of the reagent used for phenolics determination, which has been reported to be reactive also towards AsA (Everette *et al.*, 2010). The antioxidant activity mirrored exactly what happened with the antioxidant molecules, without showing any variation along the experiment (Fig 7.5 d).

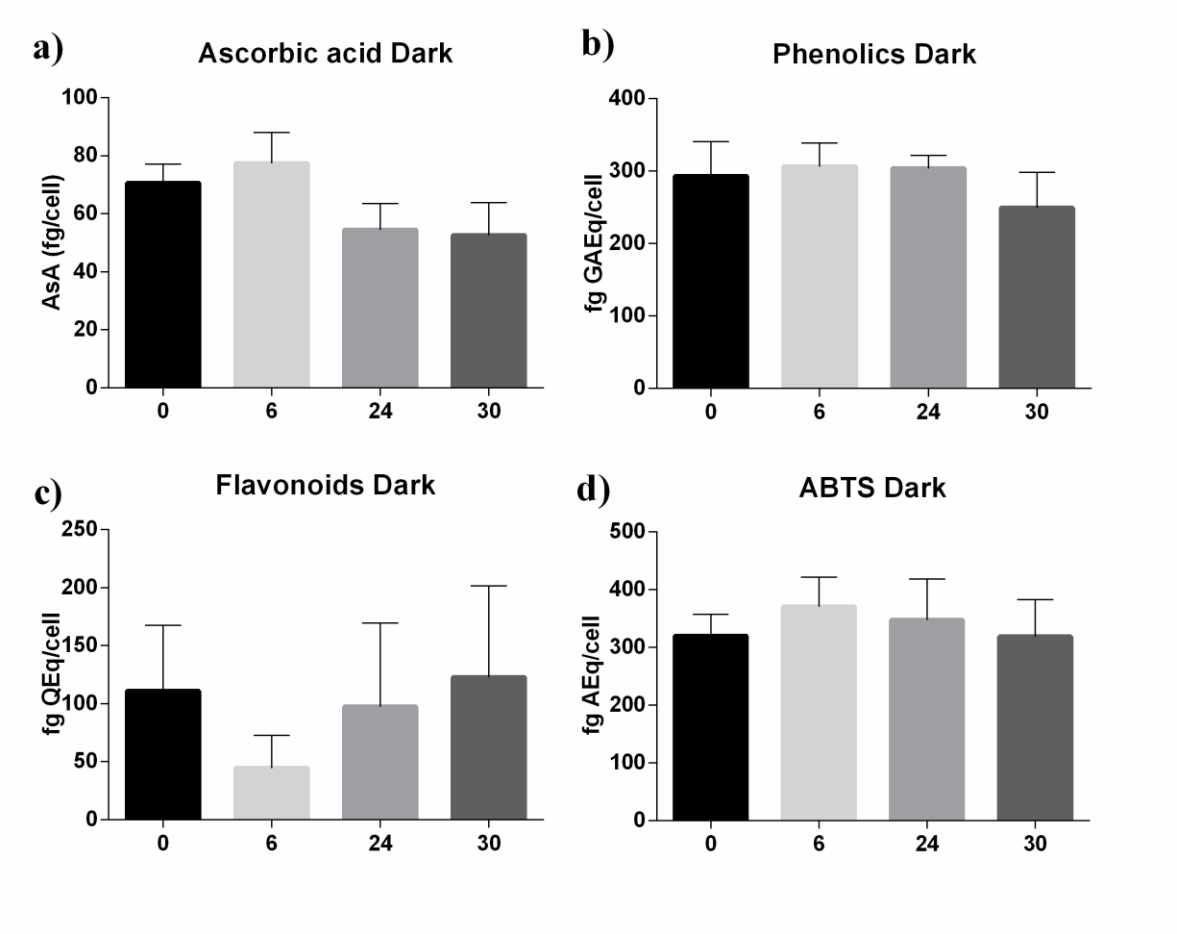

Figure 7.5: Antioxidant molecules and antioxidant activity. a) Ascorbic acid (AsA in fg/cell); b) Phenolics (in fg GAEq/cell); c) Flavonoids (in fg QEq/cell); d) ABTS test (in fg AEQ/cell). Samples were collected at pre-dawn (0), and after 6, 24, and 30 hours. Data are reported as mean ±SD of three biological replicates (n=3).

7.3.3 Continuous 10

7.3.3.1 Growth rate and photosynthesis

Cells exposed to the continuous extremely low light showed at 24 hours a negative growth rate (μ) equal to -1.5 d^{-1} (Table 7.4).

Table 7.4: Growth properties of the cultures. Cell concentration expressed as cell mL^{-1}, and growth rate expressed as μ, d^{-1}at 0 (pre-dawn) and 24 hours later.

	0	24
Cell concentration Cells mL^{-1}	676'100 ± 49'619	76'102 ± 37'561
Growth rate μ, d^{-1}	1.0 ± 0.1	-1.5 ± 0.6

The photosynthetic rate decreased at 6 hours, reaching its minimum value at 24 hours ($p<0.05$, Fig. 7.6), and increasing a bit at 30 hours.

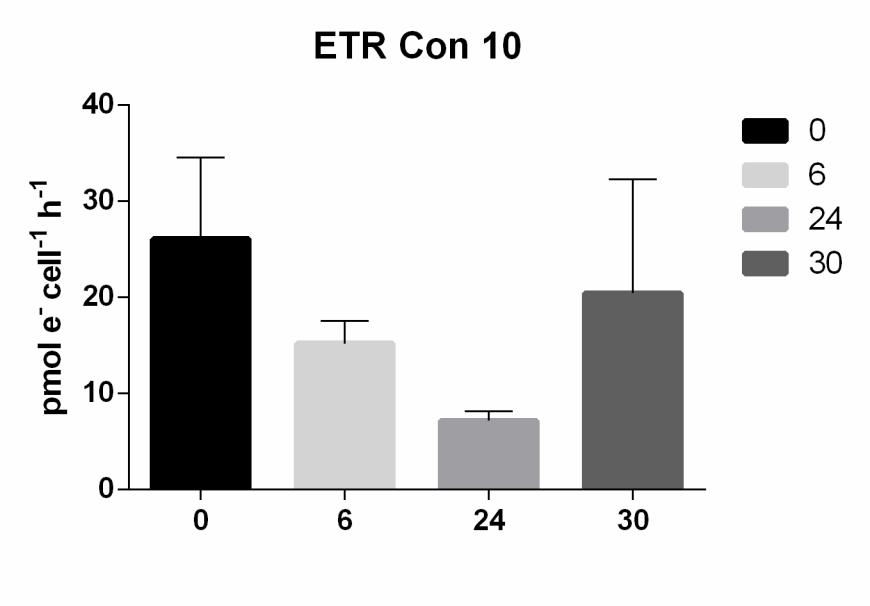

Figure 7.6: Electron Transport Rate (ETR, pmol e^- $cell^{-1}$ h^{-1}) of Continuous 10. Samples were collected at pre-dawn (0), and after 6, 24, and 30 hours. Data are reported as mean ±SD of three biological replicates (n=3).

7.3.3.2 Photosynthetic acclimation and pigments

The quantum yield of photochemistry (Fv/Fm) decreased significantly both after 6 and 24 hours respect to the pre-dawn sampling ($p<0.05$ and $p<0.01$, respectively, Fig. 7.7 a). The values of α (Fig. 7.7 b) were lower both at 6 and 24 hours, but not consistently respect to pre-dawn. Differently, Ek lowered significantly (Fig. 7.7 c), reaching its minimum value after 24 hours under this light regime ($p<0.05$). Like ETR, the values of Fv/Fm, α, and Ek came back to the initial values at 30 hours.

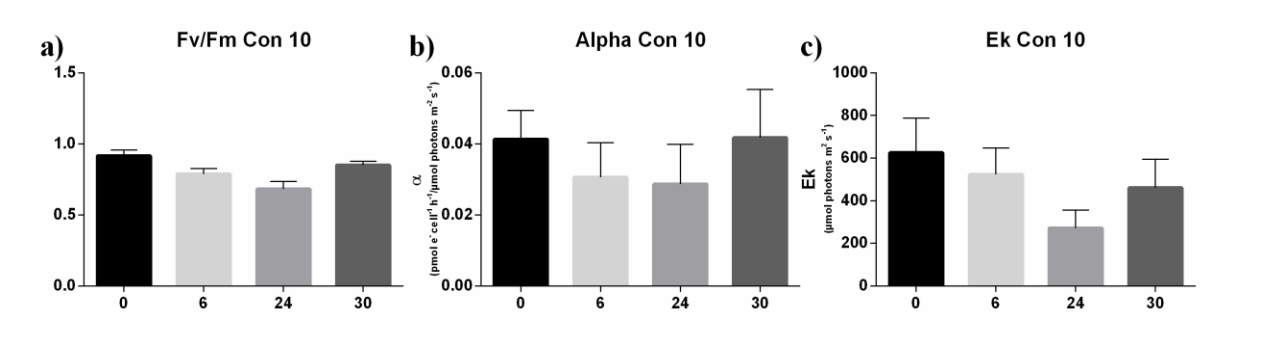

Figure 7.7: Photosynthetic parameters of Continuous 10. a) Fv/Fm (maximum quantum yield of the PSII); b) α (maximum light use efficiency, in pmol e^- $cell^{-1}$ h^{-1}/µmol photons m^{-2} s^{-1}); c) Ek (light saturation index for photosynthesis, in µmol photons m^{-2} s^{-1}). Samples were collected at pre-dawn (0), and after 6, 24, and 30 hours. Data are reported as mean ±SD of three biological replicates (n=3).

The photosynthetic pigment content greatly varied under the continuous low light.

Chlorophyll a (Chla) had a huge increase the second day of experiment (24 hours, $p<0.05$ and 30 hours $p<0.001$, Fig. 7.8 a). The antenna pigments increased already at 6 hours (chlorophyll c (Chlc) $p<0.05$ and fucoxanthin (Fuco) $p<0.01$, Fig 7.8 b, c), and both kept accumulating at 24 and 30 hours ($p<0.01$). Although not significant, the Fuco/Chla ratio increased within the first 6 hours, but later on this ratio was lower due to the greater increase of Chla respect to the antenna pigment Fuco (Fig. 7.8. d).

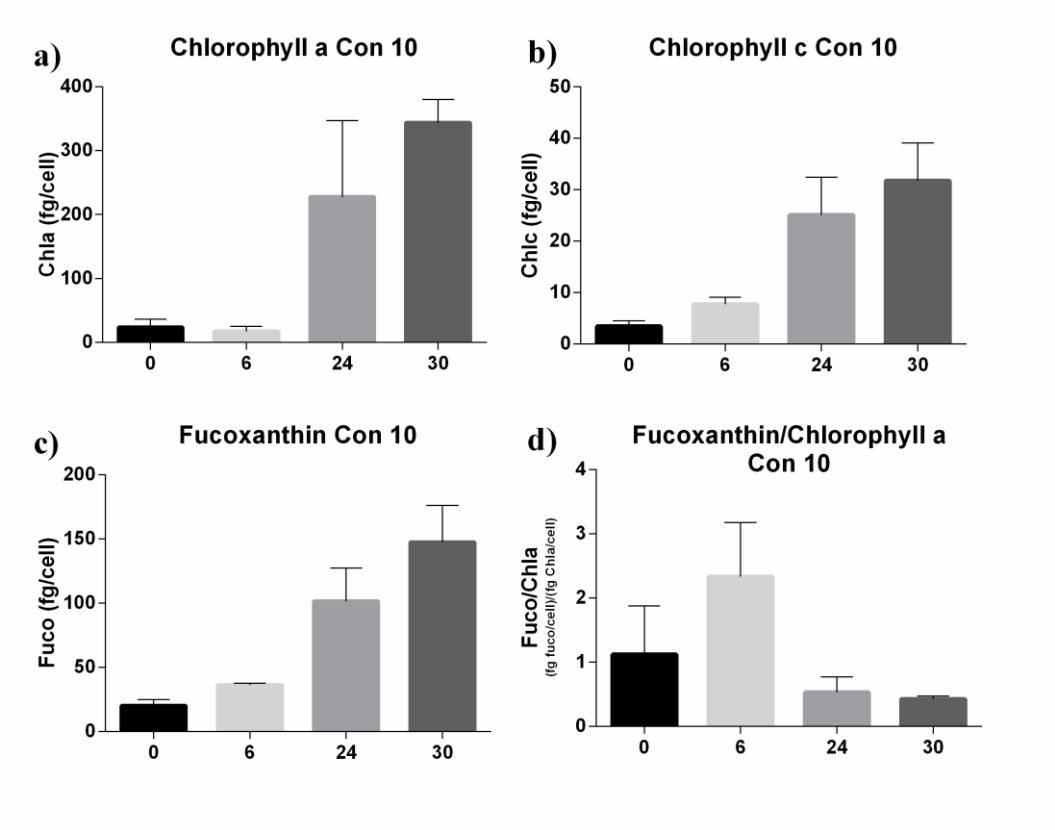

Figure 7.8: Photosynthetic pigments. a) Chlorophyll a (Chla in fg/cell); b) Chlorophyll c_s (Chlc in fg/cell); c) Fucoxanthin (Fuco in fg/cell); d) Fucoxanthin/Chlorophyll a ratio. Samples were collected at pre-dawn (0), and after 6, 24, and 30 hours. Data are reported as mean ±SD of three biological replicates (n=3).

7.3.3.3 Photoprotection

Under continuous low light, NPQ was significantly lower at all the time points respect to pre-dawn ($p<0.01$, Fig. 7.9 a), notwithstanding the strong increase of the photoprotective pigment Dt at 30 hours ($p<0.01$, Fig 7.9 b). Also its precursors diadinoxanthin (Dd) and β-carotene (β-car) were newly synthesized the second day of the experiment, since 24 hours, ($p<0.05$ at 24 and 30 hours for Dd; $p<0.001$ at 30 hours for β-car, Fig 7.9 c, d).

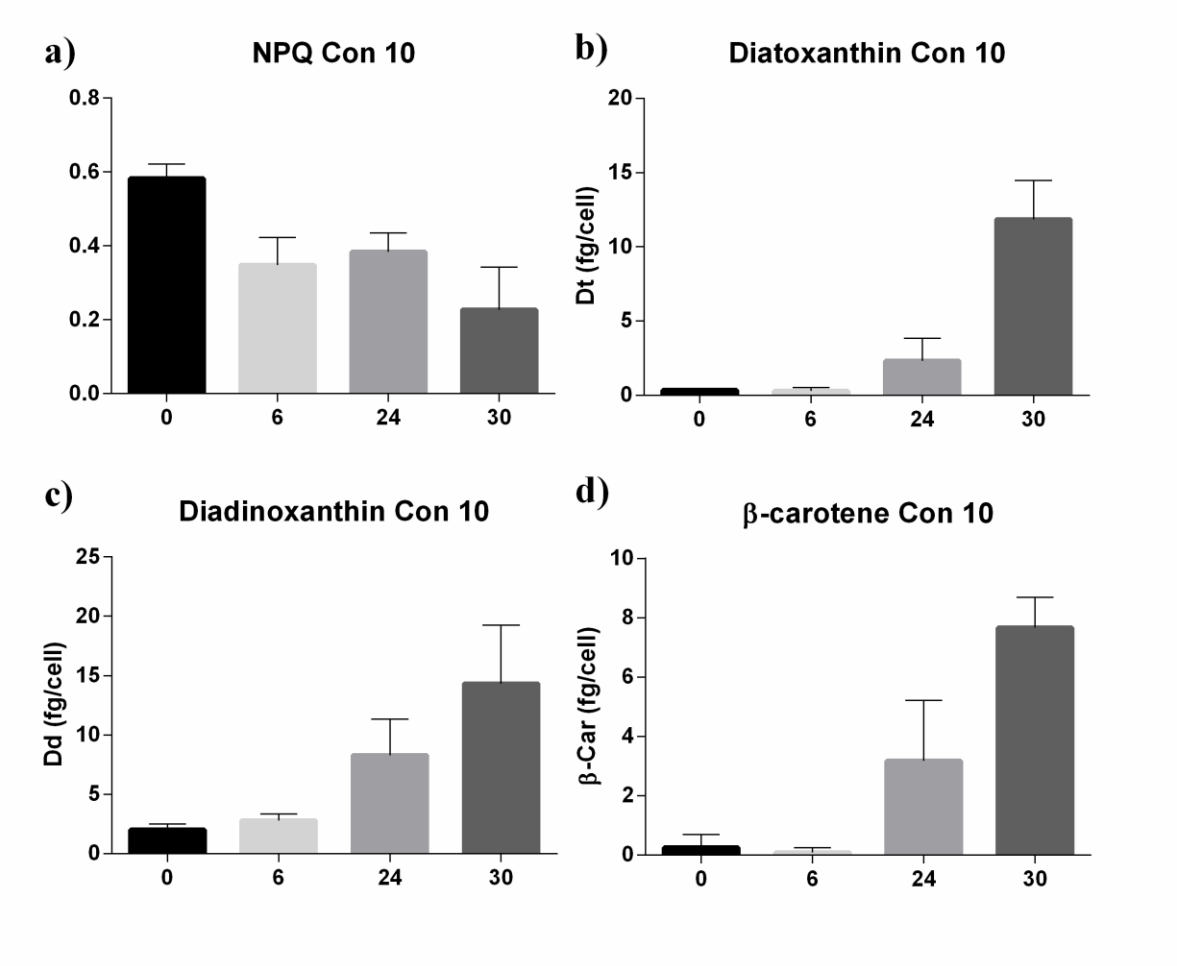

Figure 7.9: Photoprotection. a) non-photochemical quenching (NPQ); b) Diatoxanthin (Dt in fg/cell); c) Diadinoxanthin (Dd in fg/cell); d) β-carotene (β-car in fg/cell). Samples were collected at pre-dawn (0), and after 6, 24, and 30 hours. Data are reported as mean ±SD of three biological replicates (n=3).

7.3.3.4 Antioxidant molecules and activity

Under continuous low light, ascorbic acid (AsA, Fig. 7.10 a) progressively increased its concentration, reaching at 30 hours a concentration 7 times higher than at the beginning of the experiment ($p<0.01$). The same happened with the total phenolic content (Fig. 7.10 b), which started to increase at 6 hours ($p<0.01$, $p<0.001$ at 24 hours) reaching after 30 hours a concentration more than 7 times higher than the time 0 ($p<0.0001$). However, the lack of specificity of the Folin-Ciocalteu reagent (Everette *et al.*, 2010) might be responsible for the similar trend observed for both AsA and phenolic compounds. The flavonoids instead followed a slightly different trend (Fig. 7.10 c), not increasing within the first 6 hours, but showing a concentration more than 4 times higher after 24 hours. Due to the low cells' concentration, the flavonoid content at 30 hours was under the detection threshold. The results obtained with the ABTS test reflected the behavior of the antioxidant molecules (Fig. 7.10 d), being enhanced from 24 hours and reaching values at 30 hours almost 9 times higher than the time 0 ($p<0.001$).

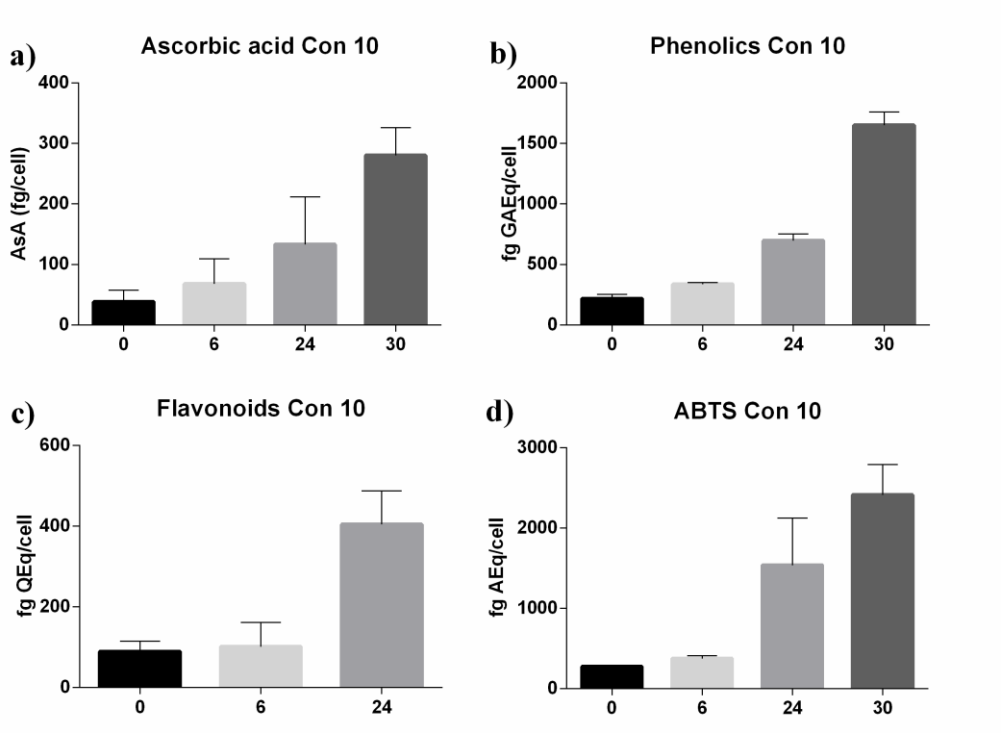

Figure 7.10: Antioxidant molecules and antioxidant activity. a) Ascorbic acid (AsA in fg/cell); b) Phenolics (in fg GAEq/cell); c) Flavonoids (in fg QEq/cell); d) ABTS test (in fg AEQ/cell). Samples were collected at pre-dawn (0), and after 6, 24, and 30 hours. Data are reported as mean ±SD of three biological replicates (n=3).

7.3.4 Sinusoidal 10

7.3.4.1 Growth rate and photosynthesis

The growth rate (μ) calculated after 24 hours under the sinusoidal low light decreased a lot (Table 7.5), but remaining positive.

Table 7.5: Growth properties of the cultures. Cell concentration expressed as cell mL^{-1}, and growth rate expressed as μ, d^{-1}at 0 (pre-dawn) and 24 hours later.

	0	24
Cell concentration Cells mL^{-1}	442'100 ± 61'802	480'077 ± 35'975
Growth rate μ, d^{-1}	1.0 ± 0.2	0.09 ± 0.07

The photosynthetic rate (ETR, Fig. 7.11) didn't change consistently, although showing lower values the second day of experiment.

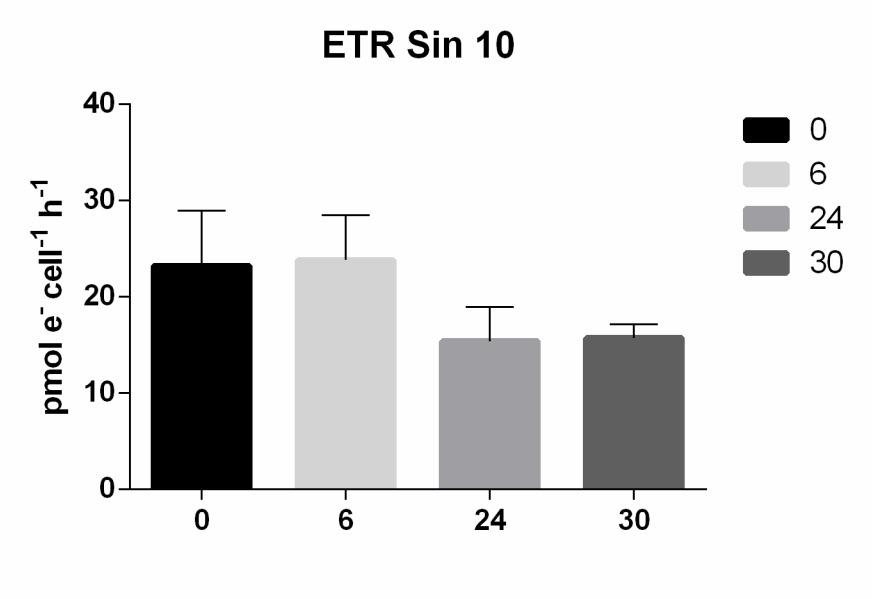

Figure 7.11: Electron Transport Rate (ETR, pmol e^- $cell^{-1}$ h^{-1}) of Dark. Samples were collected at pre-dawn (0), and after 6, 24, and 30 hours. Data are reported as mean ±SD of three biological replicates (n=3).

7.3.4.2 Photosynthetic acclimation and pigments

The quantum yield of photochemistry (Fv/Fm, Fig. 7.12 a) showed a significant decrease at 24 hours ($p<0.01$), although preserving high values during all the experiment. Both the

photosynthetic parameters α (maximum light use efficiency, Fig. 7.12 b) and Ek (light saturation index for photosynthesis Fig. 7.12 c), notwithstanding minor fluctuations, didn't change consistently.

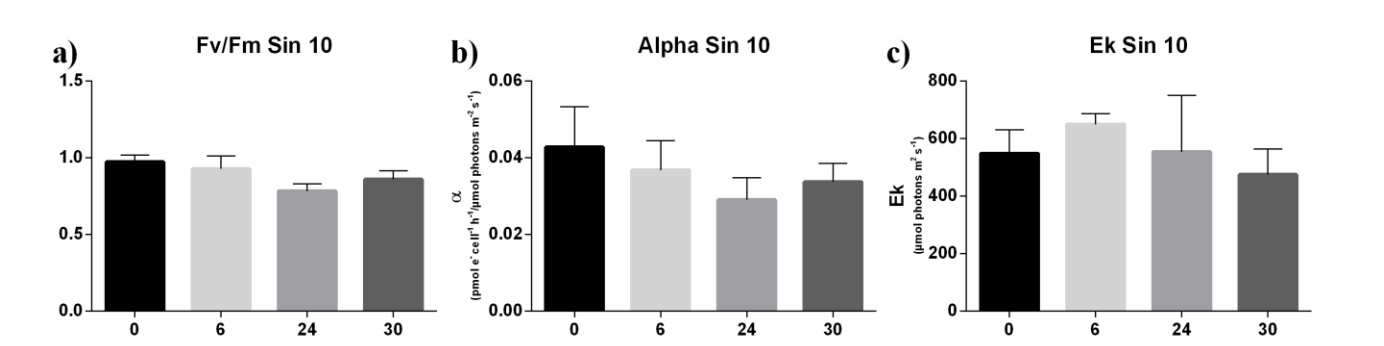

Figure 7.12: Photosynthetic parameters of Dark. a) Fv/Fm (maximum quantum yield of the PSII); b) α (maximum light use efficiency, in pmol e^- $cell^{-1}$ h^{-1}/µmol photons m^{-2} s^{-1}); c) Ek (light saturation index for photosynthesis, in µmol photons m^{-2} s^{-1}). Samples were collected at pre-dawn (0), and after 6, 24, and 30 hours. Data are reported as mean ±SD of three biological replicates (n=3).

Chlorophyll a (Chla, Fig. 7.13 a) varied over time, being enhanced only after 30 hours, although in a non-statistically significant way. The antenna pigments chlorophyll c (Chlc, Fig. 7.13 b) and fucoxanthin (Fuco, Fig. 7.13 c) showed a progressive increase, significant only for Fuco the second day (24 hours $p<0.01$ and 30 hours $p<0.05$). The Fuco/Chla ratio (Fig. 7.13 d) fluctuated as consequence of the different photosynthetic pigment content, but the change from pre-dawn was statistically significant only at 24 hours ($p<0.001$).

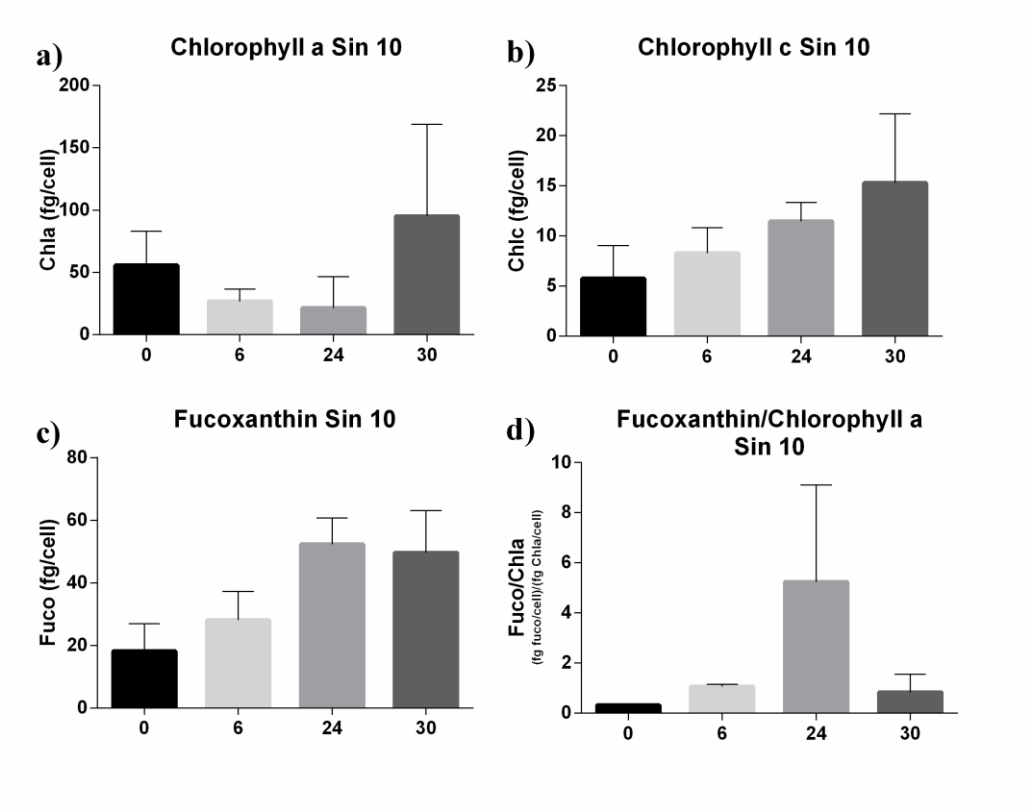

Figure 7.13: Photosynthetic pigments. a) Chlorophyll a (Chla in fg/cell); b) Chlorophyll c_s (Chlc in fg/cell); c) Fucoxanthin (Fuco in fg/cell); d) Fucoxanthin/Chlorophyll a ratio. Samples were collected at pre-dawn (0), and after 6, 24, and 30 hours. Data are reported as mean ±SD of three biological replicates (n=3).

7.3.4.3 Photoprotection

Under sinusoidal 10, NPQ decreased with time (Fig. 7.14 a). In this experiment the level of Dt was under the detection threshold (data not shown). Dd strongly increased the second day ($p<0.01$, Fig. 7.14 b) while β-car concentration firstly decreased and then enhanced at 30 hours (Fig. 7.14 c).

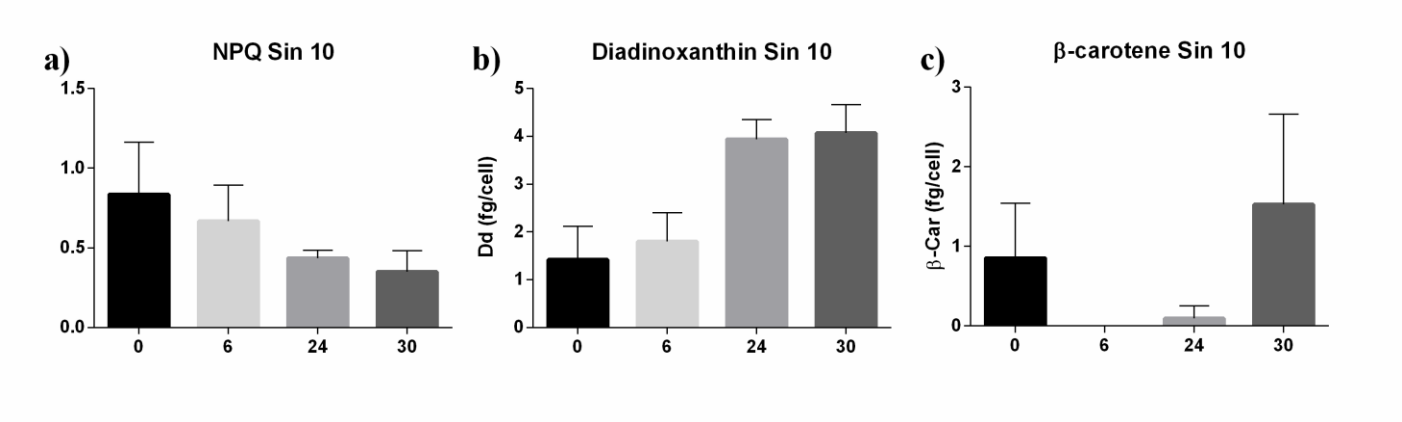

Figure 7.14: Photoprotection. a) non-photochemical quenching (NPQ); b Diadinoxanthin (Dd in fg/cell); c) β-carotene (β-car in fg/cell). Samples were collected at pre-dawn (0), and after 6, 24, and 30 hours. Data are reported as mean ±SD of three biological replicates (n=3).

7.3.4.4 Antioxidant molecules and activity

Under the sinusoidal low light, ascorbic acid content (AsA) didn't vary over time (Fig. 7.15 a). The phenolic content showed a weak increase while flavonoids followed the same trend than the one observed under dark, lowering their concentration at 6 hours ($p<0.05$) and then increasing the next day (like Dd). The ABTS correlated with the trend of these molecules, being almost unvaried until 30 hours, when a small increase was visible ($p<0.05$).

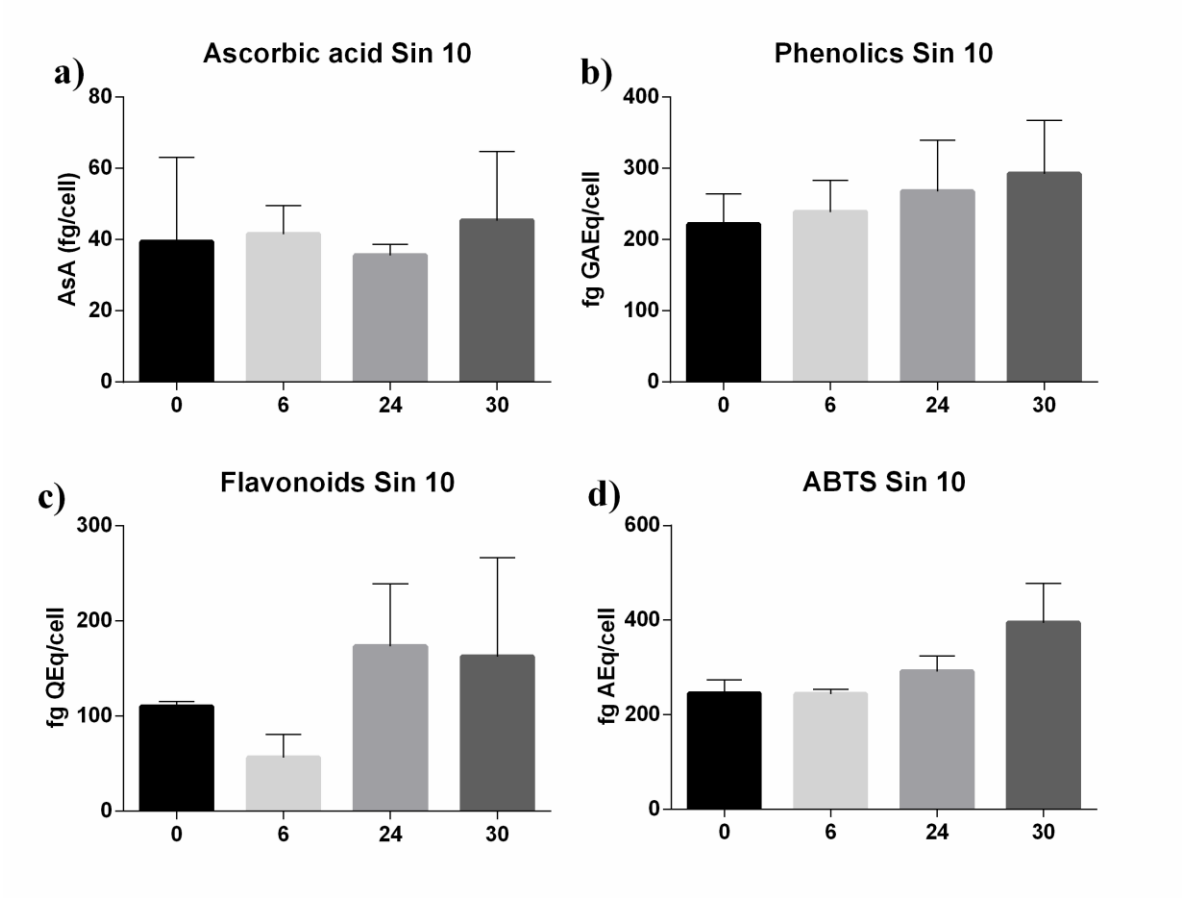

Figure 7.15: Antioxidant molecules and antioxidant activity. a) Ascorbic acid (AsA in fg/cell); b) Phenolics (in fg GAEq/cell); c) Flavonoids (in fg QEq/cell); d) ABTS test (in fg AEQ/cell). Samples were collected at pre-dawn (0), and after 6, 24, and 30 hours. Data are reported as mean ±SD of three biological replicates (n=3).

7.4 Discussion

A mismatch between growth and photosynthesis was noticed, implying that the energy was diverted toward acclimation processes and not invested into biomass enlargement. Growth rate remains positive only under sinusoidal very low light condition; under dark instead it approximates to zero, while cell death predominates under the continuous light.

The stop of cell division under dark confirms the role of light in controlling cell cycle progression. Comparisons between the results obtained on *Phaeodactylum tricornutum* and mines are interesting, notifying inter-specific differences, maybe related to the ecological/biological diversity of these two species. While in this pennate diatom the switch to prolonged darkness determined the lowering of the pigment content and lower photochemical efficiency and photosynthetic rate (Nymark *et al.*, 2013), *S. marinoi* kept constant these parameters. Indeed, at dark *P. tricornutum* was not able to newly synthesize cellular component due to insufficient energy, but was still able to divide, determining a lower pigment content due to the dilution effect (Nymark *et al.*, 2013). This feature induced a lowering of the photosynthetic capacity. Being at G_1 phase the cell cycle checkpoint in this species, the cells in S, G_2 and M phase completed the cycle before arresting in G_1. By contrast, *S. marinoi* did not grow at dark and under extremely low light condition. The reasons might be that this species probably possesses additional light dependent cell cycle checkpoints, supposedly at G_2+M, like it occurs in the centric diatom *T. weissflogii* (Vaulot *et al.*, 1986). This feature explains the almost constant photosynthetic parameters observed in this experiment and underlines the different physiology of the distinct diatoms lineages.

The correlations found among the antioxidant and photoprotective parameters suggest the coordinate operation of the different networks which respond to light, or its absence, adjusting cell physiology and metabolism. The antioxidant capacity is dependent, in addition to the antioxidant molecules concentration, also on the photoprotective pigments, reinforcing the hypothesis of the potential key antioxidant role of these molecules.

The opposite trend of the total antioxidant capacity with NPQ is intriguing, letting us suppose an alternative strategy to respond to this stressful conditions, down-regulating the

ability to dissipate the excess of energy, which was extremely low or even absent, while increasing the antioxidant capacity.
Once again, an uncoupling between NPQ and the photoprotective pigment diatoxanthin (Dt) is noticed (previous chapters) (Giovagnetti *et al.*, 2014), strengthening the hypothesis of the antioxidant role of this pigment apart from its involvement into NPQ development.

My results demonstrate that the diel cycle trend followed by different parameters such as the photoprotective and antioxidant ones during the exponential phase is under the control of a direct light stimulus and does not rely on an internal circadian clock. In fact, in absence or under an extremely low sinusoidal light, these infradiel variations disappear. This result is confirmed by those obtained in Con 10, where a continuous light regime induced a continuous synthesis of these molecules.
In a stable light environment, the presence of a circadian clock synchronized with precise and predictable daily environmental cycles represents an advantage, and is generally considered an evolutionary adaptation, able to increase the fitness of the organism (Vaze & Sharma, 2013). By contrast, under an unpredictable fluctuating environment such as the sea, the presence of a rigid scheme ruling cell physiology would represent a great handicap. In this condition, a better strategy might be to be able to promptly modify the metabolism following the external stimuli, a strategy which in fact has been always attributed to the physiologically plastic diatoms.

Another important finding regards the key role of the light distribution on the photoprotective and antioxidant network functioning, even at extremely low level of energy. The low sinusoidal light induces responses similar to the dark condition, while the continuous low light causes a strong impairment of the normal cell functioning. Indeed, under this condition, cell death is very high, while in both the Dark and the sinusoidal low light cell cultures had a comparable concentration after one day, caused by an equal rate between cell division and death or, more probably, to a block of the vegetative division.
This finding seems in contrast with what recently observed on the diatom *Thalassiosira pseudonana* (Li *et al.*, 2017). This species shows better performance in terms of growth rate in absence of a dark period in medium/low light environment, but the lower limit of continuous light used in this case was 25 µmol photons m^{-2} s^{-1}. Furthermore, growth and

photosynthesis may be influenced by light intensity and photoperiod in a species-specific way, compromising the chance of making a more general prediction on the physiologic behavior of these organisms.

The modification of the photosynthetic pigment content in Dark means that cells slowly tried to acclimate to the absence of light *via* the increase of the reaction center/antenna ratio in the first place. This result is in line with the findings of (Murphy & Cowles, 1997), whom observed in *Thalassiosira weissflogii* exposed to prolonged darkness an initial increase of Chla within the first 48 hours, followed by an increase of the relative content of Fuco to Chla, so a greater antenna size, as a longer term acclimation feature.

Also, in Con 10 and Sin 10, cells increase the light harvesting functions, enhancing pigment concentrations.

The unvaried NPQ under Dark means that cells did not lose their ability to photoprotect in case of a sudden exposure to light, as could happen in natural conditions to cells transported from deep waters to the surface. The increased concentration of Dt was probably due to the trans-thylakoid ΔpH created by the chlororespiration (Jakob *et al.*, 2001, Cruz *et al.*, 2010, Brunet *et al.*, 2011). Again, a different behavior is recorded between *S. marinoi* and *P. tricornutum*, having the latter a lower NPQ capacity at dark (Nymark *et al.*, 2013). Therefore, it is tempting to ascribe this discrepancy to a different regulation of the Lhcx proteins in these two diatom species.

The presence of extremely low level of energy in Sin 10 instead could have prevent the activation of the chlororespiratory pathway, therefore not allowing the conversion of Dd into Dt, as observed in the Dark condition.

The influence of light in terms of presence/absence and the key role of the photoperiod and distribution shape was confirmed by the principle component analysis (PCA) performed on a correlation matrix of physiological and biochemical data. The first plot corresponds to the midday sampling data set of the four light conditions (Ctrl sin 150, Dark, Con 10 and Sin 10, Fig. 7.16 a). The first two axes explain the 69% of the total variability. The four groups are markedly separated, with Dark opposed to Con 10 and the Ctrl sin 150 opposed to Sin 10. Therefore, the photophysiology and biochemistry of cells are strongly influenced by light both in terms of presence/absence and intensity.

The PCA performed on the 24 hours sampling data set is presented in Fig. 7.16 b. In this case, the two first axes account for the 64% of the total variability. The segregation of the light treatments into two distinct groups is visible: one includes Ctrl sin 150, Dark and Sin 10, opposed to the group of the Con 10. Also in this case, the quadratic light distribution is opposed to the other light conditions. The closeness of Dark, Sin 10 and Ctrl sin 150 may be explained hypothesizing that the switch to an extremely low level of energy or even to the total absence of light are conditions which resemble what can happen in nature, mimicking a sink below or at the limit of the euphotic zone. Therefore, cells acclimated to a natural-like light environment are able to respond without dramatic changes of their physiology. By contrast, the exposure to an extremely low level of light energy continuous and without a dark phase, a completely unnatural situation, strongly affects cell's physiology, leading in our case to the massive death.

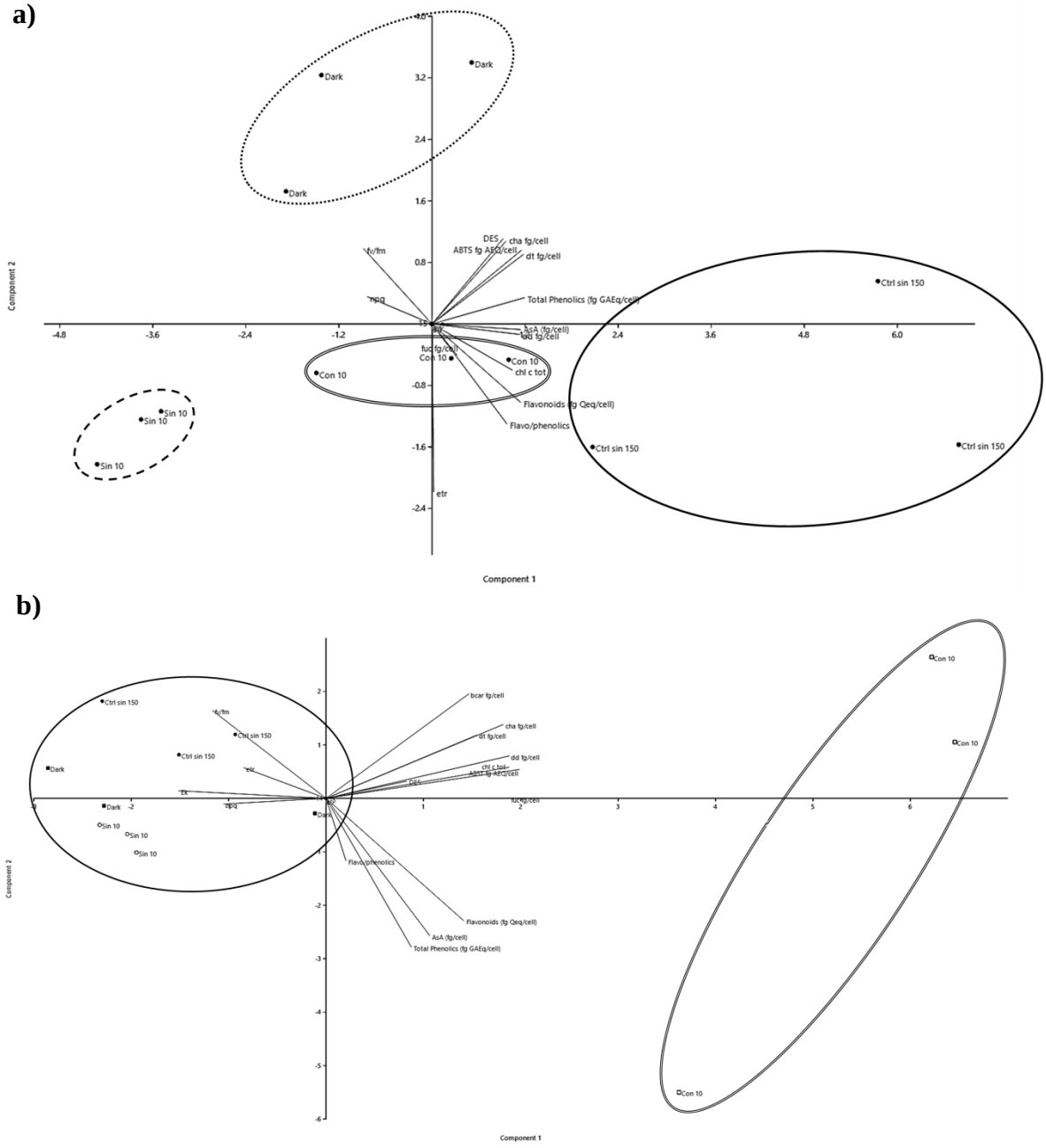

Figure 7.16: Principal components analysis (PCA). The analysis was performed on data collected a) at midday time point of the control (Ctrl sin 150) and the three treatments (Dark, Con 10 and Sin 10); b) at time zero of the control (Ctrl sin 150) and the 24 hour time point of the three light treatments (Dark, Con 10 and Sin 10). Analysis was performed on correlation matrix of the data set, which consisted in the photosynthetic, photoprotective and antioxidant network parameters such as Fv/Fm, Chla, Chlc, NPQ, Dt, Dd, DES, AsA, Phenolics, Flavonoids, ABTS, Flavonoids/Phenolics (F/P).

8. *In situ* determination of the photoprotective and antioxidant network in microalgal community: a Mesocosms experiment in the Gulf of Naples

8.1 Introduction

In this chapter, I will present a research activity I conducted at sea, i.e. on natural phytoplankton communities, investigating the photoprotective and antioxidant network functioning in the coastal water column of the Gulf of Naples.

In June 2016 I had the chance to participate in an experiment in the Gulf of Naples which foresaw the use of mesocosms, structures which can be considered "sea Laboratories". These systems provide the unique opportunity to study natural communities taking into account the "real ecosystem" dynamics, such as the indirect effects, the biological compensation and recovery, ecosystem resilience, all features/processes not visible in small scale laboratory experiment, without losing reliable reference conditions and replications (Petersen *et al.*, 2003, Riebesell *et al.*, 2013).

The advantage offered by this tool is the possibility to study a complex environment in controlled conditions, managing almost all the variables that influence a natural community. It is possible thanks to the deployment at sea of structures (for details see paragraph 8.2.1 Mesocosm setup and deployment at sea) which enclose a portion of water mass from the surrounding waters, avoiding any water advection from outside into the bag and *vice-versa*. The preservation of the biological compartments and of the hydro-chemical properties of the water masses gives the chance to maintain all the pre-existing interactions between the abiotic and biotic factors (Guieu *et al.*, 2010, Giovagnetti *et al.*, 2013, Manna, 2017).

The general aim of this experiment was the end-to-end (from viruses to zooplankton) investigation of the pelagic ecosystem functioning during a phytoplankton outburst ("bloom"), as it occurs seasonally in all temperate coastal waters. All processes from resources acquisition by primary producers to carbon flux along the trophic web, as well as the succession patterns into the communities were investigated before, during and after the microalgal outburst. Moreover, the experiment was also conceived to study the effects of microplastics on the ecosystems functioning. The approach was multi-disciplinary and multi-scale integrating physics, chemistry, biology and ecology from molecules and gene expression to ecosystem processes.

In order to stimulate the phytoplankton growth and the development of the bloom, nutrients (silicate and phosphate) were added into the bags. Samples were taken daily for the analysis of the biotic (on microalgae, zooplankton, bacteria, and viruses) and abiotic (e.g., pH, light, temperature, nutrients, organic carbon, metals, carbohydrates, CO_2, etc.) parameters.

Together with the changes over time, vertical gradient from surface to 10 meters depth was investigated. Indeed, the water mass during summer is stratified, inhibiting or limiting any vertical transport of nutrients and phytoplankton from the upper to the bottom layer and *vice-versa*. The phytoplankton community of the upper layer of the water column (above the stratification depth) has to cope with detrimental environmental conditions such as high light, UV radiations, high temperature, while the deepest one has to cope with a low light climate.

In a natural environment the food web is controlled by both top-down - i.e. predation by higher trophic level - and bottom-up - i.e. resources availability and distribution (e.g., nutrients, light, physicochemical factors). These processes although operating simultaneously, may differ in magnitude (Sinistro, 2010, Lynam *et al.*, 2017).
The top-down control exerted by grazers (both zooplankton and planktivorous fishes) on phytoplankton is not only dependent by their abundance, so is not explainable by the simple paradigm more pray more predators. The phytoplankton community composition itself affects the grazing efficiency of zooplankton. In fact, some diatoms and dinoflagellates may have some inhibitory or even toxic effects on grazers both directly or indirectly *via* the reduced egg production or hatching success (Turner & Tester, 1997, Ianora *et al.*, 2004). Also the morphology of phytoplankton affects its palatability: diatoms' big dimension of colonies and the long siliceous setae discourage their ingestion by small grazers, so the pray/predator size ratio has a key role, being larger zooplankters more efficient grazers than smaller ones (Brooks & Dodson, 1965, Kooistra *et al.*, 2007).
The influence of the zooplankton component on phytoplankton dynamics and productivity is also exerted *via* the nutrient recycling (Elser *et al.*, 2001).
In turn, the phytoplankton is a top-down controller for the microbial activity ("microbial loop"). This compartment of the food wed is responsible for the consumption of dissolved

and particulate organic carbon (DOC and POC, respectively) derived by phytoplankton exudates, aggregates and grazing activity (wound by-products, faecal pellets and urea excreted by zooplankton). This organic matter is therefore remineralized into simple inorganic forms which can be reused as nutrients by the other organisms, such as primary producers. The bacterial and phytoplankton communities control each other also through nutrient competition. There is evidence that in some conditions bacteria may choose to feed on inorganic nutrients rather than on organic matter (Danovaro, 1998). This feature would impact the phytoplankton community composition: having the bacteria a high affinity to ammonium (NH_4^+), the microalgal species which are able to use other nitrogen sources such as nitrates (NO_3^-) or show a higher-affinity uptake for ammonium are favoured (Danovaro, 1998).

All these above described ecosystem processes or interactions affect the phytoplankton performance and growth, modulating the physiological state of the cells.

In this context, I was involved in the experiment to investigate the phytoplankton photosynthetic acclimation as well as the antioxidant molecules production during the different phases of the bloom. This study is, to my knowledge, unique, being the first time that the antioxidant capacity and molecules (ascorbic acid, total phenolics, and total flavonoids) determination produced by phytoplankton community at sea is performed.

The aim of my study was to (i) describe the antioxidant molecules diversity and concentration at sea, (ii) investigate their dynamics during the different steps of a phytoplankton bloom at sea, (iii) study their role in an ecosystem context along the water column.

The production of antioxidant molecules by phytoplankton is used to counteract the oxidative stress induced by, e.g., the excess of solar radiation or physiological stress due to nutrient limitation (Snoeijs *et al.*, 2012). The excess of nutrient input into the aquatic ecosystem determines an increase of biomass, which in turns limits the light availability through the self-shading effect, therefore lowering the antioxidant production, until one nutrient becomes limiting, causing a reduction of the growth rate, increasing again the antioxidant production (Turner *et al.*, 2003).

The production of antioxidant molecules by phytoplankton is essential for heterotrophs which are not able to produce these molecules. For example, the pigment astaxanthin is the

major antioxidant carotenoid produced by crustaceans, but they need to acquire its precursors such as β-carotene and zeaxanthin from the photoautotrophs (Andersson *et al.*, 2003, Van Niewerburgh *et al.*, 2004).

Thanks to this experiment I can integrate the information retrieved from small scale controlled condition I obtained from laboratory studies (reported in the previous chapters) with the natural phytoplankton community dynamics at sea.

Results of all the analysis performed during this experiment are still not all available and analyses are still ongoing. In particular, phytoplankton community composition data are lacking and pigment content – that can be used as proxy for phytoplankton community diversity - is only partially available (see paragraph 8.2.9 HPLC Pigment analysis). Once all the data set will be accessible, this experiment will represent a unique tool to understand the complex regulation system – from gene to communities - which controls the coastal pelagic ecosystem functioning.

8.2 Materials and methods

8.2.1 Mesocosm setup and deployment at sea

Six mesocosms and sampling platforms assembled by SCUBLA S.r.l (Udine, Italy) under original project design by Dr. Christophe Brunet were deployed at sea. Each mesocosm consisted in the assemblage of four parts: a top structure, a bag, a bottom cone and a cover roof. The top structure consisted in two concentric high-density polyethen rings (PEHD, 2.8 metres diameter) stabilized by centric cross of tubes and anchored to each other by means of vertical supports of the same material (Fig. 8.1).

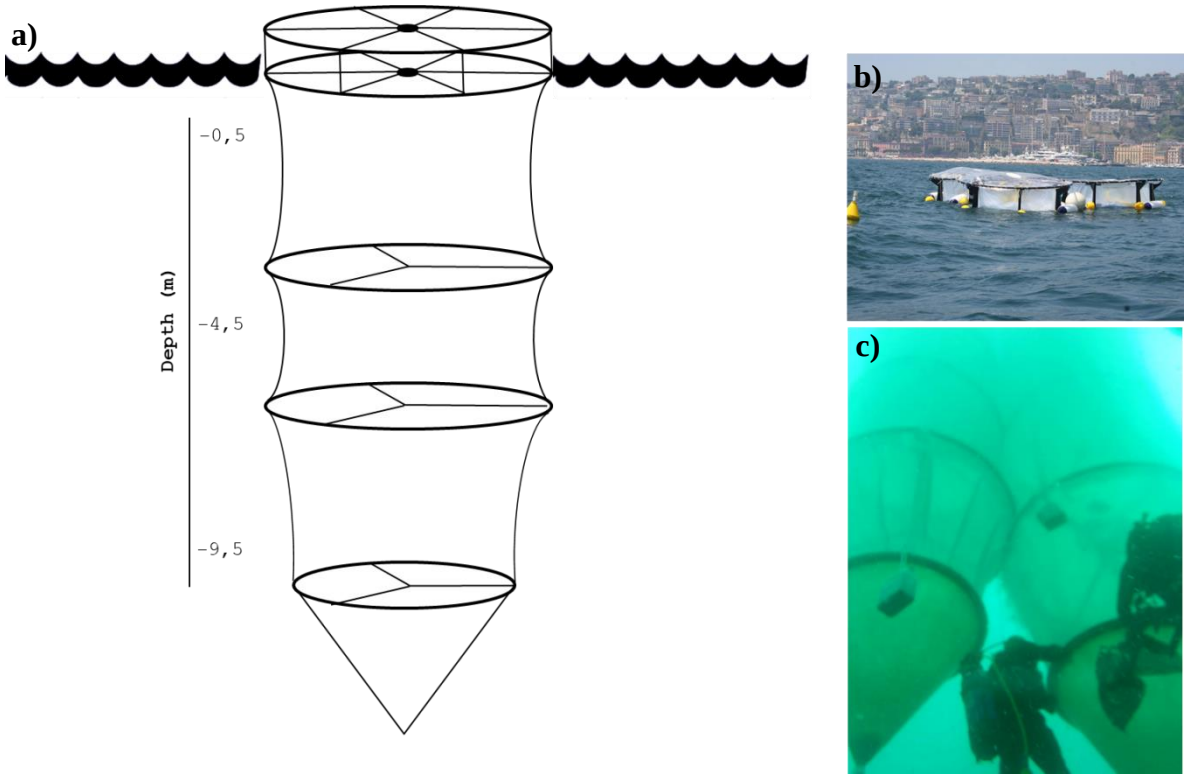

Figure 8.1: a) schematic drawing of a mesocosm; b) picture of the group of three mesocosms deployed at sea; c) view of the mesocosm from the sea floor. Pictures are courtesy of Dr Christophe Brunet and the diver Gianluca Zazo.

The bags consisted in two layers of polyethene and vinyl acetate (thickness 500 µm) with a nylon mesh in between, a composition which guaranteed transparency and strength. The

bags were fixed to the top structure and to the others rings, ensuring the maintaining of the cylindrical shape along the water column.

The bottom cone was made of fibreglass tightly connected to the bags by means of PEHD circles avoiding any water exchange. The volume of water enclosed by each mesocosm was about 52 m^3. To avoid any external disturbance (i.e. entrance of water from above, seabirds' excreta, etc.) each mesocosm was covered with a concave roof (2.8 m in diameter) made by a transparent sheet in PVC and attached to a PEHD tubes ring. A window on the roof allowed sampling operations. The roofs were tied to the vertical supports of the top structures, leaving a 10 cm space between the two, allowing air to circulate and ensure sea-air exchanges.

The mesocosms were deployed in the inner part of the gulf of Naples (coordinates: 40° 49.63' N, 14° 14.00' E), *circa* 200 meters from the coast line, in front of Stazione Zoologica "Anton Dohrn".

These structures were assembled into two groups of three mesocosms, and fastened with iron anchors to the seafloor. The flotation was guaranteed by several buoys fastened to the top structure.

The bags were lowered from the surface trapping the water column, and the bottom cones were assembled to the structure. All these operations were carried out by the divers.

8.2.2 Experimental design and sampling

The experiment lasted 14 days. The dates, experimental times, nutrient additions, and sampling times for the different parameters are summarized in Table 8.1.

Three mesocosms were amended with nutrients (see paragraph 8.2.3 Nutrient amendment), and the other three also with microplastics. This second group is not considered in this chapter.

The first sampling was carried out on 9th June 2016 (T0). In the afternoon of the same day, after the sampling operations, the first nutrient fertilization took place. Then a daily sampling was performed every morning in the same time window, between 9 and 11 a.m. A second nutrient addition took place at T6 (15th June 2016), following the same procedure described above (see paragraph 8.2.3 Nutrient amendment).

The sampling was carried out reducing as much as possible the risk of contamination and disturbance of the water mass inside the mesocosms. At this purpose, three PVC tubes were permanently installed at the centre of each mesocosm, fastened to the supporting structure. One end of these tubes was positioned at a fixed depth (0.5, 4.5 and 9.5 metres below the sea surface), while the other end was secured to the top structure. The hand pump was then connected to the emerged ends of the tubes allowing the filling of non-transparent jerry cans (10-30 L) with water coming from each depth of the various mesocosms.

The sampling and seeding operation were performed from floating plastic structures (SCUBLA S.r.l, Udine, Italy).

The jerry cans were transported from the sampling area to the laboratory and to the research vessel Vettoria with to two small boats. Once there, samples were sorted for analyses of the different parameters.

The abiotic parameters temperature and light intensity were measured daily (see paragraph 8.2.4 Temperature and light intensity measurements), as well as the Chlorophyll a (Chla) concentration and the photosynthetic parameters (see paragraph 8.2.5 Chlorophyll a concentration and 8.2.6 Photosynthetic parameters, respectively). Samples for the absorption spectra were taken at T0, T4, T6, T8, T11, and T13 (see paragraph 8.2.7 Phytoplankton absorption spectrum analysis). Samples for the antioxidant molecules and activity determination were taken at T0, T1, T4, T6, T8, T11, and T13 (see paragraph 8.2.8 Antioxidant molecules and activity determination).

Table 8.1: Dates of the experiment, relative experimental times, nutrient addition, measurements of the abiotic parameters (temperature and light intensity), and sampling times for Chla determination, photosynthetic parameters, phytoplankton absorption spectrum, antioxidant molecules and activity.

Date	Experimental time	Nutrient addition	Abiotic parameters	Chla	Photosynthetic parameters	Absorption spectrum	Antioxidants
09/06/16	T0	+	+	+	+	+	+
10/06/16	T1		+	+	+		+
11/06/16	T2		+	+	+		
12/06/16	T3		+	+	+		
13/06/16	T4		+	+	+	+	+
14/06/16	T5		+	+	+		
15/06/16	T6	+	+	+	+	+	+
16/06/16	T7		+	+	+		
17/06/16	T8		+	+	+	+	+
18/06/16	T9		+	+	+		
19/06/16	T10		+	+	+		
20/06/16	T11		+	+	+	+	+
21/06/16	T12		+	+	+		
22/06/16	T13		+	+	+	+	+

8.2.3 Nutrient amendment

In order to stimulate the phytoplankton outburst, the macronutrients were added into the mesocosms. This fertilization was preceded by a measurement of nutrient concentration at the three depths, carried out the day before. In this way it has been possible to decide which nutrient was needed and in which concentration.

Notable concentration of nitrate (NO_3^-) was recorded (mean value at the three depths equal to 1.31 ± 0.44 µmol L^{-1}), making redundant its eventual addition.

Silicate (SiO_4^-) showed a mean value at the three depths equal to 3.04 ± 0.70 µmol L^{-1}. Therefore during the first fertilization it has been added a consistent amount of it, in order to trigger a diatom bloom (see below).

Phosphate (PO_4^{3-}) was limiting (mean value at the three depths equal to 0.07 ± 0.03 µmol L^{-1}), determining a high nitrogen/phosphate (N/P) ratio, so a potential P-limitation, a frequent condition in Mediterranean Sea. Therefore, it has been added twice during the experiment, both at the first amendment and also the second week (on the 15th June 2016), to feed the ongoing bloom.

The desired final concentration of the nutrients in the mesocosm was 20 and 0.4 µmol L^{-1} for SiO_4^- and PO_4^{3-} respectively for the first fertilization and 0.4 µmol L^{-1} for PO_4^{3-} for the second fertilization.

The nutrient were weighted in laboratory and dissolved into two litres per mesocosm of filtered and sterilized sea water the day before the amendment (500 and 9.5 mmol/L of Na_2SiO_3 $9H_2O$ and NaH_2PO_4 H_2O, respectively), and left homogenizing overnight.

8.2.4 Temperature and light intensity measurements

Temperature and light intensity inside each mesocosm were recorded using HOBO Pendant® dataloggers (Onset Computer Corporation, MA, USA). The loggers were placed at the three depths (0.5, 4.5, and 9.5 metres below the sea surface) and provided measurements every five minutes during all the experiment.
The light intensity data were recorded with a planar PAR 2π sensor, which measures the incident light on a 180° arc. So the values were later multiplied by a factor of 1.9 to obtain the values of light intensity impinging from all the directions on the sensor (Brunet, personal communication; Manna, 2017).

8.2.5 Chlorophyll a concentration

Chlorophyll a (Chla) concentration was measured daily in order to have a proxy of the biomass present. Fifty mL of seawater were sampled from each mesocosm at the three depths and stored in dark bottles at 20°C until measured. The measurements were carried with a fluorimeter model 10-005R (Turner Designs, CA, USA). The values obtained with this instrument were expressed as relative fluorescence units (RFU). These values were converted into mg m^{-3} multiply them by a calibration factor equal to 0.00355, obtained with a calibration curve retrieved from HPLC measurements of Chla from *Skeletonema marinoi* cultures at known cellular density (linear regression, R^2=0.99, n=5).

8.2.6 Photosynthetic parameters

The photophysiologic parameters were measured daily on fresh collected samples with a DUAL-PAM fluorometer (Heinz Walz GmbH, Effeltrich, Germany). Due to the low cells abundance, samples were concentrated gently filtering 50 mL of seawater onto 0.45 µm polycarbonate filters (Merck, Millipore, Darmstadt, Germany). Filters were then

immediately moistened and re-suspended in 5 mL of seawater, pre-filtered on 0.22 µm polycarbonate filters. All these operations were carried out under dim light.
Then, the photochemical efficiency of photosystem II (Fv/Fm), the photosynthetic rate (relative electron transport rate - relETRmax), and the photosynthetic parameters retrieved from the P *vs* E curve, maximum light use efficiency (α), and light saturation index for photosynthesis (Ek) were obtained following the procedures reported in Chapter 2.

8.2.7 Phytoplankton absorption spectrum analysis

One litre of seawater was sampled from the three depths of each mesocosm at T0, T4, T6, T8, T11 and T13. Samples were filtered onto GF/F Filters, 25 mm (Whatman™, Buckinghamshire, UK) on the research vessel Vettoria and immediately frozen. Then, the absorption spectra were obtained following the procedures described in Chapter 2.

8.2.8 Antioxidant molecules and activity determination

The processing of the water samples for the antioxidant molecules and activity determination was carried out on the research vessel Vettoria at T0, T1, T4, T6, T8, T11 and T13. Sea water coming from the three depths of each mesocosm was filtered onto GF/F Filters, 25 mm (Whatman™, Buckinghamshire, UK). One litre was filtered for the determination of the ascorbic acid (AsA) content. Two litres instead were used for antioxidant capacity and phenolic and flavonoids content determination. The filters were immediately frozen in liquid nitrogen and then stored at -20°C.
The analyses were carried out following the procedures reported in Chapter 2 with modification due to the different concentration methods (GF/F filters instead of cell pellets).
Briefly, for AsA determination, the filters were disrupted by mechanical grounding in 1 mL of 5% trichloroacetic acid (TCA), and sonicated for 1 minute with a micro tip at 20% output on ice (S-250A Branson Ultrasonic). The homogenate was then filtered onto Whatman 25-mm GF/F filters, the volume of the extract accurately measured and immediately analysed. The same procedure described in Chapter 2 was followed.
For phenolics, flavonoids, and antioxidant capacity, the filters were disrupted by mechanical grounding in 1 mL of absolute methanol, sonicated for 1 minute with a micro

tip at 20% output on ice (S-250A Branson Ultrasonic). The homogenate was then filtered onto Whatman 25-mm GF/F filters and the volume of the extract accurately measured and directly used for the analyses. The same procedures described in Chapter 2 were followed, with the volumes adjusted for 96 well plates (150 µL<final volume<200 µL, Tecan Infinite® M1000, Switzerland).

8.2.9 HPLC Pigment analysis

The group from the Instituto de Investigaciones marinas CSIC, Vigo (Spain), leaded by the PI José L Garrido, was in charge of the HPLC pigment determination. The analyses foresee the pigment concentration determination on two different cell size fractions (> 3 µm and < 3 µm). At the present time (September 2017), the results from the greater cell size fraction from the days T0, T1, T4, T6, T8, T11 and T13 are available.

8.9.10 Statistical analysis

Data of mesocosm triplicates were presented as mean and standard deviation. Student's t-test, mean, standard deviation, Pearson linear correlation were calculated using PAST software package, version 3.10 (Hammer *et al.*, 2001).
Kriging regression analysis to draw contour maps was done using Surfer (version 11, Golden Software LLC, CO, USA, http://www.goldensoftware.com/products/surfer).

8.3 Results

8.3.1 Environmental parameters

8.3.1.1 Temperature

The temperature followed a diel cycle oscillation, showing higher values at midday due to the warming effect induced by solar radiation, which was visible up to 3-4 meters depth (Fig. 8.2). At T7 a wind burst caused the mixing of the water column, as visible by the homogenization of the temperature which narrowed its range of variation in the mesocosms (ΔT=0.3 C°).

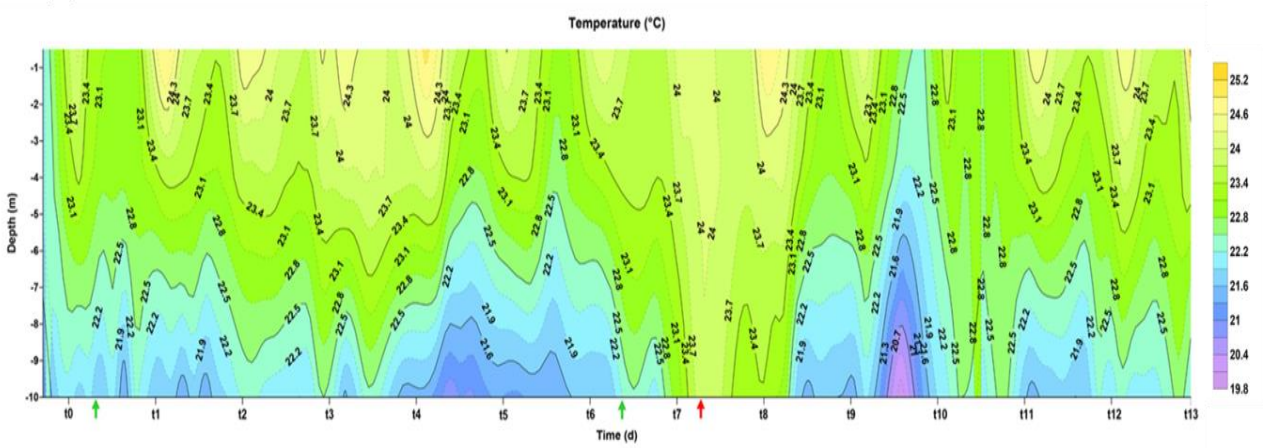

Figure 8.2: Contour maps of the temperature values (in °C) registered inside the mesocosms. Thick marks are positioned at noon of every experiment day. Green arrows mark the nutrient additions; red arrow marks the wind burst (T7)

8.3.1.2 Light intensity

At midday, light at the surface sampled depth (-0.5 m) ranged between 800 and 16 µmol photons m^{-2} s^{-1}, while at the intermediary depth (-4.5 m) between 5 and 1 µmol photons m^{-2} s^{-1}, and at the deeper depth (-9.5 m) between 0.6 and 0.1 µmol photons m^{-2} s^{-1} (Fig. 8.3).

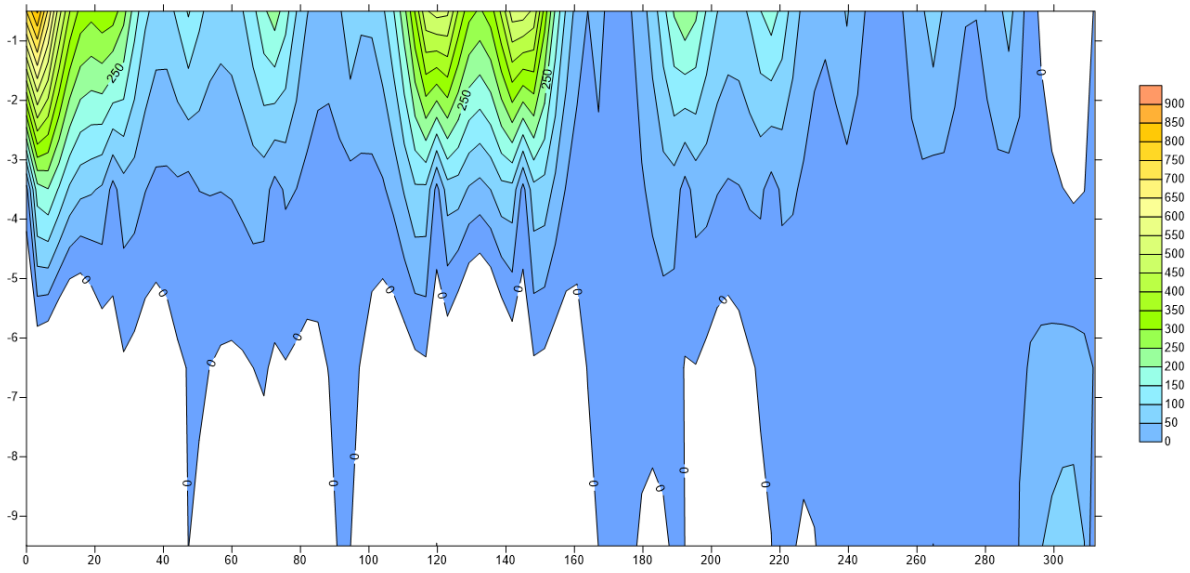

Figure 8.3: Contour map of the light intensity (in µmol photons m^{-2} s^{-1}) registered inside the mesocosms. Time is expressed in hours.

8.3.1.3 Nutrient distribution

The silicates' concentration (Fig. 8.4 a) increased up to 29 µmol L^{-1} in the surface layer after the nutrient's addition. The concentration of SiO_4^- at deep reached its maximum three days after the fertilization.

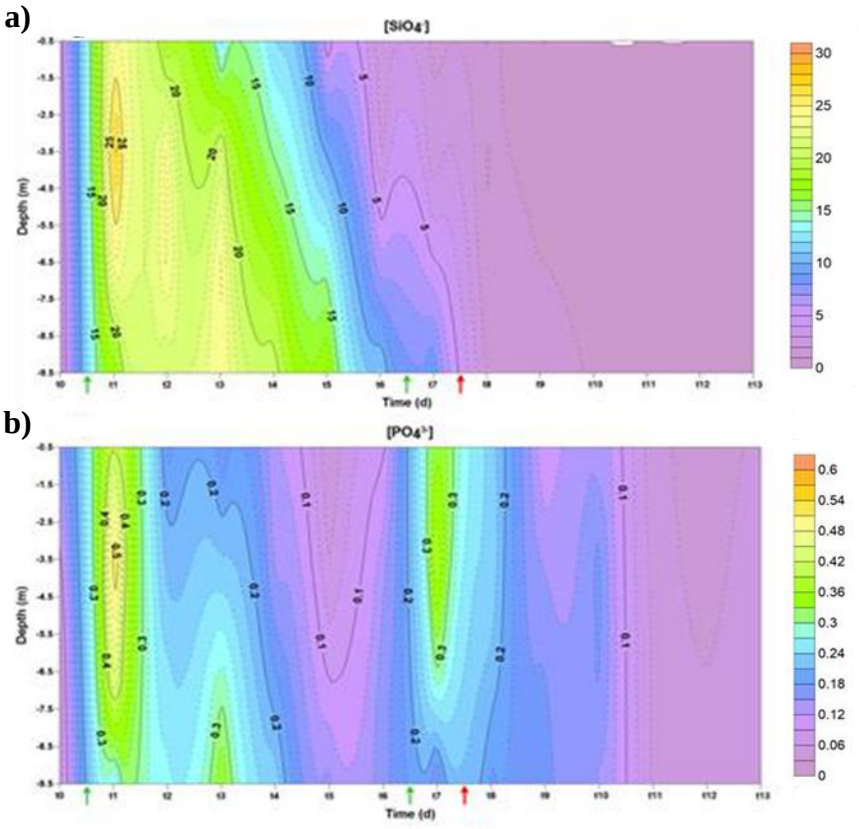

Figure 8.4: Contour maps of a) silicate (SiO_4^-) and b) phosphate (PO_4^{3-}) concentrations expressed in µmol L^{-1}. Thick marks are positioned at noon of every experiment day. Green arrows mark the nutrient additions; red arrow marks the wind burst

In the surface layer the silicates were consumed faster than at deep, reaching at T5 a concentration similar to the one before the fertilization (T0). At T7 at 9.5 meters depth instead, the silicates concentration was almost double respect to T0. The wind burst caused their redistribution along the water column. From T8 until the end of the experiment SiO_4^- concentration approximates to 0 µmol L^{-1}.

The first phosphate addition was visible until 6 meters depth, resulting in concentrations of 0.4 and 0.5 µmol L^{-1} at 0.5 and 4.5 meters depth, respectively at T1 (Fig. 8.4 b). Concentration decreased already at T2, reaching 0.2 and 0.3 µmol L^{-1} at 0.5 and 4.5 meters depth, respectively. At deep instead, the concentration of this nutrient was almost stable, showing values around 0.3 µmol L^{-1} until T4.

The presence of PO_4^{3-} at T5 was almost similar to T0 in the entire water column (0.1 µmol L^{-1}). The second addition at T6 determined the doubling in concentration of this nutrient

both at 0.5 and 4.5 meters depth (0.35 µmol L^{-1}), while in the deepest layer it stayed low (0.2 µmol L^{-1}). After that, it decreased progressively until reaching 0.1 µmol L^{-1} at T13 along the whole water column.

Nitrate (NO_3^-) kept high concentration until T3 (2.4 µmol L^{-1} at surface), when it dropped to values between 0 and 0.7 µmol L^{-1} until the end of experiment (Fig. 8.5 a).

Nitrite (NO_2^-) decreased over time (Fig. 8.5 b). Interestingly, between T3 and T5 it strongly increased at the three depths, mostly at the intermediate and deeper layers, simultaneously to the drop of the nitrates. From T6 onwards NO_2^- remained low, around 0.1 µmol L^{-1}.

The low values of ammonia (NH_4^+) recorded the first three days of experiment, started to increase at T4 especially at the intermediate and deeper layers, simultaneously to the sudden increase of the nitrite concentration (Fig. 8.5 c). It reached its maximum at T8 showing values equal to 0.8 and 0.5 µmol L^{-1} at 0.5 and 4.5 meters depth respectively, when the nitrite concentration declined. At deep instead, from T4 till T8, NH_4^+ kept stable values around 0.25 µmol L^{-1}. Then from T8 onwards ammonia dropped to low and stable values along the water column.

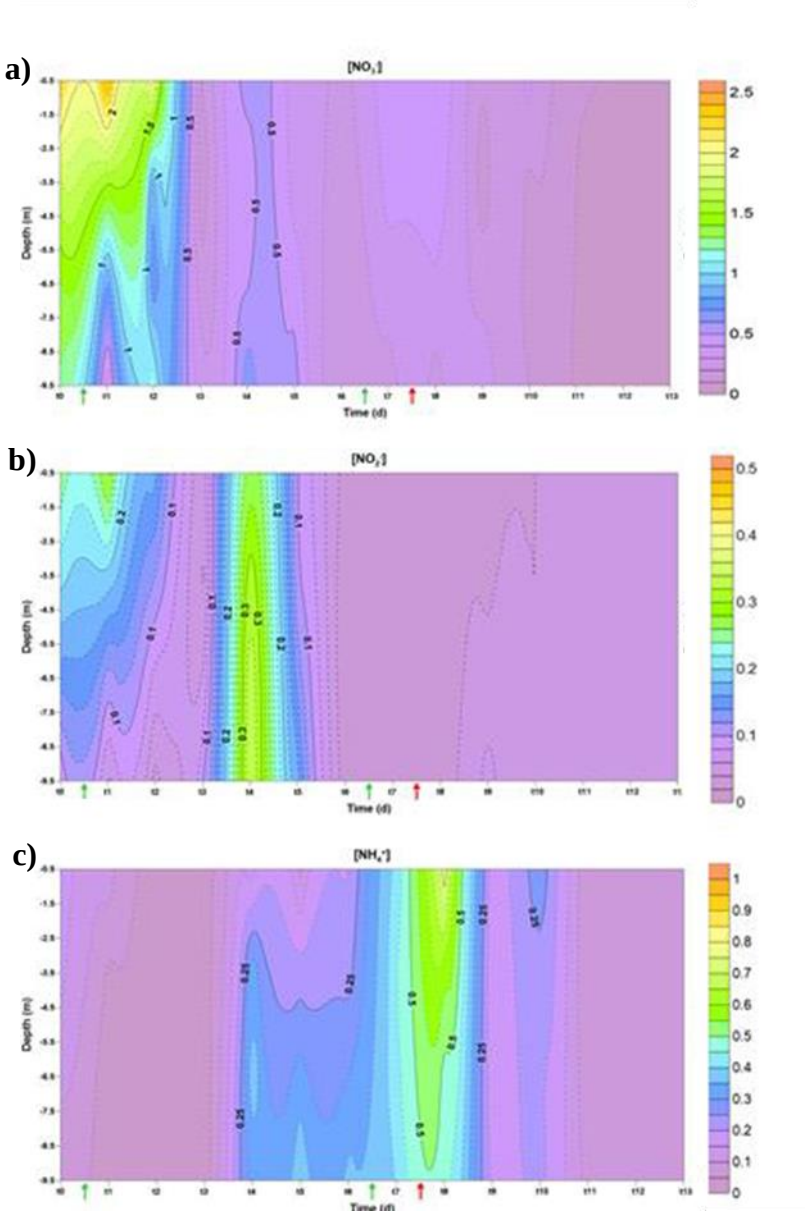

Figure 8.5: Contour maps of nutrient distribution: a) nitrate (NO_3^-), b) nitrite (NO_2^-), c) ammonium (NH_4^+) concentrations expressed in µmol L^{-1}. Thick marks are positioned at noon of every experiment day. Green arrows mark the nutrient additions; red arrow marks the wind burst.

8.3.2 Phytoplankton community

8.3.2.1 Chlorophyll a concentration

Chlorophyll a (Chla) concentration at T0 ranged from 0.5 to 1.4 mg m^{-3} along the water column (Fig. 8.6).

After the nutrient addition at T1 and T2, Chla increased in the upper and intermediate layers, reaching values up to 2 mg m^{-3}.

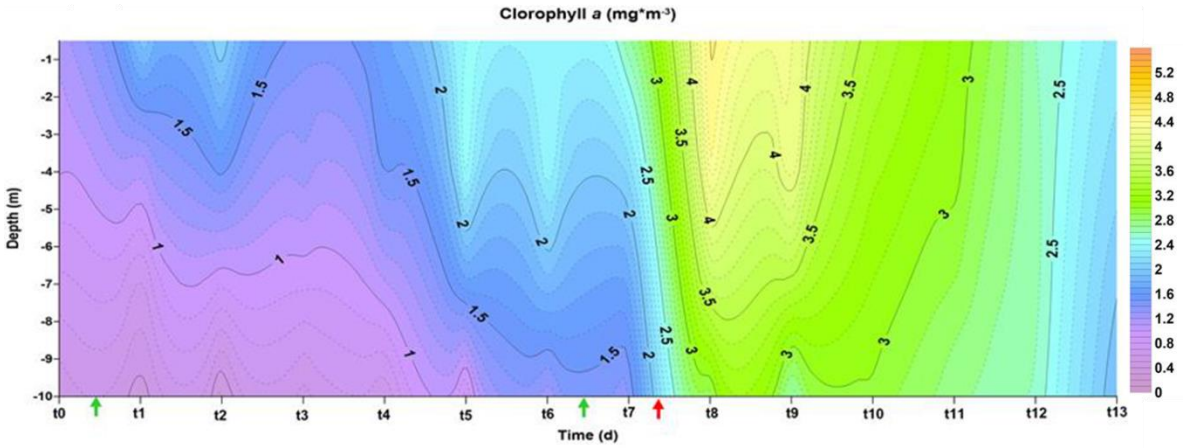

Figure 8.6: Contour maps of the Chla concentration (in mg m^{-3}). Thick marks are positioned at noon of every experiment day. Green arrows mark the nutrient additions; red arrow marks the wind burst.

After a decrease T3, a consistent increment started from T4 and lasted until T11. From T4 to T7, this increase regarded mainly the upper and intermediate layers. Thereafter, Chla distribution changed in the mesocosms, probably as a consequence of the second nutrient addition and the wind burst. In fact, while at T7 the Chla concentration at surface was *circa* 2 mg m^{-3}, at T8 it reached 4.5 mg m^{-3}. It kept increasing its concentration at the three depths until T9, and then it started to decrease, although showing high concentrations until T11.

Chla concentration was correlated with depth ($p<0.05$, $r= 0.38$), with a negative gradient from surface to deep. Moreover, Chla was inversely correlated with silica ($p<0.0001$, $r= -0.66$) and the different nitrogen sources ($p<0.05$, $r= -0.34$; $p<0.01$, $r= 0.42$; $p<0.05$, $r= 0.37$ for NO_3, NO_2 and NH_4^+, respectively).

8.3.2.2 Photophysiology

The photosynthetic rate (relative electron transport rate - relETRmax) sharply increased after the first nutrient addition (Fig. 8.7 a), reaching at T1 the maximum value recorded in the whole experiment at the surface layer (18 mol e^- g $chla^{-1}$ h^{-1}). In the deeper layer, this increase was less pronounced (7 and 2 mol e^- g $chla^{-1}$ h^{-1} at 4.5 and 9.5 meters depth, respectively). After this first enhancement, the photosynthetic rate decreased, showing values ranging from 10 to 7 mol e^- g $chla^{-1}$ h^{-1} until T7. During the second part of the experiment (after T7), the relETRmax was low all along the water column, reaching 4 mol e^- g $chla^{-1}$ h^{-1} until T13. It is noteworthy that while Chla was increasing, the photosynthetic rate had an opposite trend. Furthermore, this parameter was quite stable along the water column despite the vertical gradient, at the exception of T1.

The integrated phytoplankton absorption coefficient (a^*_{ph}) increased after the first nutrient addition, reaching at T1 its maximum value (0.27 m^{-2} mg $Chla^{-1}$) (Fig. 8.7 b). The nutrient input modulated the physiological state of cells and/or the phytoplankton community dominance or diversity, resulting in a higher light harvesting capacity. Then at T2 and T3 this parameter decreased, stabilizing on values around 0.15 m^{-2} mg $Chla^{-1}$ until the end of the experiment. Interestingly, a^*_{ph} did not vary along the water column, revealing an absence of depth-acclimation.

From T0 to T1, the photochemical efficiency of photosystem II (Fv/Fm) decreased ranging from 0.35 in surface to 0.20 at deep (Fig. 8.7 c). From T2 to T7, Fv/Fm increased reaching its maximum value at T5 (0.48), without presenting any vertical variability. Then after T7, it decreased until the end of the experiment, reaching its minimal value at T12 (0.20).

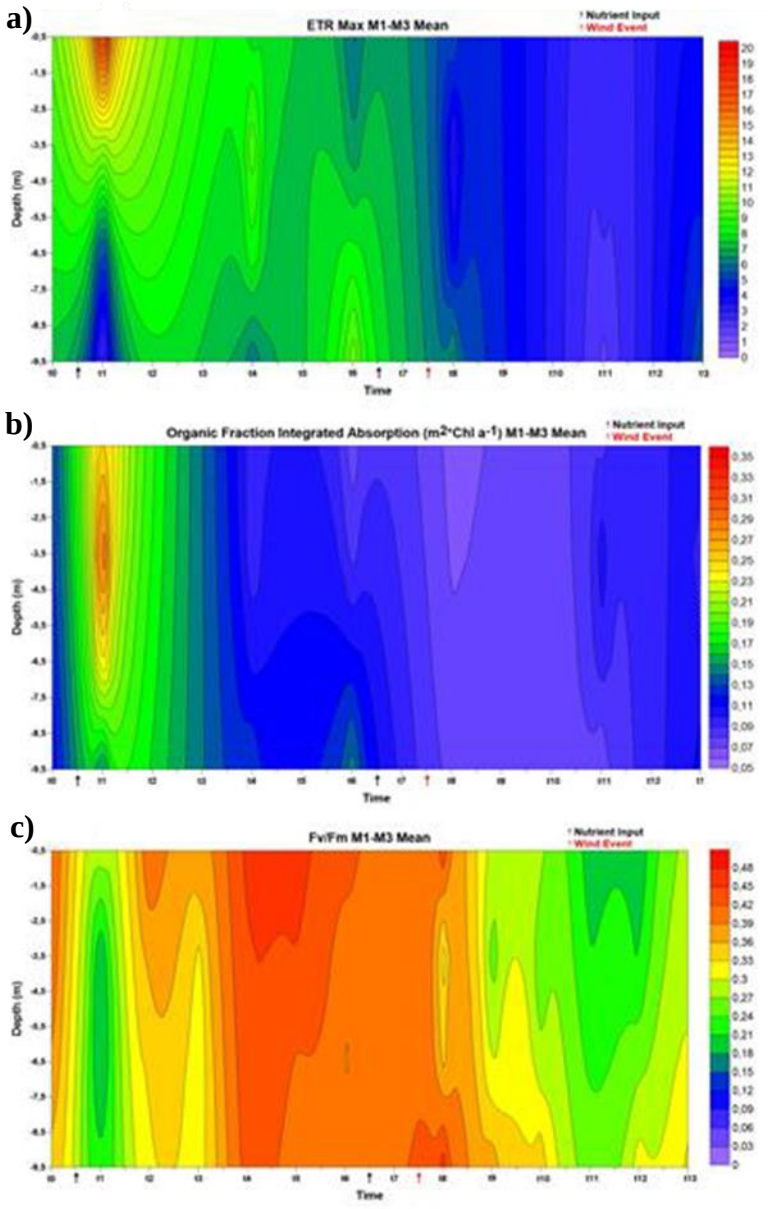

Figure 8.7: Contour maps of the photosynthetic parameters: a) relative electron transport rate (relETRmax, mol e^- g $chla^{-1}$ h^{-1}); b) integrated phytoplankton absorption coefficient (a^*_{ph}, m^{-2} mg $Chla^{-1}$); c) photochemical efficiency of photosystem II (Fv/Fm).

The photosynthetic parameters retrieved from the P *vs* E curve, α (the slope) and Ek (light saturation index for photosynthesis), varied during the experiment (Fig.8.8).

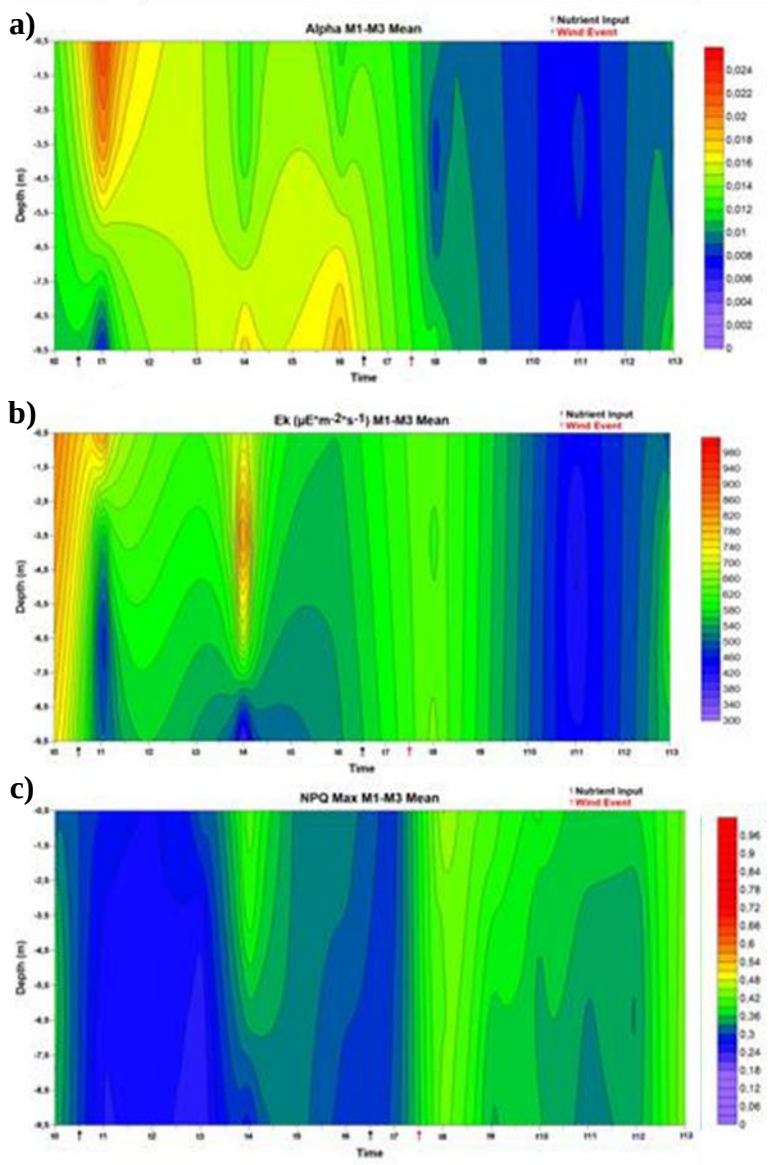

Figure 8.8: Contour maps of the photosynthetic parameters: a) maximum light use efficiency (α); b) light saturation index for photosynthesis (Ek); C) non-photochemical quenching (NPQ).

At T1, α increased in the surface layer, presenting a vertical negative gradient from surface to deep (Fig. 8.8 a). This feature, together with the increase of relETRmax and the decrease of Fv/Fm confirmed the change in the photo-physiological state of the phytoplankton community. After this first response, α decreased progressively and then dropped at T8, without presenting any vertical variability.

Ek decreased after the first nutrient addition, keeping almost stable values until T4, when it increased both at the surface and intermediate depths (Fig. 8.8 b). Then Ek lowered again

keeping stable values until T9, when it dropped and stabilized on lower values until the end of the experiment. Also Ek did not display vertical variability, with the exception of T1.

The non-photochemical quenching (NPQ) showed low values from T0 to T3 (between 0.06 and 0.01 along the water column), then at T4 it increased both at the surface and intermediate layers, reaching values around 0.40 and 0.55, respectively (Fig. 8.8 c). Then, it decreased between T5 and T7. After the second fertilization (T7), NPQ increased again, keeping high values until the end of the experiment. This feature may explain the low relETRmax recorded during the second week of experiment, being NPQ a process aimed to dissipate the excess of energy, lowering the amount of photons reaching the photosynthetic apparatus. As the other photosynthetic parameters, NPQ did not show significant vertical variations.

8.3.2.3 Total antioxidant capacity and molecules

The total antioxidant capacity (ABTS test) showed a progressive increase over time (Fig. 8.9 a). During the first four days of experiment, this parameter was relatively stable with values ranging from 2.5 ± 1.0 to 7.2 ± 3.3 µg AEq/L (mean value for the three depths during the first four days equal to 4.4 ± 1.7 µg AEq/L). At T6, the total antioxidant capacity started to increase, with values ranged from 11.1 ± 0.5 to 13.9 ± 4.2 µg AEq/L (mean value for the three depths equal to 12.5 ± 1.4 µg AEq/L). The total antioxidant capacity reached its maximum at T8, peaking at surface at 26.1 ± 5.1 µg AEq/L (mean values of the three depths 24.0 ± 2.9 µg AEq/L), slightly decreasing the subsequent days. Interestingly, while during the first week no vertical trend was visible, at T8, T11 and T13 the antioxidant capacity decreased along the water column.

The overall distribution of the total antioxidant capacity was similar to Chla concentration suggesting a link between biomass increase and the enhanced antioxidant capacity. Indeed, negative correlations between the total antioxidant capacity and SiO_4, NO_3, and NO_2 concentrations were detected (Table 8.2). A positive correlation between the total antioxidant capacity and temperature was also noticed (Table 8.2).

The total antioxidant capacity was correlated to the *Chromalveolata* group [determined by the positive correlation with Chlorophyll c, (Chlc, Table 8.3)] a polyphyletic assemblage which includes *Cryptophyta*, *Haptophyta*, *Alveolata* and *Stramenopiles* (see Chapter 1). Also, a correlation with the diatoms' fucoxanthin pigment, Fuco, was noticeable (Table 8.3).

The antioxidant capacity resulted positively correlated to the pigment Dd belonging to the xanthophyll cycle present in many Chlc–containing algae. Furthermore, it was positively linked with the pigment β-car, confirming the antioxidant role of this pigment.

Intriguingly, the antioxidant capacity was positively correlated with Chlorophyllide a, a degradation product of Chla, biomarker of cell senescence (Table 8.3) suggesting that older cells might have a higher antioxidant capacity.

The ascorbic acid (AsA) was more stable with respect to the total antioxidant capacity (Fig. 8.9 b). Excluding T6, it showed values ranging between 1.2 ± 0.5 and 2.7 ± 0.2 µg AsA/L

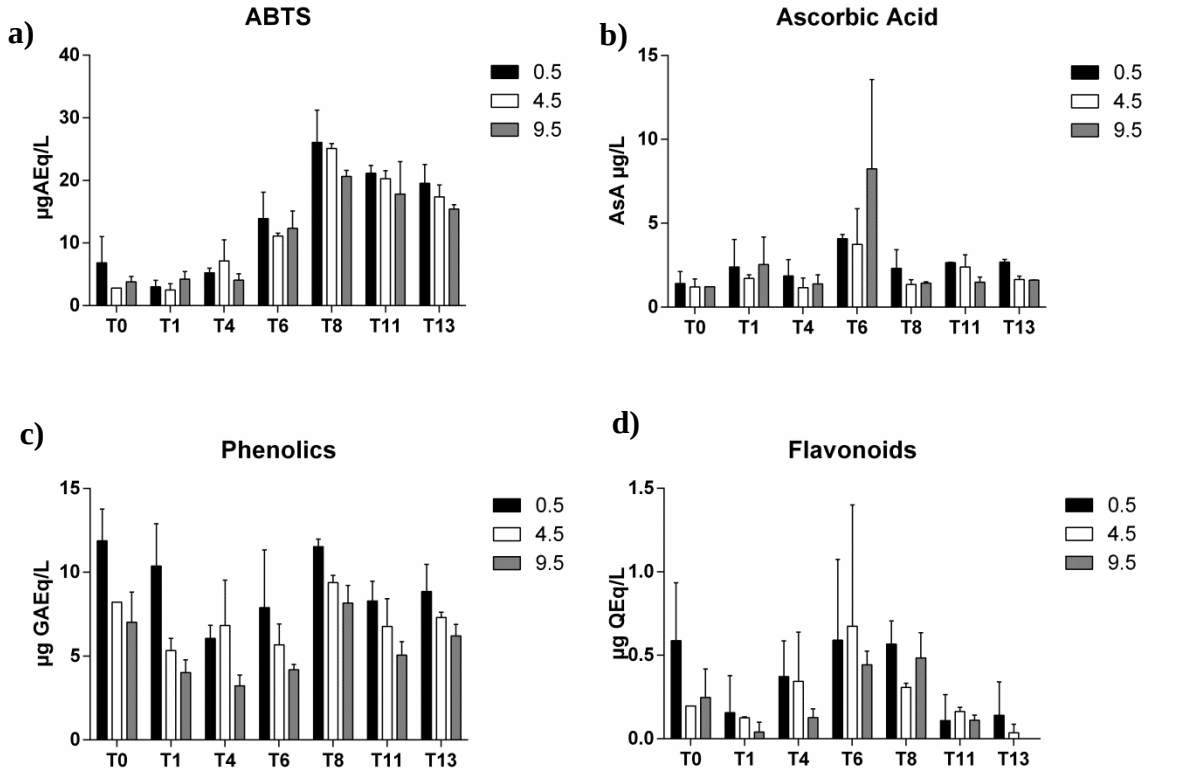

Figure 8.9: Antioxidant molecules content and antioxidant activity: a) ABTS test (µgAEq L^{-1}); Ascorbic acid (µgAsA L^{-1}); c) Phenolics (µgGAEq L^{-1}); d) Flavonoids (µgQEq L^{-1}). Samples were collected at the surface (0.5, black bars), intermediate (4.5, white bars), deeper (9.5, grey bars) layers.

(mean values of the three depths equal to 1.8 ± 0.5 µg AsA/L in all the time points with the exception of T6). At T6 this molecule displayed its highest concentration, peaking at 9.5 meters depth at 8.2 ± 5.3 µg AsA/L (mean value of the three depths was 5.4 ± 2.5 µg AEq/L). Like the total antioxidant capacity, AsA displayed a vertical trend at T8, T11 and T13, with higher surface values respect to the deeper one.

Asa concentration was not correlated to any abiotic parameters, underlining the complex behaviour of this versatile molecule which is produced and consumed rapidly by the living cells.

However, AsA concentration was positively linked to Dt, the photoprotective pigment characteristic of the *Chromalveolata* (Table 8.3).

The phenolic compounds concentration clearly showed a vertical gradient along the water column, confirmed by the positive correlation with depth, light and temperature (Fig. 8.9 c, Table 8.2). The surface values were always higher with respect to those recorded at 4.5 and 9.5 meters depth, with the only exception of T4, when the intermediate layer showed a slightly higher value respect to the surface. Temporal distribution of the phenolic compounds revealed a lowering between T0 to T4, with values from 11.9 ± 1.9 µg GAEq/L at T0 to 7.9 ± 3.4 µg GAEq/L at T4 at surface. From T6, their concentration increased reaching the initial value at T8 (surface: 11.5 ± 0.5 µg GAEq/L, mean value of the three depths: 9.7 ± 1.7 µg GAEq/L), decreasing again in the two last sampling time points, reaching values of 8.3 ± 1.2 and 8.9 ± 1.6 GAEq/L at T11 and T13, respectively.

The concentration of these molecules was correlated to the nitrogen availability, mainly NO_3 (Table 8.2).

Table 8.2: Correlations between the antioxidant capacity and molecules (expressed as µg L^{-1}) and abiotic or biotic parameters. Significance values (P) and Pearson's correlation coefficients (r).

		P	r
ABTS in µgAEq L^{-1}	Temperature	<0.05	0,46
	SiO_4	<0.01	-0,65
	NO_3	<0.05	-0,49
	NO_2	<0.01	-0,58
Phenolics in µgGAEq L^{-1}	ABTS	<0.05	0,44
	Depth	<0.001	0,68
	Temperature	<0.001	0,74
	Light	<0.001	0,67
	NO_3	<0.05	0,47
	Total nitrogen	<0.05	0,50
Flavonoids in µgQEq L^{-1}	Light	<0.05	0,51
	NH_4^+	<0.01	0,59

Phenolics' concentration was positively correlated with the *Chromalveolata* group pigments, such as $Chlc_1$, $Chlc_2$, Peridinin and Fucoxanthin (Table 8.3). It was also correlated with the total antioxidant capacity and the antioxidant pigment β-car, as well as with Dd (Table 8.3).

The flavonoid concentration showed a trend similar to the phenolic compounds, confirmed by the positive relationship of its concentration with the light availability (Fig. 8.9 d, Table 8.2).

Their concentration decreased from T0 to T1, then increased from T4 to T6, where they reached the highest value at the intermediate depth: 0.7 ± 0.7 µg QEq/L (mean values of the three depths at T6 equal to 0.57 ± 0.16 µg QEq/L). Then, they lowered reaching the lowest concentration at T13.

Intriguingly, the flavonoid concentration presented few and peculiar correlations. Indeed, it was positively correlated to ammonia (Table 8.2) and to the antioxidant pigment β-car (Table 8.3), while no relationship with phytoplankton groups or the xanthophyll cycle was revealed.

Table 8.3: Correlations between the antioxidant capacity and molecules with the pigment concentration expressed in µg L^{-1}. Significance values (P) and Pierson's correlation coefficients (r).

		P	r
ABTS in µgAEq L^{-1}	$Chlc_1$	<0.001	0,51
	$Chlc_2$	<0.001	0,55
	$Chlc_3$	<0.05	0,36
	Dd	<0.001	0,45
	Fuco	<0.0001	0,57
	β-car	<0.01	0,46
	Chlorophyllide a	<0.01	0,41
AsA in µg L^{-1}	Dt	<0.001	0,50
Phenolics in µgGAEq L^{-1}	$Chlc_1$	<0.05	0,33
	$Chlc_2$	<0.05	0,38
	Peridinin	<0.05	0,31
	Dd	<0.01	0,43
	Fuco	<0.05	0,37
	β-car	<0.05	0,31
Flavonoids in µgQEq L^{-1}	β-car	<0.05	0,35

Since the aforementioned molecules are produced by phytoplankton cells, their concentration distribution should be dependent on the phytoplankton biomass distribution. Indeed, the total antioxidant capacity was correlated to Chla concentration ($p<0.0001$, $r=0.88$, Fig. 8.10 a). The same trend was revealed for the phenolic compounds ($p<0.05$, $r=0.50$, Fig. 8.10 c). No significant relationship between Chla concentration and AsA was found (Fig. 8.10 b). As regards the flavonoids and Chla, they were correlated following two distinct kinetics: one corresponding to the first week of experiment, when Chla was lower

(Fig. 8.10 d, p<0.001, r=0.67, closed dots), and a second one during the second week, at higher Chla concentration (Fig. 8.10 d, p<0.05, r=0.76, open dots). These two distinct dynamics suggest a different production of flavonoids related to phytoplankton community shift.

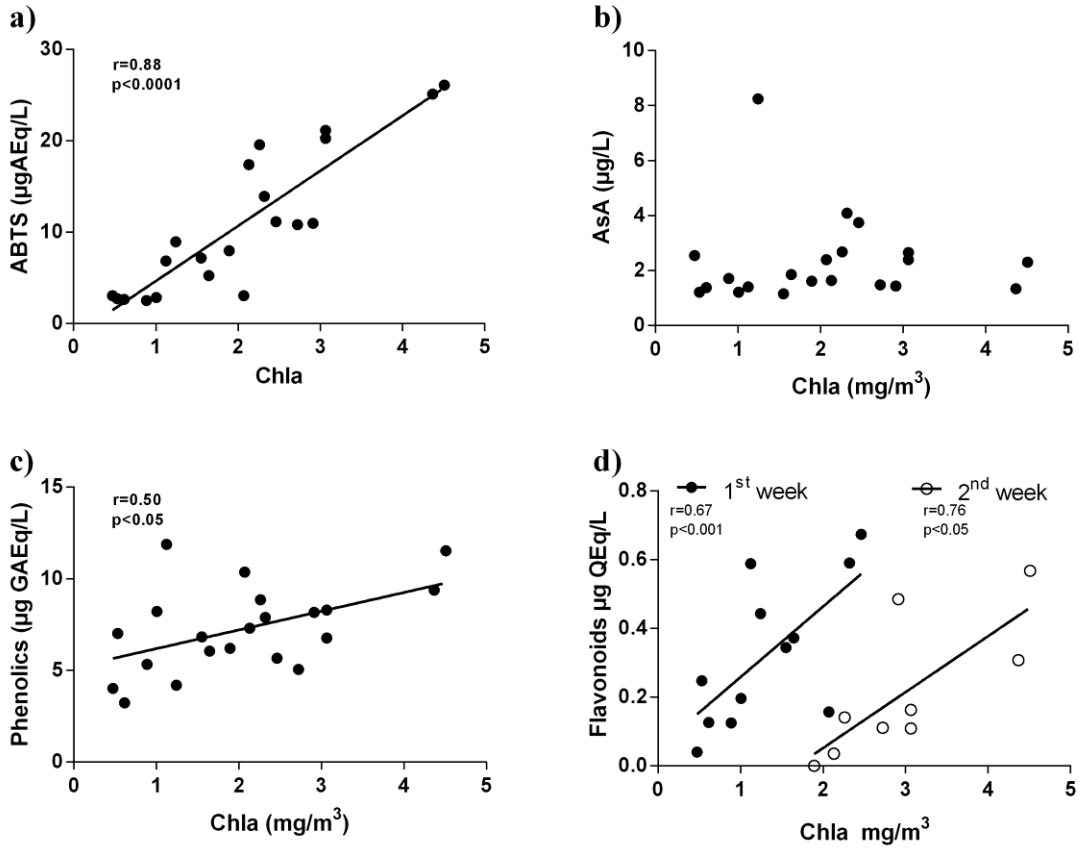

Figure 8.10: Correlations between the antioxidant capacity and molecules and Chla: a) ABTS in µgAEq L^{-1} vs Chla in mg/m^3; b) AsA in µ/L vs Chla in mg/m^3; c) Phenolics in µgGAEq L^{-1} vs Chla in mg/m^3; d)Flavonoids in µgQEq L^{-1} vs Chla in mg/m^3; first week of experiment empty dots, second week of experiment closed dots.

Being these parameters almost dependent on the autotrophic biomass, we normalized these data by the Chla concentration in order to remove the effect "biomass" from the antioxidant

distribution obtaining therefore the antioxidant capacity (mg AEQ/mg Chla) or antioxidant molecules concentration per unit of biomass (mg/mgChla).

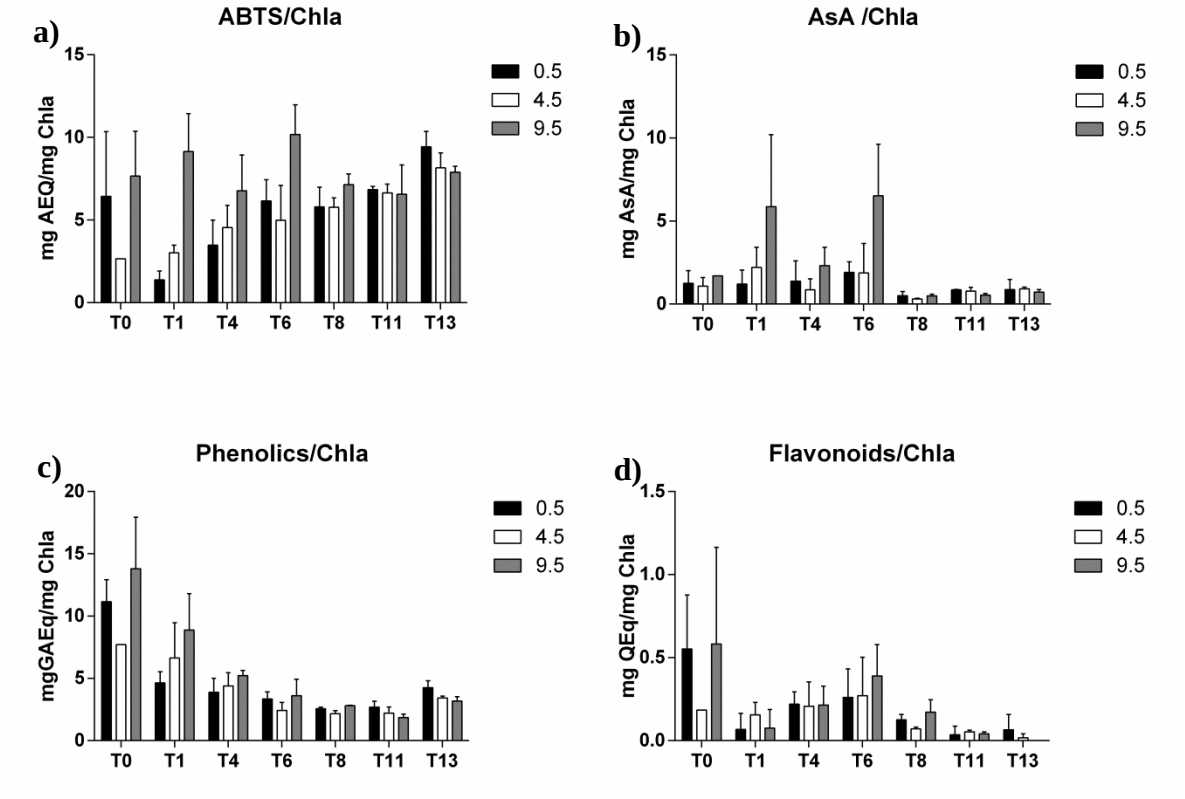

Figure 8.11: Antioxidant molecules content and antioxidant activity: a) ABTS test (mgAEq mg Chla^{-1}); Ascorbic acid (mgAsA mg Chla^{-1}); c) Phenolics (mgGAEq mg Chla^{-1}); d) Flavonoids (mgQEq mg Chla^{-1}). Samples were collected at the surface (0.5, black bars), intermediate (4.5, white bars), deeper (9.5, grey bars) layers.

The antioxidant activity per unit of phytoplankton biomass at T0 showed high values both at the surface and the deeper layer (Fig. 8.11 a). After the nutrient addition, this parameter dropped at the surface layer, keeping high values at deep (1.4 ± 0.5 and 9.1 ± 2.2 mg AEq/mg Chla at the surface and deep layer respectively at T1). Then, the total antioxidant capacity increased progressively until the end of the experiment both at the surface and intermediate depths.

Interestingly, while during the first week the higher activity was recorded at deep, from T8 onwards the antioxidant capacity was homogeneously distributed along the water column, probably as a consequence of the water mixing caused by the wind burst occurred after T7.
The greater antioxidant capacity recorded at deep determined the negative correlation of this parameter with depth (Table 8.4), suggesting a consumption of the antioxidant molecules to counteract the detrimental condition of the upper layer. The consumption of nitrogen and phosphate determined an increase of the antioxidant activity (Table 8.4).
Interestingly, the higher the antioxidant capacity, the lower the photosynthetic rate measured as relETRmax (Table 8.5), revealing a lower photosynthetic efficiency of cells which "invested" in a high antioxidant protection.

Table 8.4: Correlations between the antioxidant capacity and molecules expressed in mg/mg Chla among each other and with the environmental parameters. Significance values (P) and Pearson's correlation coefficients (r).

		P	r
ABTS in mg AEq mg Chla^{-1}	Depth	<0.05	-0,44
	PO_4	<0.05	-0,47
	NO_3	<0.01	-0,58
	NO_2	<0.01	-0,55
AsA in mg Asa mg Chla^{-1}	Temperature	<0.05	-0,45
Phenolics in mg GAEq mg Chla^{-1}	NO_3	<0.01	0,59
	N/P	<0.001	0,75
Flavonoids in mg QEq mg Chla^{-1}	Phenolics/Chla	<0.001	0,68
	NO_3	<0.05	0,45
	N/P	<0.001	0,68

After the first fertilization, an increase of AsA content per mg Chla was visible at deep (Fig. 8.11 b). This ratio kept almost stable values until T6, while from T8 until the end of the experiment it lowered respect to the previous week. During the first week the deepest layer showed higher values, while during the second week no vertical gradient was visible.
The content of AsA per Chla decreased with the water warming (Table 8.4), maybe due to its consumption in order to counteract the heat stress or in relation with changes in phytoplankton community composition.
Interestingly, AsA/Chla and NPQ showed an opposite trend, being negatively correlated to each other (Table 8.5).

Table 8.5: Correlations between the antioxidant capacity and molecules expressed in mg/mg Chla with the photosynthetic parameters. Significance values (P) and Pearson's correlation coefficients (r).

		P	r
ABTS in mg AEq mg Chla^{-1}	relETRmax	<0.05	-0,53
AsA in mg Asa mg Chla^{-1}	NPQ	<0.01	-0,64
Flavonoids in mg QEq mg Chla^{-1}	Fv/Fm	<0.05	0,47

The ratio between phenolics and Chla decreased over time (Fig. 8.11 c). The higher values were recorded at T0 (11.5 ± 1.8 mg GAEq/mg Chla at the surface), while almost halved already at T1 (4.6 ± 0.9 mg GAEq/mg Chla at the surface), showing a vertical trend with higher values at deep respect to surface. Then this ratio decreased until T13, when it was recorded a slight increase of this parameter.

The phenolics/Chla ratio was positively correlated with nitrogen, mostly linked to the nitrate concentration, and to the nitrogen/phosphate ratio (N/P) (Table 8.4).

The flavonoids/Chla ratio, like the phenolics/Chla ratio, displayed higher values at T0 (Fig. 8.11 d), lowering consistently at all depths from T1. At T4 and T6 this ratio increased, but although from T8 it decreased reaching the lowest value at the end of the experiment.

This ratio was positively related to the phenolics/Chla ratio, as well as to the nitrate concentration and N/P (Table 8.4)

Interestingly, the higher the flavonoids/Chla the higher Fv/Fm, revealing that the production of this class of molecules might be mostly related to high performing cells (Table 8.5).

8.4 Discussion

The results obtained from this experiment highlight the key role played by nutrients in controlling the phytoplankton community composition, physiological state, growth, and the synthesis of the antioxidant molecules.

The positive correlations between the different nitrogen sources and the phenolic and flavonoid compounds underline the subtle control of cell metabolism in response to nutrient availability and/or a shift in the phytoplankton community nutrient-dependent, which by consequence show a different antioxidant molecules profile. The more reduced state of ammonia respect to nitrate makes the former less energetically expensive to assimilate, although the latter is the main N form at sea. Anyway, ammonia can become toxic by inducing oxidative stress and inhibition of photosynthesis (Wang *et al.*, 2008). By consequence, the higher flavonoid content recorded at higher NH_4^+ concentration could represent an adaptation to counteract the toxicity, being these molecules signals and therefore regulators of the antioxidant cascade (Mouradov & Spangenberg, 2014).

The presence of flavonoids, phenolics and ascorbic acid as well as the total antioxidant capacity were mostly related to the *Chromalveolata* group, i.e., the Chlc-containing algae, including diatoms and Prymnesiophyceae. These groups are the main actors of the microflora communities in coastal environments. Diatoms are the most successful autotrophs in turbulent, nutrient-rich waters (Falkowski *et al.*, 2004). This is due to their high plasticity and functional diversity derived from their mix-and-match genome, the result of endosymbiotic events between heterotroph, red alga and bacteria (Armbrust *et al.*, 2004, Finazzi *et al.*, 2010). This high plasticity allows their survival under fluctuating light regimes and their thriving after a nutrient pulse, thanks to their efficient nutrient uptake, storage ability and photoprotective mechanisms (see chapter 1). Diatoms are able to assimilate nitrogen from different sources such as ammonia, nitrite, and nitrate, as well as urea, amino acids, and purines, thanks to the numerous transporters and enzymes involved in the catabolism of the nitrogen organic forms (Armbrust *et al.*, 2004).

From my results (e.g., correlation between antioxidant capacity and fucoxanthin), we can hypothesize also the role of an efficient antioxidant production system on the diatoms success at sea.

Interestingly, the flavonoid content is linked to the photochemical efficiency, suggesting that higher flavonoid content allows cells to maintain a high photosynthetic performance. It is known that the flavonoids may have different localization in the cells, and can be found in the chloroplast where they play a major role in photoprotection mainly due to their antioxidant activity (Agati & Tattini, 2010, Agati *et al.*, 2013).

The nutrient fertilization induced the phytoplankton outburst, as visible by increased Chla concentration. The biomass enhancement was paralleled to the increased photosynthetic rate (relETRmax), photochemical efficiency (Fv/Fm), and to the phytoplankton absorption coefficient (a_{ph}^{*}), indicators of a better physiological performance in nutrient-replete condition.

The greater biomass consumed the nutrients present in the water column, determining the switch of the autotrophic cells into their senescent stage. The nutrient limitation during the second week of experiment, together with the increased biomass and the consequent lower light environment, determined the lower photosynthetic rate, photochemical efficiency, and light harvesting ability.

The greater antioxidant capacity can be ascribed to the final stage of the diatom bloom thanks to the positive correlation both with the pigment fucoxanthin, characteristic of this group of microalgae, as well as with Chlorophyllide a, biomarker of senescent cells.

This growth phase was characterized by the increased antioxidant activity as well as an increased NPQ, confirming the results obtained in the laboratory experiment described in Chapter 5 on the change in photophysiology of cells during the different growth phases.

The higher antioxidant capacity was not ascribable to the antioxidant molecules analyzed in my study (AsA, phenolics, flavonoids), but it did show a link with the pigments Dd and β-car, confirming the antioxidant role of the latter and suggesting the role as antioxidants of the XC pigments (see chapter 9).

As regards the link between the photosynthetic parameters and the antioxidant network, it is noteworthy the negative correlation between NPQ and AsA. This opposite trend might be due to the fact that higher NPQ may be related to higher XC activation which relies on the AsA consumption, being a cofactor of the XC enzymes (see Chapter 1). Otherwise, this feature may reveal the alternative behaviour in front of a light stress adopted by the

different phytoplankton communities: those more able to perform a high NPQ to dissipate the excess of energy may need a lower concentration of this antioxidant and *vice-versa.*

Phytoplankton biomass in the coastal area of the Gulf of Naples during spring bloom is constituted mainly by large colonial diatoms, including *Chaetoceros* spp., *Pseudo-nitzschia delicatissima*, *Thalassionema bacillaris* and phytoflagellates. Then, in summer stratified waters, the above mentioned diatoms are substituted by smaller size ones generally in a non-colonial form, such as *Skeletonema pseudocostatum*, *Chaetoceros socialis*, *C. tenuissimus* together with phytoflagellates, dinoflagellates and coccolitophorids (Ribera d'Alcalà *et al.*, 2004).
Therefore, based on the knowledge coming from literature, we can hypothesize that during our experiment the initial diatom bloom stimulated by the silica addition, should be lately substituted by a community composed by smaller phytoplankton cell size, such as coccolithophorids or small flagellates (Ribera d'Alcalà *et al.*, 2004, Van Oostende *et al.*, 2017), and by picoplanktonic species (cell size less than 3 µm, e.g. the cyanophyte S*ynechococcus*) as already observed in this study area during the summery low nutrient conditions (Modigh *et al.*, 1996).
Unfortunately, the data on the phytoplankton community composition are not yet available, so at this time this hypothesis still has to be confirmed.

This study, which foresaw the analysis of numerous parameters at different scale of biological organization, from molecular to cellular levels up to community structure and trophic interactions, is pioneer. The results discussed in this chapter represent to my knowledge the first study of the antioxidant properties and their link with photoprotective mechanisms conducted at sea.
I showed that the antioxidant molecules and the total antioxidant capacity follow a complex dynamics being dependent on the phytoplankton community composition, (photo)physiological state and environmental stresses.

The main role played by diatoms in this bloom context, and their link with the antioxidant properties of the water column strengthen their choice as model organisms whose physiology and consequent biotechnological application are still too underexplored.

This awareness is encouraging and confirms the importance of diatoms as key-species for biotechnological investigations in modulating the photoprotective and antioxidant synthesis in these organisms, key components of our blue planet with a great potential largely neglected.

9. Antioxidant property of purified diatom’s pigments

9.1 Introduction

Carotenoids are natural fat-soluble isoprenoid compounds with important biological functions. Their structure constituted by a long system of alternating single and double bonds forms a conjugated system in which the π electrons can be easily delocalized all over the molecule. This feature is responsible for their light absorption properties, and so for their color, as well as for their chemical reactivity (Britton, 1995). Among their biological effects with positive outcomes on health, these compounds have a proven antioxidant, anticancer, anti-inflammatory, anti-obesity, neuroprotective, and anti-angiogenic activities (Stahl & Sies, 2003, Mata *et al.*, 2010, Pangestuti & Kim, 2011).

Currently, the high value carotenoids that reached the food and feed market produced by microalgae are limited to astaxanthin and β-carotene harvested mainly from *Haematococcus pluvialis* and *Dunaliella salina*, respectively (Enzing *et al.*, 2014). Although natural pigments produced by microalgae are way more than the aforementioned two, the others are not commercially available. The main drawback associated with their production and commercialization regards the optimization of their yield, which up to now is too scarce to justify their large scale production (Borowitzka, 2013).

A possible way to enhance the production of these molecules could be achieved through genetic transformation, but unfortunately the genes involved in the carotenoid biosynthetic pathway are still partially unknown (Lohr & Wilhelm, 2001, Dambek *et al.*, 2012).

It has been proven that with light manipulation the content of the carotenoids change, being them responsible both for the light harvesting, as well as for their main role in photoprotection and antioxidant activity (this thesis) (Erickson *et al.*, 2015, Goss & Lepetit, 2015). By consequence, a higher extraction yield could be obtained through a selected light climate during their cultivation able to maximize their biosynthesis.

Diatoms are an important source of natural carotenoids. They produce fucoxanthin (Fuco) as main accessory pigment in the antennae, which has been showed to have antioxidant, anti-inflammatory, anticancer, anti-obese, and antidiabetic activities (Peng *et al.*, 2011).

In addition, they produce the xanthophyll cycle (XC) pigments diadinoxanthin (Dd), diatoxanthin (Dd), their precursor β-carotene (β-car), and also violaxanthin (Vx),

antheraxanthin (Ax) and zeaxanthin (Zeax), but in a less pronounced fashion (Kuczynska *et al.*, 2015).

It has been hypothesized that the photoprotective Dt molecules possess a double role: those bounded to the proteic component of the antennae participate in the non-photochemical quenching development, while the pool dissolved in the lipid phase should play an antioxidant role, being responsible of the scavenging of the singlet oxygen ($^1O_2$) and functioning as chain breaker during lipid peroxidation (Lepetit *et al.*, 2010). It exerts the same functions of the photoprotective pigments of the green lineage Ax and Zeax (Havaux *et al.*, 2007).

It has been proven that the xanthophylls Zeax and its stereoisomer lutein have important beneficial effect on human health linked to their antioxidant power, preventing macular degeneration, reducing the intensity of cardiovascular disease, stroke, cancer, and neurodegenerative disorders (Jia *et al.*, 2017, Zaheer, 2017) and bibliography therein).

Therefore, also diatom's carotenoids must have some important biological functions which can be exploited in human health.

Despite the fact that the antioxidant power has been attributed to Dd and Dt, this feature has never been directly tested. Therefore, the aim of this chapter was to shed light on the potential antioxidant activity of diatom's pigments.

9.2 Materials and methods

9.2.1 Culture conditions

The experiment has been conducted on the diatom *Skeletonema marinoi* grown at 20°C in 2 litres polycarbonate bottles with air bubbling. The cells were long term acclimated to a sinusoidal white light distribution with a midday peak equal to 150 µmol photons s^{-1} m^{-2} and with a photoperiod of 12:12 dark:light, following the results obtained by Chandrasekaran *et al.* (2014), Orefice *et al.* (2016), Smerilli *et al.* (2017) and the chapters 5, 6 and 7. The white light was composed by Red:Green:Blue (RGB) with a ratio of 10:40:50.

In order to enhance the production of the photoprotective pigments without decreasing the growth rate, cells were switched to a sinusoidal light with a photon flux density peaking at midday at 400 µmol photons s^{-1} m^{-2}, with the same spectral composition. The mean growth rate measured was ≈ 0.7 d^{-1}.
Cells were harvested when reaching a concentration of *circa* $1x10^6$ cells ml^{-1}.
Cells were collected by centrifugation at 3600 g for 15 min at 4°C, the pellets were pooled together and centrifuged again in the same conditions. The final pellet was weighed, frozen in liquid nitrogen and then stored at -20°C.

9.2.2 Pigment extraction

The extraction of pigments from frozen cells (≈ $1x10^9$ cells) was performed in 6 mL absolute methanol. This solvent was selected due to its known higher xanthophyll's extraction efficiency (Xia *et al.*, 2013).

The sample was thoroughly mixed by vortexing, sonicated for 1 minute with a micro tip at 20% output on ice, and centrifuged at 14000g for 4 min at 4°C. The supernatant was collected for the subsequent saponification. All the operations were conducted under dim light on ice in order to reduce the risk of pigment degradation and photooxidation.

9.2.3 Saponification and carotenoid fraction recovery

After extraction, a saponification step was performed to separate the carotenoid fraction from the chlorophylls, the major pigments interfering with the spectrophotometric determination of carotenes, and to hydrolyze lipids at the same time (Lesellier *et al.*, 1993, Huo *et al.*, 1997, Kuczynska & Jemiola-Rzeminska, 2017). To the extracts, 23% of potassium hydroxide (60% w/v) was added. The mixture was left overnight (20-22 hours) in gentle swirling at dark at 4°C.

The extraction was performed following (Huo *et al.*, 1997). Briefly, a solution of petroleum ether-diisopropyl ether (3:1 v/v) was added to the mixture (final concentration 45%), and the extraction was performed by 2 minutes of vortexing. The supernatant obtained after centrifugation (2000 rpm 10 min, 4°C), was dried through rotary evaporation.

9.2.4 Preparative High Performance Liquid Chromatography

In order to maximize high-purity target compounds yield, preparative high performance liquid chromatography (prep-HPLC) has been performed.
The HPLC was the same as previously described in Chapter 2 (paragraph 2.8 Pigment analysis). The column was a reverse-phase C8, 5 µm particle size, 250 mm length, 10 mm internal diameter (Phenomenex®, Torrance, CA, USA) and the sample was injected into a 10 mL loop (Rheodyne®, Rohnert Park, CA, USA). Various attempts were made in order to determine the most efficient mobile phase and gradient able to separate the different fractions, and we used the following mobile phase:

solution A methanol:543 mM aqueous ammonium acetate (70:30 v/v)
solution B methanol:acetonitrile (70:30 v/v).

The temperature of the column was steadily maintained at 20° C and the flow rate of the mobile phase was set up at 4 mL min^{-1}. The selected gradient for the 35 minutes elution course is summarized in Table 9.1.

Table 9.1: Elution gradient for prep-HPLC

Time (minute)	Solution A	Solution B
0	100 %	0%
8	90%	10%
18	0%	100%
28	0%	100%
33	90%	10%
35	100%	0%

Prior to injection into the HPLC, the sample was resuspended in methanol:acetonitrile (70:30 v/v) and an Ion Pairing Agent (ammonium acetate 1 mol L^{-1}, final concentration 0.33 mol L^{-1}) was added to the pigment extract and incubated for 5 minutes in darkness at 4° C. The ion pairing agent was used to increase pigments hydrophobicity in order to obtain a better retainment on the column improving the peaks quality (Mantoura & Llewellyn, 1983).

Pigments were detected at 440 nm using a Hewlett Packard photodiode array detector model DAD series 1100 which gives the 350-700 nm spectrum for each detected pigment. A fluorometer (Hewlett Packard standard FLD cell series 1100) with excitation at 407 nm and emission at 665 nm allowed the detection of fluorescent molecules (chlorophylls and their degraded products).

The chromatogram revealed the presence of five major peaks, which were collected and subsequently analyzed with the analytic HPLC (Fig. 9.1).

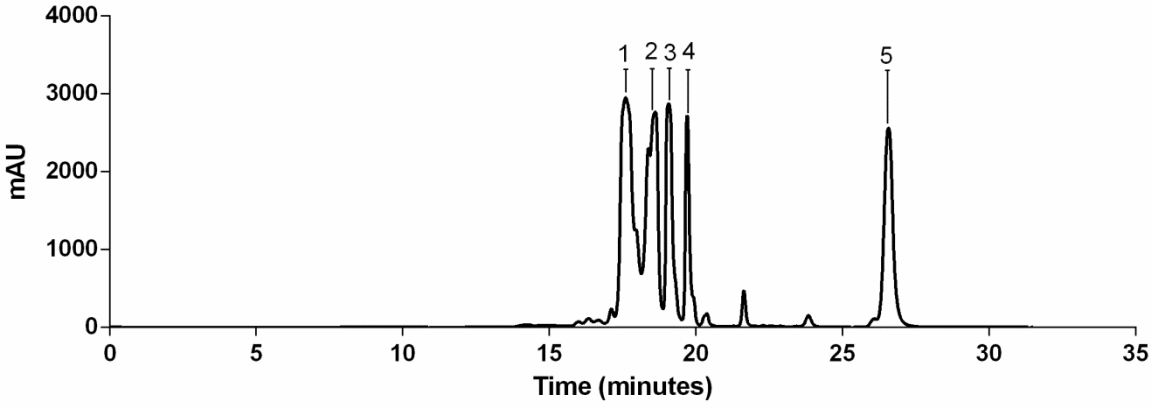

Figure 9.1: Chromatogram of the prep-HPLC. Five major peaks were detected and collected. mAU: milli absorbance units.

9.2.5 Analytic High Performance Liquid Chromatography

The different fractions collected after the prep-HPLC were subsequently injected into the analytic HPLC in order to check their purity and concentration, being already available the standard calibration curves for this column. The procedure is described in Chapter 2 (paragraph 2.8 Pigment analysis).

Fucoxanthin was not found in the collected fractions being sensitive to the saponification step (Rodriguez-Amaya, 2015).

The first fraction (peak 1 on Fig. 9.1) collected between the minutes 17 and 18.3 corresponded to an unresolved mixture of different pigments (data not shown), therefore it was not considered in the following analysis.

The second fraction (peak 2 on Fig. 9.1) collected between the minutes 18.3 and 19, consisted into a mixture of the two pigments neochrome and diadinoxanthin (Fig. 9.2). More specifically, the first peak of the chromatogram (Fig. 9.2 a) was constituted by pure 9'-*cis*-neochrome, as visible by the absorption spectrum (Fig. 9.2 b) (Roy *et al.*, 2011). The second peak instead was constituted by a mixture of both 9'-*cis*-neochrome (Fig. 9.2 b) and diadinoxanthin linked to it, which determined the switch of classic absorption spectrum of this latter pigment towards slightly lower wavelengths (Fig. 9.2 c).

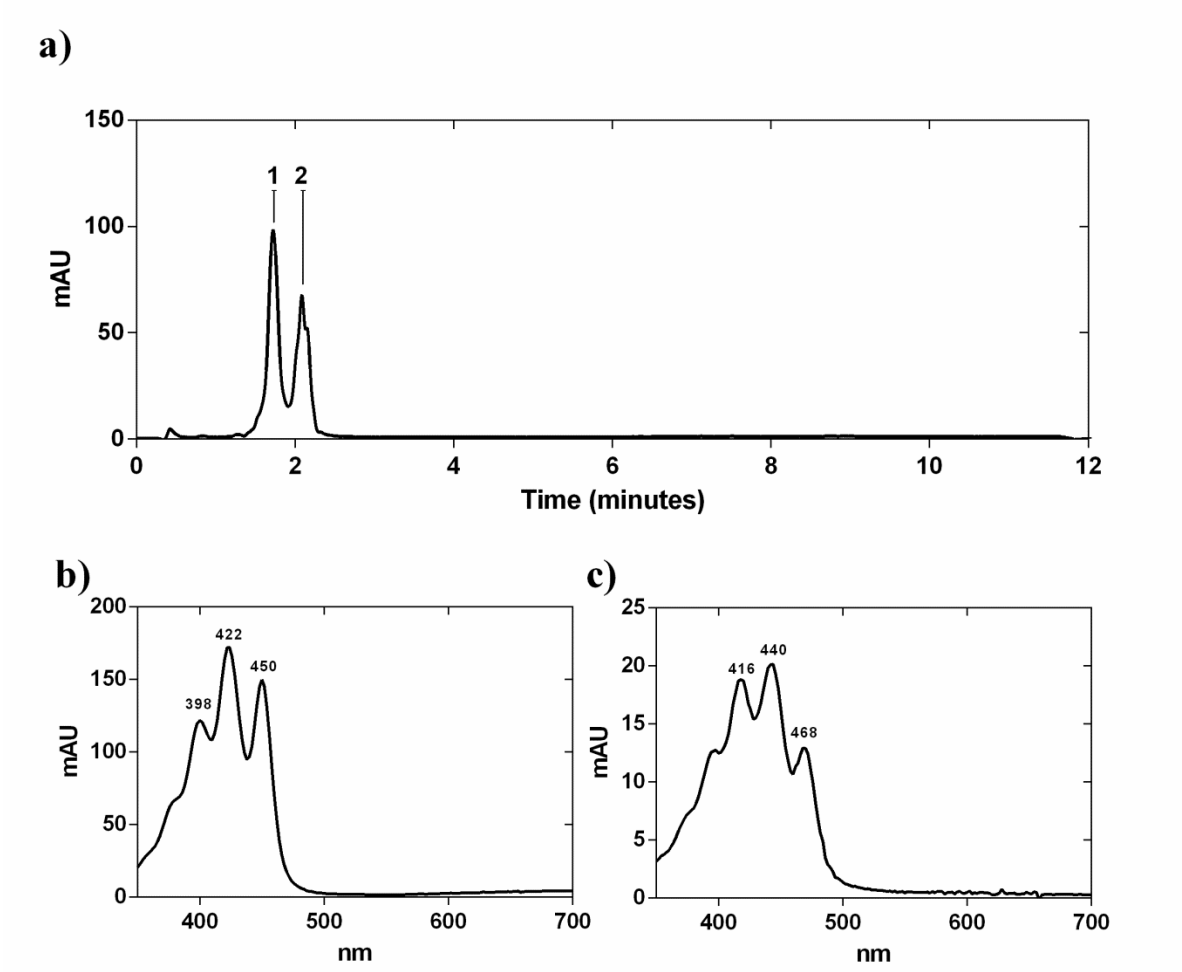

Figure 9.2: a) Chromatogram of the second fraction collected after the prep-HPLC; b) absorption spectrum visible in both the peaks number 1 and number 2 of the chromatogram which corresponds to 9'-*cis*-neochrome; c) absorption spectrum of the peak 2 of the chromatogram which corresponds to a mix of 9'-*cis*-neochrome and diadinoxanthin.

The third fraction (peak 3 on Fig. 9.1) collected between the minutes 19 and 19.7 was constituted by pure diadinoxanthin (Fig. 9.3), as visible by the unique peak of the chromatogram whose absorption spectrum corresponded to the one of diadinoxanthin (Roy *et al.*, 2011).

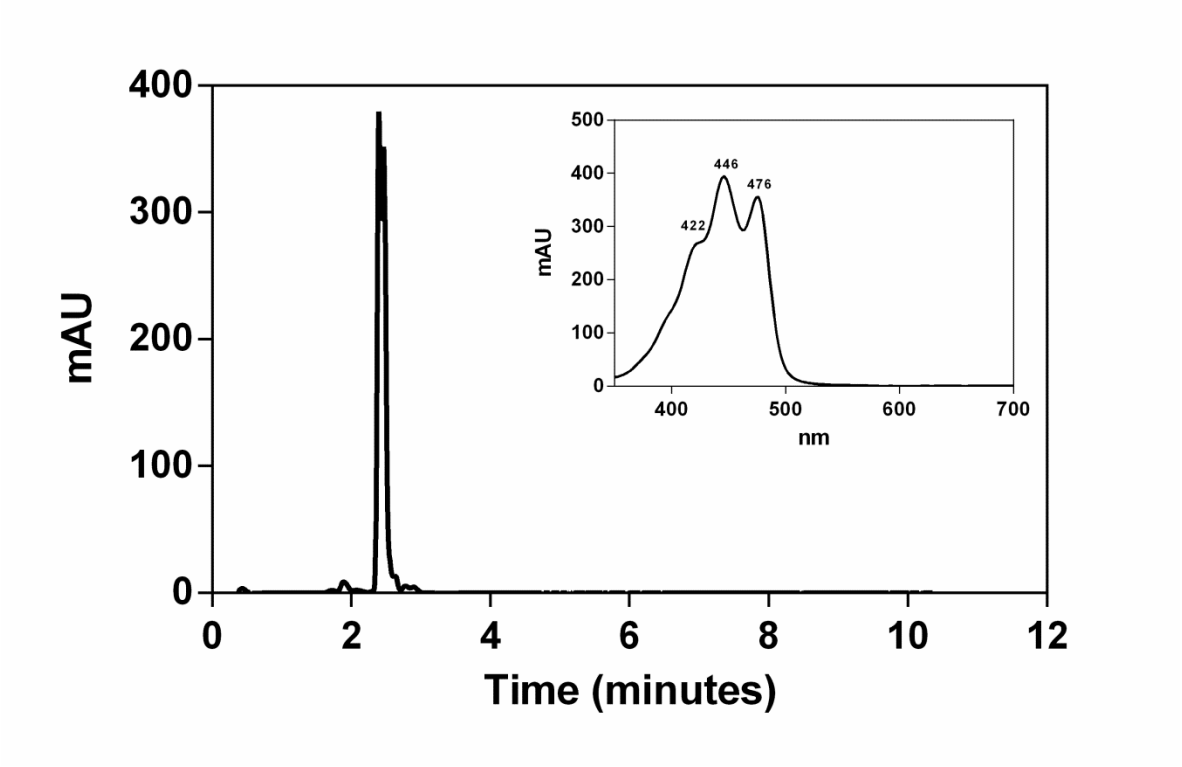

Figure 9.3: Chromatogram of the third fraction collected after the prep-HPLC. The inset plot is the absorption spectrum of the peak which corresponds to diadinoxanthin.

The fourth fraction (peak 4 on Fig. 9.1) collected between the minutes 19.7 and 20.3 corresponded to diatoxanthin (Fig. 9.4).

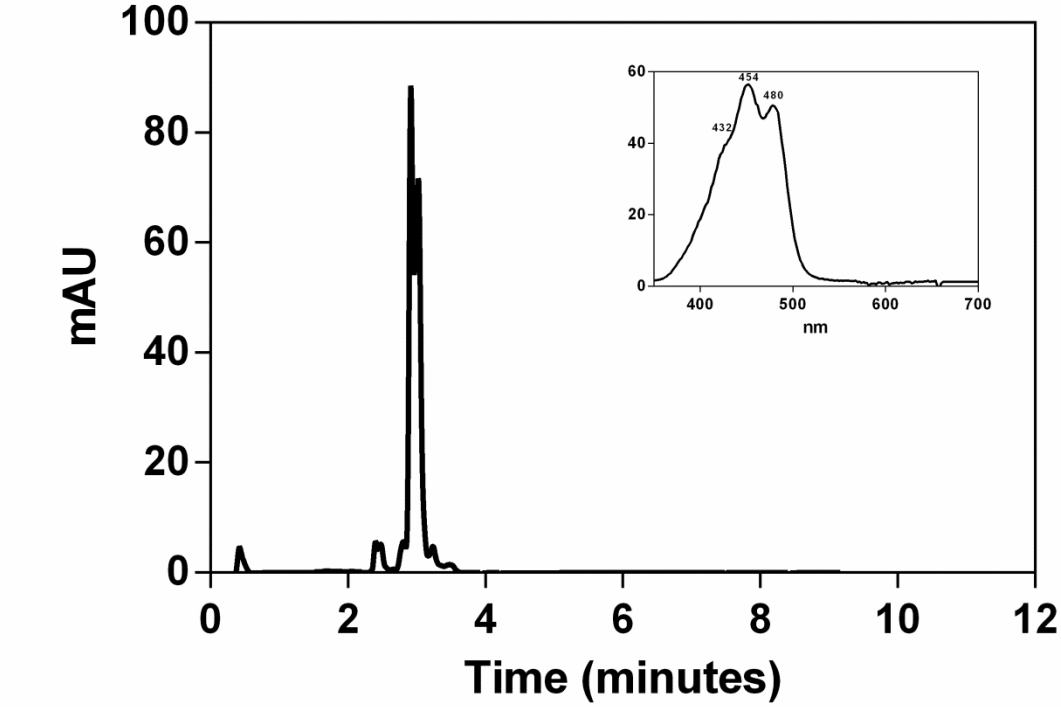

Figure 9.4: Chromatogram of the fourth fraction collected after the prep-HPLC. The inset plot is the absorption spectrum of the peak which corresponds to diatoxanthin.

The fifth fraction (peak 5 on Fig. 9.1) collected between the minutes 26.0 and 27.5 of the prep-HPLC corresponded to the pigment β-carotene (Fig. 9.5).

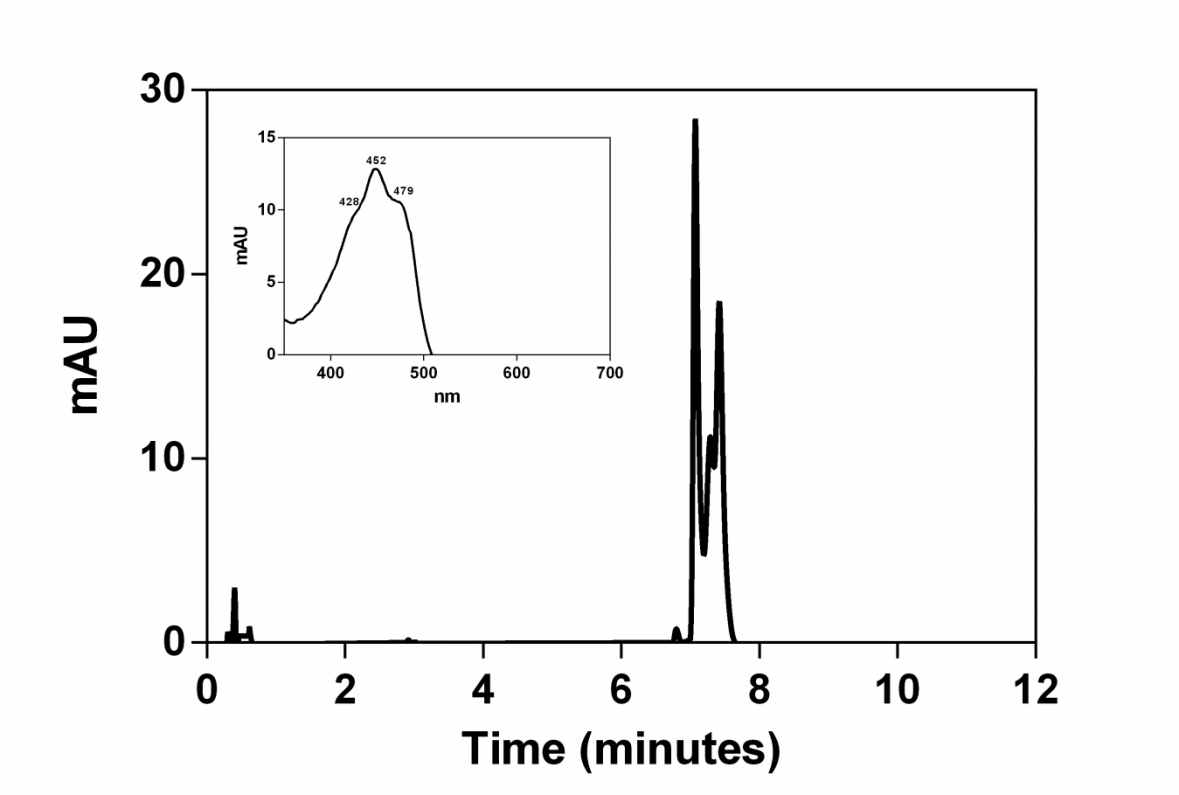

Figure 9.5: Chromatogram of the fifth fraction collected after the prep-HPLC. The inset plot is the absorption spectrum of the peak which corresponds to β-carotene.

9.2.6 ABTS radical scavenging activity

The different fractions were tested for their ABTS radical scavenging activity. The procedure is described in Chapter 2. Modifications were made in order to adjust the volumes for 96 well plates. Results were expressed as percent of inhibition calculated as follows (Xia *et al.*, 2013):

$$ABTS\ radical\ scavenging\ activity\ (\%) = \left(\frac{Ao-A}{Ao}\right) x100$$

where A_0=Abs radical and A= Abs sample.

9.2.7 Data treatment

Graphs and data analyses (best fit curves) were performed with the software Graph Pad PRISM® version 6.1.

9.3 Results and discussion

The pigments separated through prep-HPLC, and checked for their purity and concentration through analytic HPLC were subsequently screened for their antioxidant activity. The fractions resulted having different antioxidant activity (Fig. 9.6). Tocopherol standard were used as positive control.

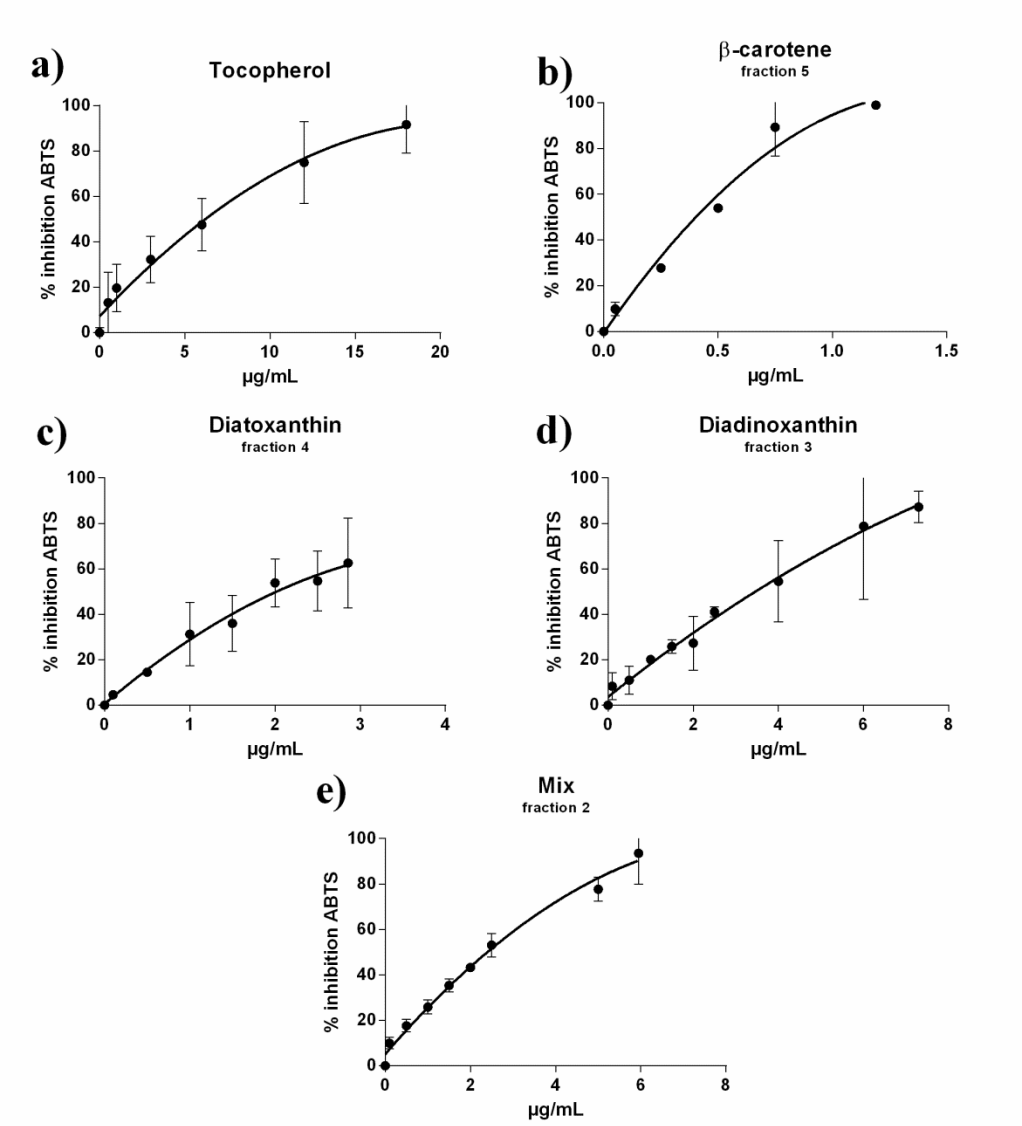

Figure 9.6: ABTS radical scavenging activity of the purified pigments expressed as % of inhibition per µg/mL: a) tocopherol; b) β-carotene, fraction 5; c) diatoxanthin, fraction 4; d) diadinoxanthin, fraction 3; e) carotenoid mix, fraction 2. Note that different concentrations of the substances were used (axis 1).

The regression curve which best fitted the data points was a second order polynomial, described by the general equation:

$$y = B_2x^2 + B_1x + B_0$$

The best-fit values with relative standard errors which describe the best fit curves of each data set and the relative goodness of fit parameters such as the degrees of freedom, R squared, absolute sum of squares (SS), and the standard deviation of the residuals (Sy.x) are reported in Table 9.1.

Table 9.1: Best-fit values and relative standard errors of the five curves obtained from the samples analyzed [Tocopherol, β-carotene (fraction 5), Diatoxanthin (fraction 4), Diadinoxanthin (fraction 3), Mix (fraction 2)]. The goodness of fit is described through the degree of freedom, R squared, absolute sum of squares (SS), and the standard deviation of the residuals (Sy.x).

	Tocopherol	β-carotene fraction 5	Diatoxanthin fraction 4	Diadinoxanthin fraction 3	Mix fraction 2
Best-fit values					
B_0	7.18	$2.3\ 10^{-10}$	0.55	3.61	5.11
B_1	8.08	146.20	31.94	15.05	21.69
B_2	-0.19	-50.85	-3.69	-0.47	-1.24
St. error					
B_0	4.00	3.06	4.13	3.86	2.06
B_1	1.50	14.13	7.72	3.21	2.10
B_2	0.08	11.74	2.69	0.44	0.34
Goodness of fit					
Degrees of Freedom	18	15	21	27	24
R squared	0.90	0.97	0.84	0.87	0.97
Absolut SS	2290	800	2203	3451	771
Sy.x	11.28	7.301	10.24	11.31	5.67

The fit of the data % inhibition ABTS *vs* molecule concentration was different for each fraction ($p<0.0001$), revealing that each fraction has its own antioxidant behavior. All the pigments showed a higher antioxidant activity than the standard tocopherol.

The half maximal inhibitory concentration (IC_{50}) of the standard was 6.20 µg/mL. The highest IC_{50} recorded was that of β-carotene (0.41 µg/mL) confirming the strong antioxidant activity of this pigment (Miller *et al.*, 1996, Mueller & Boehm, 2011).

Diatoxanthin showed an IC_{50} equal to 2.02 µg/mL, higher respect to diadinoxanthin, the latter having an IC_{50} equal to 3.45 µg/mL. The mix of carotenoids showed a high IC_{50} (2.39 µg/mL), although being the composition of this fraction not clearly distinguishable, an error

in the estimation of its concentration could have been made. Another possible reason explaining the high antioxidant activity of this fraction could be the co-presence of other bioactive molecules such as phenolic compounds. In order to verify this hypothesis, further analyses are necessary (see section 9.4 Future perspective).

Overall the results demonstrate the antioxidant power of the extracted diatom's pigment diadinoxanthin (Dd) and diatoxanthin (Dt), a feature which until now was only hypothesized but never tested. The higher antioxidant activity of Dt respect to Dd confirms the similar function of this molecule carried out by Zeax in higher plants, which besides its role in physical quenching, it's a chemical trap for ROS and it functions also as membrane stabilizer (Havaux *et al.*, 2007).

9.4. Future perspectives

The beneficial effect of carotenoids on human health as well as their application in food, feed and cosmetic industries gained great attention these years, justifying the improvement of chemical/biological methods for their large-scale production in order to meet the industrial demand (Álvarez *et al.*, 2013, Vandamme & Revuelta, 2016). The production of these compounds from microbial origin compared to chemical synthesis methods represents a more sustainable and environmental-friendly solution (Vandamme & Revuelta, 2016). Unfortunately, industrial production from microalgal origin up to now is strongly limited by the poor yield, hindering the economic feasibility of the process (Borowitzka, 2013). A way for improving carotenoids yield is represented by genetic engineering. However, the biosynthetic pathway of these compounds is not totally clarified, and another problem is associated to the highly restrictive regulatory environment on genetically modified organisms (GMOs) (Lucht, 2015).

Alternatively, improved yield could be achieved by the manipulation of the culturing condition, aiming to enhance the production of microalgal biomass and/or the production of targeted molecules. The know-how gained through the physiological studies carried out by different research groups paves the way to this option. Thus, this knowledge should be used to design new-generation of photobioreactors which by the simple manipulation of

parameters such as light and nutrient concentration could maximize both the biomass and its content of specific products of interests (e.g. carotenoids).

In this chapter, I demonstrated that the aforementioned objectives can be successfully reached: the method used to grow cells maximizing the production of the xanthophyll cycle pigments based solely on the exposure to a high light intensity with a sinusoidal distribution allows the achievement of a high growth rate of cells with a high xanthophyll cycle pigments concentration. The light condition used mirrored a natural-like light climate (which this thesis demonstrates to be better tolerated with respect to unnatural light environment) characterized by medium high intensity, which promoted the synthesis of the photoprotective pigments without affecting growth capacity. The biomass obtained contained high concentration of xanthophyll cycle pigments favoring a good separation, purification and recovery of the target molecules, used for further tests.

The results obtained in this chapter are mainly preliminary and opens the door for complementary studies.

Firstly, the next step aims to confirm the purity of the extracts through liquid chromatography-mass spectrometry (LC/MS) analysis, taking advantage of collaborations with a specialized chemical laboratory. Although HPLC analysis demonstrated the good separation and purity of the pigment extracted, the samples might contain other molecules not visible by the detection at 440 nm used. Therefore, a chemical characterization of the samples is needed in order to assess the purity of the compounds, and therefore on their antioxidant activities.

Once the purity verified, we are interested in investigating the biological activity of the xanthophylls on different cell lines, testing therefore the biotechnological application of these xanthophylls in cosmetics or pharmaceutics field.

Pigments exert numerous biological functions on human health mostly linked to their antioxidant activity (Stahl & Sies, 2005, Zhang *et al.*, 2014, Galasso *et al.*, 2017). It is known that oxidative molecules can be either potentially harmful as well as beneficial cell-signaling molecules which for example activate stress response or are used against infectious agents (Zhang *et al.*, 2014). Anyway, an impairment of redox homeostasis and the accumulation of free radicals cause the oxidative stress, which plays a major role in the development of chronic and degenerative illness (e.g., cancer, autoimmune disorders, aging, cataract, etc.) (Bubici *et al.*, 2006, Pham-Huy *et al.*, 2008). Humans or animals

developed an efficient antioxidant machinery which also depends on exogenous antioxidants obtained from the daily diet. Carotenoids' lipophilic nature allows them to pass through biological membranes reaching different regions of the human body (including the brain by crossing the blood-brain barrier) exerting their biological function (Galasso *et al.*, 2017). They can scavenge radical species by electron transfer, radical adduct formation and hydrogen atom transfer. The beneficial effects of carotenoids are not limited to the direct scavenging of oxidants; it has been proved that they possess many other biological activities acting in more indirect ways: they can interact with cellular signaling cascades modulating transcription (Sharoni *et al.*, 2004, Kaulmann & Bohn, 2014).

It has been demonstrated that carotenoids might interact with the pathway involved in the resistance to oxidants mediated by the nuclear factor erythroid 2-related factor 2 (Nrf2) (Ma, 2013). This transcription factor promotes the gene expression of enzymes with antioxidant and detoxifying functions, protecting cells against oxidative stress and thus carcinogenesis (Itoh *et al.*, 1997, Kwak *et al.*, 2002, Gorrini *et al.*, 2013). For example, Nrf2 is the sole controller of the enzymes responsible for the production of glutathione (GSH), the most abundant antioxidant cofactor within cells (Gorrini *et al.*, 2013). Carotenoids interact with this pathway by removing the Nrf2 repressor in the cytoplasm, allowing its migration into the nucleus, where it binds to the antioxidant responsive elements (ARE), leading to the transcription of the aforementioned enzymes (Kaulmann & Bohn, 2014). The activation of the Nrf2 defense metabolism by natural compounds might offer a greater protection than the antioxidant capacity alone (Foyer & Noctor, 2009).

Yet, it has been proved that carotenoids interfere with the inflammation process (Kaulmann & Bohn, 2014). Although inflammation is a key defending and self-healing process, its chronicity may provoke extensive tissue damage associated with various progressive diseases such as cancer, metabolic disorders, neurodegenerative diseases and so on (Libby, 2007, Pham-Huy *et al.*, 2008). This process involves the production of various inflammatory chemicals such as cytokines, ROS, nitric oxide, and prostaglandins whose regulation is mediated by a transcription factor: the nuclear factor-kB (NF-kB). Its abnormal activation is associated with chronic inflammatory diseases (Zhang *et al.*, 2014). It has been demonstrated that carotenoids can interfere with inflammation pathway by

inhibiting the nuclear translocation of a NF-kB subunit, preventing its activation (Salminen *et al.*, 2008).

All these studies refer to the most common carotenoids extracted from higher plants or some microorganisms. Among these compounds, it has been verified the *in vitro* and *in vivo* biological activity of the carotenoids precursor phytoene, the carotenes lycopene and β-carotene, and the xanthophylls astaxanthin, lutein, zeaxanthin, chantaxanthin, alocynthiaxanthin, fucoxanthin and its derivate fucoxanthinol (reviewed in (Kaulmann & Bohn, 2014, Galasso *et al.*, 2017).

However, no information is available on the xanthophylls diadinoxathin or diatoxanthin from diatoms. It would be thus interesting to assess their biological activity on mammalian cell lines, hypothesizing a direct scavenging activity of oxidant as well as an indirect effect exerted by their interference on the aforementioned pathways. This knowledge has important spillover on biomedical research, being these molecules potential candidates for drug discovery studies. This is a crucial step for the discovery of new products to be launched in the blue biotechnology field and for *de novo* enhancing the role of diatoms into applicative research.

10. General conclusions

The extraordinary ecological success of diatoms, group of organisms which dominates the modern oceans, is generally attributed to their extreme physiological plasticity. Indeed, they are able to grow under the harshest conditions, and are the most successful phytoplankton group in turbulent waters. This ability derives from their dynamic light harvesting systems, able to adjust to the variable light climate and rapidly cope with excess of income energy (Falkowski & Raven, 2013).

Undoubtedly, the key-role of light as one of the most important forces ruling the physiology of photosynthetic organisms is incontrovertible. This form of energy is necessary to reduce the inorganic carbon into carbohydrates, used for the synthesis of the other organic compounds, respiration and so growth. Indeed, the efficiency of biomass production is not only a function of the yield of photosynthetic light reactions, it also depends on the energetic costs of the metabolism, as well as of the defense and repair activities induced by different types of stress.

Light must be considered as a function of its multiple properties such as the instantaneous intensity, the distribution along the daylight, the integrated daily dose and the spectral composition. Therefore, it is not easy to put in direct relation the physiological responses it exerts on living organisms.

The general purpose of this thesis was to improve this knowledge through laboratory experiments which aimed to separate these different properties, and measure what happens to the photosynthetic, photoprotective and antioxidant networks which are simultaneously regulated. The information retrieved from this set of experiments was put in relation with what has been observed in a field experiment carried out in the coastal waters of the Gulf of Naples.

Being the photosynthetic energy flux in dynamic equilibrium with the carbon flux for the synthesis of macromolecules, light is responsible for the carbon allocation patters in cells (Wagner *et al.*, 2017). So, the first set of experiment reported in this thesis aimed to see whether and to what extent the light spectrum controls the carbon metabolism, determining a spectral-dependent synthesis and accumulation of macromolecules. It was found that the co-presence of blue and red light was able to increase the carbohydrate content without substantially altering the total production of proteins and lipids. Also, the light spectrum,

although not greatly modulating the lipid concentration, was able to modify their composition: the presence of red together with blue favored the synthesis of saturated fatty acids. Being this class of lipid the most stable towards oxidation, their higher presence means that cells were acclimated to the fluctuating light environment being less susceptible to lipid peroxidation.

By contrast, the square-wave light treatment, which foresaw the exposition to pure blue light, determined the dominance of the polyunsaturated fatty acids (PUFA). The fact that under this higher light treatment the most represented lipids were also the most vulnerable to the oxidative stress seems nonsense. Anyway, PUFA are precursors of signaling molecules, so they were probably involved in stress responses. In fact, although showing photophysiological alterations, cells exposed to this light treatment were still able to grow and did not show photoinhibition, in spite of a low non-photochemical quenching (NPQ) capacity.

A possible explanation to the absence of photoinhibition was probably the involvement of one other key-player of cell physiology: the antioxidant network. The transcriptional levels of the antioxidant enzymes did not change consistently, even though the light spectrum composition strongly influences these enzymes. In fact, they were activated in presence of both blue and red light and inhibited by the monospectral blue light, notwithstanding the comparable light intensity, implying a possible role of the photoreceptor signaling.

The blue light instead induced an increased production of an important class of antioxidants: the phenolic compounds.

Skeletonema marinoi turned out to be a rich source of these compounds, one of the most widespread substances in plants showing antioxidant activity, able to act both directly against radical species as well as indirectly *via* the inhibition of pro-oxidant enzymes such as lipoxygenase or through metal chelation, preventing the occurrence of the Haber-Weiss and the Fenton reactions, important sources of radical species (Quideau *et al.*, 2011).

These molecules reached under intermediate-high blue light (300 µmol photons m^{-2} s^{-1}) a concentration of *circa* 700 fg gallic acid equivalents (GAE) $cell^{-1}$, while under the pre-acclimation condition used during my work the concentration was around 300 GAE $cell^{-1}$. High similar concentration was reached when cells were suddenly exposed to a very high light (square-wave light course, with a PDF equal to 600 µmol photons m^{-2} s^{-1}). Interestingly, the latter spectral light condition (R:G:B equal to 10:40:50) has the similar

contribution of blue light to the former experiment (300 µmol photons m^{-2} s^{-1}), strengthening the idea of a blue light intensity-dependent regulation of this class of compounds.

As expected, not only environmental forcing controls the concentration of these molecules, but, also the physiological state of the cells. Indeed, high antioxidant molecules were found in senescent/dying cells, with an increase from the healthy state up to *circa* 3.5 times.

Also, *S. marinoi* highly synthesized these molecules when shifted to very low light, with a photoperiod of 24:0 light:dark. Concentration in this case became higher than 1500 fg GAE $cell^{-1}$. Probably, cells invest in the synthesis of these molecules to counteract the detrimental effect of the radical species at the chloroplast level, allowing the maintaining of a good photosynthetic performance, as visible by the high photochemical efficiency measured. Since under dark or very low light with a sinusoidal distribution and a photoperiod of 12:12 h light:dark, these compounds did not increase, keeping values between 200 and 300 fg GAE $cell^{-1}$, the main factor responsible for such huge concentration of these compounds might be the absence of dark period.

Thus, I can conclude that light is one of the environmental forcing driving phenolic compounds synthesis in *S. marinoi*. High light (instantaneous and integrated over time) induces an increase of these compounds, as also confirmed by the mesocosm experiment, where it was measured a higher content of these compounds at surface compared to depth. Also, their concentration is enhanced by the blue light and by the absence of a dark period.

Among this class, recent findings demonstrated diatoms' ability to produce flavonoids (Goiris *et al.*, 2015). These molecules are important antioxidant, exerting this function with the aforementioned mechanisms, and can also act as signaling molecules able to up-regulate the defense strategies (Pietta, 2000, Goiris *et al.*, 2015). They show different localizations inside the cells, and due to their presence in chloroplasts, these compounds are considered as important photoprotectors, scavenging radical species and stabilizing membranes containing non-bilayer lipids such as monogalactosyldiacylglycerol (MGDG) (Agati *et al.*, 2013).

Indeed, flavonoids seem to be related to photosynthesis and photoprotection, as revealed by the significant link between them and the photochemical efficiency during the mesocosm experiment.

Flavonoids concentration showed the same trend observed for the phenolic compounds, displaying light-dependent infradiel variations and enhanced synthesis during cell senescence up to *circa* 400 fg quercetin equivalent (QEq) $cell^{-1}$.

One other important actor of the antioxidant network is the ascorbic acid (AsA), which is a hydrophilic compound able to directly neutralize reactive species, reduce other oxidized compounds such as tocopherols and phenolic compounds, and function as electron donor for different enzymes such as ascorbate peroxidase (APX), and violaxanthin de-epoxidase (VDE), the enzyme responsible for the conversion of diadinoxanthin (Dd) into diatoxanthin (Dt) in diatoms (see chapter 1).

AsA appears to be controlled by different properties of the light. The blue light with a PDF equal to 500 µmol photons m^{-2} s^{-1} determined an enhancement in its concentration up to *circa* 400 fg $cell^{-1}$, while during the pre-acclimation condition it was lower than 100 fg $cell^{-1}$. Like the phenolic compounds, it followed an infradiel variation with higher midday values respect to pre-dawn, dependent on the direct light stimulus and not due to an endogenous regulation, as demonstrated by the results of cells' exposure to prolonged darkness. It accumulated in senescent/dying cells, reaching a concentration between 200 and 300 fg $cell^{-1}$, while during the exponential phase it showed values around 100 fg $cell^{-1}$. This increase, together with the presence of the other antioxidants, probably allowed the maintaining of a good photosynthetic performance despite the stressful condition by preventing the oxidation of the photosystems.

Indeed, all the aforementioned molecules were responsible for the total antioxidant activity measured in the cells, as visible by the positive correlation among these parameters and the ABTS test.

The xanthophylls, key-elements of the photoprotective processes in diatoms, are also active players of the antioxidant network.

In fact, the xanthophyll cycle pigments Dd and Dt were correlated with the antioxidant compounds as well as with the ABTS test. Furthermore, it was frequently observed a mismatch between the concentration of these pigments and the NPQ development, strengthening the hypothesis of the additional antioxidant role of these compounds, beyond the involvement of Dt in the quenching of excess energy.

These pigments were strongly dependent on the light experienced. The spectral quality as well as the intensity controlled Dt concentration: at low blue fluence rate it was scarce or

even undetected. Instead, the co-presence of red light induced its synthesis. A blue PDF equal or higher than 300 µmol photons m^{-2} s^{-1} was able to increase this pigment up to almost 20 fg $cell^{-1}$. Also the light shape distribution influenced the accumulation of this xanthophyll: under the square-wave light courses Dt was higher respect to the other conditions, reaching a value of *circa* 40 fg $cell^{-1}$ after the exposure to a quadratic light peaking at 300 µmol photons m^{-2} s^{-1}. Like the antioxidant molecules, this pigment accumulated in senescent/dying cells, where it probably exerted the same function of scavenger of radical species. As hypothesized, these pigments showed a high antioxidant activity, and a necessary next step to be undertaken in the immediate future would be the testing for their bioactivity on mammalian systems.

In conclusion, my work demonstrates that diatoms are a good model for obtaining and optimizing the production of bioactive molecules. It is possible to control the synthesis of different compounds such as pigments and antioxidants through the manipulation of the light environment, being these molecules involved in the photoprotective response.

It is interesting to notice that the conditions which allowed the best growth performance and photophysiological state of cells were the ones most close to the natural environment. This feature indicates that diatoms developed acclimation and regulation processes which allow them to survive to the natural fluctuations they may experience in the water column. By contrast, the completely unnatural light conditions such as the continuous or the square-wave light courses impaired the normal cell functioning and the biological processes subsequent to the light capture, leading generally to culture collapse.

This represents a key-discovery which has important spillover on the biotechnological exploitation of these organisms. In fact, in order to cut the costs of microalgal bioproducts manufacturing, the main problem which has to be solved is the optimization of the culturing condition which allows at the same time to obtain of a high quantum yield of growth and to maximize of the concentration of the desired product.

Therefore, this aspect must be considered for the design of efficient enclosed photobioreactors. In this way it will be possible to boost microalgal cultivation and subsequent exploitation in numerous fields such as the pharmacologic, cosmetic, nutraceutic and biofuel industries only by light modulation.

BIBLIOGRAPHY

Aebi, H. 1984. Catalase *in vitro*. *Method Enzymol* **105**:121–26.

Agati, G., Brunetti, C., Di Ferdinando, M., Ferrini, F., Pollastri, S. & Tattini, M. 2013. Functional roles of flavonoids in photoprotection: new evidence, lessons from the past. *Plant Physiol Biochem* **72**:35-45.

Agati, G. & Tattini, M. 2010. Multiple functional roles of flavonoids in photoprotection. *New Phytol* **186**:786-93.

Allen, A., Vardi, A. & Bowler, C. 2006. An ecological and evolutionary context for integrated nitrogen metabolism and related signaling pathways in marine diatoms. *Curr Opin Plant Biol* **9**:264-73.

Álvarez, R., Vaz, B., Gronemeyer, H. & de Lera, A. R. 2013. Functions, therapeutic applications, and synthesis of retinoids and carotenoids. *Chem Rev* **114**:1-125.

Amin, L., Jahi, J. M. & Nor, A. R. M. 2013. Stakeholders' attitude to genetically modified foods and medicine. *Scientific World J* **516742**:1-14.

Andersen, C. L., Jensen, J. L. & Ørntoft, T. F. 2004. Normalization of real-time quantitative reverse transcription-PCR data: a model-based variance estimation approach to identify genes suited for normalization, applied to bladder and colon cancer data sets. *Cancer Res* **64**:5245-50.

Andersen, R. A. 1992. Diversity of eukariotic algae. *Biodivers Conserv* **1**:267-92.

Andersson, M., Van Niewerburgh, L. & Snoeijs, P. 2003. Pigment trasfer from phytoplankton to zooplankton with emphasis on astaxanthin prodiction in the Baltic Sea food web. *Mar Ecol Prog Ser* **254**:213-24.

Anning, T., MacIntyre, H. L., Pratt, S. M., Sammes, P. J., Gibb, S. & Geider, R. J. 2000. Photoacclimation in the marine diatom *Skeletonema costatum*. *Limnol Oceanogr* **45**:1807-17.

Armbrust, E. 2009. The life of diatoms in the world's oceans. *Nature* **459**:185 - 92.

Armbrust, E., Berges, J., Bowler, C., Green, B., Martinez, D., Putnam, N., Zhou, S., Allen, A., Apt, K., Bechner, M., Brzezinski, M., Chaal, B., Chiovitti, A., Davis, A., Demarest, M., Detter, J., Glavina, T., Goodstein, D., Hadi, M., Hellsten, U., Hildebrand, M., Jenkins, B., Jurka, J., Kapitonov, V., Kroger, N., Lau, W., Lane, T., Larimer, F., Lippmeier, J. & Lucas, S. 2004. The genome of the diatom Thalassiosira pseudonana: Ecology, evolution, and metabolism. *Science* **306**:79 - 86.

Asada, K. 1999. The water-water cycle in chloroplasts: scavenging of active oxygens and dissipation of excess photons. *Annu Rev Plant Physiol Plant Mol Biol* **50**:601–39.

Ashworth, J., Coesel, S., Lee, A., Armbrust, E. V., Orellana, M. V. & Baliga, N. S. 2013. Genome-wide diel growth state transitions in the diatom *Thalassiosira pseudonana*. *Proc Nat Acad Sci USA* **110**:7518–23.

Bailleul, B., Rogato, A., de Martino, A., Coesel, S., Cardol, P., Bowler, C., Falciatore, A. & Finazzi, G. 2010. An atypical member of the light-harvesting complex stress-related protein family modulates diatom responses to light. *Proc Natl Acad Sci USA* **107**:18214 - 19.

Ballottari, M., Truong, T., De Re, E., Erickson, E., Stella, G., Fleming, G., Bassi, R. & Niyogi, K. 2016. Identification of pH-sensing sites in the Light Harvesting Complex Stress-Related 3 protein essential for triggering non-photochemical quenching in *Chlamydomonas reinhardtii*. *J Biol Chem* **291**:7334–46.

Barbarino, E. & Lourenço, S. O. 2005. An evaluation of methods for extraction and quantification of protein from marine macro-and microalgae. *J. Appl. Phycol.* **17**:447-60.

Barofsky, A., Simonelli, P., Vidoudez, C., Troedsson, C., Nejstgaard, J. C., Jakobsen, H. H. & Pohnert, G. 2010. Growth phase of the diatom Skeletonema marinoi influences the metabolic profile of the cells and the selective feeding of the copepod Calanus spp. *J Plankton Res* **32**:263-72.

Barra, L., Chandrasekaran, R., Corato, F. & Brunet, C. 2014. The challenge of ecophysiological biodiversity for biotechnological applications of marine microalgae. *Mar Drugs* **12**:1641-75.

Barra, L., Ruggiero, M. V., Sarno, D., Montresor, M. & Kooistra, W. C. H. F. 2013. Strengths and weaknesses of microarray approaches to detect *Pseudo-nitzschia* species in the field. *Environ Sci Pollut R* **20**:6705-18.

Bassham, J. A. 2003. Mapping the carbon reduction cycle, a personal retrospective. *Photosynth Res* **76**:35-52.

Beardall, J., Quigg, A. & Raven, J. A. 2003. Oxygen consumption: photorespiration and chlororespiration. *In*: Larkum, A. W. D., Douglas, S. E. & Raven, J. [Eds.] *Photosynthesis in algae - Advances in photosynthesis and respiration.* Kluwer Academic Publishers, pp. 157-81.

Beer, A., Gundermann, K., Beckmann, J. & Büchel, C. 2006. Subunit composition and pigmentation of fucoxanthin-chlorophyll proteins in diatoms: evidence for a subunit involved in diadinoxanthin and diatoxanthin binding. *Biochemistry* **45**:13046-53.

Begara-Morales, J. C., Sánchez-Calvo, B., Chaki, M., Valderrama, R., Mata-Pérez, C., López-Jaramillo, J., Padilla, M. N., Carreras, A., Corpas, F. J. & Barroso, J. B. 2014. Dual regulation of cytosolic ascorbate peroxidase (APX) by tyrosine nitration and S-nitrosylation. *J Exp Bot* **65**:527-38.

Begum, H., Yusoff, F., Banerjee, S., Khatoon, H. & Shariff, M. 2016. Availability and utilization of pigments from microalgae. *Crit Rev Food Sci Nutr* **56**:2209-22.

Bell-Pedersen, D., Cassone, V. M., Earnest, D. J., Golden, S. S., Hardin, P. E., Thomas, T. L. & Zoran, M. J. 2005. Circadian rhythms from multiple oscillators: lessons from diverse organisms. *Nat Rev Genet* **6**:544–56.

Bellou, S., Baeshen, M. N., Elazzazy, A. M., Aggeli, D., Sayegh, F. & Aggelis, G. 2014. Microalgal lipids biochemistry and biotechnological perspectives. *Biotechnol Adv* **32**:1476-93.

Bengtson, S., Sallstedt, T., Belivanova, V. & Whitehouse, M. 2017. Three-dimensional preservation of cellular and subcellular structures suggests 1.6 billion year-old crown-group red algae. *PLoS Biol* **15**:e2000735.

Benson, A. A. 2002. Paving the path. *Annu Rev Plant Biol* **53**:1-23.

Berry, J. P., Gantar, M., Perez, M. H., Berry, G. & Noriega, F. G. 2008. Cyanobacterial toxins as allelochemichals with potential applications as algaecides, herbicides and insecticides. *Mar Drugs* **6**:117-46.

Bertrand, M. 2010. Carotenoid biosynthesis in diatoms. *Photosynth Res* **106**:89-102.

Bidle, K. D. & Bender, S. J. 2008. Iron starvation and culture age activate metacaspases and programmed cell death in the marine diatom *Thalassiosira pseudonana*. *Eukaryot Cell* **7**:223-36.

Bidle, K. D. & Falkowski, P. G. 2004. Cell death in planktonic, photosynthetic microorganisms. *Nat Rev Microbiol* **2**:643-55.

Bidle, K. D. & Vardi, A. 2011. A chemical arms race at sea mediates algal host–virus interactions. *Curr Opin Microbiol* **14**:449-57.

Bienert, G. P., Møller, A. L. B., Kristiansen, K. A., Schulz, A., Møller, I., Schjoerring, J. & Jahn, T. 2007. Specific aquaporins facilitate the diffusion of hydrogen peroxide across membranes. *J Biol Chem* **282**:1183–92.

Bilger, W., Rimke, S., Schreiber, U. & Lange, O. 1989. Inhibition of energy-transfer to photosystem II in lichens by dehydration: different properties of reversibility with green and blue-green phycobionts. *J Plant Physiol* **134**:261–68.

Bína, D., Herbstová, M., Gardian, Z., Vácha, F. & Litvín, R. 2016. Novel structural aspect of the diatom thylakoid membrane: lateral segregation of photosystem I under red-enhanced illumination. *Sci Rep* **6**:1-10.

Boon, C. S., McClements, D. J., Weiss, J. & Decker, E. A. 2010. Factors influencing the chemical stability of carotenoids in foods. *Crit Rev Food Sci Nutr* **50**:515-32.

Borowitzka, M. A. 1995. Microalgae as sources of pharmaceuticals and other biologically active compounds. *J Appl Phycol* **7**:3-15.

Borowitzka, M. A. 2013. High-value products from microalgae—their development and commercialisation. *J Appl Phycol* **25**:743-56.

Bowler, C., Allen, A. E., Badger, J. H., Grimwood, J., Jabbari, K., Kuo, A., Maheswari, U., Martens, C., Maumus, F., Otillar, R. P., Rayko, E., Salamov, A., Vandepoele, K., Beszteri, B., Gruber, A., Heijde, M., Katinka, M., Mock, T., Valentin, K., Verret, F., Berges, J. A., Brownlee, C., Cadoret, J.-P., Chiovitti, A., Choi, C. J., Coesel, S., De Martino, A., Detter, J. C., Durkin, C., Falciatore, A., Fournet, J., Haruta, M., Huysman, M. J. J., Jenkins, B. D., Jiroutova, K., Jorgensen, R. E., Joubert, Y., Kaplan, A., Kröger, N., Kroth, P. G., La Roche, J., Lindquist, E., Lommer, M., Martin–Jézéquel, V., Lopez, P. J., Lucas, S., Mangogna, M., McGinnis, K., Medlin, L. K., Montsant, A., Marie-Pierre, Oudot–Le Secq, M.-P., Napoli, C., Obornik, M., Schnitzler Parker, M., Petit, J.-L., Porcel, B. M., Poulsen, N., Robison, M.,

Rychlewski, L., Rynearson, T. A., Schmutz, J., Shapiro, H., Siaut, M., Stanley, M., Sussman, M. R., Taylor, A. R., Vardi, A., von Dassow, P., Vyverman, W., Willis, A., Wyrwicz, L. S., Rokhsar, D. S., Weissenbach, J., Armbrust, E. V., Green, B. R., Van de Peer, Y. & Grigoriev, I. V. 2008. The *Phaeodactylum* genome reveals the evolutionary history of diatom genomes. *Nature* **456**:239-44.

Bowler, C., De Martino, A. & Falciatore, A. 2010a. Diatom cell division in an environmental context. *Curr Opin Plant Biol* **13**:623-30.

Bowler, C., Karl, D. M. & Colwell, R. R. 2009. Microbial oceanography in a sea of opportunity. *Nature* **459**:180-84.

Bowler, C., Vardi, A. & Allen, A. 2010b. Oceanographic and biogeochemical insights from diatom genomes. *Annu Rev Marine Sci* **2**:333 - 65.

Bozarth, A., Maier, U.-G. & Zauner, S. 2009. Diatoms in biotechnology: modern tools and applications. *Appl Microbiol Biotechnol* **82**:195-201.

Britton, G. 1995. Structure and properties of carotenoids in relation to function. *FASEB J* **9**:1551-58.

Brooks, J. L. & Dodson, S. I. 1965. Predation, body size, and composition of plankton. *Science* **150**:28–35.

Brown, M. R. & Miller, K. A. 1992. The ascorbic acid content of eleven species of microalgae used in mariculture. *J Appl Phycol* **4**:205-15.

Brunet, C., Casotti, R., Vantrepotte, V., Corato, F. & Conversano, F. 2006. Picophytoplankton diversity and photoacclimation in the Strait of Sicily (Mediterranean Sea) in summer. I. Mesoscale variations. *Aquat Microb Ecol* **44**:127-41.

Brunet, C., Chandrasekaran, R., Barra, L., Giovagnetti, V., Corato, F. & Ruban, A. V. 2014. Spectral radiation dependent photoprotective mechanism in the diatom *Pseudo-nitzschia multistriata*. *PLoS ONE* **9**:e87015.

Brunet, C., Conversano, F., Margiotta, F., Dimier, C., Polimene, L., Tramontano, F. & Saggiomo, V. 2013. The role of light and photophysiological properties on phytoplankton succession during the spring bloom in the North Western Mediterranean sea. *AIOL* **4**:1-19.

Brunet, C., Johnsen, G., Lavaud, J. & Roy, S. 2011. Pigments and photoacclimation processes. *In*: Roy, S., Llewellyn, C. A., Egeland, E. S. & Johnsen, G. [Eds.] *Phytoplankton Pigments. Characterization, Chemotaxonomy and Applications in Oceanography.* Cambridge University Press, pp. 445-71.

Bubici, C., Papa, S., Dean, K. & Franzoso, G. 2006. Mutual cross-talk between reactive oxygen species and nuclear factor-kappa B: molecular basis and biological significance. *Oncogene* **25**:6731-48.

Büchel, C. 2015. Evolution and function of light harvesting proteins. *J Plant Physiol* **172**:62-75.

Cai, Y., Luo, Q., Sun, M. & Corke, H. 2004. Antioxidant activity and phenolic compounds of 112 traditional Chinese medicinal plants associated with anticancer. *Life Sci* **74**:2157–84.

Cardozo, K. H. M., Guaratini, T., Barros, M. P., Falcão, V. R., Tonon, A. P., Lopes, N. P., Campos, S., Torres, M. A., Souza, A. O., Colepicolo, P. & Pinto, E. 2007. Metabolites from algae with economical impact. *Comp Biochem Physiol C Toxicol Pharmacol* **146**:60–78.

Cartaxana, P., Domingues, N., Cruz, S., Jesus, B., Laviale, M., Serodio, J. & Marques da Silva, J. 2013. Photoinhibition in benthic diatom assemblages under light stress. *Aquat Microb Ecol* **70**:87-92.

Casotti, R., Mazza, S., Brunet, C., Vantrepotte, V., Ianora, A. & Miralto, A. 2005. Growth inhibition and toxicity of the diatom aldehyde 2-trans, 4-trans-decadienal on *Thalssiosira weissflogii* (Bacillariophyceae). *J Phycol* **41**:7-20.

Chandrasekaran, R., Barra, L., Carillo, S., Caruso, T., Corsaro, M. M., Dal Piaz, F., Graziani, G., Corato, F., Pepe, D., Manfredonia, A., Orefice, I., Ruban, A. V. & Brunet, C. 2014. Light modulation of biomass and macromolecular composition of the diatom *Skeletonema marinoi*. *J Biotechnol* **192, Part A**:114-22.

Chen, T., Liu, J., Guo, B., Ma, X., Sun, P., Liu, B. & Chen, F. 2015. Light attenuates lipid accumulation while enhancing cell proliferation and starch synthesis in the glucose-fed oleaginous microalga *Chlorella zofingiensis*. *Sci Rep* **5**:14936.

Cheynier, V., Comte, G., Davies, K. M., Lattanzio, V. & Martens, S. 2013. Plant phenolics: recent advances on their biosynthesis, genetics, and ecophysiology. *Plant Physiol Biochem* **72**:1-20.

Cirulis, J., Scott, J. & Ross, G. 2013. Management of oxidative stress by microalgae. *Can J Physiol Pharmacol* **91**:15-21.

Claquin, P., Kromkamp, J. C. & Martin-Jezequel, V. 2004. Relationship between photosynthetic metabolism and cell cycle in a synchronized culture of the marine alga *Cylindrotheca fusiformis* (Bacillariophyceae). *Eur J Phycol* **39**:33-41.

Clemens, P. & Christian, W. 2013. *Microalgal biotechnology: potential and production.* De Gruyter, Berlin, 266.

Cleveland, J. S. & Weidemann, A. D. 1993. Quantifying absorption by aquatic particles: A multiple scattering correction for glass-fiber filters. *Limnol Oceanogr* **38**:1321-27.

Coesel, S., Mangogna, M., Ishikawa, T., Heijde, M., Rogato, A., Finazzi, G., Todo, T., Bowler, C. & Falciatore, A. 2009. Diatom PtCPF1 is a new cryptochrome/photolyase family member with DNA repair and transcription regulation activity. *Embo Reports* **10**:655-61.

Coesel, S., Obornik, M., Varela, J., Falciatore, A. & Bowler, C. 2008. Evolutionary origins and functions of the carotenoid biosynthetic pathway in marine diatoms. *PLoS ONE* **3**:e2896.

Cohen, P. T. W. 2010. Sorting the protein phosphatases: okadaic acid led the way. *Biochem J* **256**:1-5.

Consalvey, C., Perkins, R. G., Paterson, D. M. & Underwood, G. 2005. PAM fluorescence: a beginners guide for benthic diatomists. *Diatom res* **20**:1–22.

Cruz, S., Goss, R., Wilhelm, C., Leegood, R., Horton, P. & Jakob, T. 2010. Impact of chlororespiration on non-photochemical quenching of chlorophyll fluorescence and on the regulation of the diadinoxanthin cycle in the diatom *Thalassiosira pseudonana*. *J Exp Bot* **62**:509-19.

Dambek, M., Eilers, U., Breitenbach, J., Steiger, S., Büchel, C. & Sandmann, G. 2012. Biosynthesis of fucoxanthin and diadinoxanthin and function of initial pathway genes in *Phaeodactylum tricornutum*. *J Exp Bot* **63**:5607–12.

Danovaro, R. 1998. Do bacteria compete with phytoplankton for inorganic nutrients? Possible ecological implications. *Chem Ecol* **14**:83-96.

de Jesus Raposo, M. F., de Morais, A. M. B. & de Morais, R. M. S. C. 2015. Marine polysaccharides from algae with potential biomedical applications. *Mar Drugs* **13**:2967-3028.

Demmig-Adams, B. & Adams III, W. 2006. Photoprotection in an ecological context:the remarkable complexity of thermal energy dissipation. *New Phytol* **172**:11-21.

Demmig-Adams, B., Garab, G., Adams III, W. & Govindjee 2014. *Non-photochemical quenching and energy dissipation in plants, algae and cyanobacteria.* Springer Netherlands, 645.

Depauw, F., Rogato, A., Ribera d'Alcalà, M. & Falciatore, A. 2012. Exploring the molecular basis of response to light in marine diatoms. *J Exp Bot* **63**:1575–91.

Derks, A., Schaven, K. & Bruce, D. 2015. Diverse mechanisms for photoprotection in photosynthesis. Dynamic regulation of photosystem II excitation in response to rapid environmental change. *BBA Bioenergetics* **1847**:468-85.

Di Dato, V., Orefice, I., Amato, A., Fontanarosa, C., Amoresano, A., Cutignano, A., Ianora, A. & Romano, G. 2017. Animal-like prostaglandins in marine microalgae. *ISME J* **11**:1722-26.

Dimier, C., Giovanni, S., Ferdinando, T. & Brunet, C. 2009. Comparative ecophysiology of the xanthophyll cycle in six marine phytoplanktonic species. *Protist* **160**:397-411.

Diner, B. A. & Babcock, G. T. 1996. Structure, dynamics and energy conversion efficiency in photosystem II. *In*: Ort, D. & Yocum, C. [Eds.] *Oxygenic photosynthesis: the light reactions.* Kluwer Academic Publishers, Dordrecht, pp. 137–64.

Dodd, A. N., Salathia, N., Hall, A., Kévei, E., Tóth, R., Nagy, F., Hibberd, J. M., Millar, A. J. & Webb, A. A. 2005. Plant circadian clocks increase photosynthesis, growth, survival, and competitive advantage. *Science* **309**:630-33.

Dong, H.-P., Dong, Y.-L., Cui, L., Balamurugan, S., Gao, J., Lu, S.-H. & Jiang, T. 2016. High light stress triggers distinct proteomic responses in the marine diatom *Thalassiosira pseudonana*. *BMC Genomics* **17-994**:1-14.

Dubinsky, Z. & Stambler, N. 2009. Photoacclimation processes in phytoplankton: Mechanisms, consequences, and applications. *Aquat Microb Ecol* **56**:163–76.

Dunahay, T. G., Jarvis, E. E. & Roessler, P. G. 1995. Genetic transformation of the diatoms *Cyclotella cryptica* and *Navicula saprophila*. *J Phycol* **31**:1004-12.

Duval, B., Shetty, K. & Thomas, W. H. 2000. Phenolic compounds and antioxidant properties in the snow alga *Chlamydomonas nivalis* after exposure to UV light. *J Appl Phycol* **11**:559-66.

Eilers, P. H. C. & Peeters, J. C. H. 1988. A model for the relationship between light intensity and the rate of photosynthesis in phytoplankton. *Ecol Modell* **42**:199-215.

Elser, J. J., Gudex, L., Kyle, M., Ishikawa, T. & Urabe, J. 2001. Effects of zooplankton on nutrient availability and seston C: N: P stoichiometry in inshore waters of Lake Biwa, Japan. *Limnology* **2**:91-100.

Enzing, C., Ploeg, M., Barbosa, M. & Sijtsma, L. 2014. Microalgae-based products for the food and feed sector: an outlook for Europe. *In*: Vigani, M., Parisi, C. & Cerezo, E. R. [Eds.] *JRC Scientific and policy reports.*

Erickson, E., Wakao, S. & Niyogi, K. K. 2015. Light stress and photoprotection in *Chlamydomonas reinhardtii*. *Plant J* **82**:449-65.

Everette, J. D., Bryant, Q. M., Green, A. M., Abbey, Y. A., Wangila, G. W. & Walker, R. B. 2010. Thorough study of reactivity of various compound classes toward the Folin− Ciocalteu reagent. *J Agric Food Chem* **58**:8139-44.

Falkowski, P., Katz, M. E., Knoll, A. H., Quigg, A., Raven, J. A., Schofield, O. & Taylor, F. J. R. 2004. The evolution of modern eucaryotic phytoplankton. *Science* **305**:354-60.

Falkowski, P. G. & Owens, T. G. 1980. Light-shade adaptation: two strategies in marine phytoplankton. *Plant Physiol* **66**:592–95.

Falkowski, P. G. & Raven, J. A. 1997. *Aquatic photosynthesis.* Princeton University Press,

Falkowski, P. G. & Raven, J. A. 2013. *Aquatic photosynthesis.* Princeton University Press, 465.

FAO 1996. Micro-algae. *In*: Lavens, P. & Sorgeloos, P. [Eds.] *Manual on the production and use of live food for aquaculture.* FAO, Rome.

Field, C. B., Behrenfeld, M. J., Randerson, J. T. & Falkowski, P. 1998. Primary production of the biosphere: integrating terrestrial and oceanic components. *Science* **281**:237–40.

Fields, M. W., Hise, A., Lohman, E. J., Bell, T., Gardner, R. D., Corredor, L., Moll, K., Peyton, B. M., Characklis, G. W. & Gerlach, R. 2014. Sources and resources: importance of nutrients, resource allocation, and ecology in microalgal cultivation for lipid accumulation. *Appl Microbiol Biotechnol* **98**:4805–16.

Finazzi, G., Moreau, H. & Bowler, C. 2010. Genomic insights into photosynthesis in eukaryotic phytoplankton. *Trends Plant Sci* **15**:565-72.

Fortunato, A. E., Jaubert, M., Enomoto, G., Bouly, J.-P., Raniello, R., Thaler, M., Malviya, S., Bernardes, J. S., Rappaport, F., Gentili, B., Huysman, M. J. J., Carbone, A., Bowler, C., Ribera d'Alcalà, M., Ikeuchi, M. & Falciatore, A. 2016. Diatom phytochromes reveal the existence of far-red-light-based sensing in the ocean. *Plant Cell* **28**:616-28.

Foyer, C. & Noctor, G. 2005a. Oxidant and antioxidant signalling in plants: a re-evaluation of the concept of oxidative stress in a physiological context. *Plant Cell Environ* **28**:1056–71.

Foyer, C. & Noctor, G. 2005b. Redox homeostasis and antioxidant signaling: a metabolic interface between stress perception and physiological responses. *Plant Cell Environ* **17**:1866–75.

Foyer, C. H. & Noctor, G. 2009. Redox regulation in photosynthetic organisms: signaling, acclimation, and practical implications. *Antioxid Redox Signal* **11**:861-905.

Foyer, C. H. & Noctor, G. 2011. Ascorbate and glutathione: the heart of the redox hub. *Plant Physiol* **155**:2-18.

Foyer, C. H. & Shigeoka, S. 2011. Understanding oxidative stress and antioxidant functions to enhance photosynthesis. *Plant Physiol* **155**:93-100.

Gadjev, I., Vanderauwera, S., Gechev, T. S., Laloi, C., Minkov, I. N., Shulaev, V., Apel, K., Inzé, D., Mittler, R. & Van Breusegem, F. 2006. Transcriptomic footprints disclose specificity of reactive oxygen species signaling in *Arabidopsis*. *Plant Physiol* **141**:436-45.

Galasso, C., Corinaldesi, C. & Sansone, C. A., 6(4), 96. 2017. Carotenoids from marine organisms: biological functions and industrial applications. *Antioxidants* **6**:96.

Genty, B., Briantais, J.-M. & Baker, N. R. 1989. The relationship between the quantum yield of photosynthetic electron transport and quenching of chlorophyll fluorescence. *Biochim Biophys Acta* **990**:87–92.

Gibson, J. H. 2000. UVB Radiation: definition and characteristics. *In UV-B Monitoring and Research Program.* Retrieved from http://uvb.nrel.colostate.edu/UVB/publications/uvb_primer.pdf, Colorado.

Giovagnetti, V., Brunet, C., Conversano, F., Tramontano, F., Obernosterer, I., Ridame, C. & Guieu, C. 2013. Assessing the role of dust deposition on phytoplankton ecophysiology and succession in a low-nutrient low-chlorophyll ecosystem: a mesocosm experiment in the Mediterranean sea. *Biogeosciences* **10**:2973–91.

Giovagnetti, V., Flori, S., Tramontano, F., Lavaud, J. & Brunet, C. 2014. The velocity of light intensity increase modulates the photoprotective response in coastal diatoms. *Plos ONE* **9**:e103782.

Giovagnetti, V. & Ruban, A. 2017. Detachment of the fucoxanthin chlorophyll a/c binding protein (FCP) antenna is not involved in the acclimative regulation of photoprotection in the pennate diatom *Phaeodactylum tricornutum*. *Biochim Biophys Acta* **1858**:218-30.

Godhe, A. 2017. *Skeletonema marinoi*. University of Gothenburg, http://cemeb.science.gu.se/research/target-species-imago%20/skeletonema-marinoi.

Godhe, A., Kremp, A. & Montresor, M. 2014. Genetic and microscopic evidence for sexual reproduction in the centric diatom *Skeletonema marinoi*. *Protist* **165**:401-16.

Goiris, K., Muylaert, K., Fraeye, I., Foubert, I., Brabanter, J. D. & Cooman, L. D. 2012. Antioxidant potential of microalgae in relation to their phenolic and carotenoid content. *J Appl Phycol* **24**:1477–86.

Goiris, K., Van Colen, W., Wilches, I., León-Tamariz, F., De Cooman, L. & Muylaert, K. 2015. Impact of nutrient stress on antioxidant production in three species of microalgae. *Algal Res* **7**:51-57.

Gorrini, C., Harris, I. S. & Mak, T. W. 2013. Modulation of oxidative stress as an anticancer strategy. *Nat Rev Drug Discov* **12**:931-47.

Goss, R. & Jakob, T. 2010. Regulation and function of xanthophyll cycle-dependent photoprotection in algae. *Photosynth Res* **106**:103-22.

Goss, R. & Lepetit, B. 2015. Biodiversity of NPQ. *J Plant Physiol* **172**:13-32.

Goss, R., Pinto, E., Wilhelm, C. & Richter, M. 2006. The importance of a highly active and ΔpH-regulated diatoxanthin epoxidase for the regulation of the PS II antenna functionin diadinoxanthin cycle containing algae. *J Plant Physiol* **163**:1008-21.

Gouveia, L., Marques, A. E., Sousa, J. M., Moura, P. & Bandarra, N. M. 2010. Microalgae – source of natural bioactive molecules as functional ingredients. *Food Sci Tech Bull Funct Foods* **7**:21-37.

Grasshoff, K., Kremling, K. & Erhrhardt, M. 2009. *Methods of seawater analysis.* Wiley-VCH, New York, 632.

Graziani, G., Schiavo, S., Nicolai, M. A., Buono, S., Fogliano, V., Pinto, G. & Pollio, A. 2013. Microalgae as human food: chemical and nutritional characteristics of the thermo-acidophilic microalga Galdieria sulphuraria. *Food Funct* **4**:144-52.

Grobbelaar, J. U. 2013. Mass production of microalgae at optimal photosynthetic rates. *In*: Dubinsky, Z. [Ed.] *Photosynthesis.* Intech, pp. 357-71.

Grouneva, I., Jakob, T., Wilhelm, C. & Goss, R. 2006. Influence of ascorbate and pH on the activity of the diatom xanthophyll cycle-enzyme diadinoxanthin de-epoxidase. *Physiol Plant* **126**:205–11.

Grouneva, I., Jakob, T., Wilhelm, C. & Goss, R. 2008. A new multicomponent NPQ mechanism in the diatom *Cyclotella meneghiniana*. *Plant Cell Physiol* **49**:1217-25.

Grouneva, I., Jakob, T., Wilhelm, C. & Goss, R. 2009. The regulation of xanthophyll cycle activity and of non-photochemical fluorescence quenching by two alternative electron flows in the diatoms *Phaeodactylum tricornutum* and *Cyclotella meneghiniana*. *Biochim Biophys Acta* **1787**:929-38.

Grouneva, I., Rokka, A. & Aro, E. 2011. The thylakoid membrane proteome of two marine diatoms outlines both diatom-specific and species-specific features of the photosynthetic machinery. *J Prot Res* **10**:5338–53.

Grover, A. 1993. How do senescing leaves lose photosynthetic activity? *Curr Sci* **64**:226-34.

Guerra, L. T., Levitan, O., Frada, M. J., Sun, J. S., Falkowski, P. G. & Dismukes, G. C. 2013. Regulatory branch points affecting protein and lipid biosynthesis in the diatom *Phaeodactylum tricornutum*. *Biomass Bioenerg* **59**:306-15.

Guieu, C., Dulac, F., Desboeufs, K., Wagener, T., Pulido-Villena, E., Grisoni, J.-M., Louis, F., Ridame, C., Blain, S., Brunet, C., Bon Nguyen, E., Tran, S., Labiadh, M. & Dominici, J.-M. 2010. Large clean mesocosms and simulated dust deposition: a new methodology to investigate responses of marine oligotrophic ecosystems to atmospheric inputs. *Biogeosciences* **7**:2681-738.

Guillard, R. R. L. 1975. Culture of phytoplankton for feeding marine invertebrates. *In*: Smith, W. L. & Chanley, M. H. [Eds.] *Culture of Marine Invertebrate Animals.* Plenum Press, New York, pp. 29-60.

Guiry, M. D. 2012. How many species of algae are there? *J Phycol* **48**:1057-63.

Gutteridge, J. & Halliwell, B. 1990. The measurement and mechanism of lipid peroxidation in biological systems. *Trends Biochem Sci* **15**:129-35.

Häder, D. P., Kumar, H. D., Smith, R. C. & Worrest, R. C. 2007. Effects of solar UV radiation on aquatic ecosystems and interactions with climate change. *Photochem Photobiol Sci* **6**:267–85.

Hajimahmoodi, M., Faramarzi, M. A., Mohammadi, N., Soltani, N., Oveisi, M. R. & Nafissi-Varcheh, N. 2010. Evaluation of antioxidant properties and total phenolic contents of some strains of microalgae. *J Appl Phycol* **22**:43–50.

Hammer, Ø., Harper, D. A. T. & Ryan, P. D. 2001. PAST: Paleontological Statistics Software Package for education and data analysis. *Palaeontol Electron* **4**:1-9.

Havaux, M., Dall'Osto, L. & Bassi, R. 2007. Zeaxanthin has enhanced antioxidant capacity with respect to all other xanthophylls in *Arabidopsis* leaves and functions independent of binding to PSII antennae. *Plant Physiol* **145**:1506-20.

Hildebrand, M., Davis, A. K., Smith, S. R., Traller, J. C. & Abbriano, R. 2012. The place of diatoms in the biofuels industry. *Biofuels* **3**:221–40.

Hormann , H., Neubauer , C. & Schreiber , U. 1994. An active Mehler–peroxidase sequence can prevent cyclic PSI electron transport in the presence of dioxygen in intact chloroplasts. *Photosynth Res* **57**:61-70.

Horton, P. & Ruban, A. 1992. Regulation of photosystem II. *Photosynth Res* **34**:375–85.

Hu, Q., Sommerfeld, M., Jarvis, E., Ghirardi, M., Posewitz, M., Seibert, M. & Darzins, A. 2008. Microalgal triacylglycerols as feedstocks for biofuelproduction: perspectives and advances. *Plant J* **54**:621-39.

Humby, P. L., Snyder, E. C. R. & Durnford, D. G. 2013. Conditional senescence in *Chlamydomonas reinhardtii* (Chlorophyceae). *J Phycol* **49**:389-400.

Huo, J. Z., Nelis, H. J., Lavens, P., Sorgeloos, P. & De Leenheer, A. 1997. Determination of E vitamers in microalgae using high-performance liquid chromatography with fluorescence detection. *J Chromatogr A* **782**:63-68.

Huysman, M. J., Fortunato, A. E., Matthijs, M., Costa, B. S., Vanderhaeghen, R., Van den Daele, H., Sachse, M., Inzé, D., Bowler, C., Kroth, P. G., Wilhelm, C., Falciatore, A., Vyverman, W. & De Veylder, L. 2013. AUREOCHROME1a-mediated induction of the diatom-specific cyclin dsCYC2 controls the onset of cell division in diatoms (*Phaeodactylum tricornutum*). *Plant Cell* **25**:215-28.

Huysman, M. J. J., Martens, C., Vandepoele, K., Gillard, J., Rayko, E., Heijde, M., Bowler, C., Inze, D., Van de Peer, Y., De Veylder, L. & Vyverman, W. 2010. Genome-wide analysis of the diatom cell cycle unveils a novel type of cyclins involved in environmental signaling. *Genome Biol* **11**.

Ianora, A., Turner, J. T., Esposito, F., Carotenuto, Y., d'Ippolito, G., Romano, G., Fontana, A., Guisande, C. & Miralto, A. 2004. Copepod egg production and hatching success is reduced by maternal diets of a non-neurotoxic strain of the dinoflagellate *Alexandrium tamarense*. *Mar Ecol Prog Ser* **280**:199-210.

Imlay, J. A. 2008. Cellular defenses against superoxide and hydrogen peroxide. *Annu Rev Biochem*:755-76.

Ingebrigtsen, R. A., Hansen, E., Andersen, J. H. & Eilertsen, H. C. 2016. Light and temperature effects on bioactivity in diatoms. *J Appl Phycol* **28**:939–50.

Itoh, K., Chiba, T., Takahashi, S., Ishii, T., Igarashi, K., Katoh, Y., Oyake, T., Hayashi, N., Satoh, K., Hatayama, I., Yamamoto, M. & Nabeshima, Y. 1997. An Nrfs/small Maf eterodimer mediates the induction of phase II detoxifying enzyme genes through antioxidant response elements. *Biochem Biophys Res Commun* **236**.

Ivleva, N. B., Bramlett, M. R., Lindahl, P. A. & Golden, S. S. 2005. LdpA: a component of the circadian clock senses redox state of the cell. *EMBO J* **24**:1202-10.

Jakob, T., Goss, R. & Wilhelm, C. 2001. Unusual pH-dependence of diadinoxanthin de-epoxidase activation causes chlororespiratory induced accumulation of diatoxanthin in the diatom *Phaeodactylum tricornutum*. *J Plant Physiol* **158**:383–90.

Jakob, T., Wagner, H., Stehfest, K. & Wilhelm, C. 2007. A complete energy balance from photons to new biomass reveals a light- and nutrient-dependent variability in the metabolic costs of carbon assimilation. *J Exp Bot* **58**:2101–12.

Janknegt, P. J., Graaff, C. M. D., van de Poll, W. H., Visser, R. J. W., Rijstenbil, J. W. & Buma, A. G. J. 2009. Short-term antioxidative responses of 15 microalgae exposed to excessive irradiance including ultraviolet radiation. *Eur J Phycol* **44** 525–39.

Janknegt, P. J., Rijstenbil, J. W., van de Poll, W. H., Gechev, T. S. & Buma, A. G. J. 2007. A comparison of quantitative and qualitative superoxide dismutase assays for application to low temperature microalgae. *J Photochem Photobiol B* **87**:218–26.

Jensen, G. S., Ginsberg, D. I. & Drapeau, M. S. 2001. Blue-green algae as an immuno-enhancer and biomodulator. *J Am Nutraceutical Assoc* **3**:24–30.

Jia, Y. P., Sun, L., Yu, H. S., Liang, L. P., Li, W., Ding, H., Song, X. B. & Zhang, L. J. 2017. The pharmacological effects of lutein and zeaxanthin on visual disorders and cognition diseases. *Molecules* **22**:610.

Jochem, F. J. 1999. Dark survival strategies in marine phytoplankton assessed by cytometric measurement of metabolic activity with fluorescein diacetate. *Mar Biol* **135**:721-28.

Johnston, A. M., Raven, J. A., Beardall, J. & Leegood, R. C. 2001. Photosynthesis in a marine diatom. *Nature* **412**:40-41.

Jungandreas, A., Schellenberger Costa, B., Jakob, T., von Bergen, M., Baumann, S. & Wilhelm, C. 2014. The acclimation of *Phaeodactylum tricornutum* to blue and red light does not influence the photosynthetic light reaction but strongly disturbs the carbon allocation pattern. *PLoS ONE* **9**:e99727.

Kaulmann, A. & Bohn, T. 2014. Carotenoids, inflammation, and oxidative stress—implications of cellular signaling pathways and relation to chronic disease prevention. *Nutr Res* **34**:907-29.

Kedare, S. B. & Singh, R. P. 2011. Genesis and development of DPPH method of antioxidant assay. *J Food Sci Technol* **48**:412-22.

Keeling, P. J. 2010. The endosymbiotic origin, diversification and fate of plastids. *Philos Trans R Soc Lond B* **365**:729-48.

Keeling, P. J. 2013. The number, speed and impact of plastid endosymbioses in eukaryotic evolution. *Annu Rev Plant Biol* **64**:27.1–27.25.

Kirk, J. T. O. 1983. *Light and photosynthesis in aquatic systems.* Cambridge University Press, New York,

Kirk, J. T. O. 1994. *Light and photosynthesis in aquatic ecosystems.* Cambridge University Press, 662.

Klejdus, B., Lojková, L., M. Plaza, M. Snóblová & Sterbová, D. 2010. Hyphenated technique for the extraction and determination of isoflavones in algae: Ultrasound-assisted supercritical fluid extraction followed by fast chromatography with tandem mass spectrometry. *J Chromatogr A* **1217**:7956-65.

Kobata, A. 1972. Isolation of oligosaccharides from human milk. *Methods Enzymol.* **28**:262-71.

Kobayashi, N. & DellaPenna, D. 2008. Tocopherol metabolism, oxidation and recycling under high light stress in *Arabidopsis*. *Plant J* **55**:607-18.

Kolber, Z. 2007. Energy cycle in the ocean: powering the microbial world. *Oceanography* **20**:79-87.

Kolber, Z. & Falkowski, P. G. 1993. Use of active fluorescence to estimate phytoplankton photosynthesis in situ. *Limnol Oceanogr* **38**:1646-65.

Kooistra, W. H. C. F., Gersonde, R., Medlin, L. K. & Mann, D. G. 2007. The origin and evolution of the diatoms: their adaptation to a planktonic existence. *In*: Falkowski, P. G. & Knoll, A. H. [Eds.] *Evolution of Primary Producers in the Sea*. Elsevier Academic Press, Burlington, pp. 207-50.

Kovacik, J., Klejdus, B. & Backor, M. 2010. Physiological responses of *Scenedesmus quadricauda* (Chlorophyceae) to UV-A and UV-C light. *Photochem Photobiol* **86**:612-16.

Kraan, S. 2012. Algal polysaccharides, novel aapplications and outlook *In*: Chang, C.-F. [Ed.] *Carbohydrates - comprehensive studies on glycobiology and glycotechnology*. InTech, pp. 489-532.

Krieger-Liszkay, A. 2006. Singlet oxygen production in photosynthesis. *J Exp Bot* **56**:337–46.

Kuczynska, P. & Jemiola-Rzeminska, M. 2017. Isolation and purification of all-trans diadinoxanthin and all-trans diatoxanthin from diatom *Phaeodactylum tricornutum*. *J Appl Phycol* **29**:79-87.

Kuczynska, P., Jemiola-Rzeminska, M. & Strzalka, K. 2015. Photosynthetic pigments in diatoms. *Mar Drugs* **13**:5847-81.

Kwak, M. K., Itoh, K., Yamamoto, M. & Kensler, T. W. 2002. Enhanced expression of the transcription factor Nrf2 by cancer chemopreventive agents: role of antioxidant response element-like sequences in the nrf2 promoter. *Mol Cell Biol* **22**:2883–92.

Lamaison, J. L. C. & Carnet, A. 1990. Teneurs en principaux flavonoids des fleurs de *Crataegeus monogyna* Jacq et de *Crataegeus laevigata* (Poiret D. C) en fonction de la vegetation. *Pharm Acta Helv* **65**:315–20.

Laohavisit, A., Anderson, A., Bombelli, P., Jacobs, M., Howe, C. J., Davies, J. M. & Smith, A. G. 2015. Enhancing plasma membrane NADPH oxidase activity increases current output by diatoms in biophotovoltaic devices. *Algal Res* **12**:91-98.

Lattanzio, V., Lattanzio, V. M. T. & Cardinali, A. 2006. Role of phenolics in the resistance mechanisms of plants against fungal pathogens and insects. *In*: Imperato, F. [Ed.]

Phytochemistry: advances in research. Research Signpost, Trivandrum, Kerala, India, pp. 23-67.

Lauritano, C., Andersen, J. H., Hansen, E., Albrigtsen, M., Escalera, L., Esposito, F., Helland, K., Hanssen, K. Ø., Romano, G. & Ianora, A. 2016. Bioactivity screening of microalgae for antioxidant, anti-inflammatory, anticancer, anti-diabetes, and antibacterial activities. *Front Mar Sci* **3**:1-12.

Lavaud, J. 2007. Fast regulation of photosynthesis in diatoms: mechanisms, evolution and ecophysiology. *Funct Plant Sci Biotechnol* **1**:267-87.

Lavaud, J. & Goss, R. 2014. The peculiar features of non-photochemical fluorescence quenching in diatoms and brown algae *In*: Demmig-Adams, B., Garab, G., Adams III, W. & Govindjee [Eds.] *Non-photochemical quenching and energy dissipation in plants, algae and cyanobacteria* pp. 421-43.

Lavaud, J., Rousseau, B. & Etienne, A.-L. 2004. General features of photoprotection by energy dissipation in planktonic diatoms (Bacillariophyceae). *J Phycol* **40**:130-37.

Lavaud, J., Rousseau, B. & Etienne, A. 2002a. In diatoms, a transthylakoid proton gradient alone is not sufficient to induce a non-photochemical fluorescence quenching. *FEBS Letts* **523**.

Lavaud, J., Strzepek, R. F. & Kroth, P. G. 2007. Photoprotection capacity differs among diatoms: Possible consequences on the spatial distribution of diatoms related to fluctuations in the underwater light climate. *Limnol Oceanogr* **52**:1188-94.

Lavaud, J., Van Gorkom, H. & Etienne, A. 2002b. Photosystem II electron transfer cycle and chlororespiration in planktonic diatoms. *Photosynth Res* **74**:51-59.

Lebeau, T. & Robert, J.-M. 2003. Diatom cultivation and biotechnologically relevant products. Part II: Current and putative products. *Appl Microbiol Biotechnol* **60**:624-32.

Lemoine, Y. & Schoefs, B. 2010. Secondary ketocarotenoid astaxanthin biosynthesis in algae: a multifunctional response to stress. *Photosynth Res* **106**:155-77.

León-Bañares, R., González-Ballester, D., Galván, A. & Fernánez, E. 2004. Transgenic microalgae as gree cell-factories. *Trends Biotechnol* **22**:45-52.

Lepetit, B. & Dietzel, L. 2015. Light signaling in photosynthetic eukaryotes with ‘green’ and ‘red’ chloroplasts. *Environ Exp Bot* **114**:30-47.

Lepetit, B., Gélin, G., Lepetit, M., Sturm, S., Vugrinec, S., Rogato, A., Kroth, P. G., Falciatore, A. & Lavaud, J. 2017. The diatom *Phaeodactylum tricornutum* adjusts nonphotochemical fluorescence quenching capacity in response to dynamic light via fine-tuned Lhcx and xanthophyll cycle pigment synthesis. *New Phytol* **214**:205–18.

Lepetit, B., Goss, R., Jakob, T. & Wilhelm, C. 2012. Molecular dynamics of the diatom thylakoid membrane under different light conditions. *Photosynth Res* **111**:245–57.

Lepetit, B., Sturm, S., Rogato, A., Gruber, A., Sachse, M., Falciatore, A., Kroth, P. G. & Lavaud, J. 2013. High light acclimation in the secondary plastids containing diatom *Phaeodactylum tricornutum* is triggered by the redox state of the plastoquinone pool. *Plant Physiol* **161**:853–65.

Lepetit, B., Volke, D., Gilbert, M., Wilhelm, C. & Goss, R. 2010. Evidence for the existence of one antenna-associated, lipid-dissolved and two protein-bound pools of diadinoxanthin cycle pigments in diatoms. *Plant Physiol* **154**:1905–20.

Lesellier, E., Tchapla, A., Marty, C. & Lebert, A. 1993. Analysis of carotenoids by high-performance liquid chromatography and supercritical fluid chromatography. *J Chromatogr A* **663**:9-23.

Levitan, O., Dinamarca, J., Hochman, G. & Falkowski, P. G. 2014. Diatoms: a fossil fuel of the future. *Trends Biotechnol* **32**:117-24.

Li, G., David Talmy & Campbell, D. A. 2017. Diatom growth responses to photoperiod and light are predictable from diel reductant generation. *J Phycol* **53**:95-107.

Li, H.-B., Cheng, K.-W., Wong, C.-C., Fan, K.-W., Chen, F. & Jiang, Y. 2007. Evaluation of antioxidant capacity and total phenolic content of different fractions of selected microalgae. *Food Chem* **102**:771–76.

Li, H.-Y., Lu, Y., Zheng, J.-W., Yang, W.-D. & Liu, J.-S. 2014. Biochemical and genetic engineering of diatoms for polyunsaturated fatty acid biosynthesis. *Mar Drugs* **12**:153-66.

Li, Y., Wang, Z., Sun, X. & Tang, K. 2008. Current opinions on the functions of tocopherol based on the genetic manipulation of tocopherol biosynthesis in plants. *J Integr Plant Biol* **50**:1057-69.

Li, Z., Wakao, S., Fischer, B. B. & Niyogi, K. K. 2009. Sensing and responding to excess light. *Annu Rev Plant Biol* **60**:239-60.

Libby, P. 2007. Inflammatory mechanisms: the molecular basis of inflammation and disease. *Nutr Rev* **65(suppl 3)**:S140-S46.

Lin, C. & Todo, T. 2005. The cryptochromes. *Genome Biol* **6**:220.1-20.9.

Litchman, E. 2000. Growth rates of phytoplankton under fluctuating light. *Freshw Biol* **44**:223-35.

Litchman, E. & Klausmeier, C. A. 2001. Competition of phytoplankton under fluctuating light. *Am Nat* **157**:170-87.

Litchman, E., Klausmeier, C. A. & Yoshiyama, K. 2009. Contrasting size evolution in marine and freshwater diatoms. *Proc Natl Acad Sci USA* **106**:2665-70.

Litvín, R., Bína, D., Herbstovà, M. & Gardian, Z. 2016. Architecture of the light-harvesting apparatus of the eustigmatophyte alga *Nannochloropsis oceanica*. *Photosynth Res* **130**:137-50.

Llewellyn, L. E. 2006. Saxitoxin, a toxic marine natural product that targets a multitude of receptors. *Nat Prod Rep* **23**:200-22.

Lohr, M. & Wilhelm, C. 2001. Xanthophyll synthesis in diatoms: quantification of putative intermediates and comparison of pigment conversion kinetics with rate constants derived from a model. *Planta* **212**:382-91.

Lowry, O., Rosebrough, N., Farr, A. & Randall, R. 1951. Protein measurement with the Folin phenol reagent. *J Biol Chem* **193**:297-314.

Lü, J. M., Lin, P. H., Yao, Q. & Chen, C. 2010. Chemical and molecular mechanisms of antioxidants: experimental approaches and model systems. *J Cell Mol Med* **14**:840-60.

Lucht, J. M. 2015. Public acceptance of plant biotechnology and GM crops. *Viruses* **7**:4254-81.

Luo, C.-S., Liang, J.-R., Lin, Q., Li, C., Bowler, C., Anderson, D. M., Wang, P., Wang, X.-W. & Gao, Y.-H. 2014. Cellular responses associated with ROS production and cell fate decision in early stress response to iron limitation in the diatom *Thalassiosira pseudonana*. *Proteome* **13**:5510-23.

Lynam, C. P., Llope, M., Möllmann, C., Helaouët, P., Bayliss-Brown, G. A. & Stenseth, N. C. 2017. Interaction between top-down and bottom-up control in marine food webs. *Proc Natl Acad Sci USA* **114**:1952-57.

Ma, Q. 2013. Role of Nrf2 in oxidative stress and toxicity. *Annu Rev Pharmacol Toxicol* **53**:401-26.

MacIntyre, H. L. & Geider, R. J. 1996. Regulation of Rubisco activity and its potential effect on photosynthesis during mixing in a turbid estuary. *Mar Ecol Prog Ser* **144**:247-64.

MacIntyre, H. L., Kana, T. M., Anning, T. & Geider, R. J. 2002. Photoacclimation of photosynthesis irradiance response curves and photosynthetic pigments in microalgae and cyanobacteria. *J Phycol* **38**:17-38.

MacIntyre, H. L., Kana, T. M. & Geider, R. J. 2000. The effect of water motion on short-term rates of photosynthesis by marine phytoplankton. *Trends Plant Sci* **5**:12-17.

Mae, T., Thomas, H., Gay, A. P., Makino, A. & Hidema, J. 1993. Leaf development in *Lolium temulentum*: photosynthesis and photosynthetic proteins in leaves senescing under different irradiances. *Plant Cell Physiol* **34**:391-99.

Mann, D. G. & Droop, S. J. M. 1996. Biodiversity, biogeography and conservation of diatoms. *Hydrobiologia* **336**:19-32.

Manna, V. 2017. *Phytoplankton community response to nutrients fertilization and microplastics addition: a mesocosm experiment in the Gulf of Naples.* Master Degree, Università degli Studi di Napoli "Federico II" - Stazione Zoologica Anton Dohrn, 132 pp.

Mantoura, R. F. C. & Llewellyn, C. A. 1983. The rapid determination of algal chlorophyll and carotenoid pigments and their breakdown products in natural waters by reverse phase H.P.L.C. *Anal Chim Acta* **151**:297–314.

Marchetti, A., Schruth, D. M., Durkin, C. A., Parker, M. S., Kodner, R. B., Berthiaume, C. T., Morales, R., Allen, A. E. & Armbrust, E. V. 2012. Comparative metatranscriptomics identifies molecular bases for the physiological responses of phytoplankton to varying iron availability. *Proc Nat Acad Sci USA* **109**:E317–E25.

Marchetti, J., Bougaran, G., Jauffrais, T., Lefebvre, S., Rouxel, C., Saint-Jean, B., Lukomska, E., Robert, R. & Cadoret, J. P. 2013. Effects of blue light on the biochemical composition and photosynthetic activity of *Isochrysis* sp. (T-iso). *J Appl Phycol* **25**:109-19.

Marí, M., Morales, A., Colell, A., García-Ruiz, C. & Fernández-Checa, J. C. 2009. Mitochondrial glutathione, a key survival antioxidant. *Antioxid Redox Signal* **11**:2685-700.

Martin, S. J. & Sabina, E. P. 2017. Comparative modulation of levels of oxidative stress in the liver of anti-tuberculosis drug treated Wistar rats by vitamin B12, beta-carotene and *Spirulina fusiformis*: role of NF-kB, iNOS, IL-6 and IL-10. *J Cell Biochem*.

Massot, C., Stevens, R., Génard, M., Longuenesse, J.-J. & Gautier, H. 2012. Light affects ascorbate content and ascorbate-related gene expression in tomato leaves more than in fruits. *Planta* **235**:153-63.

Mata, T. M., Martins, A. A. & Caetano, N. S. 2010. Microalgae for biodiesel production and other applications: a review. *Renew Sust Energ Rev* **14**:217-32.

McCord, J. M. & Fridovich, I. 1968. The reduction of cytochrome c by milk xanthine oxidase. *J Biol Chem* **243**:5753-60.

McLean, R. J. 1968. Ultrastructure of *Spongiochloris typica* during senescence. *J Phycol* **4**:277–83.

McQuoid, M. R., Godhe, A. & Nordberg, K. 2002. Viability of phytoplankton resting stages in the sediments of a coastal Swedish fjord. *Eur J Phycol* **37**:191-201.

Mehler, A. H. 1951. Studies on reactivity of illuminated chloroplasts. I. Mechanism of the reduction of oxygen and other Hill reagents. *Arch Biochem Biophys* **33**:65-77.

Meiser, A., Schmid-Staiger, U. & Trösch, W. 2004. Optimization of eicosapentaenoic acid production by *Phaeodactylum tricornutum* in the flat panel airlift (FPA) reactor. *J Appl Phycol* **16**:215-25.

Mergenhagen, D. & Mergenhagen, E. 1987. The biological clock of *Chlamydomonas reinhardii* in space. *Eur J Cell Biol* **43**:203–07.

Mhamdi, A., Noctor, G. & Baker, A. 2012. Plant catalases: peroxisomal redox guardians. *Arch Biochem Biophys* **525**:181-94.

Miller, N. J., Sampson, J., Candeias, L. P., Bramley, P. M. & Rice-Evans, C. A. 1996. Antioxidant activities of carotenes and xanthophylls. *FEBS Lett* **384**:240-42.

Miloslavina, Y., Grouneva, I., Lambrev, P., Lepetit, B., Goss, R., Wilhelm, C. & Holzwarth, A. 2009. Ultra-fast fluorescence study on the location and mechanism of non-photochemicalquenching in diatoms. *Biochim Biophys Acta* **1787**:1189-97.

Miralto, A., Barone, G., Romano, G., Poulet, S. A., Ianora, A., Russo, G. L., Buttino, I., Mazzarella, G., Laabir, M., Cabrini, M. & Giacobbe, M. G. 1999. The insidious effect of diatoms on copepod reproduction. *Nature* **402**:173-76.

Mittag, M., Kiaulehn, S. & Hirschie Johnson, C. 2005. The circadian clock in *Chlamydomonas reinhardtii*. What is it for? What is it similar to? *Plant Physiol* **137**:399-409.

Mittag, M. & Wagner, V. 2003. The circadian clock of the unicellular eukaryotic model organism *Chlamydomonas reinhardtii*. *Biol Chem* **384**:689 – 95.

Mittler, R. 2002. Oxidative stress, antioxidants and stress tolerance. *Trends Plant Sci* **7**:405-10.

Mittler, R. & Zilinskas, B. A. 1993. Detection of ascorbate peroxidase activity in native gels by inhibition of the ascorbate-dependent reduction of nitroblue tetrazolium. *Anal Biochem* **212**:540–46.

Miyake, C. 2010. Alternative electron flows (water-water cycle and cyclic electron flow around PSI) in photosynthesis: molecular mechanisms and physiological functions. *Plant Cell Physiol* **51**:1951-63.

Modigh, M., Saggiomo, V. & Ribera d'Alcalà, M. 1996. Conservative features of picoplankton in a Mediterranean eutrophic area, the Bay of Naples. *J Plankton Res* **18**:87-95.

Morel, A., Lazzara, L. & Gostan, J. 1987. Growth rate and quantum yield time response for a diatom to changing irradiances (energy and color). *Limnol Oceanogr* **32**:1066–84.

Mouradov, A. & Spangenberg 2014. Flavonoids: a metabolic network mediating plants adaptation to their real estate. *Front Plant Sci* **5**:620.

Moustafa, A., Beszteri, B., Maier, U. G., Bowler, C., Valentin, K. & Bhattacharya, D. 2009. Genomic footprints of a cryptic plastid endosymbiosis in diatoms. *Science* **324**:1724–26.

Mueller, L. & Boehm, V. 2011. Antioxidant activity of β-carotene compounds in different *in vitro* assays. *Molecules* **16**:1055-69.

Müller, P., Li, X. P. & Niyogi, K. K. 2001. Non-photochemical quenching. A response to excess light energy. *Plant Physiol* **125**:1558-66.

Munekage, Y., Hashimoto, M., Miyake, C., Tomizawa, K.-I., Endo, T., Tasaka, M. & Shikanai, T. 2004. Cyclic electron flow around photosystem I is essential for photosynthesis. *Nature* **429**:579.

Murphy, A. M. & Cowles, T. J. 1997. Effects of darkness on multi-excitation in vivo fluorescence and survival in a marine diatom. *Limnol Oceanogr* **42**:1444-53.

Murphy, M. 2009. How mitochondria produce reactive oxygen species. *Biochem J* **417**:1-13.

Nelson, D. M., Tréguer, P., Brzezinski, A., Leynaert, A. & Quéguiner, B. 1995. Production and dissolution of biogenic silica in the ocean: revised global estimates, comparison with regional data and relationship to biogenic sedimentation. *Global Biogeochem Cycles* **9**:359-72.

Nelson, N. & Ben-Shem, A. 2004. The complex architecture of oxygenic photosynthesis. *Nat Rev Mol Cell Biol* **5**.

Nicklisch, S. C. T. & Waite, J. H. 2014. Optimized DPPH assay in a detergent-based buffer system for measuring antioxidant activity of proteins. *MethodsX* **1**.

Nimse, S. B. & Pal, D. 2015. Free radicals, natural antioxidants, and their reaction mechanisms. *RSC Adv* **5**:27986–8006.

Niyogi, K. 1999. Photoprotection revisited: genetic and molecular approaches. *Annu Rev Plant Physiol Plant Mol Biol* **50**:333–59.

Noctor, G. & Foyer, C. H. 1998. Ascorbate and glutathione: keeping active oxygen under control. *Annu Rev Plant Physiol Plant Mol Biol* **49**:249-79.

Noctor, G., Veljovic-Jovanovic, S. & Foyer, C. H. 2000. Peroxide processing in photosynthesis: antioxidant coupling and redox signalling. *Philos Trans R Soc Lond B Biol Sci* **355**:1465-75.

Noodén, L. D. 2003. *Plant cell death processes.* Elsevier, Academic Press, 392.

Noordally, Z. B. & Millar, A. J. 2015. Clocks in algae. *Biochemistry* **54**:172-83.

Nymark, M., Valle, K. C., Brembu, T., Hancke, K., Winge, P., Andresen, K., Johnsen, G. & Bones, A. M. 2009. An integrated analysis of molecular acclimation to high light in the marine diatom *Phaeodactylum tricornutum*. *PLoS ONE* **4**:e7743.

Nymark, M., Valle, K. C., Hancke, K., Winge, P., Andresen, K., Johnsen, G., Bones, A. M. & Brembu, T. 2013. Molecular and photosynthetic responses to prolonged darkness and subsequent acclimation to re-illumination in the diatom *Phaeodactylum tricornutum*. *PLoS one* **8**:e58722.

Olaizola, M. 2003. Commercial development of microalgal biotechnology: from the test tube to the marketplace. *Biomol Eng* **20**:459-66.

Oliveri, P., Fortunato, A. E., Petronea, L., Ishikawa-Fujiwara, T., Kobayashi, Y., Todo, T., Antonova, O., Arboleda, E., Zantke, J., Tessmar-Raible, K. & Falciatore, A. 2014. The Cryptochrome/Photolyase Family in aquatic organisms. *Mar Genomics* **14**:23-37.

Omaye, S., Turnbull, J. & Sauberlich, H. 1979. Selected methods for the determination of ascorbic acid in animal cells, tissues, and fluids. *Methods Enzymol* **62**:3-11.

Onno Feikema, W., Marosvölgyi, M., Lavaud, J. & van Gorkom, H. 2006. Cyclic electron transfer in photosystem II in the marine diatom *Phaeodactylum tricornutum*. *Biochim Biophys Acta* **1757**.

Orefice, I., Chandrasekaran, R., Smerilli, A., Corato, F., Caruso, T., Casillo, A., Corsaro, M. M., Dal Piaz, F., Ruban, A. V. & Brunet, C. 2016. Light-induced changes in the photosynthetic physiology and biochemistry in the diatom *Skeletonema marinoi*. *Algal Res* **17**:1-13.

Orefice, I., Lauritano, C., Procaccini, G., Ianora, A. & Romano, G. 2015. Insights into possible cell-death markers in the diatom *Skeletonema marinoi* in response to senescence and silica starvation. *Mar Genomics* **24**:81-88.

Ouyang, Y., Andersson, C. R., Kondo, T., Golden, S. S. & Hirschie Johnson, C. 1998. Resonating circadian clocks enhance fitness in cyanobacteria. *Proc Natl Acad Sci USA* **95**:8660–64.

Pangestuti, R. & Kim, S. K. 2011. Biological activities and health benefit effects of natural pigments derived from marine algae. *J Funct Foods* **3**:255-66.

Parker, M. S., Armbrust, E. V., Piovia-Scott, J. & Keil, R. G. 2004. Induction of photorespiration by light in the centric diatom *Thalassiosira weissflogi* (Bacillariophyceae): Molecular characterization and physiological consequences. *J Phycol* **40**:557-67.

Paul, T. 2000. Effect of a prolonged superoxide flux on transferrin and ferritin. *Arch Biochem Biophys* **382**:253–61.

Peltier, G. & Cournac, L. 2002. Chlororespiration. *Annu Rev Plant Biol* **53**:523-50.

Peng, J., Yuan, J.-P., Wu, C.-F. & Wang, J.-H. 2011. Fucoxanthin, a marine carotenoid present in brown seaweeds and diatoms: metabolism and bioactivities relevant to human health. *Mar Drugs* **9**:1806–28.

Pérez-López, P., González-García, S., Ulloa, R. G., Sineiro, J., Feijoo, G. & Moreira, M. T. 2014. Life cycle assessment of the production of bioactive compounds from *Tetraselmis suecica* at pilot scale. *J Clean Prod* **64**:323-31.

Perrine, Z., Negi, S. & Sayre, R. T. 2012. Optimization of photosynthetic light energy utilization by microalgae. *Algal Res* **1**:134-42.

Peterhansel, C., Horst, I., Niessen, M., Blume, C., Kebeish, R., Kürkcüoglu, S. & Kreuzaler, F. 2010. Photorespiration. *Arabidopsis Book* **8**:e0130.

Peters, E. 1996a. Prolonged darkness and diatom mortality. II. Marine temperate species. *J Exp Mar Bio Ecol* **207**:43-58.

Peters, E. 1996b. Prolonged darkness and diatom mortality: I. Marine Antarctic species. *J Exp Mar Bio Ecol* **207**:24-41.

Petersen, J. E., Kemp, W. M., Bartleson, R., Boynton, W. R., Chen, C. C., Cornwell, J. C., Gardner, R. H., Hinkle, D. C., Houde, E. D., Malone, T. C., Mowitt, W. P., Murray, L., Sanford, L. P., Stevenson, J. C., Sundberg, K. L. & Suttles, S. E. 2003. Multiscale experiments in coastal ecology: improving realism and advancing theory. *AIBS Bulletin* **53**:1181-97.

Pfaffl, M. W., Horgan, G. W. & Dempfle, L. 2002. Relative expression software tool (REST©) for group-wise comparison and statistical analysis of relative expression results in real-time PCR. *Nucleic Acids Res* **30**:e36-e36.

Pfaffl, M. W., Tichopad, A., Prgomet, C. & Neuvians, T. P. 2004. Determination of stable housekeeping genes, differentially regulated target genes and sample integrity: BestKeeper - Excel-based tool using pair-wise correlations. *Biotechnol Lett* **26**:509-15.

Pham-Huy, L. A., He, H. & Pham-Huy, C. 2008. Free radicals, antioxidants in disease and health. *Int J Biomed Sci* **4**:89-96.

Pietta, P.-G. 2000. Flavonoids as antioxidants. *J Nat Prod* **63**:1035-42.

Pohnert, G. 2005. Diatom/copepod interactions in plankton: The indirect chemical defense of unicellular algae. *Chembiochem* **6**:946-59.

Popovich, C., Damiani, C., Constenla, D. & Leonardi, P. 2012. Lipid quality of the diatoms *Skeletonema costatum* and *Navicula gregaria* from the South Atlantic Coast (Argentina): evaluation of its suitability as biodiesel feedstock. *Journal of Applied Phycology* **24**:1-10.

Pulz, O. & Gross, W. 2004. Valuable products from biotechnology of microalgae. *Appl Microbiol Biotechnol* **65**:635-48.

Pyszniak, A. M. & Gibbs, S. P. 1992. Immunocytochemical localisation of photosystem I and the fucoxanthin-chlorophyll a/c light-harvesting complex in the diatom *Phaeodactylum tricornutum*. *Protoplasma* **166**:208–17.

Quideau, S., Deffieux, D., Douat-Casassus, C. & Pouysegu, L. 2011. Plant polyphenols: chemical properties, biological activities, and synthesis. *Angew Chem Int Ed Engl* **50**:586-621.

Ramos, M. J., Fernández, C. M., Casas, A., Rodríguez, L. & Pérez, Á. 2009. Influence of fatty acid composition of raw materials on biodiesel properties. *Bioresour Technol* **100**:261–68.

Raven, J. A. 2013. Iron acquisition and allocation in stramenopile algae. *J Exp Bot* **64**:2119-27.

Raven, J. A., Beardall, J. & Giordano, M. 2014. Energy costs of carbon dioxide concentrating mechanisms in aquatic organisms. *Photosynth Res* **121**:111-24.

Raven, J. A., Giordano, M., Beardall, J. & Maberly, S. C. 2012. Algal evolution in relation to atmospheric CO_2: carboxylases, carbon-concentrating mechanisms and carbon oxidation cycles. *Phil Trans R Soc Lond B* **367**:493-507.

Ribalet, F., Berges, J. A., Ianora, A. & Casotti, R. 2007a. Growth inhibition of cultured marine. phytoplankton by toxic algal-derived polyunsaturated aldehydes. *Aquat Toxicol* **85**:219-27.

Ribalet, F., Vidoudez, C., Cassin, D., Pohnert, G., Ianora, A., Miralto, A. & Casotti, R. 2009. High plasticity in the production of diatom-derived polyunsaturated aldehydes under nutrient limitation: physiological and ecological implications. *Protist* **160**:444-51.

Ribalet, F., Wichard, T., Pohnert, G., Ianora, A., Miralto, A. & Casotti, R. 2007b. Age and nutrient limitation enhance polyunsaturated aldehyde production in marine diatoms. *Phytochemistry* **68**:2059-67.

Ribera d'Alcalà, M., Conversano, F., Corato, F., Licandro, P., Mangoni, O., Marino, D., Mazzocchi, M. G., Modigh, M., Montresor, M., Nardella, M., Saggiomo, V., Sarno, D. & Zingone, A. 2004. Seasonal patterns in plankton communities in a pluriannual time series at a coastal Mediterranean site (Gulf of Naples): an attempt to discern recurrences and trends. *Sci Mar* **68**:65-83.

Riebesell, U., Czerny, J., von Bröckel, K., Boxhammer, T., Büdenbender, J., Deckelnick, M., Fisher, M., Hoffmann, D., Krug, S. A., Lentz, U., Ludwig, A., Muche, R. & Schulz, K. G. 2013. A mobile sea-going mesocosm system–new opportunities for ocean change research. *Biogeosciences* **10**:1835-47.

Rivkin, R. B. 1989. Influence of irradiance and spectral quality on the carbon metabolism of phytoplankton I. Photosynthesis, chemical composition and growth. *Mar Ecol Prog Ser* **55**:291-304.

Rockwell, N. C., Duanmu, D., Martin, S. S., Bachy, C., Price, D. C., Bhattacharya, D., Worden, A. Z. & Lagarias, J. C. 2014. Eukaryotic algal phytochromes span the visible spectrum. *Proc Nat Acad Sci USA* **111**:3871–76.

Rodriguez-Amaya, D. 2015. *Food Carotenoids: Chemistry, Biology and Nutrition.* John Wiley & Sons Incorporated, 429.

Roy, S., Llewellyn, C. A., Skarstad Egeland, E. & Johnsen, G. 2011. *Phytoplankton pigments - Characterization, chemotaxonomy and applications in oceanography*. Cambridge University Press, 890.

Ruban, A. 2016. Nonphotochemical chlorophyll fluorescence quenching: mechanism and effectiveness in protecting plants from photodamage. *Plant Physiol* **170**:1903-16.

Ruban, A. V. 2009. Plants in light. *Commun Integr Biol* **2**:50-55.

Ruban, A. V. & Johnson, M. 2015. Visualizing the dynamic structure of the plant photosynthetic membrane. *Nat Plants* **3**:15161.

Ruban, A. V., Lavaud, J., Rousseau, B., Guglielmi, G., Horton, P. & Etienne, A.-L. 2004. The super-excess energy dissipation in diatom algae: comparative analysis with higher plants. *Photosynth Res* **82**:165-75.

Ruban, A. V. & Murchie, E. H. 2012. Assessing the photoprotective effectiveness of non-photochemical chlorophyll fluorescence quenching: A new approach. *Biochim Biophys Acta* **1817**:977-82.

Running, J., Severson, D. & Schneider, K. 2002. Extracellular production of L-ascorbic acid by *Chlorella protothecoides*, Prototheca species and mutants of *P. moriformis* during aerobic culturing at low pH. *J Ind Microbiol Biotechnol* **29**:93-98.

Salminen, A., Lehtonen, M., Suuronen, T., Kaarniranta, K. & Huuskonen, J. 2008. Terpenoids: natural inhibitors of NF-κB signaling with anti-inflammatory and anticancer potential. *Cell Mol Life Sci* **65**:2979-99.

Sanchez-Rangel, J. C., Benavides, J., Heradia, J. B., Cisneros-Zevallos, L. & Jacobo-Velazquez, D. A. 2013. The Folin–Ciocalteu assay revisited: improvement of its specificity for total phenolic content determination. *Anal Methods* **5**:5990-99

Sangeetha, R. K., Bhaskar, N. & Baskaran, V. 2009. Comparative effects of β-carotene and fucoxanthin on retinol deficiency induced oxidative stress in rats. *Mol Cell Biochem* **331**:59-67.

Sansone, C., Galasso, C., Orefice, I., Nuzzo, G., Luongo, E., Cutignano, A., Romano, G., Brunet, C., Fontana, A., Esposito, F. & Ianora, A. 2017. The green microalga *Tetraselmis suecica* reduces oxidative stress and induces repairing mechanisms in human cells. *Sci Rep* **7**:41215.

Schaller, S., Latowski, D., Jemiola-Rzeminska, M., Wilhelm, C., Strzalka, K. & Goss, R. 2010. The main thylakoid membrane lipid monogalactosyldiacylglycerol (MGDG) promotes the de-epoxidation of violaxanthin associated with the light-harvesting complex of photosystem II (LHCII). *Biochim Biophys Acta* **1797**:414-24.

Schaub, I., Wagner, H., Graeve, M. & Karsten, U. 2017. Effects of prolonged darkness and temperature on the lipid metabolism in the benthic diatom *Navicula perminuta* from the Arctic Adventfjorden, Svalbard. *Polar Biol* **40**:1425-39.

Schellenberger Costa, B., Jungandreas, A., Jakob, T., Weisheit, W., Mittag, M. & Wilhelm, C. 2013a. Blue light is essential for high light acclimation and photoprotection in the diatom *Phaeodactylum tricornutum*. *J Exp Bot* **64**:483–93.

Schellenberger Costa, B., Sachse, M., Jungandreas, A., Rio Bartulos, C., Gruber, A., Jakob, T., Kroth, P. G. & Wilhelm, C. 2013b. Aureochrome 1a is involved in the photoacclimation of the diatom *Phaeodactylum tricornutum*. *PLoS ONE* **8**:e74451.

Segev, E., Wyche, T. P., Kim, K. H., Petersen, J., Ellebrandt, C., Vlamakis, H., Barteneva, N., Paulson, J. N., Chai, L., Clardy, J. & Kolter, R. 2016. Dynamic metabolic exchange governs a marine algal-bacterial interaction. *eLIFE* **17473**:1-28.

Shang, W. & Feierabend, J. 1999. Dependence of catalase photoinactivation in rye leaves on light intensity and quality and characterization of a chloroplast-mediated inactivation in red light. *Photosynth Res* **59**:201–13.

Sharma, O. P. & Bhat, T. K. 2009. DPPH antioxidant assay revisited. *Food Chem* **113**:1202-05.

Sharma, P., Jha, A. B., Dubey, R. S. & Pessarakli, M. 2012. Reactive oxygen species, oxidative damage, and antioxidative defense mechanism in plants under stressful conditions. *J Bot*:1-26.

Sharoni, Y., Danilenko, M., Dubi, N., Ben-Dor, A. & Levy, J. 2004. Carotenoids and transcription. *Arch Biochem Biophys* **430**:89-96.

Sheppard, V., Poulsen, N. & Kröger, N. 2010. Characterization of an endoplasmic reticulum-associated silaffin kinase from the diatom *Thalassiosira pseudonana*. *J Biol Chem* **285**:1166-76.

Sigaud-Kutner, T. C. S., Neto, A. M. P., Pinto, E. & Colepicolo, P. 2005. Diel activities of antioxidant enzymes, photosynthetic pigments and malondialdehyde content in stationary-phase cells of *Tetraselmis gracilis* (Prasinophyceae). *Aquat Bot* **82**:239–49.

Singleton, V. L. & Rossi, J. A. 1965. Colorimetry of total phenolics with phosphomolybdic-phosphotungstic acid reagents. *Am J Enol Vitic* **16**:144-58.

Sinistro, R. 2010. Top-down and bottom-up regulation of planktonic communities in a warm temperate wetland. *J Plankton Res* **32**:209-20.

Six, C., Finkel, Z. V., Rodriguez, F., Marie, D., Partensky, F. & Campbell, D. A. 2008. Contrasting photoacclimation costs in ecotypes of the marine eukaryote picoplankter *Ostreococcus*. *Limnol Oceanogr* **53**:255–65.

Smerilli, A., Orefice, I., Corato, F., Gavalás Olea, A., Ruban, A. & Brunet, C. 2017. Photoprotective and antioxidant responses to light spectrum and intensity variations in the coastal diatom *Skeletonema marinoi*. *Environ Microbiol* **19**:611-27.

Smetacek, V. 1999. Diatoms and the ocean carbon cycle. *Protist* **150**:25-32.

Smirnoff, N. & Wheeler, G. L. 2000. Ascorbic acid in plants: biosynthesis and function. *Crit Rev Biochem Mol Biol* **35**:291-314.

Snoeijs, P., Busse, S. & Potapova, M. 2002. The importance of diatom cell size in community analysis. *J Phycol* **38**:265-72.

Snoeijs, P., Sylvander, P. & Häubner, N. 2012. Oxidative stress in aquatic primary producers as a driving force for ecosystem responses to large-scale environmental changes. *In*: Abele, D., Vázquez-Medina, J. P. & Zenteno-Savín, T. [Eds.] *Oxidative stress in aquatic ecosystems.* Wiley-Blackwell, pp. 72-88.

Spolaore, P., Joannis-Cassan, C., Duran, E. & Isambert, A. 2006. Commercial application of microalgae. *J Biosci Bioeng* **101**:87-96.

Stahl, W. & Sies, H. 2003. Antioxidant activity of carotenoids. *Mol Aspects Med* **24**:345-51.

Stahl, W. & Sies, H. 2005. Bioactivity and protective effects of natural carotenoids. *Biochim Biophys Acta* **1740**:101-07.

Su, W., Jakob, T. & Wilhelm, C. 2012. The impact of nonphotochemical quenching of fluorescence on the photon balance in diatoms under dynamic light conditions. *J Phycol* **48**:336–46.

Suzuki, K., Iwamoto, K., Yokoyama, S. & Ikawa, T. 1991. Glycolate-oxidizing enzymes in algae. *J Phycol* **27**:492-98.

Taddei, L., Stella, G., Rogato, A., Bailleul, B., Fortunato, A., Annunziata, R., Sanges, R., Thaler, M., Lepetit, B., Lavaud, J., Jaubert, M., Finazzi, G., Bouly, J. & Falciatore, A. 2016. Multisignal control of expression of the LHCX protein family in the marine diatom *Phaeodactylum tricornutum*. *J Exp Bot* **67**:3939-51.

Tassan, S. & Ferrari, G. M. 1995. An alternative approach to absorption measurements of aquatic particles retained on filters. *Limnol Oceanogr* **40**:1358-68.

Telfer, A. 2002. What is carotene doing in the photosystem II reaction centre? *Philos Trans R Soc Lond* **357**:1431–40.

Tiwari, B. S., Belenghi, B. & Levine, A. 2002. Oxidative stress increased respiration and generation of reactive oxygen species, resulting in ATP depletion, opening of mitochondrial permeability transition, and programmed cell death. *Plant Physiol* **128**:1271-81.

Triantaphylides, C., Krischke, M., Hoeberichts, F. A., Ksas, B., Gresser, G., Havaux, M., Van Breusegem, F. & Mueller, M. J. 2008. Singlet oxygen is the major reactive oxygen species involved in photooxidative damage to plants. *Plant Physiol* **148**: 960–68.

Tuchman, N. C., Schollett, M. A., Rier, S. T. & Geddes, P. 2006. Differential heterotrophic utilization of organic compounds by diatoms and bacteria under light and dark conditions. *Hydrobiologia* **561**:167–77.

Turner, J. T. & Tester, P. A. 1997. Toxic marine phytoplankton, zooplankton grazers, and pelagic food webs. *Limnol Oceanogr* **42**:1203-14.

Turner, R. E., Rabalais, N. N., Justic, D. & Dortch, Q. 2003. Future aquatic nutrient limitations. *Mar Pollut Bull* **46**:1032-34.

Van Amerongen, H. & Dekker, J. P. 2003. Light-harvesting in photosystem II. *In*: Green, B. & Parson, W. W. [Eds.] *Light-Harvesting Antennas in Photosynthesis: Advances in Photosynthesis and Respiration.* Kluwer Academy Publisher, Dordrecht, pp. 493.

van de Poll, W. H., Visser, R. J. W. & Buma, A. G. J. 2007. Acclimation to a dynamic irradiance regime changes excessive irradiance sensitivity of *Emiliania huxleyi* and *Thalassiosira weissflogii*. *Limnol Oceanogr* **52**:1239-48.

Van Leeuwe, M. A., Sikkelerus, B. v., Gieskes, W. W. C. & Stefels, J. 2005. Taxon-specific differences in photoacclimation to fluctuating irradiance in an Antarctic diatom and a green flagellate. *Mar Ecol Prog Ser* **288**:9-19.

Van Niewerburgh, L., Wanstrand, I. & Snoeijs, P. 2004. Growth and C:N:P ratios in copepod grazing on N- or Si-limited phytoplankton blooms. *Hydrobiol* **514**:57-72.

Van Oostende, N., Fawcett, S. E., Marconi, D., Lueders-Dumont, J., Sabadel, A. J. M., Woodward, E. M. S., Jonsson, B. F., Sigman, D. M. & Ward, B. B. 2017. Variation of summer phytoplankton community composition and its relationship to nitrate and regenerated nitrogen assimilation across the North Atlantic Ocean. *Deep Sea Res Part 1 Oceanogr Res Pap* **121**:79-94.

Vandamme, E. J. & Revuelta, J. L. 2016. *Industrial Biotechnology of Vitamins, Biopigments, and Antioxidants.* John Wiley & Sons, 548.

Vandesompele, J., De Preter, K., Pattyn, F., Poppe, B., Van Roy, N., De Paepe, A. & Speleman, F. 2002. Accurate normalization of real-time quantitative RT-PCR data by geometric averaging of multiple internal control genes. *Genome Biol* **3**:1-12.

Vardi, A., Berman-Frank, I., Rozenberg, T., Hadas, O., Kaplan, A. & Levine, A. 1999. Programmed cell death of the dinoflagellate Peridinium gatunense is mediated by CO2 limitation and oxidative stress. *Curr Biol* **9**:1061-64.

Vardi, A., Bidle, K. D., Kwityn, C., Hirsh, D. J., Thompson, S. M., Callow, J. A., Falkowski, P. & Bowler, C. 2008. A diatom gene regulating nitric-oxide signaling and susceptibility to diatom-derived aldehydes. *Curr Biol* **18**:895-99.

Vardi, A., Formiggini, F., Casotti, R., De Martino, A., Ribalet, F., Miralto, A. & Bowler, C. 2006. A stress surveillance system based on calcium and nitric oxide in marine diatoms. *PLoS Biol* **4**:419-11.

Vaulot, D., Olson, R. J. & Chisholm, S. W. 1986. Light and dark control of the cell cycle in two marine phytoplankton species. *Exp Cell Res* **167**:38-52.

Vaze, K. M. & Sharma, V. K. 2013. On the adaptive significance of circadian clocks for their owners. *Chronobiol Int* **30**:413-33.

Veith, T., Brauns, J., Weisheit, W., Mittag, M. & Büchel, C. 2009. Identification of a specific fucoxanthin-chlorophyll protein in the light harvesting complex of photosystem I in the diatom *Cyclotella meneghiniana*. *Biochim Biophys Acta* **1787**:905–12.

Vermaas, W. 1993. Molecular-biological approaches to analyze photosystem II structure and function. *Annu Rev Plant Physiol Plant Mol Biol* **44**:457–81.

Vidoudez, C. & Pohnert, G. 2012. Comparative metabolomics of the diatom *Skeletonema marinoi* in different growth phases. *Metabolomics* **8**:654-69.

Vigani, M., Parisi, C., Rodriguez-Cerezo, E., Barbosa, M. J., Sijtsma, L., Ploeg, M. & Enzing, C. 2015. Food and feed products from microalgae: market opportunities and challenges for the EU. *Trends Food Sci Tech* **42**:81-92.

Vogel, C. & Marcotte, E. M. 2012. Insights into the regulation of protein abundance from proteomic and transcriptomic analyses. *Nat Rev Genet* **13**:227–32.

Wagner, H., Jakob, T., Fanesi, A. & Wilhelm, C. 2017. Towards an understanding of the molecular regulation of carbon allocation in diatoms: the interaction of energy and carbon allocation. *Phil Trans R Soc B* **372**:20160410.

Wagner, H., Jakob, T., Lavaud, J. & Wilhelm, C. 2016. Photosystem II cycle activity and alternative electron transport in the diatom *Phaeodactylum tricornutum* under dynamic light conditions and nitrogen limitation. *Photosynth Res* **128**:151-61.

Wagner, H., Jakob, T. & Wilhelm, C. 2006. Balancing the energy flow from captured light to biomass under fluctuating light conditions. *New Phytol* **169**:95-108.

Wang, C., Zhang, S. H., Wang, P. F., Hou, J., Li, W. & Zhang, W. J. 2008. Metabolic adaptation to ammonia-induced oxidative stress in leaves of the submerged macrophyte *Vallisneria natans* (Lour.) Hara. *Aquat Toxicol* **87**:88-98.

Wang, C. Y., Chen, C.-T. & Wang, S. Y. 2009. Changes of flavonoid content and antioxidant capacity in blueberries after illumination with UV-C. *Food Chem* **117**:426-31.

Wang, J., Zhang, Z. & Huang, R. 2013. Regulation of ascorbic acid synthesis in plants. *Plant Signal Behav* **8**:e24536.

Wang, J. K. & Seibert, M. 2017. Prospects for commercial production of diatoms. *Biotechnol Biofuels* **10**:1-13.

Waring, J., Klenell, M., Bechtold, U., Underwood, G. J. C. & Baker, N. R. 2010. Light-induced responses of oxigen photoreduction, reactive oxigen species production and scavenging in two diatom species. *J Phycol* **46**:1206–17.

White, A. J. & Critchley, C. 1999. Rapid light curves:a new fluorescence methos to assess the state of the photosynthetic apparatus. *Photosynthesis Res.* **59**:63–72.

Wilhelm, C., Jungandreas, A., Jakob, T. & Goss, R. 2014. Light acclimation in diatoms: From phenomenology to mechanisms. *Marine Genomics* **16**:5-15.

Wilson, K. E., Thompson, J. E., Huner, N. P. A. & Greenberg, B. M. 2001. Effects of ultraviolet-A exposure on ultraviolet-B–induced accumulation of specific flavonoids in *Brassica napus*. *Photochem Photobiol* **76**:678–84.

Wolfe-Simon, F., Grzebyk, D. & Schofield, O. 2005. The role and evolution of superoxide dismutase in algae. *J Phycol* **41**:453-65.

Xia, S., Wang, K., Wan, L., Li, A., Hu, Q. & Zhang, C. 2013. Production, characterization, and antioxidant activity of fucoxanthin from the marine diatom *Odontella aurita*. *Mar Drugs* **11**:2667-81.

Xiong, J., Jee, G. & Subramaniam, S. 1996. Modeling of the D1/D2 proteins and cofactors of the photosystem II reaction center: Implications for herbicide and bicarbonate binding. *Prot Sci* **5**:2054-73.

Young, J. N., Heureux, A. M. C., Sharwood, R. E., Rickaby, R. E. M., Morel, F. M. M. & Whitney, S. M. 2016. Large variation in the Rubisco kinetics of diatoms reveals diversity among their carbon-concentrating mechanisms. *J Exp Bot* **67**:3445-56.

Zaheer, K. 2017. Hen egg carotenoids (lutein and zeaxanthin) and nutritional impacts on human health: a review. *CYTA J FOOD* **15**:474-87.

Zhang, J., Sun, Z., Sun, P., Chen, T. & Chen, F. 2014. Microalgal carotenoids: beneficial effects and potential in human health. *Food Funct* **5**:413-25.